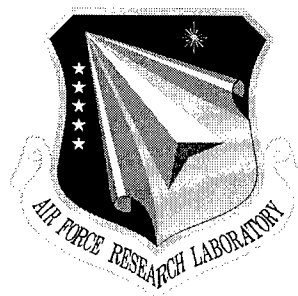


**RL-TR-97-233**  
**Final Technical Report**  
**February 1998**



# **DATABASE MANAGEMENT USING OPTICAL ASSOCIATIVE MEMORY**

**Harris Corporation**

**Sponsored by**  
**Advanced Research Projects Agency**  
**ARPA Order No. 7892**

*APPROVED FOR PUBLIC RELEASE; DISTRIBUTION UNLIMITED.*

19980430 104

The views and conclusions contained in this document are those of the authors and should not be interpreted as necessarily representing the official policies, either expressed or implied, of the Advanced Research Projects Agency or the U.S. Government.


**AIR FORCE RESEARCH LABORATORY**  
**ROME RESEARCH SITE**  
**ROME, NEW YORK**

**DTIC QUALITY INSPECTED 8**

This report has been reviewed by the Air Force Research Laboratory, Information Directorate, Public Affairs Office (IFOIPA) and is releasable to the National Technical Information Service (NTIS). At NTIS it will be releasable to the general public, including foreign nations.

RL-TR-97-233 has been reviewed and is approved for publication.

APPROVED:



FRED N. HARITATOS  
Project Engineer



FOR THE DIRECTOR:

JOSEPH CAMERA, Technical Director  
Intelligence & Reconnaissance Directorate

If your address has changed or if you wish to be removed from the Air Force Research Laboratory mailing list, or if the addressee is no longer employed by your organization, please notify AFRL/IFED, 32 Hangar Road, Rome, NY 13441-4114. This will assist us in maintaining a current mailing list.

Do not return copies of this report unless contractual obligations or notices on a specific document require that it be returned.

**ALTHOUGH THIS REPORT IS BEING PUBLISHED BY AFRL, THE RESEARCH WAS ACCOMPLISHED BY THE FORMER ROME LABORATORY AND, AS SUCH, APPROVAL SIGNATURES/TITLES REFLECT APPROPRIATE AUTHORITY FOR PUBLICATION AT THAT TIME.**

## DATABASE MANAGEMENT USING OPTICAL ASSOCIATIVE MEMORY

Lynda M. Ralston  
Andrew M. Bardos  
William R. Beaudet  
Lee M. Burberry

Contractor: Harris Corporation  
Contract Number: F30602-91-C-0015  
Effective Date of Contract: 27 Mar 91  
Contract Expiration Date: 30 Sep 97  
Program Code Number: 4Y10  
Short Title of Work: Database Management Using Optical Associative  
Memory  
Period of Work Covered: Mar 91 - Sep 97

Principal Investigator: Lynda Ralston  
Phone: (407) 727-5110  
AFRL Project Engineer: Fred N. Haritatos  
Phone: (315) 330-4582

Approved for public release; distribution unlimited.

This research was supported by the Advanced Research Projects  
Agency of the Department of Defense and was monitored by  
Fred N. Haritatos, AFRL/IFED, 32 Hangar Road, Rome, NY.

**DTIC QUALITY INSPECTED 3**

REPORT DOCUMENTATION PAGE			Form Approved OMB No. 0704-0188	
Public reporting burden for this collection of information is estimated to average 1 hour per response, including the time for reviewing instructions, searching existing data sources, gathering and maintaining the data needed, and completing and reviewing the collection of information. Send comments regarding this burden estimate or any other aspect of this collection of information, including suggestions for reducing this burden, to Washington Headquarters Services, Directorate for Information Operations and Reports, 1215 Jefferson Davis Highway, Suite 1204, Arlington, VA 22202-4302, and to the Office of Management and Budget, Paperwork Reduction Project (0704-0188), Washington, DC 20503.				
1. AGENCY USE ONLY (Leave blank)		2. REPORT DATE February 1998		3. REPORT TYPE AND DATES COVERED Final Mar 91 - Sep 97
4. TITLE AND SUBTITLE  DATABASE MANAGEMENT USING OPTICAL ASSOCIATIVE MEMORY			5. FUNDING NUMBERS c - F30602-91-C-0015 PE - 62712E PR - G143 TA - 00 WU - 01	
6. AUTHOR(S)  Lynda M. Ralston, Andrew M. Bardos, William R. Beaudet, and Lee M. Burberry				
7. PERFORMING ORGANIZATION NAME(S) AND ADDRESS(ES) Harris Corporation Government Communications Systems Division P.O. Box 91000 Melbourne FL 32902			8. PERFORMING ORGANIZATION REPORT NUMBER  N/A	
9. SPONSORING/MONITORING AGENCY NAME(S) AND ADDRESS(ES) Advanced Research Projects Agency      Air Force Research Laboratory/IFED 3701 North Fairfax Drive                      32 Hangar Road Arlington VA 22203-1714                      Rome NY 13441-4114			10. SPONSORING/MONITORING AGENCY REPORT NUMBER  RL-TR-97-233	
11. SUPPLEMENTARY NOTES  Air Force Research Laboratory Project Engineer: Fred N. Haritatos/IFED/(315)330-4582				
12a. DISTRIBUTION AVAILABILITY STATEMENT  Approved for public release; distribution unlimited.			12b. DISTRIBUTION CODE	
13. ABSTRACT (Maximum 200 words)  A concept was developed for an optical based associative memory system that accepts a query request from a user, searches the disk for the location of the information and ensures maximum efficiency in data recovery. The system was divided into three parts; user interface and controls, optical correlation, and post processing and analysis. Concepts were developed for the user interface and control subsystem and for the post processing and analysis subsystem. A breadboard was developed to test the correlation subsystem concepts. Two basic concepts were tested; both were successful to some level. The first is an all optical approach in which the data correlation is performed by a space integrating optical correlator. The second is a hybrid opto-electronic approach in which the data is read back in parallel and fed into an electronic correlator.  The optical correlator is a space integrating image plane architecture. The output of the correlation is the number of bits in the query that match bits recorded in that section of the data. The nature of ASCII coding resulted in excessive background fluctuations during readout. The implementation of a custom code and bias subtraction processing reduced the background fluctuations making it possible to set a threshold that locates the correlations. However, any threshold that ensures 100% detection will generate a high false correlation rate.  (Continued)				
14. SUBJECT TERMS  Database Management, Database Search, Associative Memory, Photonics			15. NUMBER OF PAGES 176	
			16. PRICE CODE	
17. SECURITY CLASSIFICATION OF REPORT  UNCLASSIFIED	18. SECURITY CLASSIFICATION OF THIS PAGE  UNCLASSIFIED	19. SECURITY CLASSIFICATION OF ABSTRACT  UNCLASSIFIED	20. LIMITATION OF ABSTRACT  UL	

The opto-electronic correlator is a more compact design with fewer components and therefore will be easier to package. The data is read off the optical disk in parallel, detected by the photodetector electronics that are an integral part of the opto-electronic integrated circuit, and then the correlation is performed electronically. The output of the opto-electronic correlator gives the number of matching characters between the query and the recorded data. This results in a cleaner correlation output than that from the optical correlator. As a result, it is a straightforward process to define a threshold that ensures 100% probability of detection with a low false correlation rate. The one risk area in the opto-electronic correlator is mechanical tolerances. The data is written along radii of the disk and the photodetector must be aligned with a high degree of precision with the disk radii. In order to ensure proper operation, disk eccentricities and drive wobble must be kept lower than  $\pm 10\mu\text{m}$ .

## **ACKNOWLEDGEMENTS**

We would like to acknowledge the contribution of Dr. Philippe Marchand of Parallel Solutions Inc. Dr. Marchand developed the concept of the opto-electronic integrated circuit for use as a combined photodetector and electrical correlator in the Optical Associative Memory system. The opto-electronic correlator concept reported in Chapter 4 was developed by the combined efforts of Parallel Solutions and Harris.

## Table of Contents

<b>1. INTRODUCTION.....</b>	<b>1-1</b>
1.1 Background .....	1-1
1.2 System Requirements.....	1-2
1.3 Summary of Results .....	1-3
1.4 Report Structure .....	1-3
<b>2. SYSTEM OVERVIEW.....</b>	<b>2-1</b>
2.1 Control and Interface Electronics.....	2-2
2.1.1 Control Electronics.....	2-2
2.1.2 Interface System .....	2-2
2.1.2.1 Controller .....	2-2
2.1.2.2 Diagnostics .....	2-3
2.2 Post-Processing System.....	2-3
2.2.1 Degree of Match Processors.....	2-3
2.2.2 Fuzzy Set Processors .....	2-5
2.2.3 Mask Composer.....	2-5
2.2.4 Man Machine Interface (MMI).....	2-5
2.2.4.1 Database Mode Interface .....	2-5
2.2.4.2 System Mode Interface.....	2-6
2.2.5 Optical Correlation Queries .....	2-6
2.2.6 Query Results .....	2-7
2.3 Correlation Subsystem .....	2-7
2.3.1 Optical Correlation Trade Study .....	2-7
2.3.2 Optical Correlator Architecture.....	2-11
2.3.3 Opto-electronic Correlator Architecture .....	2-12
2.3.4 Summary .....	2-13
<b>3. OPTICAL CORRELATOR ARCHITECTURE .....</b>	<b>3-1</b>
3.1 Optical Correlator Concept.....	3-1
3.2 Optical Correlator Design Trades.....	3-3
3.2.1 Data Format Trades .....	3-3
3.2.1.1 Correlation Simulation Using the 4/15 Code .....	3-4
3.2.1.2 Correlation Simulation Using the RLL (2,7) Code .....	3-11
3.2.1.3 Custom Correlation Code.....	3-15
3.2.2 Source.....	3-24
3.2.2.1 Coherent Sources.....	3-24
3.2.2.2 Discrete High-Power LEDs.....	3-34
3.2.2.3 LED Arrays .....	3-37
3.2.2.4 Summary of the Source Trade.....	3-39
3.2.3 SLM.....	3-39

3.2.3.1 Liquid Crystal Spatial Light Modulators.....	3-42
3.2.3.2 Magneto-Optic SLM .....	3-43
3.2.3.3 Electro-optic SLMs .....	3-43
3.2.3.4 Deformable Mirrors.....	3-43
3.2.3.5 SLM Trade Summary .....	3-44
3.2.3.6 Spatial Light Modulator Testing .....	3-46
3.2.4 Disk Media Trades .....	3-47
3.2.4.1 Optical Correlator Disk Size Limits.....	3-48
3.2.4.2 Disk Type .....	3-49
3.2.4.3 Substrate Effects.....	3-53
3.2.5 Photodetector Array .....	3-53
3.2.6 Objective Lens.....	3-55
3.2.7 Servo System.....	3-56
3.3 <i>Breadboard Results</i> .....	3-58
3.3.1 Breadboard Description.....	3-58
3.3.2 Breadboard Development Measurements and Simulations.....	3-61
3.3.3 Optical Correlator Breadboard Results .....	3-84
3.4 <i>Optical Correlator Architecture Summary</i> .....	3-88
<b>4. OPTO-ELECTRONIC CORRELATOR ARCHITECTURE.....</b>	<b>4-1</b>
4.1 <i>Opto-Electronic Correlator Concept</i> .....	4-1
4.2 <i>Opto-Electronic Integrated Circuit Development Summary</i> .....	4-3
4.2.1 Data Coding.....	4-6
4.2.2 Optical Data Detector Circuits .....	4-6
4.3 <i>Disk Data Format</i> .....	4-7
4.4 <i>Detector Structures</i> .....	4-10
4.5 <i>Detection Reliability and Speed Comparison of Single Bit Vs. Manchester-Coded</i> <i>Input Detection</i> .....	4-11
4.5.1 Detection Reliability.....	4-11
4.5.1.1 Single-bit detection .....	4-13
4.5.2 Manchester-coded input detection.....	4-13
4.5.3 Detection Speed.....	4-15
4.5.3.1 Single-bit detection .....	4-15
4.5.3.2 Manchester-coded input detection.....	4-15
4.6 <i>Mathcad Analysis of single-bit vs. Manchester Inputs</i> .....	4-17
4.6.1 Detection Reliability.....	4-17
4.6.1.1 Single-Bit input .....	4-18
4.6.1.2 Manchester Inputs .....	4-19
4.6.2 Speed Analysis .....	4-21
4.6.2.1 Single-Bit Input .....	4-21
4.6.2.2 Manchester Inputs .....	4-23
4.6.2.3 Comparison .....	4-24



<i>4.7 Input Detector Circuits</i> .....	4-25
4.7.1 Data .....	4-25
4.7.2 Clock .....	4-25
4.7.3 Tracking and Alignment.....	4-27
<i>4.8 Typical simulations of the chip operation</i> .....	4-28
4.8.1 Query Loading.....	4-28
4.8.2 Perfect match Simulation .....	4-29
<i>4.9 Fabricated Parts</i> .....	4-29
4.9.1 Correlator Chip.....	4-30
4.9.2 Chip and Interface Board.....	4-30
4.9.3 Test Board .....	4-31
4.9.4 Test Setups .....	4-31
<i>4.10 Breadboard Experiments</i> .....	4-32
<i>4.11 Opto-Electronic Correlator Summary</i> .....	4-41
<b>5. SUMMARY AND RECOMMENDATIONS</b> .....	<b>5-1</b>
<i>5.1 Correlator Design</i> .....	5-1
5.1.1 Storage Capacity.....	5-1
5.1.2 Thresholding.....	5-2
5.1.3 Packaging .....	5-4
<i>5.2 Component Development Status</i> .....	5-4
<i>5.3 Alternative Technologies</i> .....	5-6
<i>5.4 Summary and Recommendations</i> .....	5-7

## List of Illustrations

Figure 2.0-1 Optical Associative Memory System .....	2-1
Figure 2.2-1 Post Processing Electronics Concept.....	2-4
Figure 2.3.1-1 Data Format Options .....	2-9
Figure 2.3.2-1 Generic Space Integrating Correlator Architecture .....	2-12
Figure 3.1-1 The Space Integrating Correlator Architecture.....	3-1
Figure 3.1-2 Phase Correlator Optics.....	3-2
Figure 3.1-3 Intensity Correlator Optics .....	3-3
Figure 3.2.1.1-1a .....	3-9
Figure 3.2.1.1-1b .....	3-9
Figure 3.2.1.1-1c .....	3-9
Figure 3.2.1.1-1d .....	3-10
Figure 3.2.1.1-1e .....	3-10
Figure 3.2.1.1-1 Simulation Results of the Keyword "search" encoded in the 4/15 code with noise effects included. ....	3-10
Figure 3.2.1.1-2 The qualitative effect of correlation normalization .....	3-11
Figure 3.2.1.2-1 Data flow for the generation of a code word in the RLL(2,7) code .....	3-12
Figure 3.2.1.2-2 Analog Correlation Output for the Keyword "Harris" .....	3-13
Figure 3.2.1.2-3 Highest False Correlation vs. Number of Mask 'ON' bits .....	3-14
Figure 3.2.1.2-4 Ratio of ON/TOTAL Channel Bits .....	3-15
Figure 3.2.1.3-1 Performance of the Custom 16 Bit Code.....	3-20
Figure 3.2.1.3-2 Performance of the Custom 16 Bit Code with a Nonsense String in the Search Text.....	3-21
Figure 3.2.1.3-3 Performance of the Custom 24 Bit Code.....	3-22
Figure 3.2.1.3-4 Performance of the Custom 32 Bit Code.....	3-23
Figure 3.2.2.1-1 Phase Encoded Data.....	3-26
Figure 3.2.2.1-2 Amplitude Encoded Data.....	3-27
Figure 3.2.2.1-3 Illumination Effects on Phase Encoded Data.....	3-28
Figure 3.2.2.1-4 Illumination Effects on Amplitude Encoded Data.....	3-30
Figure 3.2.2.1-5 Transform Plane Aberrations.....	3-31
Figure 3.2.2.1-6 The Effect of Varying Degrees of Speckle Noise.....	3-32
Figure 3.2.2.1-7 Classic Speckle Effects on Correlation Output.....	3-33
Figure 3.2.2.2-1 TRW SLED Power Curve.....	3-36
Figure 3.2.2.3-1 LED Array Format to Image Format Transfer.....	3-37
Figure 3.2.4.2-1 WORM Readout Configuration.....	3-50
Figure 3.2.6-1 Measure MTF of the 4mm CD Player Objective Lens.....	3-56

Figure 3.3.1-1 Breadboard Layout .....	3-59
Figure 3.3.2-1 One sector of correlation output using a standard calibration pattern. ....	3-61
Figure 3.3.2-2 Sample breadboard correlation output in the RLL(2,7) code .....	3-62
Figure 3.3.2-3 Bias subtraction processing algorithm.....	3-63
Figure 3.3.2-4 Breadboard output using the bias subtraction algorithm.....	3-64
Figure 3.3.2-5 Processed Correlation Output Example.....	3-66
Figure 3.3.2-6 Keyword Discrimination .....	3-66
Figure 3.3.2-7 Disk Orientation with respect to the test pattern and CCD array .....	3-67
Figure 3.3.2-8 Full CCD scan through the mask.....	3-68
Figure 3.3.2-9 Correlation data region Run A, through the mask.....	3-69
Figure 3.3.2-10 Correlation Output Histograms .....	3-71
Figure 3.3.2-11 Data scan including resynch bytes.....	3-73
Figure 3.3.2-12 Scans of extreme data patterns .....	3-73
Figure 3.3.2-13 MTF calibration pattern.....	3-75
Figure 3.3.2-14 Alternative MTF simulations .....	3-76
Figure 3.3.2-15 Two character repetitive pattern .....	3-77
Figure 3.3.2-16 Keyword "Harris".....	3-78
Figure 3.3.2-17 Comparison of Simulated MTF with Measured MTF.....	3-79
Figure 3.3.2-18 Exponential MTF Model Contributors.....	3-80
Figure 3.3.2-19 Simulations of scaling errors .....	3-82
Figure 3.3.2-20 Analysis of measurements from frame grab data .....	3-83
Figure 3.3.2-21 DFT analysis of Frame Grab Data.....	3-85
Figure 3.3.3-1 Highest false correlations as a function of the number to channel bits .....	3-87
Figure 3.3.3-2 Comparison of the highest false correlations for the selected o keywords.....	3-87
Figure 3.3.3-3 Optical Correlator Output for a Regular Grating Pattern .....	3-89
Figure 3.3.3-4 Optical Correlator Output for the Query Word 'advance'.....	3-90
Figure 3.3.3-5 Optical Correlator Output for the Query Word 'multiple' .....	3-91
Figure 4.1-1 Opto-Electronic Correlator Concept.....	4-1
Figure 4.1-2 Opto-electronic Correlation Tree.....	4-2
Figure 4.1-2 Electronic Correlation Process in Time.....	4-3
Figure 4.2-1: View of the delivered chip and the interface board.....	4-4
Figure 4.2-2: Simplified Functional Diagram of the correlator chip .....	4-5
Figure 4.2-3: Schematic view of the disk and principle of correlation .....	4-6
Figure 4.3-1: General disk specifications.....	4-8
Figure 4.3-2: Physical dimensions of the detectors on the chip.....	4-9
Figure 4.3-3: Descriptions of the various signal to be stored on the disk .....	4-9
Figure 4.4-1: Possible photodiode implementations based on P-substrate N-well silicon technology .....	4-10
Figure 4.5.1-1: Single bit detection circuitry .....	4-11
Figure 4.5.1-2: Manchester coded input detection circuitry .....	4-11
Figure 4.7.1-1: Differential Optical Input Detector Circuitry .....	4-25

Figure 4.7.2-1: Differential Clock Detector Circuitry with Double Photodiodes and hysteresis compensation circuit .....	4-26
Figure 4.7.3-1: Split Detector layout based on the ST1 detector Structure.....	4-27
Figure 4.7.3-2: Split detector Current Amplifier Circuitry .....	4-27
Figure 4.8.1-1: Query Loading simulations .....	4-28
Figure 4.8.2-1: Perfect Match simulation.....	4-29
Figure 4.9.1-1: Picture of the correlator chip .....	4-30
Figure 4.9.2-1: Picture of the interface board with mounted chip .....	4-30
Figure 4.9.3-1: Picture of the test board connected to the interface board.....	4-31
Figure 4.9.4-1: Electrical and Optical test set-ups .....	4-31
Figure 4.10-1 Opto-Electronic Correlator Breadboard .....	4-32
Figure 4.10-3 Breadboard Query Process .....	4-34
Figure 4.10-4 Opto-Electronic correlation of the query word 'cards. ....	4-35
Figure 4.10-5 Expanded Correlation Output.....	4-36
Figure 4.10-6 Correlation Outputs for different query lengths .....	4-37
Figure 4.10-7 Effect of Readout Speed on the Correlator Output.....	4-40
Figure 4.10-8 Effect of the Internal Chip Threshold on Correlation Output .....	4-41
Figure 5.1-1 PDA Disk Alignment .....	5-2
Figure 5.1.2-1 Threshold Characteristics of the Optical Correlator.....	5-3
Figure 5.1.2-2 Thresholding Characteristics of the Opto-Electronic Correlator.....	5-3

## List of Tables

Table 1.2-1 System Design Specifications.....	2-9
Table 2.3.1-1 Correlator Architecture Trades.....	2-10
Table 3.1-1 Collection Aperture Trade.....	3-4
Table 3.2.1.1-1 Correlation of NO ERROR Data in 4/15 Code.....	3-6
Table 3.2.1.1-2 4/15 Code Results with Phase Effects Included.....	3-7
Table 3.2.1.2-1 Results for the Keyword "Harris".....	3-12
Table 3.2.1.2-2 Correlation Model Results.....	3-14
Table 3.2.1.3-1 Brightness distribution for all allowable code sequences of length 16.....	3-17
Table 3.2.2.1-2 Illumination Effects on Amplitude Coding.....	3-29
Table 3.2.2.1-3 Phase Aberration Effects.....	3-29
Table 3.2.2.1-4 Summary of Speckle Reduction Techniques.....	3-34
Table 3.2.2.2-1 LED Options.....	3-34
Table 3.2.2.2-2 SLED Specifications.....	3-36
Table 3.2.2.3-1 LED Array Requirements.....	3-37
Table 3.2.2.4-1 Source Trade.....	3-39
Table 3.2.3-1 Spatial Light Modulator Requirements.....	3-40
Table 3.2.3.5-2 Additional SLMs, Not Necessarily Commercially Available.....	3-44
Table 3.2.3.5-1 Commercially Available SLMs .....	3-45
Table 3.2.3.5-3 Recent Advances, Not Part of the Original Trade .....	3-46
Table 3.2.3.6-1 Characteristics of Procured & Tested SLMs .....	3-46
Table 3.2.3.6-2 Meadowlark SLM Performance.....	3-47
Table 3.2.4.1-1 Correlator Disk Size Trade .....	3-48
Table 3.2.4.2-1 WORM Disk Contrast Measurements .....	3-51
Table 3.2.4.2-2 Phase Change Disk Contrast Measurements.....	3-52
Table 3.2.5-1 Photodetector Array Requirements.....	3-54
Table 3.3.1-1 Breadboard Design and Measured Light Budget.....	3-60
Table 3.3.2-1 An Example of Statistics from a set of correlation outputs .....	3-70
Table 3.2.2-2 Standard Deviation in the Correlation Peaks.....	3-72
Table 3.3.2-3 Breadboard Contrast Measurements .....	3-72
Table 3.3.2-4 Correlation Statistics using Exponential MTF Model .....	3-81
Table 3.3.2-4 Averages from Frame Grab Measurements .....	3-84
Table 3.3.3-1 Correlation Model Results .....	3-86
Table 4.4-1 Qualitative comparison of different photodiode structures .....	4-11
Table 4.10-1 OEIC Correlator Light Budget .....	4-33
Table 4.10-2 Summary of the Opto-Electronic Correlator Testing.....	4-38
Table 4.10-3 Summary of the Correlator Results with Thresholds of '0' and '1' .....	4-42
Table 5.1.1-1 Associative Memory Design Parameters - Projected System.....	5-1
Table 5.2-1 Correlator Component Status.....	5-5
Table 5.3-1 Correlator Option Comparison .....	5-8

## 1. INTRODUCTION

The Optical Associative Memory (OAM) Program, contract number F30602-91-C-0015, is an investigation into rapid data recovery from optical disks. During the program, a concept was developed for a readout system that accepts a query request from a user, searches the disk for the location of the information and ensures maximum efficiency in data recovery. The system was divided into three parts, user interface and controls, optical correlation, and post processing and analysis. Concepts were developed for the user interface and control subsystem and for the post processing and analysis subsystem. A breadboard was developed to test the correlation subsystem concepts. Two basic concepts were tested. The first is an all optical approach in which the data correlation is performed by a space integrating optical correlator. The second is a hybrid opto-electronic approach in which the data is read back in parallel and fed into an electronic correlator.

### 1.1 Background

The mission of tactical correlation systems is to determine number, status, location and intent of tactical threats rapidly and with a high degree of confidence. Every tactical electronic surveillance system contains one or more data base correlation subsystems which are bottlenecks in obtaining efficient analysis of intercepted signals. The Optical Associative Memory development was driven by requirements for increased capacity search and retrieval in support of military information correlation systems.

Three types of correlation account for most tactical correlation requirements: parametric, textual and pattern-matching. Parametric correlation is the search of tabular data for an indexed data set satisfying specific values or ranges, such as finding the Emitter Type associated with given radio frequency and modulation parameters. Geographic correlation, such as finding the nearest threat to a waypoint, is also parametric correlation. Textual correlation matches reference text input as a keyword, number, or sentence fragment to a large unstructured text data base, such as narrative reports. Pattern-matching is the matching of a small two dimensional point array with a large library of known patterns; an example is matching a new radar track segment against a library of prior ingress paths. The optical associative memory is conceived as a general purpose tool with which to achieve any or all of these types of correlation, with emphasis on free form text.

Many correlation processors use highly efficient search algorithms based on binary trees to reduce searches from Order (N) to Order ( $\log_2 N$ ). Integration of new data or search criteria into existing search binary search trees may be impossible (CD-ROM) or impractical (WORM). If possible, as with erasable optical media, each new search criteria requires its own set of binary indices for maximum search efficiency. Each binary index overhead includes space for indices and processing time required to maintain indices. In addition, search time is directly proportional to the amount of data in the system, which can lead to unpredictable throughput in time-critical situations. Furthermore, near misses are often crucial in determining why a correlation failed. Binary tree search normally yields all or nothing results, making it necessary to redefine search criteria and rerun an entire search to achieve best correlation which dramatically increases applications execution time.

The bulk optical associative memory overcomes many of the problems of traditional approaches including binary tree search. The massive parallelism of optics produces all results in a fixed, short (30-60ms) search time. The addition of new data does not increase search time. No space is needed to index the data since physical location is determined directly by the optical correlator based on a content-oriented search mask. In addition, there is no computational penalty for installing new data, regardless of how organized, since the search does not use indices. Near-misses are stored in the internal memory of the Optical Data Finder and are available for use as a starting point for the next query, greatly increasing query efficiency. Alternatively, near misses can be read and analyzed by the host to determine why a correlation failed; e.g. due to appearance of parameters never before seen on a particular emitter type.

## **1.2 System Requirements**

The system requirement is to store multiple databases with a combined storage capacity of 300 MBytes and scan the entire memory for keyword locations within 35 msec. The system will accept structured query language (SQL) inputs, structure a search for all the included databases, and combine the resultant outputs to define the most probable location of the desired information in the memory. The user can then access the data. Key requirements for the optical associative memory system are summarized in Table 1.2-1.

**Table 1.2-1 System Design Specifications**

PARAMETER	SPECIFICATION	DESIGN MINIMUM	DESIGN GOAL
TIME TO FIRST CORRELATION*	50 msec	70 msec	35 msec
TIME FOR ALL CORRELATIONS**	500 msec	170 msec	135 msec
DATA READOUT RATE	1 MBPS	1MBPS	1MBPS
STORAGE MEDIUM		WORM	ERASABLE
KEYWORD LENGTH			
MINIMUM	3 characters	4 characters	3 characters
MAXIMUM	17 characters	12 characters	17 characters
DATABASE SIZE	300 MBytes	100 MBytes	300 MBytes
FILE TYPE	FREE FORM ALPHANUMERICS	FREE FORM ALPHANUMERICS	FREE FORM ALPHANUMERICS
PROBABILITY OF DETECTION			100%
PROBABILITY OF FALSE CORRELATION			≤ 5%

\* The time required for the system to identify the first correlation it finds and provide the data address to the user.

\*\* The time required for the system to process all correlations found in a single rotation , sort them and provide the user with a list of data addresses ranked by correlation degree of match . This does not include the possibility that query may require multiple keyword searches. If multiple keyword searches are required, it defines the time necessary to combine all the searches and resort the data after each additional keyword.

### **1.3 Summary of Results**

Concepts were developed for the user interface, control system, and post-processor. Two concepts were investigated for the correlation subsystem: an all optical correlator and an opto-electronic correlator. These were both breadboarded and tested; both were successful to some level.

The optical correlator requires a custom code and therefore a custom correlation disk. The output of the correlation is the number of bits in the query that match bits recorded in that section of the data. The nature of ASCII coding resulted in excessive background fluctuations during readout. This occurs because there are a limited number of variations in how the ASCII characters are encoded and there is always some degree of background correlation. In places, the background correlations were stronger than a valid correlation. The combination of the custom code and bias subtraction in the processing reduced the background fluctuations making it possible to set a reasonable threshold to identify true correlations. Any threshold that ensures 100% detection will generate a high false correlation rate. Although written in a normal serial mode around the tracks, the custom code removes extraneously recorded bits such as resynch bytes and error correction codes. The custom correlation disk must be written off-line and updated whenever new data is added to the database.

The opto-electronic correlator is a more compact design with fewer components and therefore will be easier to package. It also requires a custom, differential code recorded off-line on a custom correlation disk. The data is read off the optical disk in parallel, detected by the photodetector electronics that are an integral part of the opto-electronic integrated circuit, and then the correlation is performed electronically. The output of the opto-electronic correlator gives the number of matching characters between the query and the recorded data. This results in a cleaner correlation output than that from the optical correlator. Analog noise is removed from the system when the differential encoding is converted to digital 'ones' and 'zeros'. The correlation is performed on the digitized bits and only digital noise can corrupt it. The result is an output that can easily be thresholded to ensure 100% probability of detection with a low false correlation rate. The only area where the opto-electronic correlator does not surpass the optical version is in mechanical tolerances. The data is written along radii of the disk and the photodetector must be aligned with a high degree of precision with the disk radii. In order to ensure proper operation, disk eccentricities and drive wobble must be kept lower than  $\pm 10 \mu\text{m}$ .

Both correlators require 16 heads to read the entire optical disk. Packaging these will be a challenge. Packaging the opto-electronic version will be easier because there are fewer components. The Control and Post-Processing subsystems are essentially the same for both correlators. Overall, of these two options, we recommend the opto-electronic version. However, with the advances made in electronics since the inception of this program, we recommend a detailed look at an electrical solution prior to continuing with either optical approach.

### **1.4 Report Structure**

Chapter 2 discusses the overall system architecture and the concepts for controls, user interface, and post-processor. It also includes the basic trades for the correlation subsystem. Chapter 3 focuses on the all optical correlation system. It summarizes the system trades and conclusions and describes the breadboard hardware, breadboard testing and results. Chapter 4



---

provides a similar definition of the opto-electronic correlation approach, the breadboard hardware, and test results. Chapter 5 summarizes the trades between the optical correlator and the opto-electronic correlator in terms of performance and component development status. It also includes a brief analysis of the current state-of-the-art in software and hardware solutions. Conclusions and recommendations are provided in Section 5. Appendix A is a report on the concepts investigated for parametric numerics. Appendix B is the full interface definition for the opto-electronic integrated circuit. Appendix C has the details of the electrical design of the focus and tracking system.

## 2. SYSTEM OVERVIEW

The OAM system has three major subsystems: the user interface and control subsystem, the correlator subsystem, and the post correlation processing subsystem. Figure 2.0-1 shows the system block diagram. The control and interface subsystem consists of a computer terminal to provide the user interface, and a standard commercial optical drive (data disk). The correlation subsystem includes a modified optical disk drive augmented with an optical correlator (correlation disk). The processing subsystem takes the output of the correlator, combines it with the user defined logic requirements, and returns the best correlations to the user interface subsystem.

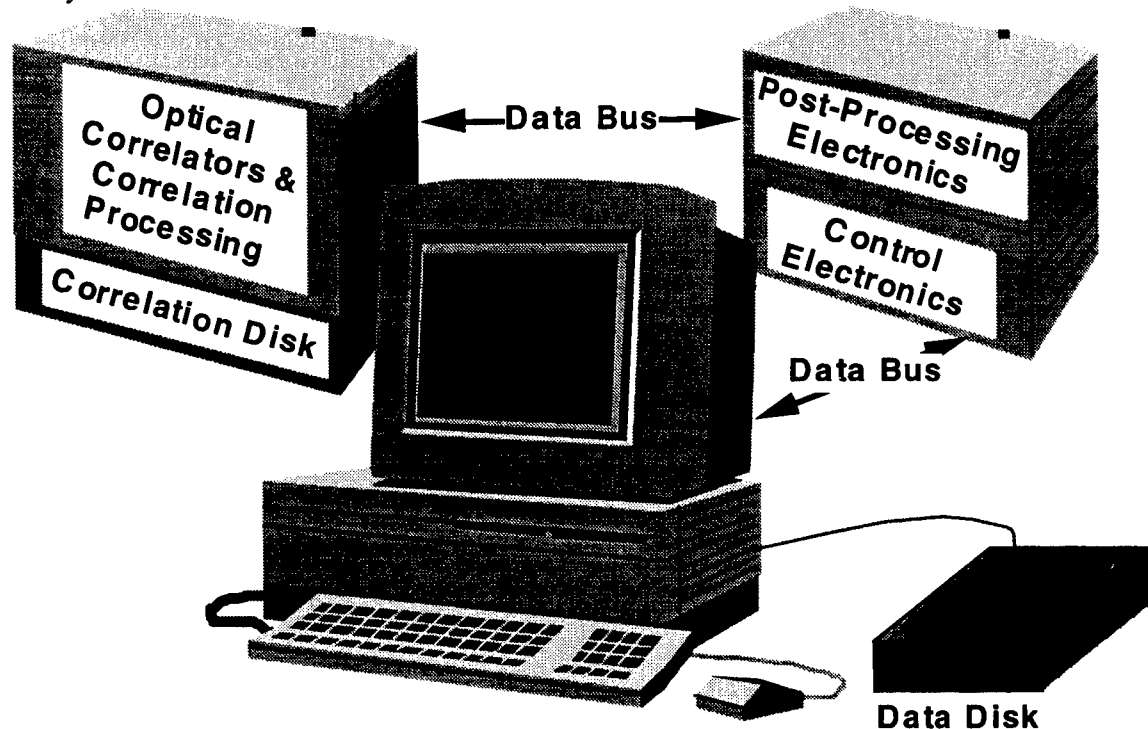


**Figure 2.0-1 Optical Associative Memory System**

Data is entered into the system through an ethernet interface or a standard disk drive. The data is stored, in parallel, in the both standard data disk drive and in the modified correlator disk drive. The modified drive records the same data in a sector by sector mapping using a format optimized for correlation. The correlator subsystem correlates one side of the disk with a 45 to 256 bit search mask every time the media passes under the correlator. Associative retrieval occurs when the user defines a keyword search mask that is input to the correlation subsystem. Each correlator stage processes 1250 tracks of the media in parallel. For each data track, the peak correlation in each sector is stored and clocked out at the end of the sector. The 8 bit Degree of Match Word (DMW) represents the best match of the keyword for each data track in the sector. Each such correlation pass creates and ranks 510,000 digital degree of match words representing degree of maximum match of the mask with the data in each of the disk sectors. The post-processor chains successive queries, combining current results with the previous

results, yielding combined results ready for chaining to the next scan. The best matching track/sector address is retrieved from the standard optical data disk on the next revolution of the media.

The OAM program concentrated primarily on the correlation subsystem. Section 2.1 presents requirements and concepts for the control and interface subsystem. Section 2.2 discusses the post processing electronics to a concept level. In Section 2.3 we discuss the correlator top level requirements, options, and trades. The remainder of the report centers on the correlator component trades, breadboards, and test results.

## **2.1 Control and Interface Electronics**

The system interfaces to the host system via a single standard Small Computer Systems Interface (SCSI) port. Either a stand-alone computer or a terminal may serve as the user interface. The host software module interfaces to the user and/or to the applications programmer.

### **2.1.1 Control Electronics**

The function of the control processor is to set up the search masks and timing registers for system control. It then extracts and formats match results into Oracle or Sybase compatible responses and handles the SCSI interface to the commercial optical drive.

The control subsystem includes a hard disk for system development and interfaces to external devices through RS-232 and SCSI ports. The Control Processor is an advanced microprocessor configured to the VME form factor. This processor accesses the control and command registers of all electronic boards throughout the VME bus. Signals flow from analog input to high speed data distribution to low speed (1 MByte/Sec) read-out. Multiple parts of the software subsystem control specific areas of operation. These include the workstation, the Control Processor, the microcontrollers and the database. The interface software will be compatible with a standard search language such as Oracle or Sybase. The software subsystem controls all system operations.

### **2.1.2 Interface System**

The User Workstation is a commercial PC that allows the developer to build multiple windows for the user interface. The Man Machine Interface (MMI) resides on the User Workstation and is where the user enters commands. There are two modes of operation for entering system commands. The first mode allows the user to enter system support commands such as commands for calibration and diagnostics. The second mode is the database access mode which allows the user to query the system for database information and display various results of the query.

The Control Processor (CP) is the interface between the workstation and the correlator. All queries are passed through the CP to generate a bit mask for searching the media. The CP returns the resultant information back to the user workstation.

#### **2.1.2.1 Controller**

The control sequence for accessing data on the optical media starts with the MMI. The user enters the database access mode by selecting the Database Mode button. At this point the user can query the database. The workstation sends the query to the CP by placing it on the

bus. The CP analyzes the query and sends it on for mask generation. The mask is returned to the CP, which waits until the start of the first sector is reached. At this time the mask is sent to the correlator. The correlator searches all data on the optical media and assigns a correlation value for each data element under the mask. The correlation values are processed by fuzzy set operations in order to determine the Degree of Match. The results are kept in a sorted list with the maximum Degree of Match as the first element. When the entire optical media has been searched the resulting sector table is returned to the workstation and displayed on the screen as the query result. The list of Degrees of Match is accessible to the user through the MMI.

### **2.1.2.2 Diagnostics**

Additional diagnostics are available in the system to aid the developer and the user. The diagnostics are accessed by selecting the System Mode button on the main window display of the MMI. The first diagnostic tool allows the user to load two falling raster displays with data. The graphs display the data as amplitude versus frequency over a period of time. This format is referred to as a 'falling raster' graph. The first graph displays the data as it is read from the disk. The second graph is the known data pattern that was written to disk. By referencing these two graphs, the user may spot problem areas on the disk. A command button on this display allows the user to overlay the data to further compare the two graphs.

The second diagnostic tool allows the user to display a known data pattern as it appears on the disk in the falling raster format. It displays additional information such as where the start of sector and the resynch byte reside in the data.

The system also includes error checking which will allow the system to exit a problem gracefully. One example is an error handler which will trap the condition that occurs when the optical disk does not respond to an input/output command. A message appears on the user's monitor of the workstation and an error log is written. System errors are kept in a log which may be referenced later to help troubleshoot potential problems.

## **2.2 Post-Processing System**

The Post-Processing System consists of custom electronic boards and software that interface to both the correlator subsystem and the control and interface subsystem. It is shown conceptually in Figure 2.2-1. The post-processing electronics performs fuzzy set operations between previously stored intermediate match results and real-time degree of match from the optical correlator. It consists of two kinds of components: the fuzzy set processors and the bulk sort processors.

### **2.2.1 Degree of Match Processors**

The Optical Data Finder's integral Degree of Match Processor (DMP) ranks the partial matches so that track/sector addresses of first-best match or all matches above a software defined threshold may be read out. The DMP also combines multiple queries using Boolean and/or fuzzy-set operators on each successive revolution of the disk. User programmable fuzzy set operators compute a new degree of match based on current and prior degree of match, such as taking the sum of current and prior degree of match, the maximum of current and prior degree of match, etc. During each revolution of the optical media, the DMP performs a full-disk fuzzy associative query. Each query has 512,000 prior partial matches plus the new optical search

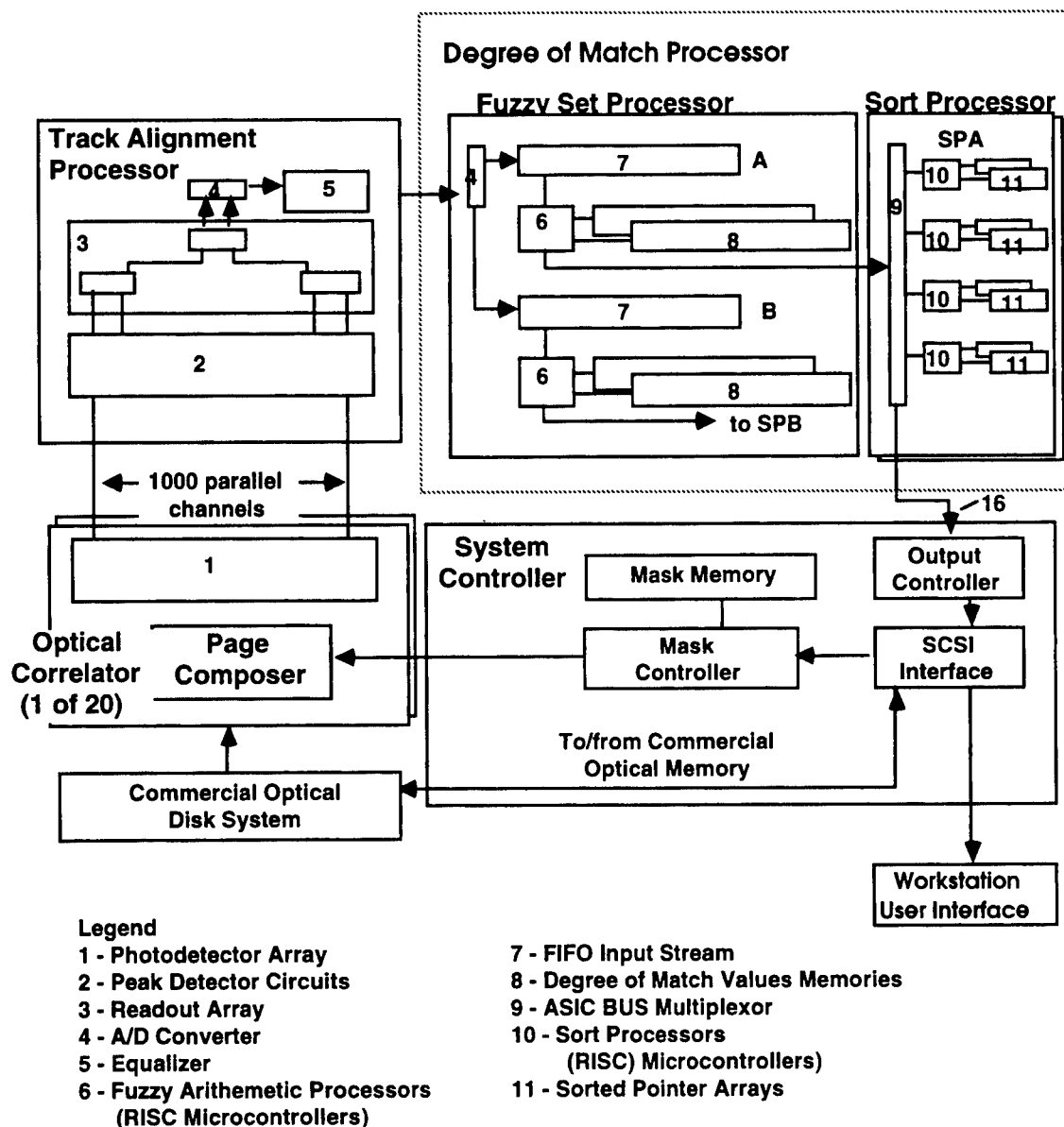


**Figure 2.2-1 Post Processing Electronics Concept**

mask results on all 512,000 sectors, yielding 512,000 rank-ordered partial match results. Partial match results may be used with each successive query, to support full text databases such as Sybase and ORACLE. Within 500 ms, the full system will find the best match (and all other partial matches) to a 15-term query or to 15 independent queries.

The Degree of Match Processor in the Post-Processing electronics provides digital processing which performs fuzzy set operations between previously stored intermediate match results and real-time degree of match from the optical correlator. Each Degree of Match Word represents the maximum match of the search term to data in the sector, and thus achieves position-independent correlation. One DMW is established for each track/sector on the disk on

every revolution. The queries may be chained by the fuzzy set processor which combines the current DMW with the corresponding DMW from a Degree of Match Processor. In each revolution of the optical medium, the DMP's 96 processors perform a systolic full-disk fuzzy associative query which yields rank-ordered partial match results.

Each bulk sort processor does a four-way heap sort of the new match results, yielding a set of pointers. The output processor obtains degree of match and track/sector addresses from the pointers for retrieving the digital data in parallel with the next optical correlation.

### **2.2.2 Fuzzy Set Processors**

Each fuzzy set processor consists of two RISC microprocessors and cache memory controllers. The processors combine current Match results with corresponding sector prior match results from Match Memory, yielding a new Match result in two streams (A and B). There is one fuzzy set processor for each optical channel.

The Fuzzy Processors and Sort Processors require small control programs for their specialized operations. The software assigns a Degree of Match (DM) for data as it is found and then sorts them in rank-order. The DM is computed and sorted by dedicated microcontroller chips in the VME chassis.

### **2.2.3 Mask Composer**

When a user enters a database query, the Mask Composer generates a bit mask for the optical disk correlation. The mask is the bit stream that corresponds to how the characters are written on the optical disk.

### **2.2.4 Man Machine Interface (MMI)**

The User Interface is created for display on a stand-alone PC or on a smart terminal. The MMI is displayed on a high resolution color monitor and is divided into windows which are dedicated to specialized activities. The MMI is mouse-driven for all commands except database access queries. Database access queries are formatted in a standard query language format; the user simply types in the string or value of interest to access the database. Colors highlight areas of interest, for example, if a keyword has synonyms associated with it in the query tree, color is used to highlight both the keyword and highlighting all synonyms in the resulting text.

#### **2.2.4.1 Database Mode Interface**

The Database Mode interface is composed of multiple windows. The window directly beneath the title pane displays the resulting data record for the item which has the greatest degree of match for the query. The displayed text highlights all keywords and any synonyms for the keyword that was entered for the query. Keywords are displayed in one color and synonyms are displayed in another for clarification. The user may select the item to be displayed in the query tree format. This format displays the resulting data block's keyword on an associative query tree which gives the user a graphic picture of how the keyword is associated with the synonyms and other keywords in the database.

The window beneath the query result window is a scrollable window that contains all Degrees of Match in descending order above a user specified threshold. The first item on the list

has the highest degree of match and is automatically displayed, in text format, on the query result window. The additional degrees of match window is scrollable; any of the items may be selected for display in the query result window. A mouse documentation line directly below this window describes how to display the result's data block in the text format or in the keyword's associative query tree format. In addition to the window interface, a C Programmer's tool kit will be available to allow integration to existing applications in the demonstration.

The next window presents graphs of relations between the query keyword and other keywords of interest. A readout describes the data point selected on the corresponding graph. Various relationships can be established through these graphs.

The bottom window is used with the database query entry pane. The defined database functions are mouse selectable and can be used in creating compound queries of the database. A compound query allows the user to create a query which encompasses different concepts in order to define a subset of user specified information. This subset is accessible through the list of degrees of match window for view on the query results window.

#### **2.2.4.2 System Mode Interface**

The System Mode command displays two windows of falling raster graphics of data patterns. The Optical Disk Pattern is the pattern read from the optical disk. The Test Pattern is the pattern written to the optical disk. By comparing the two patterns, the user can compare the input data against the output data. This display is used for diagnostics. The additional command buttons for the Data Maps display allow the user to load the Optical Disk Pattern graph, load the Test Pattern graph, overlay the two graphs for easier comparison, and page through the next set of data.

The other two commands at the top of the System Mode window are Calibration and Track Data. Selecting Calibration brings up a window that prompts the user to select which sectors on the disk to calibrate. Selecting Track Data displays a known data pattern on the optical disk. The system will also have an "automatic" mode in which tracks are calibrated without user interaction.

#### **2.2.5 Optical Correlation Queries**

A query can be a string or a field of interest. A query may be a string if the user is looking for a particular comment stored in a data record. The string is entered through the MMI on the workstation. This text string is sent over the SCSI drive to the Control Processor (CP). A bit mask is created for the text string with the Mask Composer. This bit mask is used by the optical correlator for scanning the optical medium for the queried text. All the data is searched for this string.

The optical correlators scan all data on the disk and give a degree of match to everything found. The degrees of match are sorted dynamically, stored in a list, and returned to the user. The degrees of match and the sorts are all computed with microcontrollers for optimum speed performance. The user can specify the minimum level for the Degree of Match for the items stored on the returned list.

The user can make a query of the database for a particular text string plus request the system to return all synonyms of the text. The user can also request queries by using compound

logic statements in order to combine data concepts. These types of queries are supported through the use of query trees. Query trees differ from traditional database accesses in the following ways:

- Search is performed over all fields of the data record, rather than in a few defined fields.
- Matches are given a value in the range [0,1]
- Queries may be expressed as a concept.

In order to retrieve synonyms from a query tree the user enters the keyword of interest. The keyword exists as a leaf node on the query tree. All other leaf nodes for this branch are synonyms of the keyword. The database access system traverses this branch computing the maximum degree of match for the keyword and its synonyms. The result is a data record with the maximum degree of match for the keyword or its synonyms.

Retrieval of a combined logical concept can be done with more than one database. The result of one part of a query expression is kept in a query tree to be combined with the result of the query of a second database. In other words, querying multiple databases is done by feeding the second database with the results from the first database. The result of the query expression is a query tree with branches containing concepts that are combined by the logic of the query expression.

### **2.2.6 Query Results**

The query results are sorted by Degree of Match and stored in a list that also contains the sector and track address for each match. The addresses are used by the Sector Map table for quick access to the logical block of data. The minimum value for a Degree of Match may be determined dynamically or set by the user. The user may also specify a maximum length of the Degree of Match list. The system dynamically computes the minimum Degree of Match to be the noise floor of the results, below which reside all Degrees of Match that are insignificant.

The Degree of Match list is returned to the user in descending order, with the highest match first. The first element is displayed on the MMI as the result of the query. The remaining elements and their Degree of Match values are displayed below the query result window. Any of these elements may be selected by the user for view on the screen.

## **2.3 Correlation Subsystem**

Based on an overall trade of correlator types, two optical correlator designs were investigated: an all optical space integrating correlator and an opto-electronic correlator that incorporates optical data detection and electrical correlation functions. This section reviews the overall trade and briefly summarizes each of the selected candidates. The detailed trades, breadboards, and results for each are given in Sections 3 and 4 respectively.

### **2.3.1 Optical Correlation Trade Study**

Both time integrating and space integrating correlator architectures were considered. These were combined with holographic and digital data encoding and with different bit sizes and data layouts (cross track vs. along track). In addition, we considered the effect of recording with



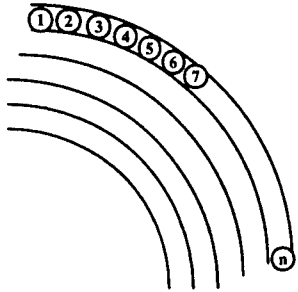
bits that were larger than those used for normal digital data storage. We were looking for an architecture with components that would not require extensive development, and that would simplify the overall system. Trade issues included:

- System complexity
- Query limitations
- Photodetector Array (PDA) complexity
- Spatial Light Modulator (SLM) complexity
- Signal-to-Noise Ratio (SNR)
- Reduction in data sent to the Post Processor subsystem
- Clocking (bit vs. sector vs. character)
- Structured formats vs. free form text formats
- Servo complexity

Common assumptions made in evaluating each candidate architecture include use of a WORM disk written off-line and use of a 24 bit custom code. Most architectures also assume a zoned constant angular momentum format with 17 sectors in the inside zone increasing to 32 in the outside zone. Once a candidate architecture was selected for further evaluation these assumptions were revisited as part of the detailed design.

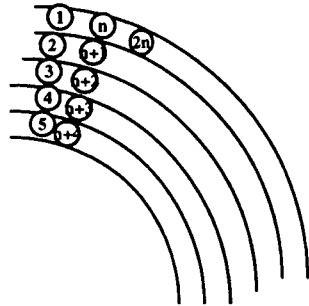
Three generic data formats were considered: serial (normal optical disk format), radial, and radial/serial. These formats are shown in Figure 2.3.1-1. In addition, the normal format might be written cross track coherent, where the data bits on adjacent tracks are written along radial lines although they have no relationship with each other. This format allows a single clock to be used for all tracks. In general, serial format provides the largest storage capacity and the greatest flexibility in defining keywords. If it is written in a cross-track coherent structure, the storage capacity is reduced. Pure radial format imposes some limitations on how the data is written and on the queries. First, it requires that the number of elements in the spatial light modulator equal the number of tracks in the data format. Next, each query must be formatted as a 17 character query since there is no way of knowing where the data starts. This requires that the data be written in 24 X 17 bit blocks along the radial line in order for the data starting point to line up with the query starting point in the SLM. The radial/serial format writes the data in bands. Each ASCII character is encoded into channel bits that are written along radial lines. The next ASCII character is written along the adjacent radial line. This requires that the query be input into the system in bands that correspond to the disk characters. It also requires cross track coherence which reduces data storage.

The various combinations of correlation type and data format are summarized in Table 2.3.1-1. The initial trades were down selected to architectures that did not reduce data storage or constrain the query format. Next, architectures that use sector level clocking are preferred in order to reduce the amount of data sent to the Post- Processing subsystem.



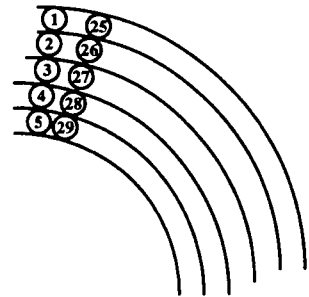
### SERIAL FORMAT

- 8 bit ASCII characters are converted into 24 coded channel bits and recorded serially around the disk
- Adjacent characters are recorded serially around the disk



### RADIAL FORMAT

- 8 bit ASCII characters are converted into 24 coded channel bits and recorded along a disk radius
- Adjacent characters are recorded along the radius
- Wrap arounds occur every n tracks for 1 correlator head.



### RADIAL/SERIAL FORMAT

- 8 bit ASCII characters are converted into 24 coded channel bits and recorded along a radius
- Adjacent characters are recorded serially around the disk.

Figure 2.3.1-1 Data Format Options

**Table 2.3.1-1 Correlator Architecture Trades**

No	Architecture	Data Format	SLM	PDA	Clocking	Data Reduction	Comments
1	Space Integrating Image Plane	• Radial/Serial • Free form	17 X 1300 24 element repeat	1 X 54	Sector	4 X 10 <sup>6</sup>	• Lenslet Array
2	Space Integrating Image Plane	• Serial • Free form • Rectilinear	1 X 408	1 X 1300	Sector	4 X 10 <sup>6</sup>	• Optical Baseline
3	Space Integrating Image Plane	• Serial • Free form • Rectilinear • Fat bits	1 X 192	1 X 650	Sector	4 X 10 <sup>6</sup>	• Custom, large disk • Reduces storage (4X) • Improves SNR • Limits query to 8 characters
4	Space Integrating Image Plane	• Serial • Free form • Rectilinear • Tall bits	1 X 408	1 X 512	Sector	4 X 10 <sup>6</sup>	• Reduces storage (2.5X) • Custom format • Improves SNR • Eases tracking
5	Space Integrating Image Plane	• Radial, Structured • Cross Track Coherent	1 X 1300 256 element repeat	1 X 5	Sector	4 X 10 <sup>6</sup>	• Lenslet Array • Single Keywords
6	Space Integrating Image Plane	• Radial/Serial • Free Form	NONE	1 X 512	Bit	NONE	• Electronic Correlation • Reduces Storage (2.5X) • Hybrid OEIC Baseline
7	Space Integrating Image Plane	• Radial/Serial • Free form • Fat bits	17 X 512 24 element repeat	1 X 27	Sector	4 X 10 <sup>6</sup>	• Lenslet array • Reduces storage (4X) • Improves SNR & Eases Focus
8	Time Integrating	• Cross-track coherent • Free form	NONE	256x1300	Bit	256 X increase	
9	Time Integrating	• Cross track coherent • Structured	NONE	1 X 1300	Bit Keyword	NONE	• Single Keyword
10	Space Integrating Fourier Plane	• Serial	High Spatial Frequency	1 X 1300	Sector	4 X 10 <sup>6</sup>	
11	Space Integrating Holographic (2-D format)	• Radial • Cross track coherent	NONE	32 X 64	Bit	NONE	• Electronic Correlation • Reduces Storage (12X) • Focus Servo Required • Insufficient Light
12	Space Integrating Holographic (1-D Format)	• Radial • Cross Track Coherent	NONE	1 X 1024	Bit	NONE	• Electronic Correlation • Reduces Storage (25X) • Focus Servo Required

The time integrating architectures were eliminated because they provided no data reduction and required bit level timing accuracy (about 46 ns). The Fourier plane architecture required a complex, custom SLM; this was determined to be a high risk. The holographic storage formats reduced data storage. The space integrating architecture with radial/serial format also reduced data storage.

Of the space integrating image plane architectures, the only one that does not either reduce data storage or increase the complexity of the SLM is number 2, which is standard optical disk data format with free form text. Within each disk zone the data is written in a rectilinear format to allow a simple linear SLM to be used. This was selected as the initial baseline. After further investigation it was determined that this architecture would require that several custom components be developed. The trade matrix was re-evaluated and the space integrating architecture with radial/serial format (Number 6) was selected for additional evaluation. Architecture No. 2 is an all optical architecture. Architecture No. 6 is an opto-electronic architecture in which the data is read optically off an optical disk but the actual correlation is done electronically. During the program, these options were investigated in detail, breadboarded, and tested. Each is discussed further below.

### **2.3.2 Optical Correlator Architecture**

The optical subsystem comprises a set of fixed optical correlation stations, spaced around the disk, that perform channel-encoded binary optical correlation in parallel across all tracks on the disk. Since the correlator input is an optical disk, optical matched filtering techniques provide the parallel readout to locate the desired data patterns on the disk. Correlation directly from an optical disk lends itself naturally to spatial domain filtering where the matched filter is a fixed spatial light modulator and the signal is automatically translated past the filter function by the rotating disk.

Figure 2.3.2-1 illustrates the generalized architecture of a space integrating signal processing system operating on data stored on an optical disk. A point source illuminates a signal,  $s(x)$ , in input plane P1. The reflected signal is imaged onto plane P3. A filter with a transmittance function,  $s(x)$ , is introduced into image plane P3. This filter is oriented parallel to the data tracks and is spread in the cross-track direction to cover 1300 tracks in parallel. As the disk rotates the input is translated relative to the filter and the convolution of the input signal with the text search string in the filter is produced. When the signal exactly matches the filter a correlation peak occurs at the output detector array. The detector array is oriented in the cross-track direction so that each element of the array corresponds to a single track on the disk.

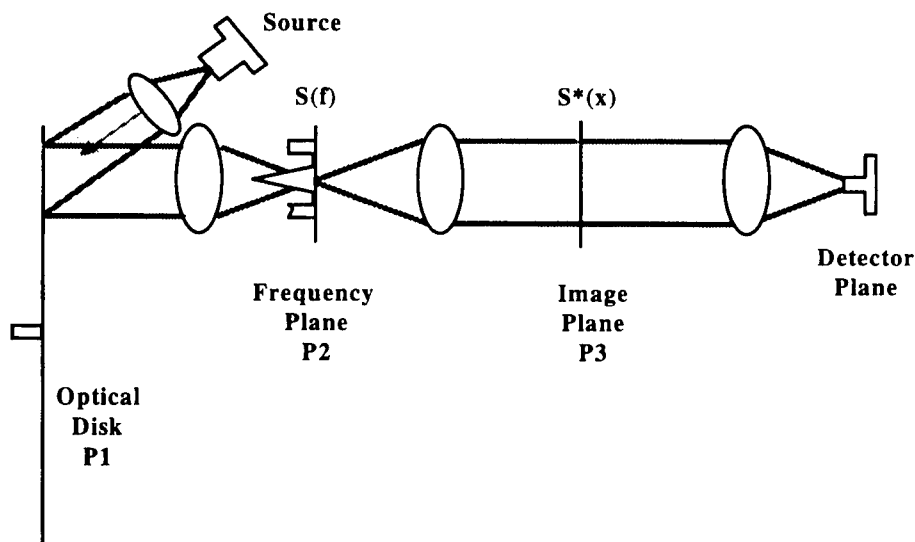


**Figure 2.3.2-1 Generic Space Integrating Correlator Architecture**

Coherent noise effects require incoherent illumination. Therefore, the optimum architecture is an amplitude modulated space integrating correlator with the matched filter in the image plane of the optical disk. Normally, the output of an image plane correlator is extremely sensitive to alignment between the filter and the data. A 2% shift in cross-track position, or along-track position, or a 0.1% scaling error between the filter and the image of the data reduces the correlation peak by about 10 dB. This risk is minimized in the proposed spatial architecture. Since the mask elements are spread in the cross-track direction to cover 1300 tracks in parallel, lateral track drift caused by disk eccentricity is irrelevant to the correlation. The signal is always aligned with the data mask in the cross-track direction. Along-track positioning is provided by the rotation of the disk and at some point the data will properly overlap with the mask. The exact time of overlap is not of interest, only the sector in which it occurred.

During operation a defined keyword is input as a matched filter reference function by computing and storing the proper density distribution in a Spatial Light Modulator (SLM). As the disk rotates past the SLM the degree of correlation between the recorded data and the keyword filter is detected as a function of time at the detector plane. The correlator output is proportional to the byte-by-byte degree of match, in bits, between search mask and data on the disk. The sector and track where a correlation is found, along with a voltage level proportional to the strength of the optical correlation, are sent into the post-processor.

### **2.3.3 Opto-electronic Correlator Architecture**

The opto-electronic architecture takes advantage of the parallel readout potential of the optical disk combined with a high-speed OptoElectronic Integrated Circuit (OEIC) that performs bitwise-matching operations. Thus, a high-capacity, high-throughput optoelectronics associative memory system is implemented that leverages on well established optical disk and VLSI technologies.

The optoelectronic associative memory system consists of a parallel readout optical disk, an exclusive-or (XOR) gate array, an opto-electronic summation circuit, a photodetector

array and a fast electronic decision circuit. A query from the host is loaded into the XOR gate array. Each bit of the query is compared to the corresponding bits of the binary bit-planes read from the optical disk (bitwise matching operations). The outputs of all the XOR operations are then summed and the resultant value gives a measure of the match between the query and the bit-plane of the disk under observation. This value is then fed into the Post-Processor.

This system can support several modes of operation. First, a threshold value is preselected in the decision circuit. The successive inner products between the query bit-plane and the stored bit-planes of the disk are computed and only those bit planes whose sums satisfy the threshold condition are retrieved. Second, the system can be used for classification where a query bit-plane is compared to all the stored bit-planes. In this case, the output does not retrieve a disk bit plane but identifies whether or not the query bit-plane belongs to the database. Finally, the system can be used to find the best match among the bit planes stored on the disk to a query bit plane. On the first rotation all the sums computed for each of the disk bit-planes are compared and the maximum Hamming distance is stored in the decision circuit. The best match is therefore identified and the corresponding bit-plane is retrieved on the subsequent rotation.

The Opto-Electronic Integrated Circuit that performs the summation operation consists of an array of unit cells, each having a light detector and local silicon circuitry that performs the exclusive-nor function. Each unit cell receives three inputs as well as control information. The query is loaded from the control subsystem. The corresponding bits from the stored binary bit-planes arrive from the disk at the detector. The third input is a clock obtained from the disk that signals when a complete bit plane is under observation. The detector circuits of the opto-electronic XOR gate array can be designed to provide large noise margins for the detected input bits. Thus the system can operate with bit-planes having low signal-to-noise ratios. The XOR logic circuits produce a high output only when a bit-match occurs. The outputs of the unit cells are then summed electronically using a tree fan-in structure. Each fan-in unit adds the inputs it receives and sends the results up the tree. The final summed output is the Hamming distance between the query word and the word stored on the optical disk.

#### **2.3.4 Summary**

The output of either type of correlator is digitized as a word defining the strength of the correlation. This word is sent to the Post-Processor that sorts the results by degree of correlation, stores the degree of correlation and the location of the data in memory, combines the results with the results of previous correlations, and outputs the location of the strongest correlation peak to the data reader. Next, the recorded data is accessed and read out. The user can then request readout of the next strongest correlation.

The next two chapters discuss the two correlation types in detail.

### 3. OPTICAL CORRELATOR ARCHITECTURE

The optical correlator is a space integrating image plane architecture. Design issues include data formatting, disk type, and optical subsystem components. A software simulation was developed to facilitate several of the design trades. Once the basic design was determined a breadboard was fabricated and tested. In this section we discuss the optical correlator development starting with the selection of a code for the correlation disk and the selection of disk type. The breadboard component requirements and performance is defined and the test breadboard described. Finally, the experimental results from the breadboard are summarized.

#### 3.1 Optical Correlator Concept

The optical subsystem is composed of a set of fixed optical correlation stations spaced around the disk that perform channel-encoded binary optical correlation in parallel across all tracks on the disk. Since the correlator input is an optical disk, optical matched filtering techniques provide the possibility of parallel readout to locate the desired data patterns on the disk. Correlation directly from an optical disk lends itself to spatial domain filtering where the matched filter is a fixed spatial light modulator and the signal is automatically translated past the filter function by the rotating disk. Because coherent noise effects require incoherent illumination, as discussed in Section 3.2.2, the optimum architecture is an amplitude modulated space integrating correlator with the matched filter in the image plane of the optical disk. Figure 3.1-1 shows the basic concept. The data is written around the tracks on the optical disk. The spatial light modulator (SLM) that holds the query word is oriented parallel to the disk tracks with one SLM element for each recorded bit. The photodetector array (PDA) is oriented perpendicular to the SLM along a radius of the disk with one photodetector element for each track on the disk. In the along track direction, the bits are imaged from the disk to the SLM. In the across track direction, the tracks are Fourier transformed to the SLM plane so that all tracks along a disk radius pass through the same element of the SLM. The optics between the SLM and the PDA Fourier transforms the SLM into the PDA. This effectively collects the throughput from the all the SLM elements onto a unique PDA element for each disk track.

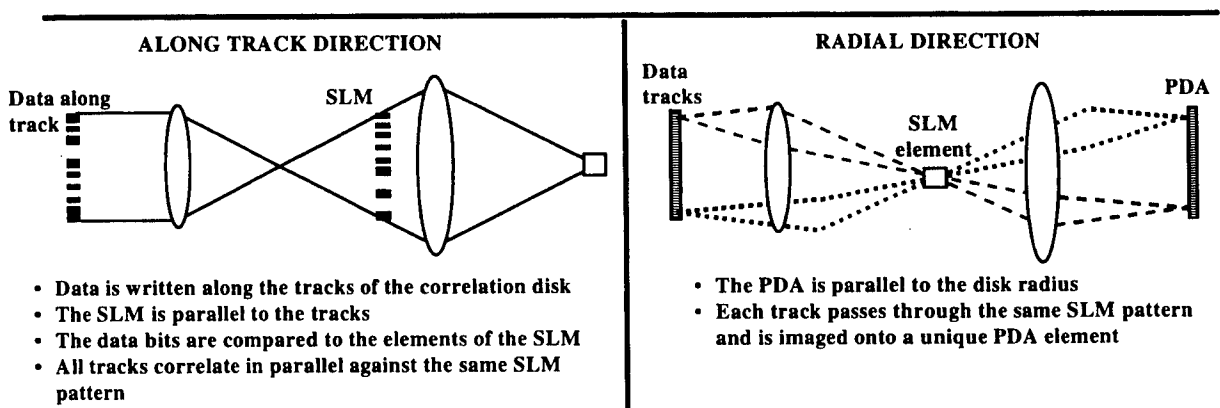


Figure 3.1-1 The Space Integrating Correlator Architecture

During operation a defined key word is input as a matched filter reference function by computing and storing the proper density distribution in a Spatial Light Modulator (SLM). As the disk rotates past the SLM, the degree of correlation between the recorded data and the keyword filter is detected as a function of time at the detector plane. The correlator output is proportional to the byte-by-byte degree of match, in bits, between search mask and data on the disk.

The space integrating architecture can be implemented using either a phase or amplitude correlation. For a phase correlator the data is written as a phase variation on a phase change disk and the query is written as a phase mask. When the data matches the query a uniform phase front is generated. The Fourier transform lens collects this into a concentrated spot at the detector plane as shown in Figure 3.1-2. When the mask and data pattern do not match a phase modulated wavefront is generated which transforms to a distributed spot at the PDA plane. To properly detect the correlations, the PDA size must be matched to the distributed spot size. However, this changes with keyword length. Figure 3.1-2 shows the equivalent conditions for an intensity correlator. Both the data and the mask are stored as amplitude variations. The output spot size is the same whether the data does or does not match the mask. Therefore, a single photodetector size is optimum.

### PHASE CORRELATOR

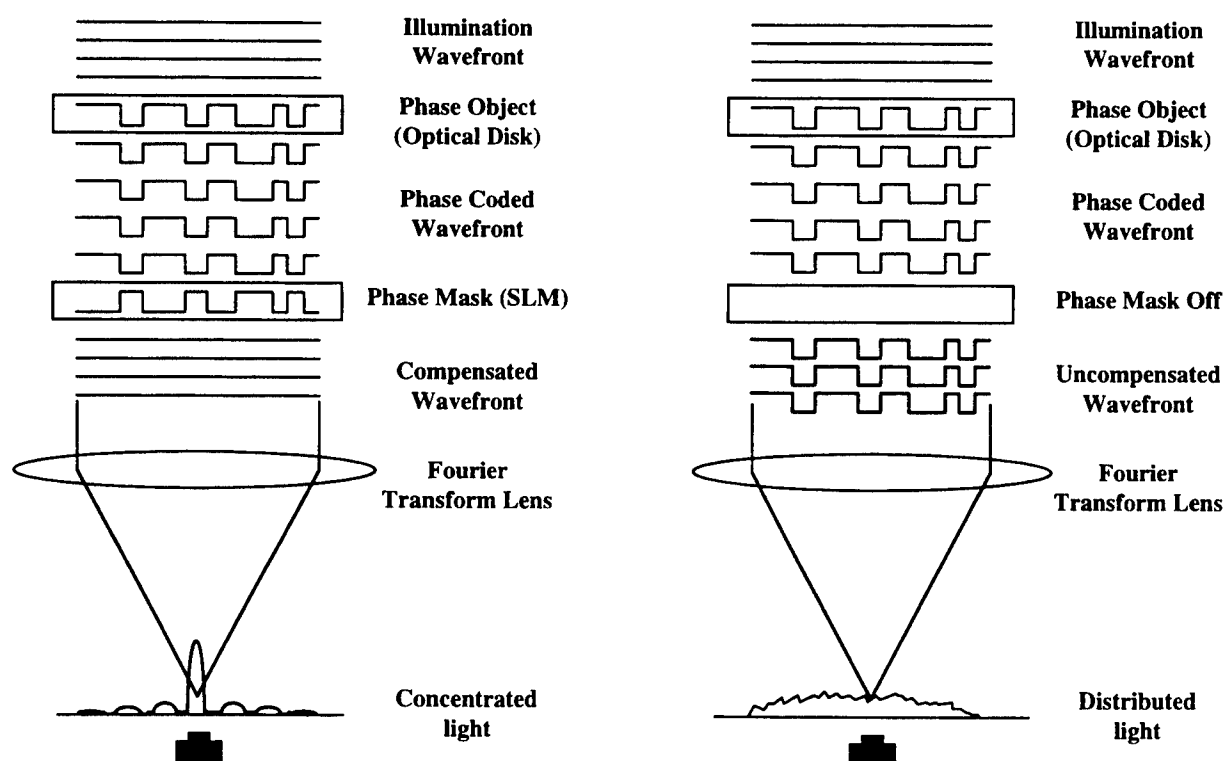
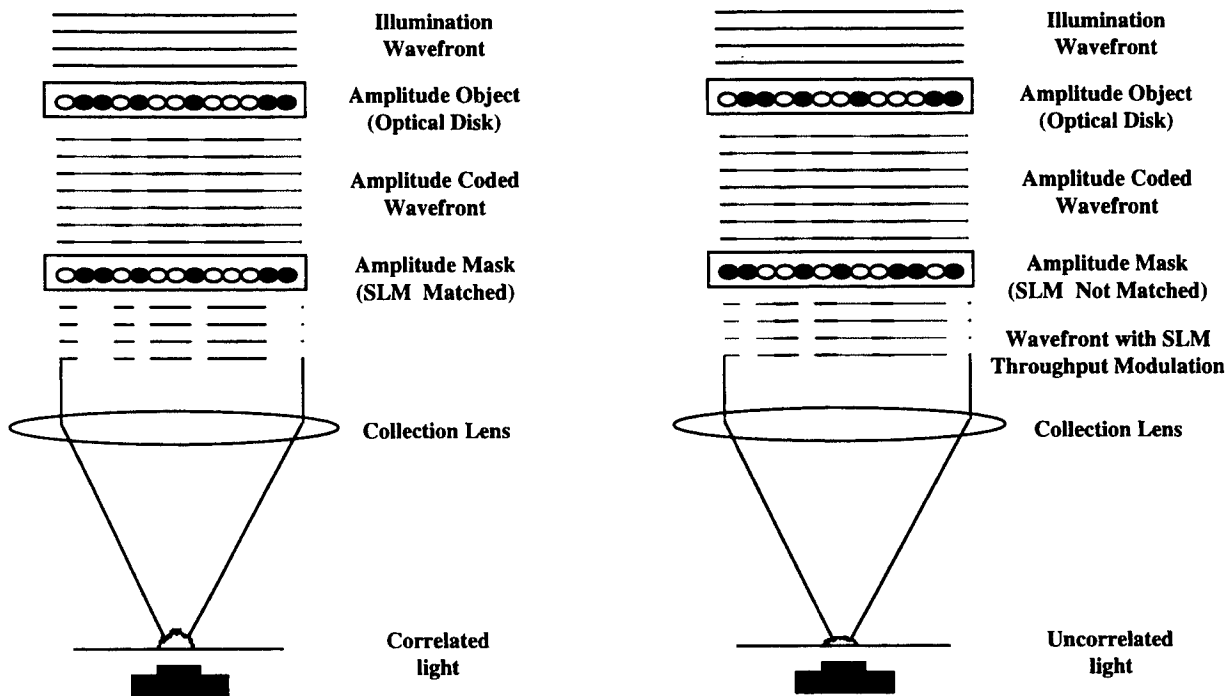


Figure 3.1-2 Phase Correlator Optics



## INTENSITY CORRELATOR



**Figure 3.1-3 Intensity Correlator Optics**

Table 3.1-1 summarizes the differences between small photodetector aperture and full aperture light collection. We selected full aperture collection for three reasons. First, coherent light will not work for this system; coherent noise swamps the image. This is discussed in detail in Section 3.2.2. Second, mechanical tolerances are reduced. Both the depth of focus and the pointing accuracy of the optics are less critical. Third, the detector size remains fixed for full aperture collection. As a result of the initial trades, the optical baseline is a space integrating, amplitude modulated, image plane correlator.

### **3.2 Optical Correlator Design Trades**

A key design trade in the development of the correlator is the code used to record the data on the correlation disk. Key hardware components in the operation of the optical correlator subsystem include the optical disk, source, spatial light modulator, optics, photodetector array, and disk control electronics. The trades and definitions of these are addressed in this section.

#### **3.2.1 Data Format Trades**

The two main coding schemes for optical disks are the '4/15' code in which the 8 bit ASCII characters are encoded as 15 channel bits, 4 of which are always on. This code has the advantage of a constant light return of 4/15. It has a disadvantage in that with only 4 bits on there are a large number of close correlations. The second common code is the 'run length limited 2,7' (RLL(2,7)). This code is defined such that there are never less than 2 nor more than 7 'zeros' between each 'one' bit. However, it is not a unique code; the code for a given ASCII

**Table 3.1-1 Collection Aperture Trade**

Small Aperture Collection	Full Aperture Collection
Needs spatially coherent light	Can use coherent or incoherent light
Collects light energy in central DC spot only	Collect all light energy after SLM
Response is quadratic with correlation	Response is linear with correlation
Uses phase object and phase SLM	Uses amplitude object and amplitude SLM
Detector size = single resolution element (e.g. 7 $\mu\text{m}$ @ F/7 or 1 $\mu\text{m}$ @ F/1)	Detector size = 256 resolution elements (e.g. 1 mm @ F/4 or 250 $\mu\text{m}$ @ F/1)
Depth of focus corresponds to resolution element size (e.g. 49 $\mu\text{m}$ @ F/7 or 1 $\mu\text{m}$ @ F/1)	Depth of focus is limited only by detector size
Pointing accuracy on all passive or active optics is a small fraction of a Rel. (‘Rel’ = resolution element expressed in waves or in spot diameters.)	Pointing accuracy much looser, determined only by detector size limitations. (Typically a few Rels)
Detection window has to change to accommodate changing word length, i.e., it has to match the DC spot size.	Detector size can remain fixed (matched to the longest word) as word length changes.

character depends on the value of the previous bit written. Also, it does not have a constant optical return which complicates the ability to set a threshold for the system. The effects of both these codes were simulated in order to determine what type of optical disk system to select for the system.

The final determination was that neither code is optimum for our application and that a custom code optimized for the correlation process is preferred. Such a code was developed and implemented in the breadboard. This new code increased the design options for the system. It also led to the concept of a dual disk system architecture in which the data is recorded on a ‘data disk’ in the standard optical disk format and, in parallel, on a ‘correlation disk’ in a format optimized for correlations. A map between the correlation disk and the data disk is maintained in the control system. When a correlation location is identified on the correlation disk, it is then recovered from the data disk. This has the advantage that a new query can be initiated while the data readout of the previous query is on-going. It has the disadvantage that, prior to starting the system operation, the data must be transferred to the correlation disk which can be a time consuming operation.

Section 3.2.1.1 discusses the simulations of the 4/15 and RLL(2,7) codes and the development of the custom code.

### 3.2.1.1 Correlation Simulation Using the 4/15 Code

We developed a FORTRAN code simulation (DISK415.FOR) to evaluate data, noise, and 4/15 encoding effects on analog correlation outputs was. The general simulation is described here. This program was used for all the simulations and the code was modified as required. For

example, additional breadboard effects were added as they were identified from the breadboard testing.

## **SIMULATION PROGRAM**

INPUT PARAMETERS are:

KEYWORD:	up to 32 characters
Mask Type (Amplitude / Phase):	amplitude blanks a nonmatched bit, phase subtracts a nonmatched bit.
Mask Noise :	Fraction of 'on' level (Amplitude pseudorandom Gaussian distribution)
Text File:	ASCII text file read from disk (Typically a file from the proposal was used)
Text Noise:	Fraction of 'on' level (Amplitude pseudorandom Gaussian distribution)
Identification Threshold:	% Correlation to treat as a "Hit"

## **ALGORITHMS**

Initialize 4/15 lookup table

Set Mask - Noise if present (encoded once per keyword definition)

Read a text page - encode w/ noise (same approach as mask)

- 1) Accumulate correlation histograms : event count, and # of characters matched
- 2) Store analog correlation values: these predict detector temporal output

Calculate histogram metrics

False Distribution Properties

Peak # of occurrences: the most common % of bits matched

10% population boundary: The top % of bit matches for 10% of the total data  
points scanned

Width: Defined at the Peak - 10% point

Upper bound of False alarm count: % of bit matches that includes the total # of  
false alarms

Match Distribution Properties

Upper bound: peak of Matched % of bits matched (can exceed 100% with noise  
added)

Lower bound: lower % of bits matched for # of hits that includes an exact ASCII  
match with the Keyword

Width: Upper bound: Lower bound (0 for no noise)

Clear % to False alarm boundary: indication of decision hardness (can be  
negative)

Average correlation Level: indication of detector DC output

A series of keywords were correlated with the first 10,000 characters of the OAM proposal in its text file format. We found that, for short keywords, the resulting histogram has a discrete nature based on the characteristics of the code. For example, using the 4/15 code a 6 character keyword is mapped into 4 'on' bits per byte. With no errors, there are only 24 possible locations of marks for the keyword encoded in 4/15 channels. Above the threshold, exact ASCII character matches are counted to determine the # of characters matched for each percentage-of-correlation bin. Longer keywords take on a more continuous distribution. For 70-80% matches, on average, about half the number of ASCII characters matched. Table 3.2.1.1-1 summarizes the results for keywords ranging from 3 to 26 characters.

**Table 3.2.1.1-1 Correlation of NO ERROR Data in 4/15 Code**

Keyword	Length	FP: FW	C%: MH
EOB	[3]	25: 17	9: 69
Byte	[4]	25: 13	19: 45
byte	[4]	25: 13	19: 235
Fuzzy	[5]	25: 16	25: 21
fuzzy	[5]	25: 16	25: 57
Harris	[6]	25: 17	21: 55
Albert	[6]	20: 22	17: 61
technology	[10]	25: 18	23: 31
Jamberdino	[10]	20: 23	20: 41
demonstration	[13]	19: 26	4: 24
Albert Jamberdino	[17]	20: 22	33: 1
associative memory	[18]	20: 21	6: 7
electronics technology	[22]	27: 16	23: 11
Harris Optical Data Finder	[26]	25: 14	13: 8

Parameter		Average	Standard Deviation
FALSE Peak	FP	23.29	2.67
FALSE Width	FW	18.14	3.87
Clear % (%)	C%	18.36	7.71
Match Hits	MH	47.57	56.20 (per 10K chars)

An analysis of distribution statistics versus keyword length shows that the distribution of false correlations remains fairly stable with the exception of the upper bound which is heavily word dependent. The hit rate follows a better trend of decreasing for increasing keyword length with the exception of the word "byte". This is in spite of producing no exact ASCII matches. Changing the "b" to "B" found the all words matching "Byte" and reduced the false correlation rate by a factor of 5.

In summary:

- No Analog Error was introduced
- Average correlation level = 23% with the width of false distribution = 18%
- At a threshold of 70%, the hit rate varies from 7/1000 for three character keywords, down to 1/1000 for Keywords with 20 characters.
- Clear space available for a match decision varies from 4% to 33% for the data examined. There is a strong dependence on word similarity. (i.e. the word "demonstration" has many cousins from the 'tion' family). A unique individual such as "Albert Jamberdino" stands alone.
- Amplitude Mask average correlation constant for differing Keywords at 26.67%.
- Phase correlation results resemble amplitudes, with a "stretched" region between the false and match distributions.
- In terms of data, there appears to be distinct separation between similar and dissimilar words (as defined by 1/2 character count)
- A fixed error of 0.1 full value was introduced in the mask, and the text stream was examined for 0.1, 0.2, and 0.3. Both distributions spread. Using the Keyword "Harris", the clear decision area reduced to about 15%, 9%, and 4% respectively. (The no error case had a safe area of 21%).

Next, a phase indicator was added to the model, and examined with several common Keywords. The following table was run for the 10,000 characters of the file 'oldprop.asc' with no mask or text noise.

**Table 3.2.1.1-2 4/15 Code Results with Phase Effects Included**

Keyword	$\phi$ phase/hits	THRESHOLD	MATCHES
THE	0/75	80	41
_data_ (_indicates a space)	0/46	80	17
data	15/160	80	19
which	2/70	75	5
optic	0/224	75	22
Total	17/575		104.00

The threshold was set for about 5.5, which was the hit rate required to yield the true population. Of this set, about 3% were non-zero phase correlations (channel bit synchronization not on a byte boundary). These were each at the lower edge of the correlation threshold. At this point, it appears out of phase correlations are present, but are not a strong influence on the matched distribution.

The Keyword "search" was used with varying combinations of mask and disk noise to characterize distribution trends. Disk noise levels were in the range of 0% to 30%, and mask noise was added at 0%, 10%, and 20%. The Clear % is the range of correlation values between

the upper bound of the false and the lower bound of the matched distributions. These behave as expected; i.e., decreasing for increasing noise of either type. The data is presented as discrete mask noise families for varying disk (text) noise. A notable point is Clear % = 0 which is where the populations boundaries are tangent. With a mask noise of 20% (14 dB) this occurs at a disk noise of 17% (15 dB). The Clear % is affected by both the upward encroachment of the false population, and the downward drift of the true population. Examination of these two distributions follows.

A false distribution produces more meaningful statistics as it accumulates the bulk of the correlations. Figure 3.2.1.1-1 provides an example of the simulation output for the keyword "search". Similar simulations were run on other keywords. The "top of the miss" shown in Figure 3.2.1.1-1a remains well behaved for Keywords where alpha searches reveal character count matches on the order of half or less for partial matches. When introducing noise, the 0 mask noise family is somewhat artificial (as 11 of the 15 channel bits per byte are completely ignored) and the fit has been replaced by an extrapolated curve generated from the mask noise cases of 10 and 20%. From the text noise (TN) coefficients it appears that the rate of boundary movement decreases with increasing noise both in linear and quadratic form. The average correlation value over the population is defined here as the "DC level" (Figure 3.2.1.1-1b). This value increases fairly uniformly with higher noise.

The match statistics appear dominated by text noise. Figure 3.2.1.1-1d shows the width of the match distribution overlapped with the families of mask noise examined. As shown in Figure 3.2.1.1-1e, the match center drifts up with mask noise. This drift effect led to an investigation of correlation normalization.

Correlation match normalization helps define the level of a true match for varying Keyword lengths in the presence of noise. The effect is shown in Figure 3.2.1.1-2. A zero noise amplitude match should consist of 4 bits per character. Noise tends to increase the correlation summation as zero bits begin to leak onto some amplitude. Noise levels, referred to here, are for Gaussian distribution with a sigma of the percent stated (of 100% full on) about the mean of 'off' or 'on'. Negative off levels are inverted and treated as positive levels of the same magnitude. The 'no normalization' case shows wider distributions (more noise) shifting upward along the correlation value axis.

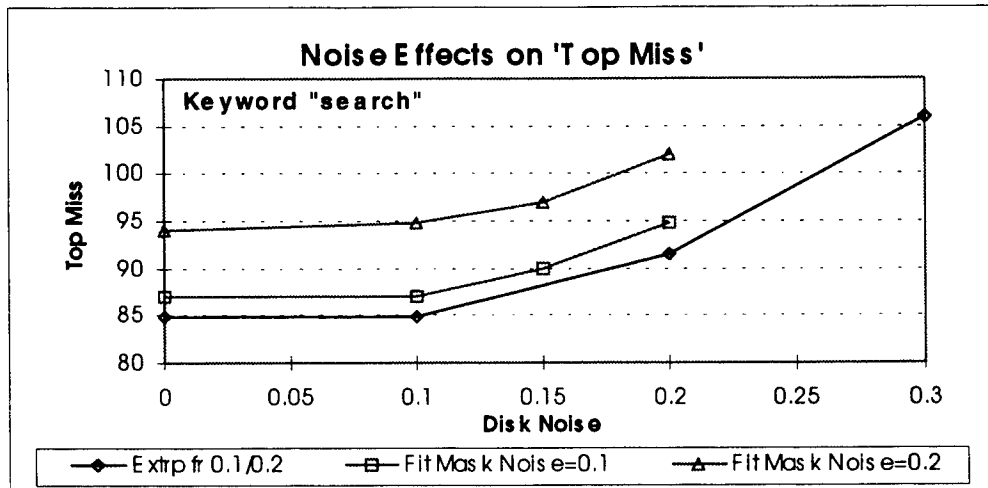


Figure 3.2.1.1-1a

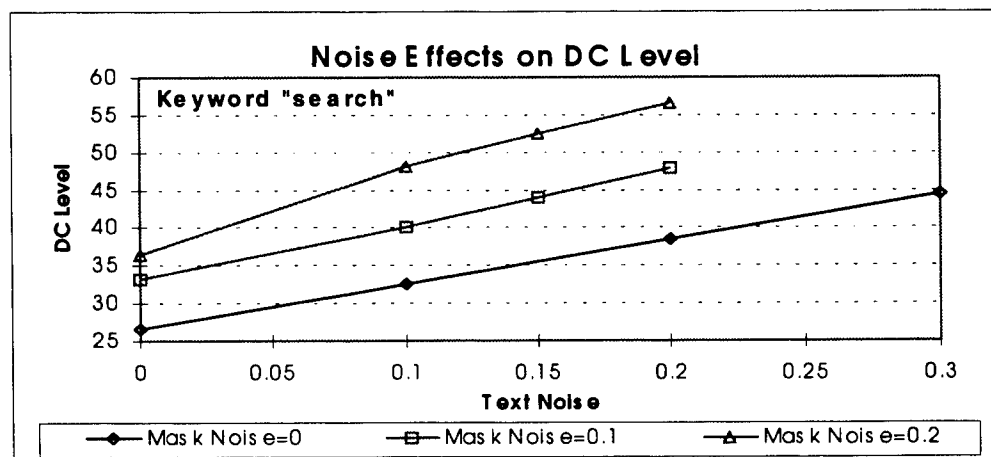


Figure 3.2.1.1-1b

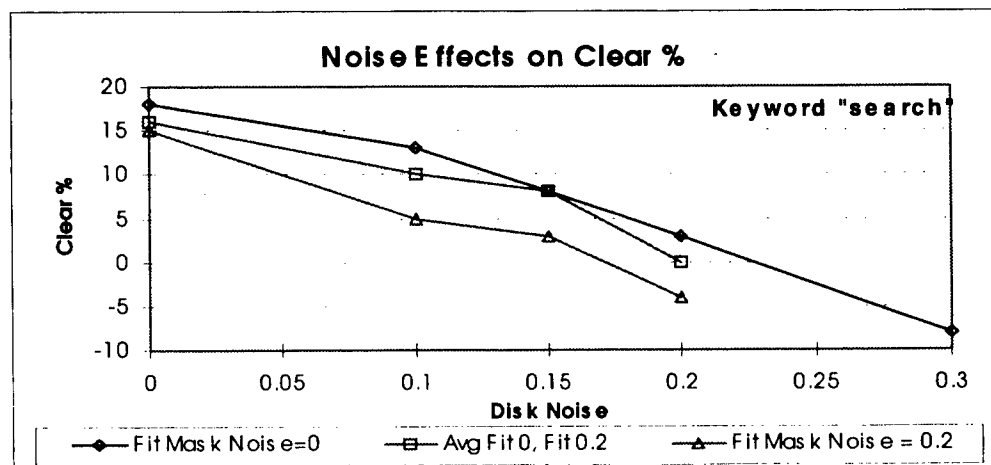


Figure 3.2.1.1-1c

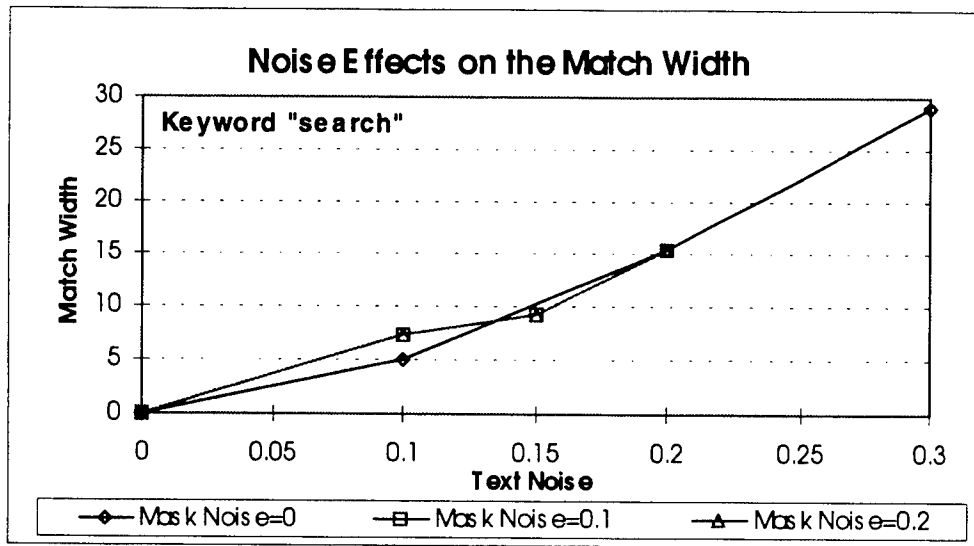


Figure 3.2.1.1-1d

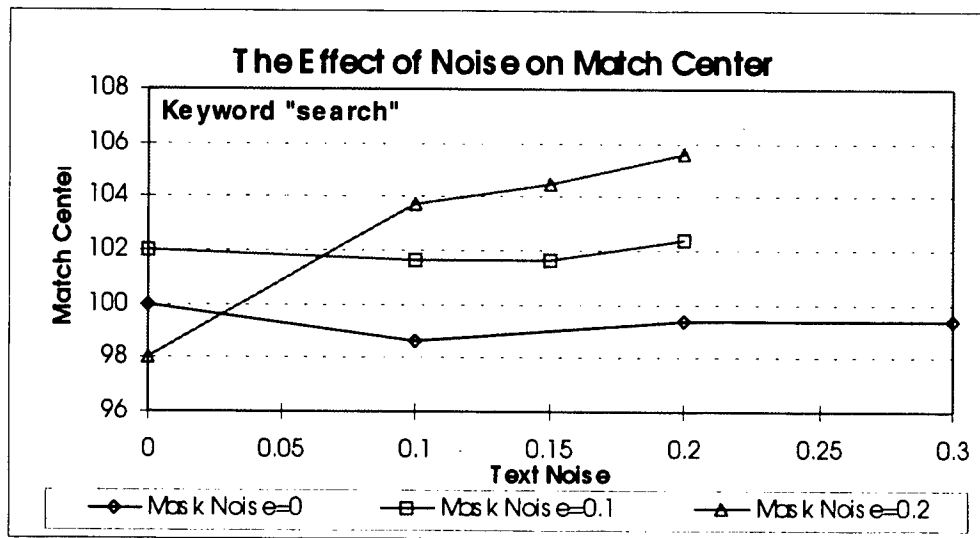
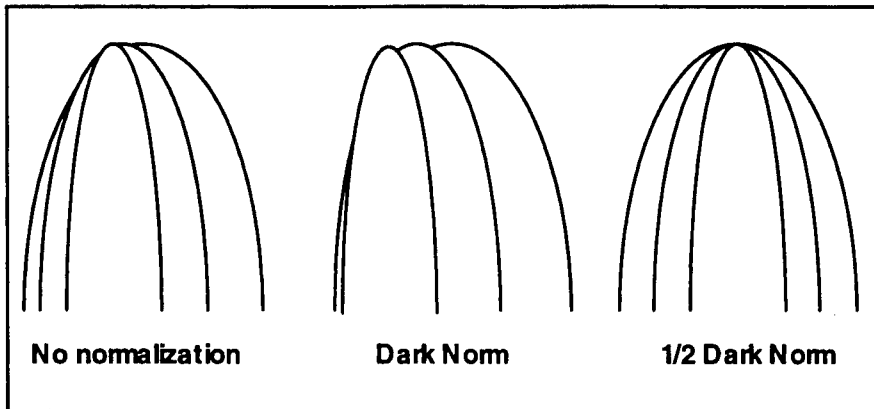


Figure 3.2.1.1-1e

Figure 3.2.1.1-1 Simulation Results of the Keyword "search" encoded in the 4/15 code with noise effects included.





**Figure 3.2.1.1-2 The qualitative effect of correlation normalization**

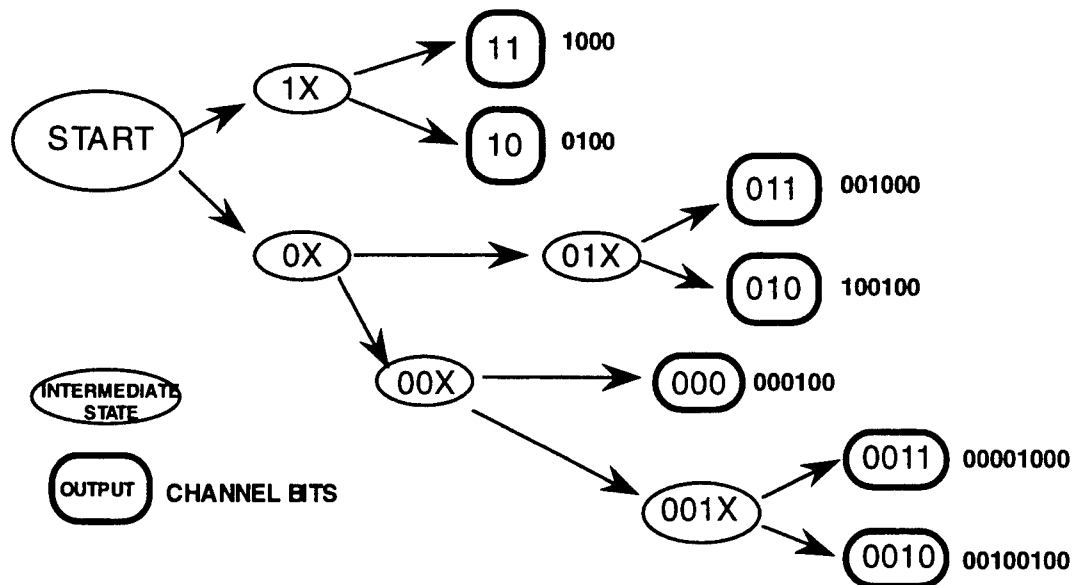
A normalization algorithm was implemented relative to the total transmission allowable through the mask. The total transmission possible through the template is compared to the number of 'on' marks. A fraction of this difference is then added to the 'on' marks to become the normalization factor. Dark norm of the above figure becomes:

$$\begin{aligned}\text{Dark Norm} &= 4/15 * (\text{mask thru} - \text{on bits}) + \text{on bits} \\ 1/2 \text{ Dark Norm} &= 2/15 * (\text{mask thru} - \text{on bits}) + \text{on bits}\end{aligned}$$

The dark norm case causes increasing noise distributions to migrate further down the correlation value axis. Use of half the dark norm correction factor maintains a constant 100% centered true distribution.

### **3.2.1.2 Correlation Simulation Using the RLL (2,7) Code**

Run Length Limited (RLL) coding is defined by the allowable spaces between coded marks. For example, (2,7) refers to no less than 2 consecutive spaces and no more than 7 consecutive spaces. The code is assigned with hysteresis, i.e. bit assignment depends on previous bit conditions. A flow chart for the generation of a coded word is shown in Figure 3.2.1.2-1. A minimum of 2 and a maximum of 4 data bits are required before assigning channel bits. The code requires a doubling of storage as 16 channel bits are used for every 8 data bits. Within a sector, every 20 user bytes are followed with a resynch byte. Thus a sector of 1024 user bytes includes 51 synch bytes. After a synch byte, the data coding resumes from the starting code state. It is significant that the ASCII character "space" also serves as a code state reset. Any starting point within the Flow will end in the start position after the "space" has been encoded. This feature allows the system to use a unique SLM pattern for matching data to a fixed keyword for any text which occurs after a "space".



RLL(2,7) FLOW CHART

Figure 3.2.1.2-1 Data flow for the generation of a code word in the RLL(2,7) code

The DISK415 simulation discussed in Section 3.2.1.1 was modified to operate in the RLL(2,7) mode. Data stream levels are altered from 0/1 (off/on) to user entered contrast levels, which are inverted and scaled in integer values to 1000. For example, an 8% contrast produces levels of 1000/920. The mask can be configured to pass either the bright bits (data "off") or dark bits (data "on"). Previous runs were done with mask passing data "on" and the disk encoded to level 1 for an "on" condition. Additionally, the "on" marks can be allowed to spill over into the "space" regions.

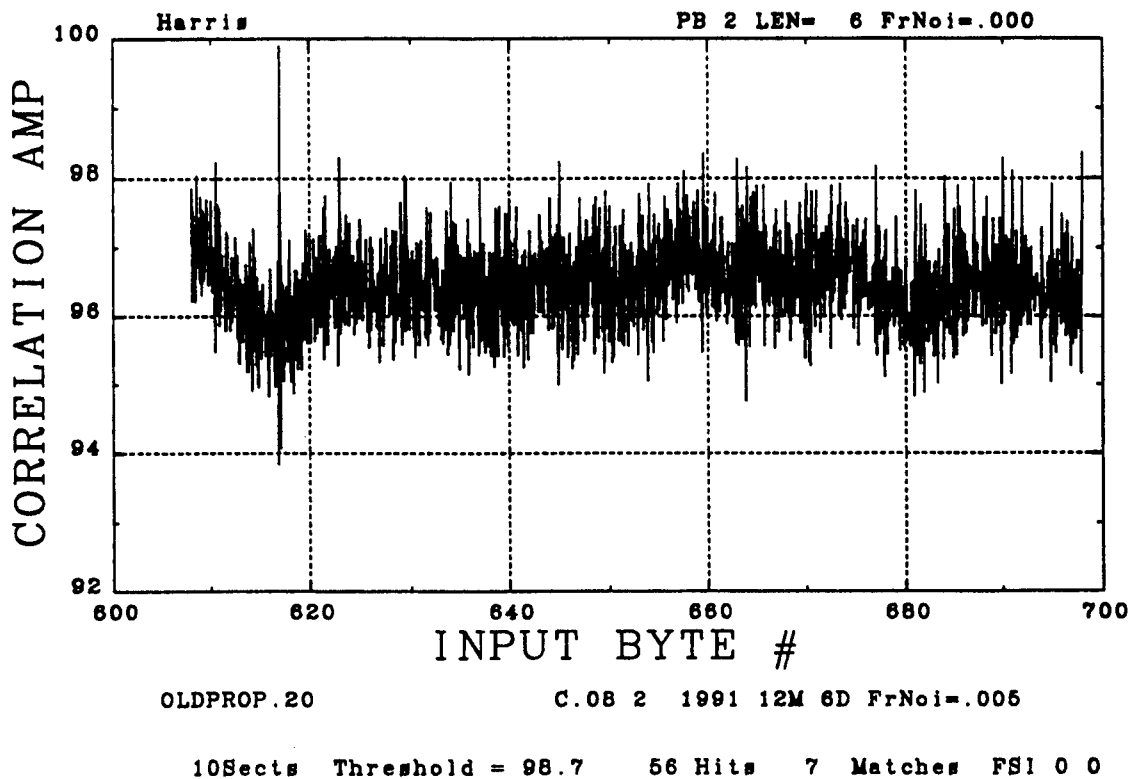
Sample sections of the OAM proposal were examined using the keyword "Harris". A contrast ratio of 8% was used with disk noise of 0.5% Gaussian distributed. In the 10 sectors examined there are 7 occurrences of the word "Harris". A threshold of 98.7% was used. The results are shown in Table 3.2.1.2-1.

Table 3.2.1.2-1 Results for the Keyword "Harris"

Synch bit	Disk noise	# Found	Clear Range	High False
No	No	7	0.6%	99.4%
Yes	No	6	None	99.4%
No	0.05%	7	0.5%	99.4%
Yes	0.05%	5	None	99.4%

By scaling the simulation to the reported contrast (8%) separates a perfect match from false conditions by about 0.5%. The program also simulated the disk characteristic of using 2 channel bits to set a mark by setting two SLM pixels dark per mark; this approach recovers the bit encoding contrast loss.

Figure 3.2.1.2-2 presents a typical analog correlation output for the case of no synch byte and disk noise of 0.05%. The dip from bytes 610 preceding the hit at byte 618 appears consistently before data matches. It occurs because of how the word "Harris" is coded in the 4/15 code. When the coded pattern is offset by a few bits, there is a strong mismatch causing a minimal throughput.



**Figure 3.2.1.2-2 Analog Correlation Output for the Keyword "Harris"**

The RLL(2,7) simulation was run for our demo baseline disk using 20 sectors of the 'oldprop' ASCII file. Disk contrast was set to 8% with bit noise at 0.5%. To select candidate keywords a single word sort was done on the text data. The results of the simulation are shown in Table 3.1.1.2-2. The first column shows the keyword used for the simulation run. Next, the number of bits in the pass mode and marks in the block mode are shown. Here, a mark consists of 2 channel bits. The "Keywords Present" is counted by examining the text file. "Keywords Found" is the number of correlation outputs above a given threshold. The only occurrences not found are the results of a synchronization byte splintering the disk text. The highest FALSE, plotted in Figure 3.2.1.2-3, is probably the most significant result. There is an overall, but not absolute, trend of improving the separation between true and false matches as the number of bits increases. "Hits for TRUE" totals the number of identifications required to include all the unsplintered exact matches. Next, the total number of mask channel bits and percentage of "on"

bits / total bits are listed. This is plotted in Figure 3.2.1.2-4. An average of the bits "on" percentage reveals that the code consistently maintains a 50% "on" level (for the double length marks).

**Table 3.2.1.2-2 Correlation Model Results**

Keyword	ON bits	marks	KW Present	KW Found	Low TRUE	Highest FALSE	Hits for TRUE	CH bits	PCT light
TRW	21	14	2	2	100	100.1	3	49	0.429
mix	24	12	2	2	99.9	100.0	6	48	0.5
EOB	24	12	3	3	99.9	100.1	11	48	0.5
two	28	10	2	2	99.75		2	48	0.583
NATO	32	16	2	2	100	99.7	2	64	0.5
SIGINT	46	25	4	3	99.9	99.2		96	0.479
unique	49	24	2	2	99.8	99.6		97	0.505
keyword	60	26	1	1	100	99.4	1	112	0.536
aircraft	70	29	4	1	100	99.2		128	0.547
Average =									0.509
St Dev =									0.041

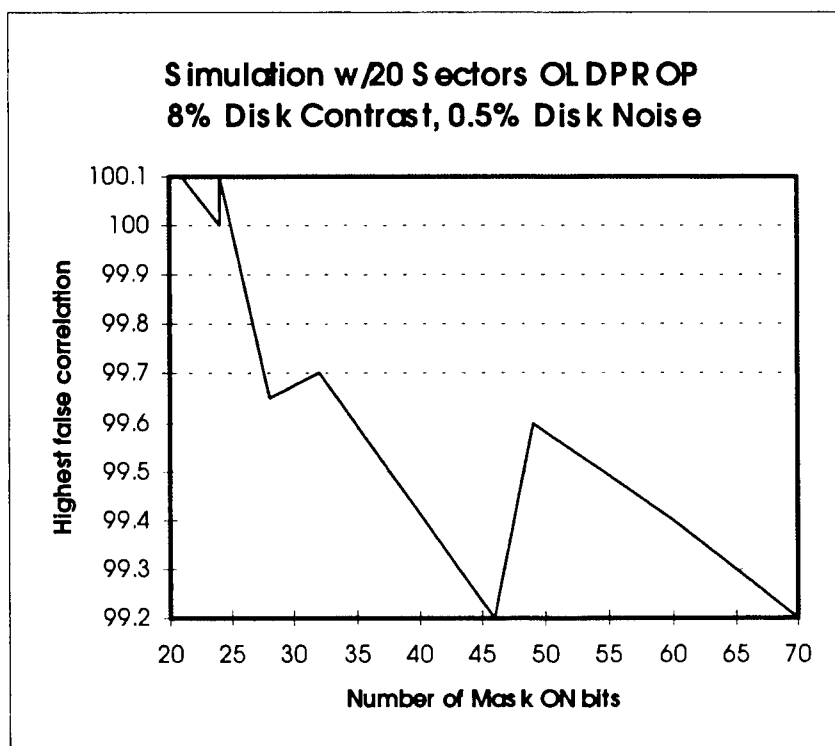


**Figure 3.2.1.2-3 Highest False Correlation vs. Number of Mask 'ON' bits**

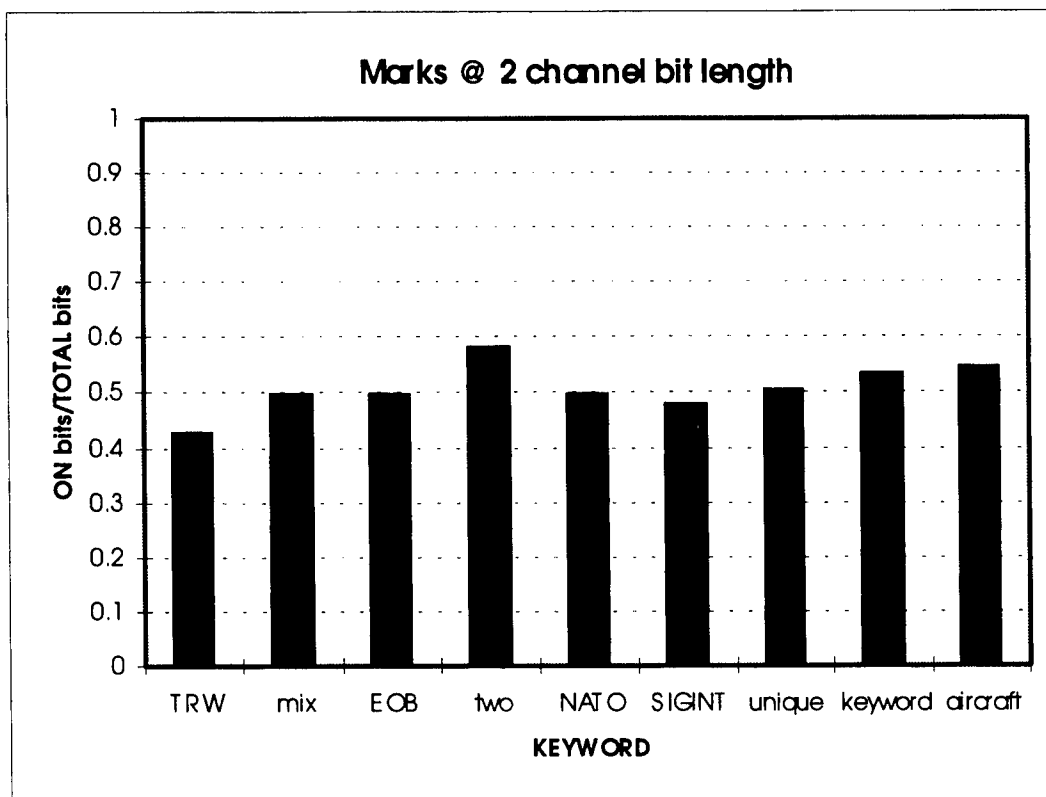


**Figure 3.2.1.2-4 Ratio of ON/TOTAL Channel Bits**

### 3.2.1.3 Custom Correlation Code

The desired output of an optical correlator is a low value for data mismatches with strong (10's of dBs) peaks when a match occurs. Neither the 4/15 or the RLL(2,7) codes provide such a strong correlation difference. Therefore, we investigated alternative coding schemes which would maximize the correlation peak and provide good correlation discrimination.

This section discusses the coding for an optical associative memory in which data bits are written to a disk in the form of non-reflecting spots and recovered using a form of incoherent optical correlation. The optical correlator works by imaging a portion of the disk on a mask containing a sequence of transparent and opaque regions which correspond to the pattern of bits in the keyword. Light transmitted through the mask is collected into a photo detector using a lens. In the ideal case, when the two patterns match, the transparent regions on the mask line up with the reflecting regions on the disk and the total amount of light impinging on the photo detector is maximized. The coding task is to choose a set of code words such that, for all other cases, the amount of light transmitted through the mask is minimized. In analysis we make several simplifying assumptions and state some partial results without proof. For the purpose of this discussion we assume that a spot is represented by a binary 'one' and the absence of a spot is represented by a binary 'zero'.

This assumption presents some interesting variations on the usual problem addressed by conventional coding theory. First of all, the non-reflecting spots on the disk are spaced at an

interval which corresponds to roughly  $1/2$  the diameter of the spot. Thus, to a first approximation a single 'one' written on the disk appears as a pair of ones. Two consecutive 'ones' written to the disk appear as three consecutive ones, etc. From a conventional signal processing perspective this is equivalent to preprocessing the signal using a partial response filter whose impulse response is two symbols long. Second, since we are operating with spot sizes that are near the resolution limit of conventional optics so that the pattern imaged on the mask is not exactly focused. Experimental evidence suggests that this defocusing has the effect of spreading the energy in a single pulse width almost uniformly into the two adjacent slots with negligible energy outside this region. Thus, when computing the energy density at the mask, we make the assumption that the energy in each of the three consecutive slots will be approximately  $1/3$  if the center slot on the disk corresponds to white space (i.e. a data zero).

Using these assumptions and a particular choice of code words, we can compute three quantities of interest; the brightness of a code word, the cross-brightness of two code words and the cross-brightness-distance between two code words. In the interest of brevity we will refer to the cross-brightness-distance as the CB-distance.

The brightness of a code word is defined as the total amount of light gathered when a code word on the disk is imaged onto a perfect mask. For example, if the apparent pattern on the disk were 110011, the brightness would be computed as:

$$(\text{sum } 0 \ 1/3 \ 2/3 \ 2/3 \ 1/3 \ 0) = 2.$$

Note that for the purposes of this calculation we assume the pattern is embedded entirely in dark spaces. If in fact we use this criteria to choose a set of words of constant brightness, there will be some variations due to contributions from the two nearest neighbors when the words are written consecutively on the mask.

The cross-brightness of two words is defined as the total amount of light gathered when a code word on the disk is imaged onto a mask representing a second code word. For example if the apparent pattern on the disk were 110011 and the mask were 111000, the cross-brightness would be computed as:

$$(\text{sum } 0 \ 0 \ 0 \ 2/3 \ 1/3 \ 0) = 1$$

or reversing the roles of image and mask,

$$(\text{sum } 0 \ 0 \ 1/3 \ 2/3 \ 0 \ 0) = 1.$$

In general one can write,

$$\text{cross-brightness}(a,b) = \text{cross-brightness}(b,a).$$

Finally we define the CB-distance between two code words as:

$$\text{CB-distance}(a,b) = \text{brightness}(a) - \text{cross-brightness}(a,b).$$

Note that whereas the cross-brightness is a symmetrical function of its two arguments, the CB-distance(a,b) is not symmetrical unless:

$$\text{brightness(a)} = \text{brightness(b)}.$$

The problem of interest is to find a code suitable for representing the standard ASCII character set. Thus we would like to find 256 members of equal brightness such that the minimum CB-distance(a,b) over all possible pairs a and b is as large as possible. By restricting ourselves to sets of equal brightness we simplify the problem of setting detection thresholds and we can take advantage of the fact that the CB-distance will be independent of the ordering of two code words.

We note in passing that the problem of finding a set of code words which meets the criteria of constant-brightness and minimum separation from all other code words falls into the general class of sphere packing problems and the optimum solution is in general NP complete. Thus we are relegated to finding a good suboptimum solution by heuristic means.

Since the current schemes for encoding information on an optical disk use code words of length 15 or 16 we use this as a point of departure. By direct enumeration we can compute the brightness distribution for all sequences of length 16 that can be generated at the output of the length 2 partial response filter. This distribution is given in Table 3.2.1.3-1.

**Table 3.2.1.3-1. Brightness distribution for all allowable code sequences of length 16.**

Brightness	Number of Words	Brightness	Number of Words	Brightness	Number of Words
0	1	16/3	289	32/3	33
1/3	14	17/3	138	11	0
2/3	68	6	378	34/3	3
1	138	19/3	176	35/3	12
4/3	126	20/3	119	12	0
5/3	144	7	280	37/3	2
2	301	22/3	91	38/3	13
7/3	276	23/3	96	13	0
8/3	201	8	180	40/3	2
3	420	25/3	6	41/3	0
10/3	371	26/3	72	14	0
11/3	212	9	90	43/3	0
4	470	28/3	5	44/3	0
13/3	370	29/3	50	15	0
14/3	185	10	55	46/3	1
5	450	31/3	4	47/3	0

Note that the maximum number of candidates occurs at a brightness level of 4 and is equal to 470. From this set of 470 words we would like to choose a subset of 256 words which minimizes the CB-distance between any two pairs. Again, by direct enumeration we can determine that every word on this list has at least 8 nearest neighbors that are at distance 1/3 or

less away. Since we have to discard at least one of these words for every word that is retained, it is clearly impossible to generate a code having minimum distance greater than  $1/3$ . Thus we can conclude that the best set of 256 code words will have a minimum CB-distance of at most  $1/3$  and that codes of length 16 are not going provide a very large discriminant for rejecting non-matching patterns. As we discuss later, it is possible to salvage this situation, somewhat, by observing that fewer than 128 of the 8 bit ASCII characters are normally used in a database. A somewhat smaller number of these, perhaps 96 or 97, account for the lion's share of all usage. Nevertheless, even with this small bit of relief it is still not possible to expand the minimum distance for a reduced set of characters beyond  $1/3$ .

With the above computations in mind, we note that we have to concentrate on codes whose members have more than 16 bits. Using heuristic search techniques we found several possible candidates corresponding to lengths 20, 24, 28 and 32. Not surprisingly, the best results are obtained using length 32 codes. However, it appears that good results may be possible with code words of length 24. We have been able to construct several sets of 256 words arranged in groups such that all of the elements in each group are guaranteed to have a certain minimum CB-distance with respect to all members of that group and all members of the groups which occur previously in the list. Although we believe that there exist codes with distance properties better than those shown below, it is doubtful that anyone will be able to improve on these codes by more than 5 or 10 percent.

Some sample statistics are shown below.

- Case 0 - Length 16 codewords of brightness 4
  - words 1 - 68 minimum distance greater than  $1/3$
  - words 67 - 256 minimum distance greater than 0
- Case 1 - Length 20 codewords of brightness 6
  - words 1 - 39 minimum distance greater than 1
  - words 40 - 81 minimum distance greater than  $2/3$
  - words 82 - 256 minimum distance greater than  $1/3$
- Case 2 - Length 20 codewords of brightness 7
  - words 1 - 47 minimum distance greater than 1
  - words 48 - 94 minimum distance greater than  $2/3$
  - words 95 - 256 minimum distance greater than  $1/3$
- Case 3 - Length 20 codewords of brightness 8
  - words 1 - 54 minimum distance greater than 1
  - words 55 - 102 minimum distance greater than  $2/3$
  - words 103 - 256 minimum distance greater than  $1/3$
- Case 4 - Length 24 codewords of brightness  $28/3$ 
  - words 1 - 37 distance greater than 2
  - words 38 - 59 distance greater than  $5/3$ ,
  - words 60 - 115 distance greater than  $4/3$ ,
  - words 116 - 243 distance greater than 1



words 244 - 256 distance greater than  $2/3$ .

Case 5 - Length 24 codewords of brightness 8

words 1 - 99 at distance  $> 4/3$

words 100 - 209 at distance  $> 1$

words 210 - 256 at distance  $> 2/3$

Case 6 - Length 28 codewords of brightness 11

words 1 - 98 distance greater than 2

words 99 - 170 distance greater than  $5/3$

words 171 - 256 distance greater than  $4/3$

Case 7 - Length 32 codewords of brightness 13

words 1 - 58 distance greater than 3

words 59 - 81 distance greater than  $8/3$

words 82 - 137 distance greater than  $7/3$

words 138 - 256 distance greater than 1

In each of the cases described above there are subsets of the codewords that have better distance properties than the overall set. Thus, if we order the ASCII characters according to their probability of usage, we can ensure that the most frequently used characters are mapped onto those codewords having the largest separation from their neighbors. As we mentioned earlier, the ASCII characters above 128 are rarely used. For the most part, databases use the alpha-numeric subset plus the common punctuation characters. A crude ordering which should gives us the lion's share of the benefits is shown below.

(65-90)	ABC.....Z
(97-122)	abc.....z
(48-57)	01 ..... 9
(32-47)	space ! " # \$ % & ' ( ) * + , - . /
(58-64)	: ; < = > ? @
(123-127)	{   } ~ rubout
(8-13)	backspace, tab, line-feed, up-arrow, page return
	followed by all the rest

Some examples using the codes discussed above and this character mapping are shown in Figures 3.2.1.3-1 through 3.2.1.3-4. In these examples we simulate a data base in which we wish to extract the word "advance" in the phrase "Now is the time to advance to go and collect \$200." This simulation uses the idealized model above. There is no attempt to model noise or other phenomena which occur in the real media. One might note that these results are optimistic since they are looking for a pattern that is 7 characters long in a sequence where there are very few partial matches. Also observe that for the 16-4-code, where we substitute the nonsensical sequence "eueeiaa" for the word "collect" in the phrase, the spread is reduced from 7 to 5. This leaves little room for random fluctuations in the media and other noise sources.

"advance" in "Now is the time to advance to go and collect \$200."

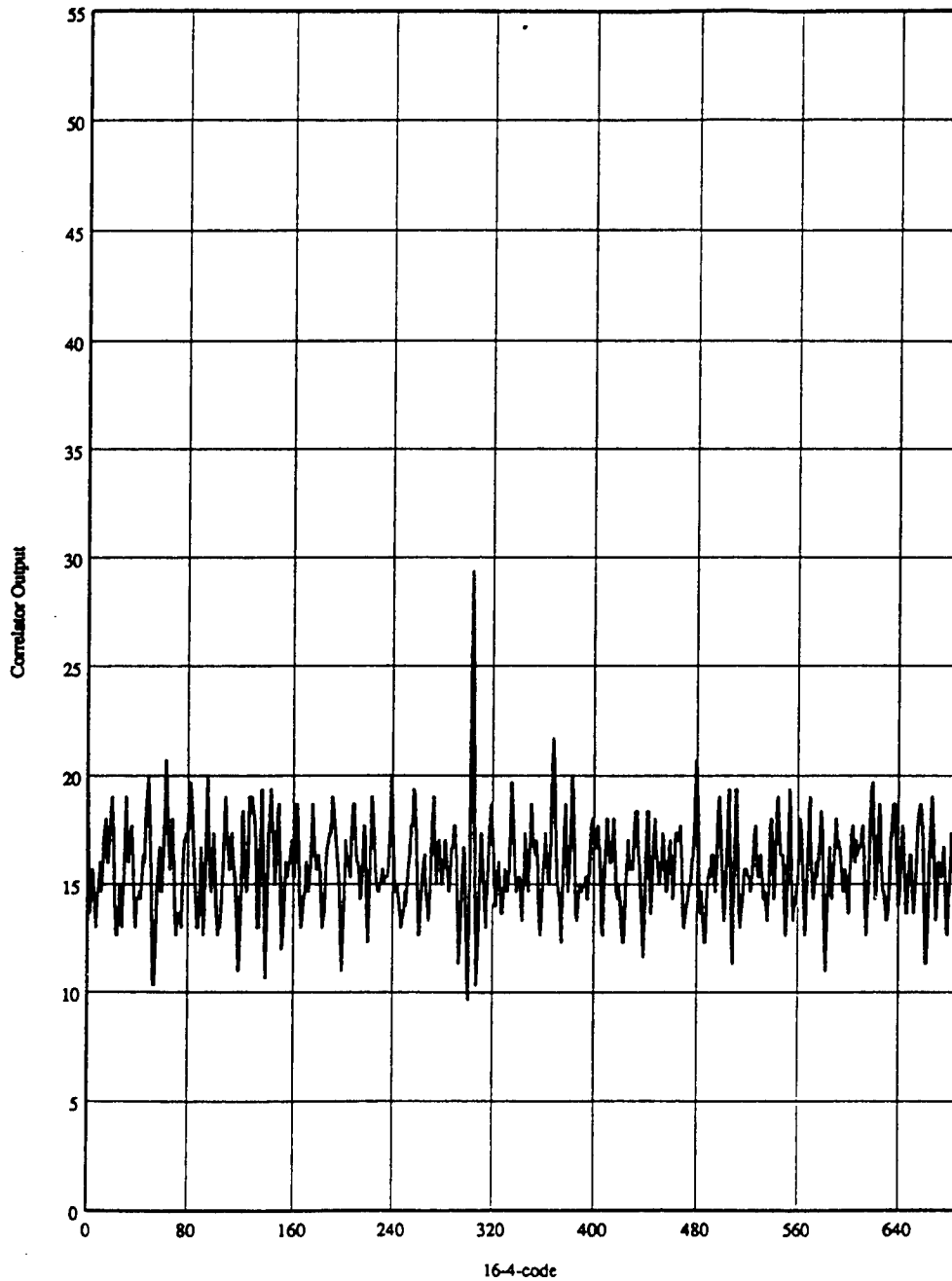


**Figure 3.2.1.3-1 Performance of the Custom 16 Bit Code**

"advance" in "Now is the time to advance to go and eueeiaa \$200."

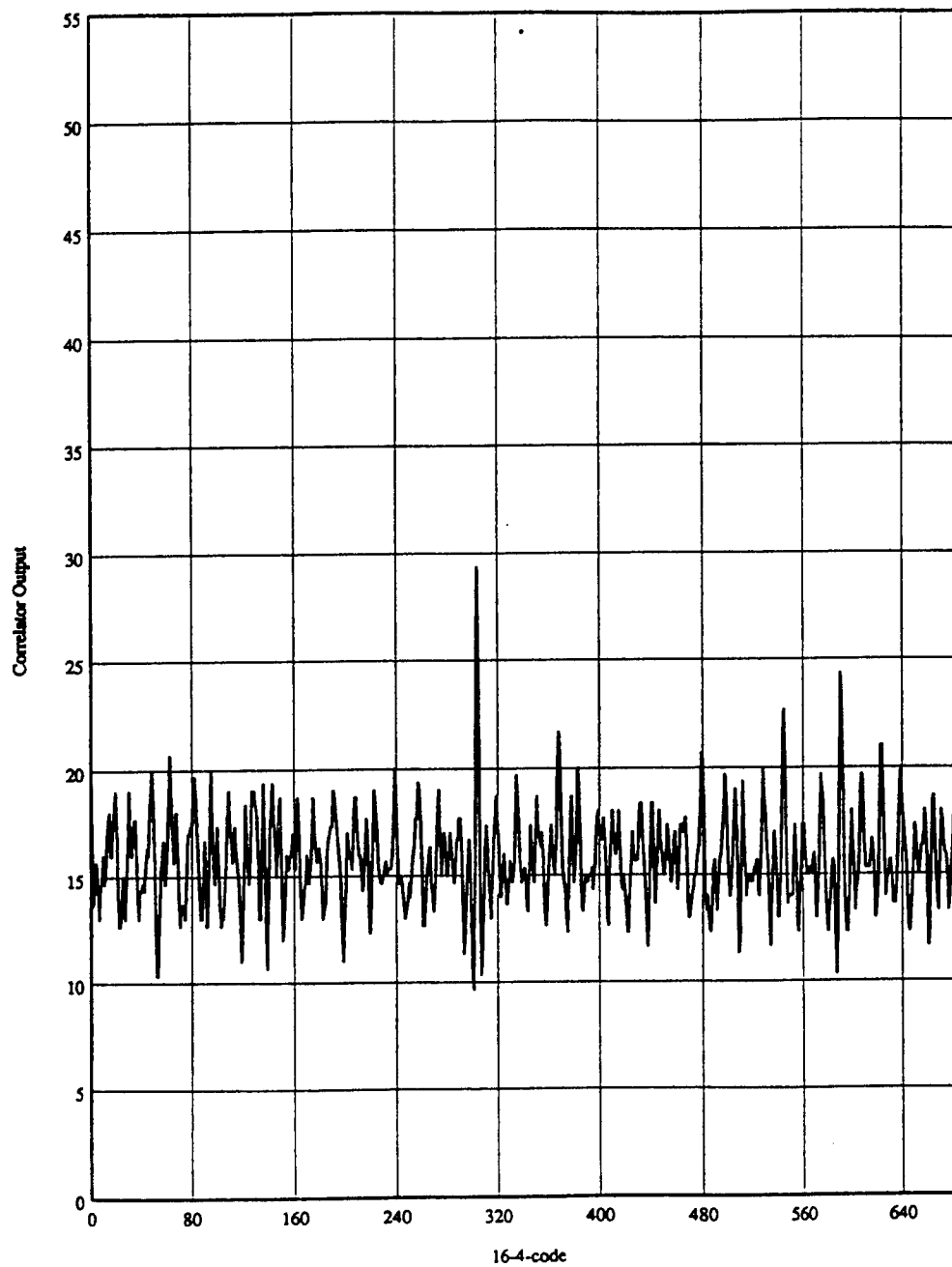


**Figure 3.2.1.3-2 Performance of the Custom 16 Bit Code with a Nonsense String in the Search Text**

"advance" in "Now is the time to advance to go and collect \$200."

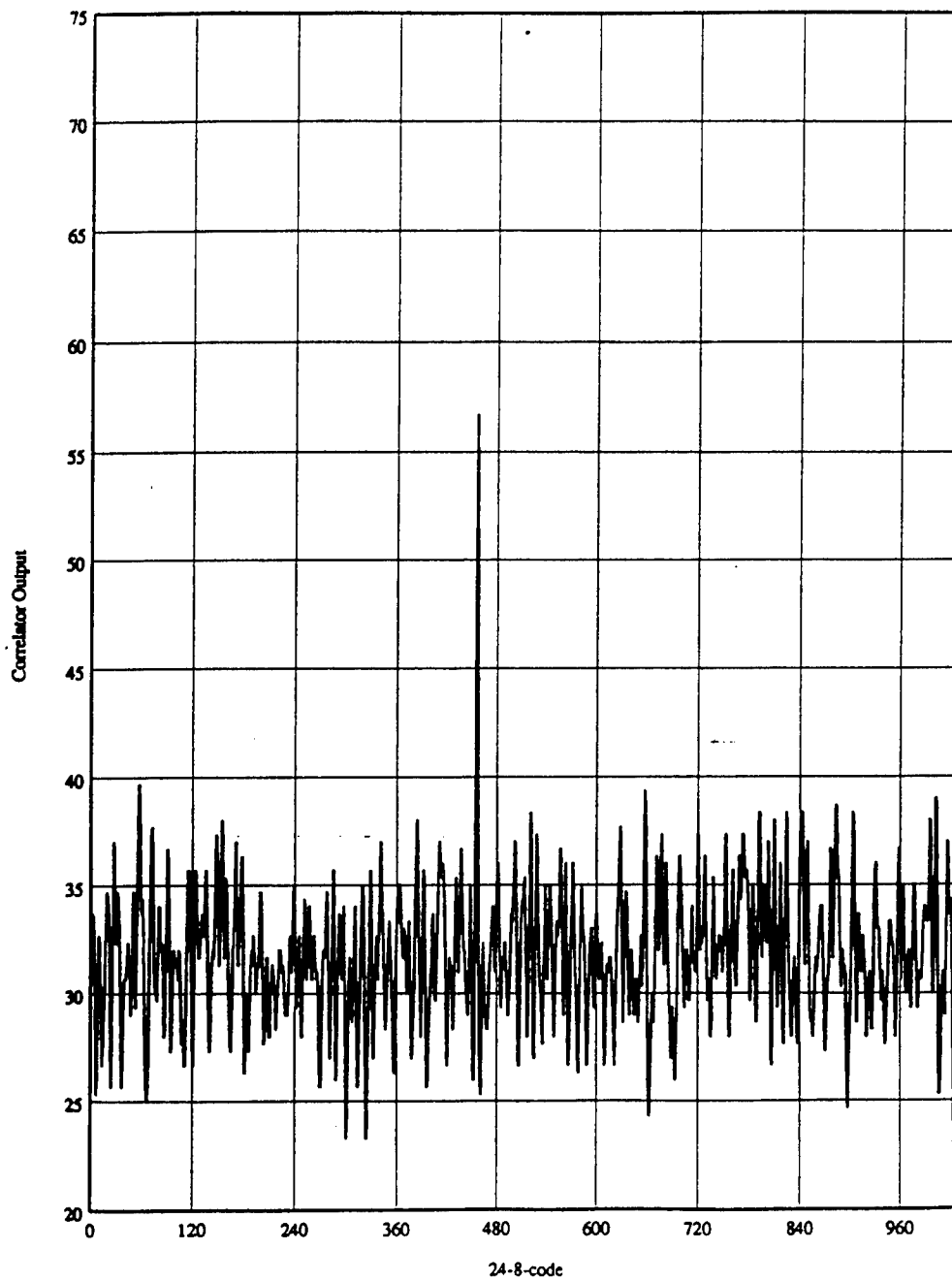


**Figure 3.2.1.3-3 Performance of the Custom 24 Bit Code**

"advance" in "Now is the time to advance to go and collect \$200."

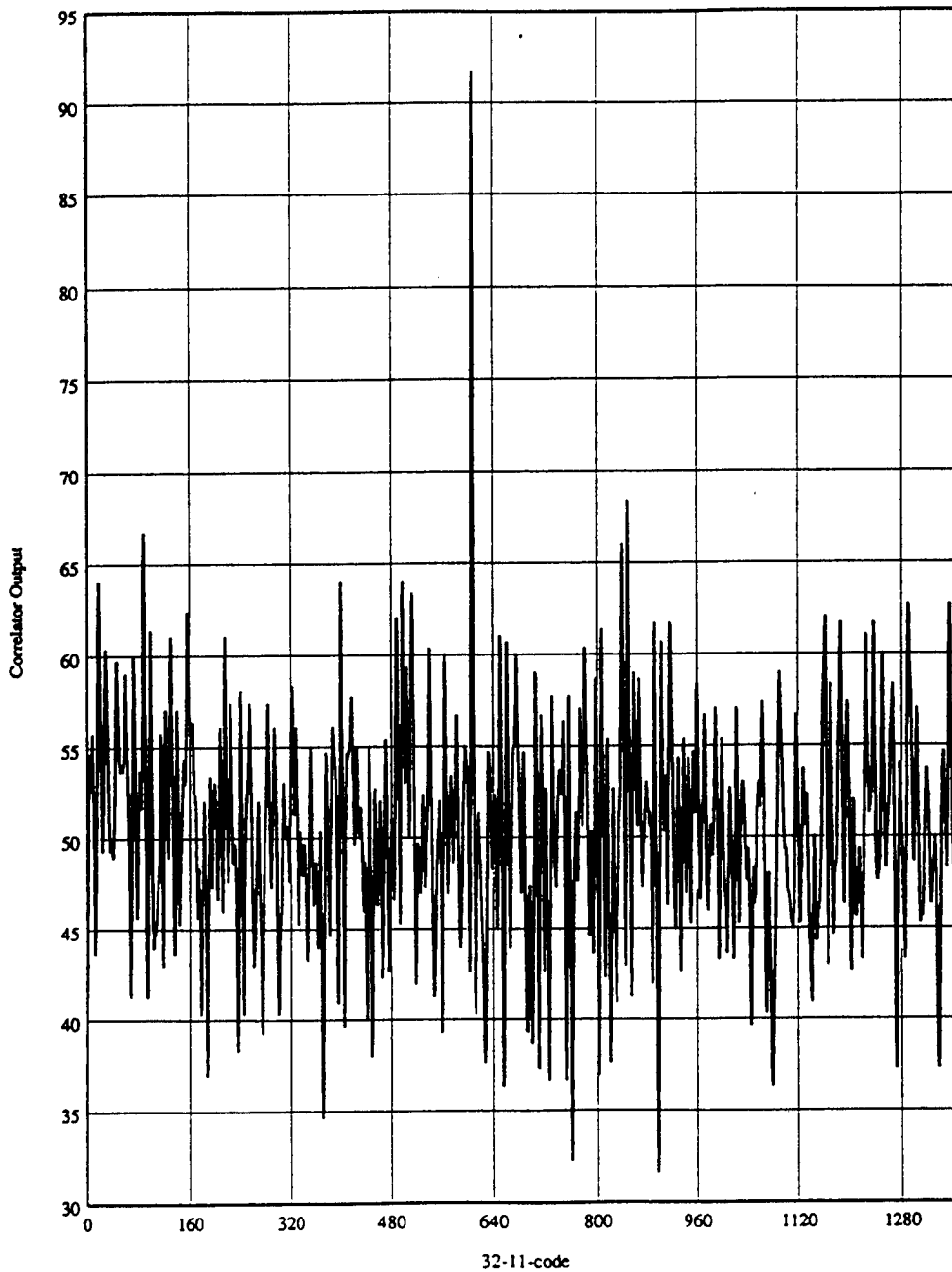


**Figure 3.2.1.3-4 Performance of the Custom 32 Bit Code**

Based on the success of the coding simulations, we used the custom code in the breadboard measurements. The measured results are discussed in Section 3.3.

### 3.2.2 Source

Candidate sources for the optical correlator include: diode lasers, light emitting diodes (LEDs) and LED arrays, superluminescent diodes (SLED), and incoherent sources. Inefficient collection characteristics make incoherent sources undesirable. The coherent noise (speckle) generated in imaging with a diode laser caused a signal to noise ratio that was less than one. The final selection was a superluminescent diode which was implemented in the breadboard and worked well in extensive system tests. This section discusses the characteristics and trades of the various sources.

#### 3.2.2.1 Coherent Sources

Semiconductor laser diodes are extensively used in the optical disk industry and were the obvious first candidate for the optical correlator. They are commercially available in small packages, provide both spatial and temporal single mode operation, and generate optical powers greater than 50 mW. Their optical emission spectrum is in the near infrared and therefore, optical disks were developed with maximum contrast at these wavelengths. Laser diode arrays become an option if more optical power is required.

A laser diode was used in the initial breadboard tests. When the disk was imaged onto the spatial light modulator plane, the coherent noise swamped the image. We found it impossible to determine where the image plane was due to the noise level. A set of experiments and simulations were performed to test speckle reduction techniques.

A FORTRAN model, SPECKLE.FOR, was developed to compare the effects of aperture truncation, illumination wavelength, illumination coherence, data configuration, and aberrations. The program constructs an object plane as a complex amplitude. The data is encoded as a series of samples in either phase only, or as a dip in amplitude plus a  $\pi$  phase shift. This is then Fast Fourier Transformed to the complex Transform plane. This transform plane can be aberrated and used for testing aperture effects. An inverse transform then produces the image plane. For multiple line or incoherent illumination the image plane is intensity averaged. The transform truncation is scaled to our implementation by a linear interpolation. This permits simulation without requiring full field, full resolution arrays. The point of truncation  $T_r$  is set by:

$$N_r = (N / N_{obj}) * (NA / (\lambda / \Lambda)), \text{ where}$$

- N = transform sample size
- $N_{obj}$  = number of samples in object to resolve
- NA = limiting lens numerical aperture
- $\lambda$  = Illumination wavelength
- $\Lambda$  = Size of object to resolve.

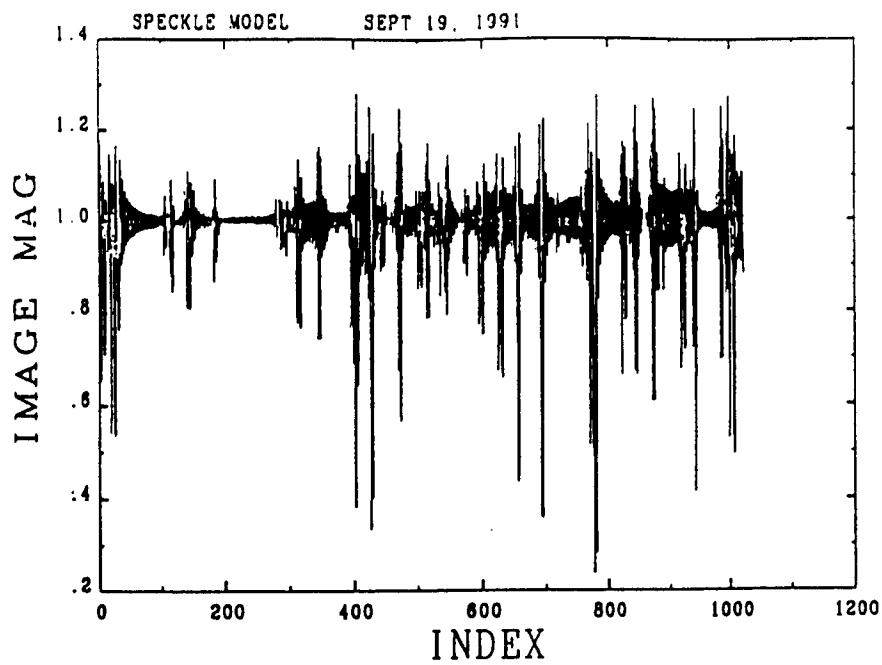
For example: a numerical aperture of 0.4, an illumination wavelength of  $0.5\mu\text{m}$ , an object size of  $1.0\mu\text{m}$ , a 1024 point transform, and a sampling rate of 10 samples in the target object produces a truncation value at 82 samples. For now, a simple brick wall low pass filter is used to block samples 82 through 942 (1024-82).

Incoherent illumination is modeled as an ensemble average of piece-wise coherent cases. Each member is uniformly phase randomized at increments of its local spatial coherence,

with the wavefront assigned a point-wise value linearly interpolated between the edges of the limits. These are processed independently and intensity averaged at the image plane.

Multi-line illumination is also treated as an ensemble average. Each member is locally coherent with a randomly assigned uniform phase across its wavefront. In the filtering algorithm the point of truncation is scaled for each member wavelength. A uniform wavelength distribution is used for the fractional bandwidth input and is centered at the value of truncation corresponding to an equivalent uniform illumination. Again, each member is treated independently until the image plane is intensity averaged.

Various image merits can be applied to rank the system performance. For phase-only data the image amplitude should maintain an input value of 1. The upper panel of Figure 3.2.2.1-1 shows a typical uniform illumination input response. Truncation of the Fourier plane occurred at the sample set midpoint. Amplitude spikes occur at the edge of data transitions. The lower panel plots the variation of the amplitude deviation for several aperture truncations. Amplitude encoded data sets an "off" bit as an amplitude of 1, and an "on" bit as an amplitude reduced to the level set by a Gaussian distribution about a given amplitude contrast ratio. Examples used here have the "off" level set at 0.7 with a 1 sigma deviation of 1/10 of its mean input level. Figure 3.2.2.1-2 illustrates the effect of amplitude deviations in the recovered image from the input data on the merit evaluation defined as RMSERR. Only errors detracting from the data decision process contribute to this value. The root mean square of "on" bits less than 1, and "off" bits greater than their object input value are accumulated and normalized to both the transform size (number of occurrences examined) and the mean input contrast. The results of different illumination conditions are summarized for phase data in Table 3.2.2.1-1.



AVE BIT SAMPLES 4.0 SIGMA=1.00

LOWPASS BAND=50.00      AVE VAL = .977      STD DEV = 12.97

## PHASE ENCODED SPECKLE

Truncation at Transform Plane

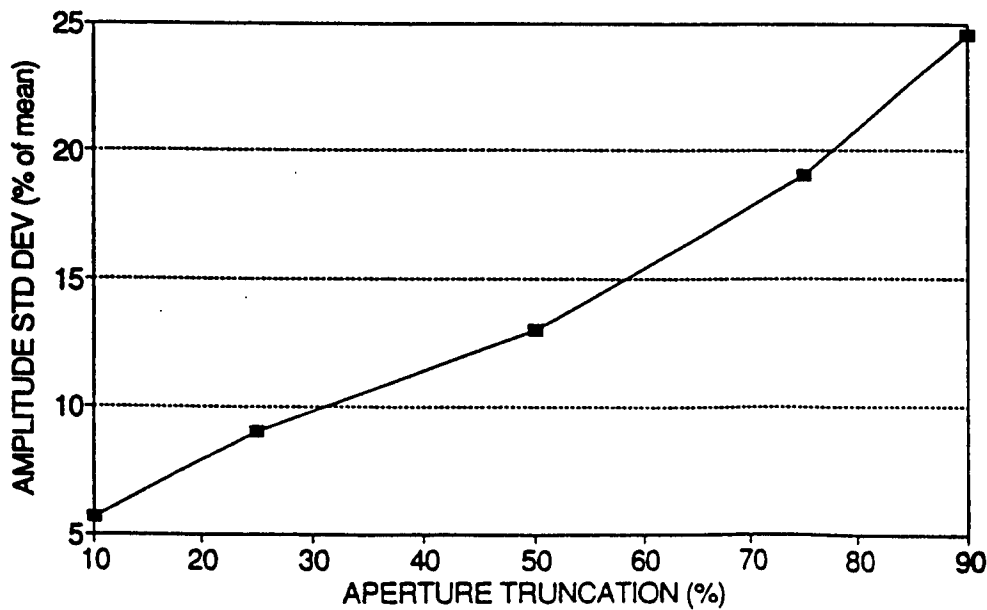
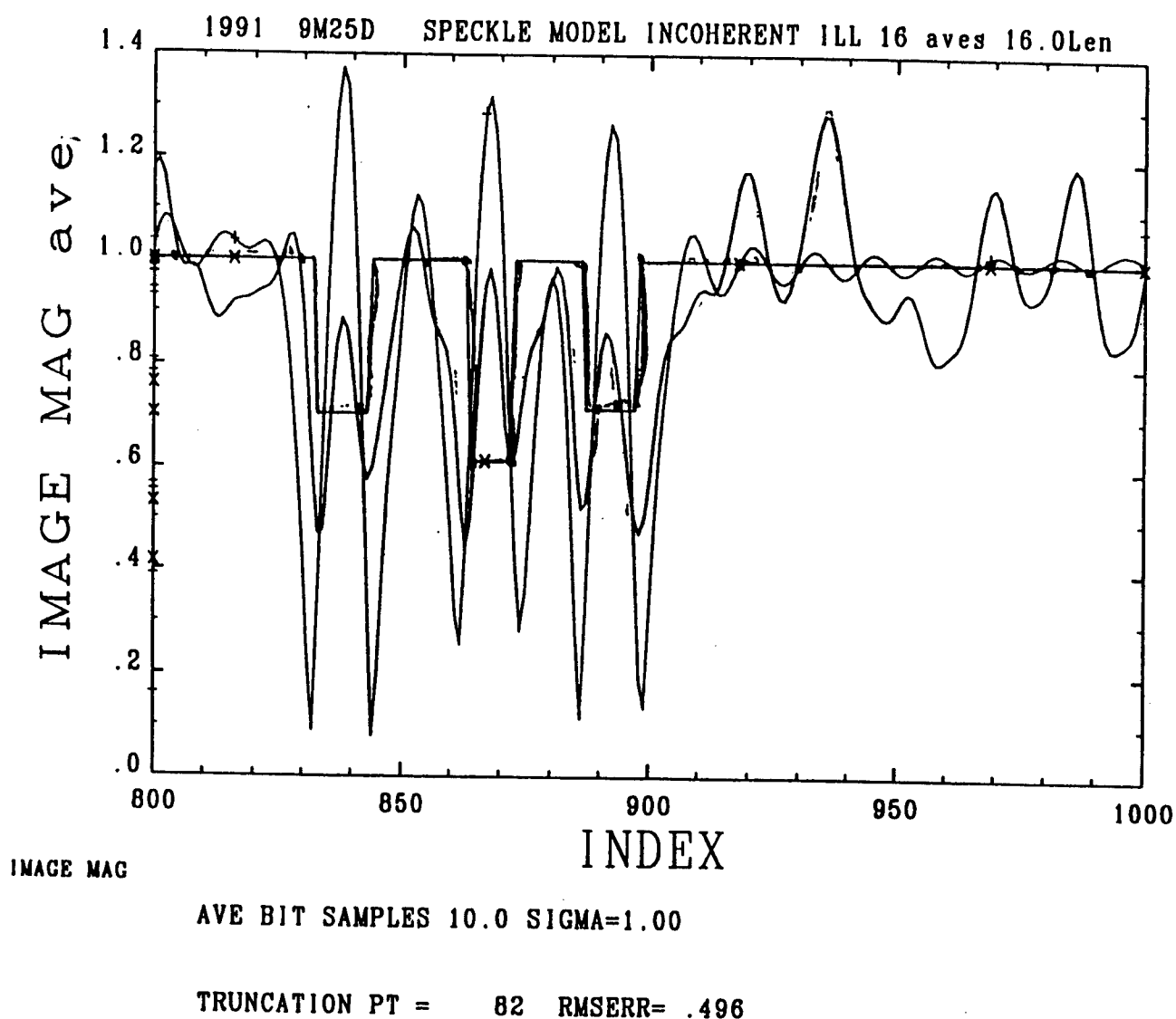


Figure 3.2.2.1-1 Phase Encoded Data





**Figure 3.2.2.1-2 Amplitude Encoded Data**

The illumination approaches for data encoded by phase transitions are compared in Figure 3.2.2.1-3. All cases have data encoded areas responding with amplitude ringing that appears to be of about the same order. The constant "off" condition is somewhat smoothed from the uniform illumination by incoherent (at 16 averages of spatial coherence increment of 16 samples). The multi-color (0.4 fractional bandwidth of 16 discrete lines) smooths the "off" areas best. Comparing the average and standard deviation of the illuminations shows no significant changes (see table 3.2.2.1-1).

Table 3.2.2.1-1 Illumination Effects on Phase Coding

Phase Only Data	NTR = 123	
	Average	St Dev
UNIFORM	0.986	9.388
Multi-Line (16/0.4)	0.986	8.98
Incoherent (16/16)	0.985	9.13

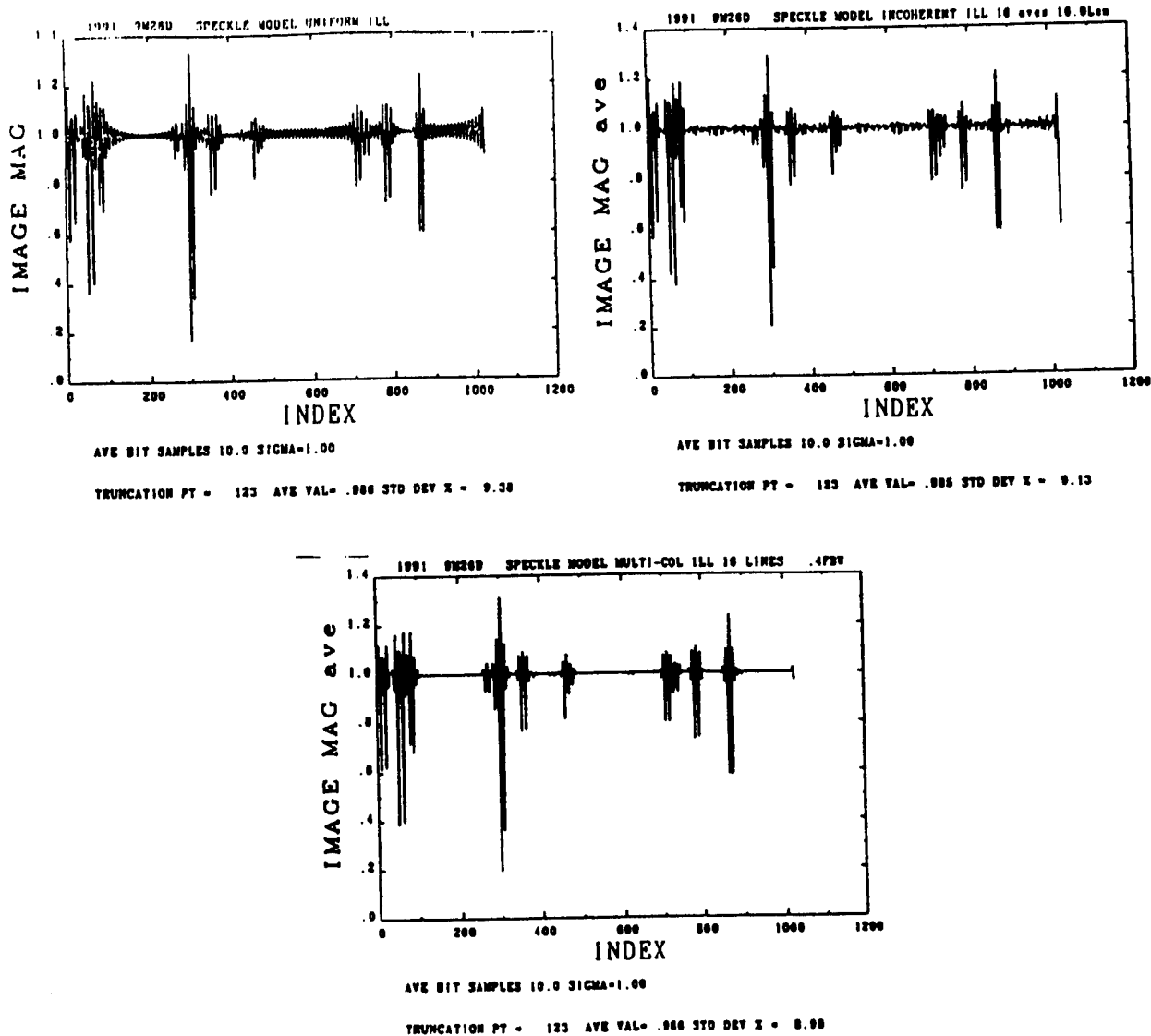


Figure 3.2.2.1-3 Illumination Effects on Phase Encoded Data

Amplitude encoded data which include a deviation about  $\pi$  in phase are shown in Figure 3.2.2.1- 4. The results are summarized in Table 3.2.2.1-2. For the milder truncation at NTR = 123, there is little advantage from using the distributed sources. A sharper truncation (NTR = 82 corresponding to  $1\mu\text{m}$  spots) shows a difference in the merit evaluation. However, a visual examination of the patterns does not reveal a strong relief in the obscuration of the data areas.

**Table 3.2.2.1-2 Illumination Effects on Amplitude Coding**

Amplitude w/ Phase Data	NTR = 123	NTR = 82
	RMSERR	RMSERR
UNIFORM	0.479	0.504
Multi-Line (16/0.4)	0.449	0.207
Multi-Line (16/0.6)	0.435	
Incoherent (16/16)	0.433	0.164

Figure 3.2.2.1-5 shows the effect of allowing a phase aberration to occur in the transform plane. Here, a 4th order deviation of about one wave of phase is introduced in the outer 20% of the image plane. Glaring errors caused by the aberration result in strong peaks for uniform and multi-color illumination. The incoherent illumination is able to at least keep the bit "on" condition from ringing above the data "off" condition. Results are summarized in Table 3.2.2.1-3.

**Table 3.2.2.1-3 Phase Aberration Effects**

Transform Aberration Data as Amp	NTR = 82 RMS ERR
UNIFORM	0.899
Multi-Line (16/0.4)	0.880
Multi-Line (16/0.6)	0.496
Incoherent (16/16)	0.465 32 averages with 16 coherence length

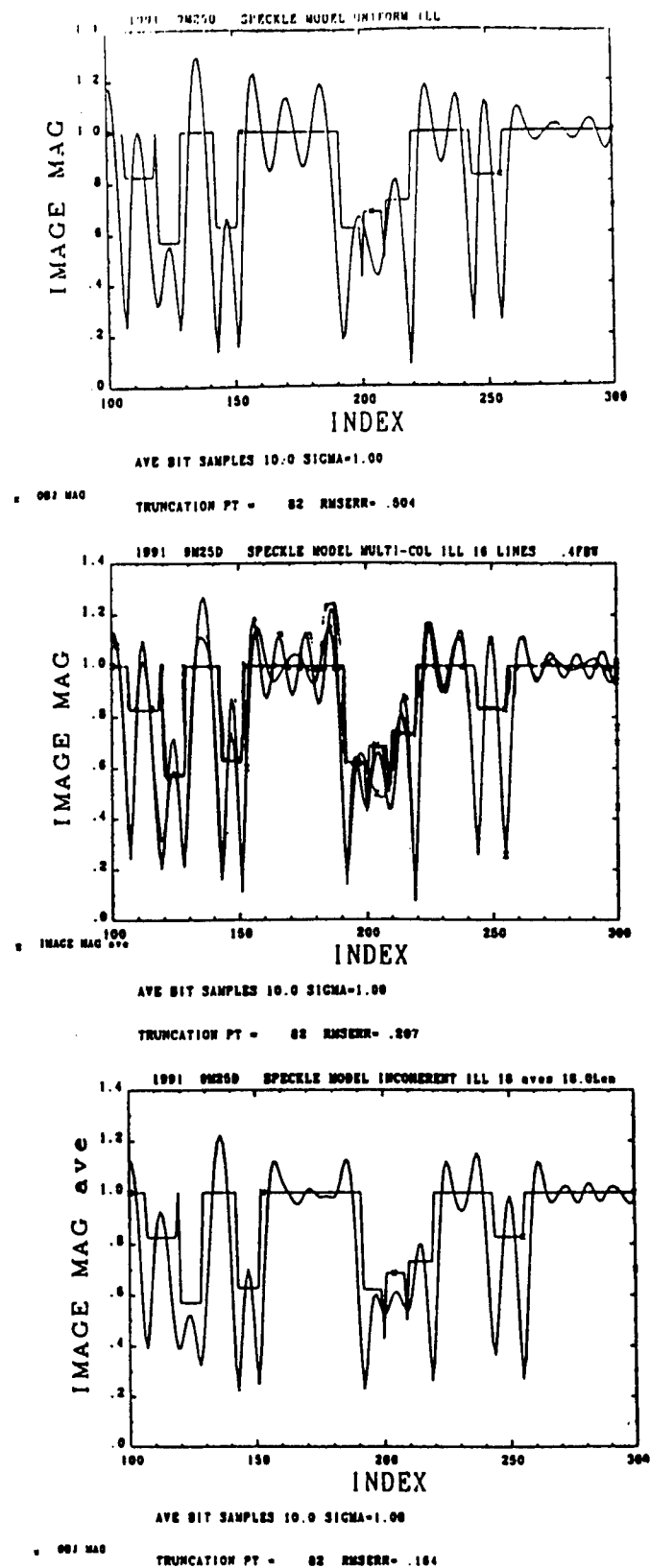


Figure 3.2.2.1-4 Illumination Effects on Amplitude Encoded Data

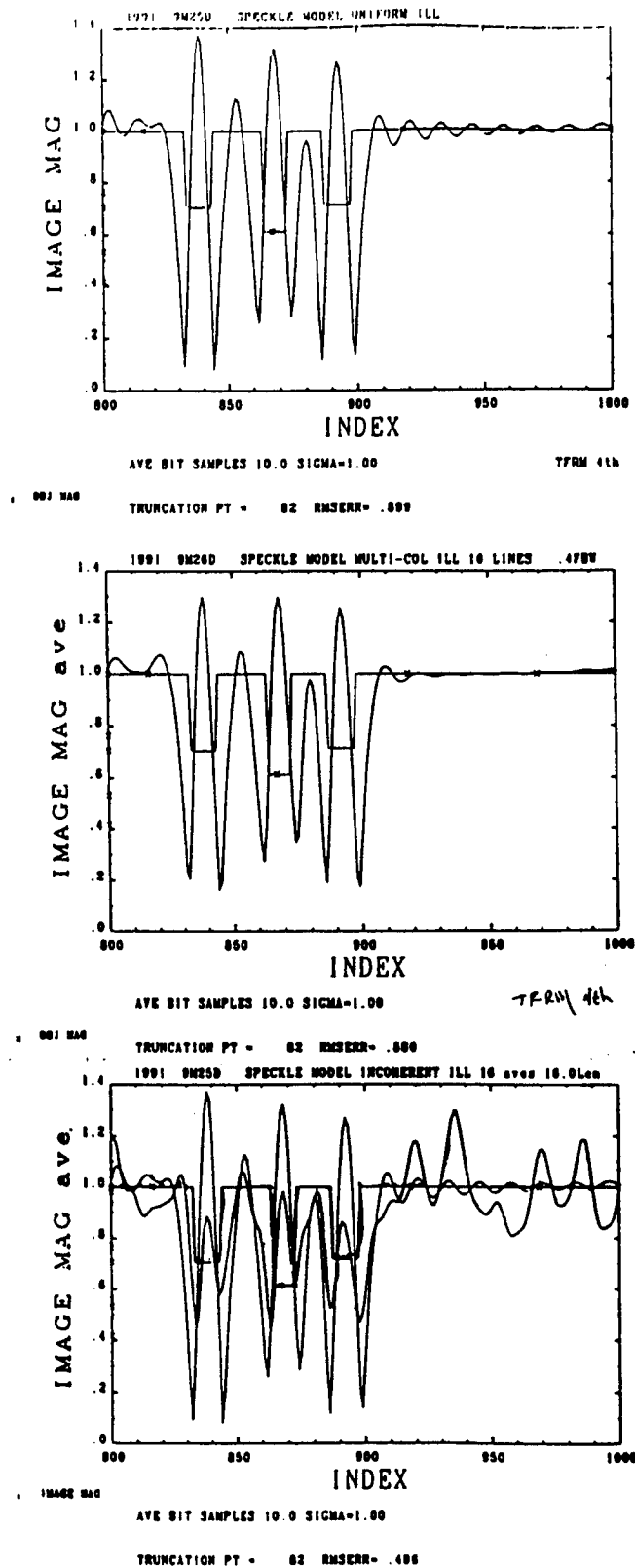


Figure 3.2.2.1-5 Transform Plane Aberrations

This analysis shows that in an unaberrated system with amplitude encoded data, a severe truncation is required before multi-source illumination improves response from a uniform source.

We reviewed the literature for information on speckle effects. A 1973 paper in Applied Optics "Measuring Speckle Effect" by Raoul van Ligten presents a probability distribution function that evaluates the effect of speckle in an image. Using this technique to determine the effect of our numerical aperture and feature size indicates that our coherent noise is not classical speckle. This implies that either our defining aperture is not at the 0.4 NA lens, or another mechanism is responsible for our coherent interference.

Raoul van Ligten presents a probability density function for speckle irradiation of the form:

$$P() = (1/S^2) * e^{-w}$$

where:  $S$  = speckle intensity

$$w = S/\langle S \rangle$$

$\langle S \rangle$  = average of  $S$ .

Varying degrees of speckle influence are shown in Figure 3.2.2.1-6. A uniform distribution plots as a line at  $w = 1$ . Extreme speckle resembles  $1/S^2$ .

Intermediate cases transition by multiplying the extreme by an exponential. He references an article by Enloe, Bell System Technical Journal, Sept. 1967, which describes the primary source of speckle as "the random phase angles associated with the scattering centers comprising the microstructure of the diffuse surface".

That is, the surface cannot be treated as varying smoothly for coherent analysis. Using these suggestions, the SPECKLE.FOR model was revamped to allow the object to influence the wavefront with a random phase at spacing set by the variable SPACOH. Figure 3.2.2.1-7 shows two extreme cases. The upper panel is 4/15 data only, encoded at a mean contrast of 70%. The 'no data' condition occurs about 0.8 of the time, with the data 'on' condition spread about the index of 70 (corresponding to 70% of data off condition).

The lower panel mimics the transitional effect shown above when the source is phase randomized at a period of 2. This corresponds to an extremely fine spatial frequency. The problem is scaled; a 10 sample period here scales to a  $1.5\mu\text{m}$  feature. The randomized source does not depart from the peak at 100 for randomization of period above 10. The results are summarized in Table 3.2.2.1-4. The results suggest that the system is apertured somewhere, or another wavefront mechanism is contributing heavily to the coherent interference. Alternatives to coherent sources were therefore considered.

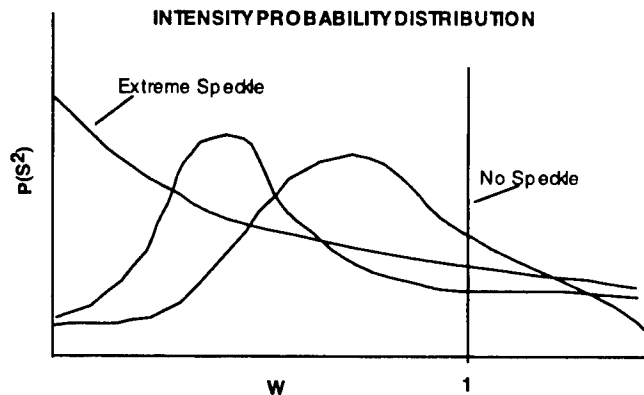
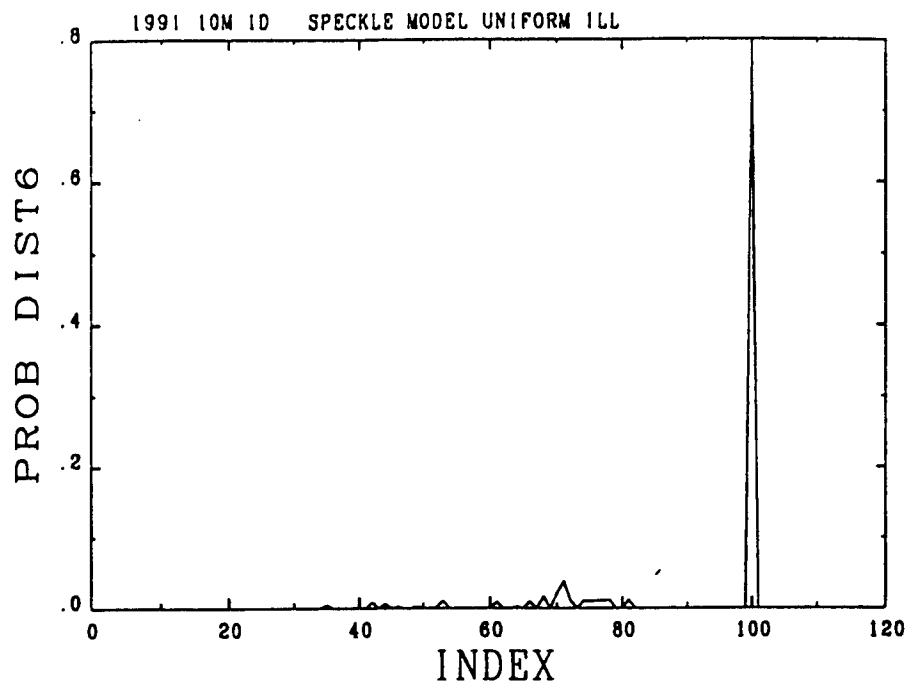
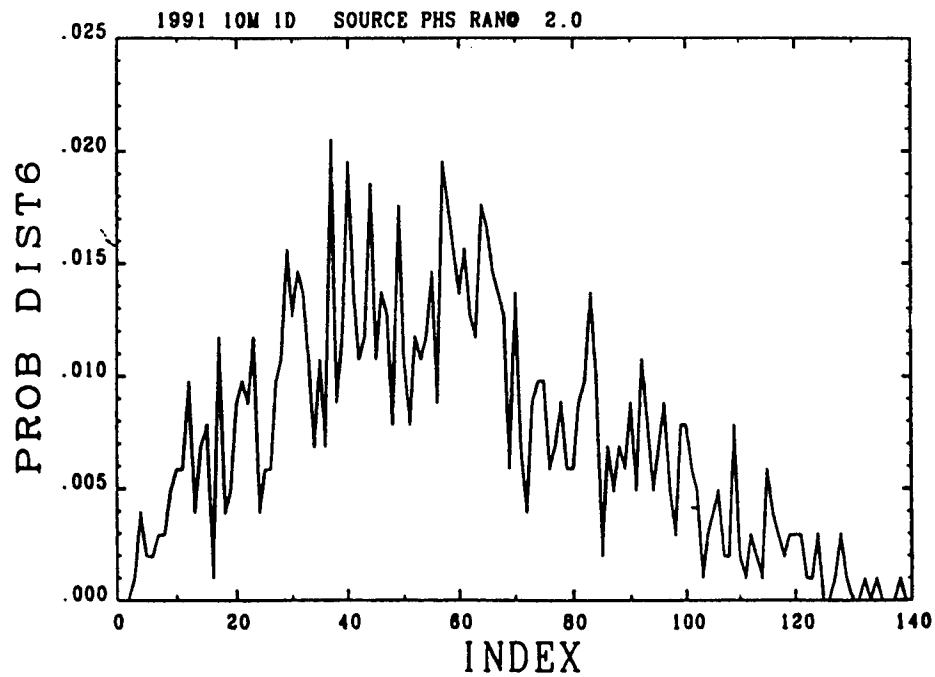


**Figure 3.2.2.1-6 The effect of varying degrees of speckle Noise**



AVE BIT SAMPLES 10.0 SIGMA=1.00

RMSERR= .000



AVE BIT SAMPLES 10.0 SIGMA=1.00

TRUNCATION PT = 123 RMSERR=1.412

**Figure 3.2.2.1-7 Classic Speckle Effects on Correlation Output**

**Table 3.2.2.1-4 Summary of Speckle Reduction Techniques**

Run Conditions	PDF Peak	PDF Half Max - Full Width
Pure Data (No truncation)	100	1
TR = 123 (1.5um features)	100	12
TR = 82 (1.0um features)	100	16
Source Ran = 16, TR=123	101	32
Source Ran = 10, TR=123	102	42
Source Ran = 5, TR=123	95	57
Source Ran = 2, TR=123	48	70

### 3.2.2.2 Discrete High-Power LEDs

These devices fall into at least three basic fabrication categories:

1. Domed semiconductor material with small emitting area at base of dome. Shaping the dome allows the total internal reflection problem at the surface of the high index semiconductor to be minimized. Relatively small junctions imply high current densities with possible performance degradation and reliability problems;
2. Surface emitting structure with basically a Lambertian distribution of light. These devices are typically operated at high currents, but due to relatively large junction areas, the current density is not excessive;
3. Edge-emitting superluminescent diodes having a Laser-like structure but no resonant cavity. This structure generates a relatively narrow optical beam with a fairly broad spectral bandwidth. The emitting junction is usually 1 to 2 microns thick, but the width and depth dimensions can be varied over several tens of microns to increase power output and modify device characteristics. This configuration will probably generate the brightest (watts/steradian) output but this conjecture is not yet verified.

Table 3.2.2.2-1 summarizes the characteristics of LEDs for various sources.

**Table 3.2.2.2-1 LED Options**

Vendor	COTS/ Custom	Wavelength (nm)	Bandwidth (nm)	Power (mW)
Hitachi	COTS	735-905		20 - 40
Opto-Diode Corporation	COTS	880	80	100
EG&G Optoelectronics	COTS & Custom	850	40	10 mW COTS
Sarnoff Research Center	COTS & Custom	830	8 to 15	15 -30
TRW	COTS & Custom	800	240	50 mW COTS; 250 mW custom



The breadboard was modified by replacing the coherent source with an incoherent LED. The resulting input efficiency from the source to the disk was on the order of 0.75%. This limit is imposed by the optical invariant combined with geometric considerations.

The LED output is collected by a 25 mm condenser, reflected off a hot mirror (to separate out the focus illumination system), through a beamsplitter and objective lens to illuminate the disk with a large area spot. Assuming the LED distribution is essentially uniform over the half sphere, its output is spread across the surface area of a hemisphere

$$A_H = 2\pi R^2.$$

A lens of diameter D on the surface of the hemisphere collects the light going through an area  $A_L = \pi D^2/4$ . For an F/1 lens,  $D=R$ , therefore the collection aperture of the lens is

$$A_L = \pi R^2/4.$$

The portion of the LED emission that is collected then is  $A_L / A_H$  where

$$A_L / A_H = \pi R^2 / (4 * 2\pi R^2) = 1/8$$

Therefore, at best only 1/8 of the LED output power can be collected by an F/1 lens; in addition, the LED canister is blocking approximately 35% of the hemisphere. The other major loss is the 50% transmission of the beamsplitter. As a result, for a 12 mW LED, the expected best case light at the disk is then about 490  $\mu$ W; the maximum measured light at the disk is 450  $\mu$ W. The difference comes from losses in the uncoated optics and at the hot mirror. The ratio of the active data area on the disk to the size of the illumination limits the amount of useful light to about 1/5 of the available 450  $\mu$ W, or about 90 $\mu$ W of useful light. Based on these measurements, we determined that an LED would not provide the light levels required by the system. A superluminescent diode with a divergence similar to a laser would have better collection efficiency without generating coherent noise.

Superluminescent diodes were procured from TRW and Sarnoff Research Center and tested in the system. Note: the TRW 50 mW device was eventually selected for the breadboard testing. The specifications for the SLED are summarized in Table 3.2.2.2-2. The SLED is essentially an edge emitting device with a laser like structure but no resonant cavity. It therefore emits a narrow optical beam that can be easily collected by the optics (50% collection efficiency compared to <5% for the LED). Because there is no resonant cavity, the spectral bandwidth is relatively broad making it temporally incoherent which reduces speckle effects. However because of the small emitting junction (1 to 2  $\mu$ m thick) it is spatially coherent resulting in improved MTF. The device we acquired from TRW has 50 mW output power. By increasing the width and depth of the device the vendors estimate that 250 to 500 mW are possible. Figure 3.2.2.2-1 shows the output power curve for the TRW SLED used in the breadboard.

**Table 3.2.2.2-2 SLED Specifications**

Parameter	Specification
Center Wavelength	800 nm $\pm$ 30
Spectral Bandwidth	30 nm FWHM
Temporal Coherence	TBD
Spatial Coherence	TBD
Divergence	10° by 30°
Polarization	500:1
Aperture Size	10 x 100 $\mu$ m
Output Power	<sup>3</sup> 50 mW
Drive Power for Max Output	<sup>2</sup> 500 mA

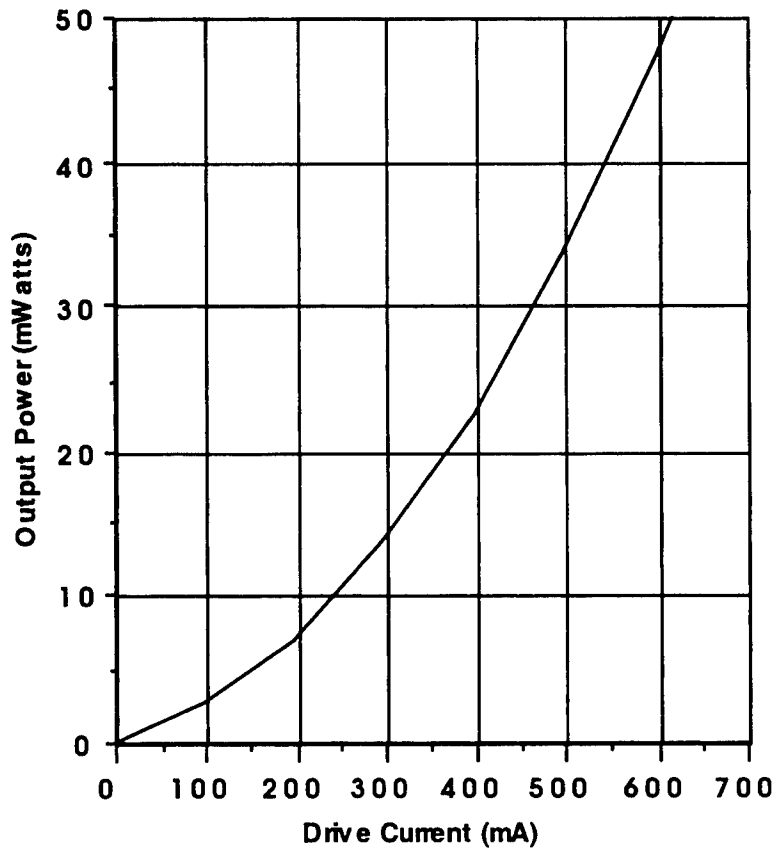


**Figure 3.2.2.2-1 TRW SLED Power Curve**

### 3.2.2.3 LED Arrays

As an alternative to a single high power LED, we considered an array of LEDs where each element of the array corresponds to one channel bit on the disk. The LED array therefore provides the light source and correlation reference pattern for the system. This has the potential to simplify the optical system, reduce components and make the correlator easier to package in a compact configuration.

In the system concept, ten to twenty optical correlators are in fixed locations around an optical disk and each correlator looks at 1000 to 2000 tracks on the disk. Each correlator will require an LED array. Optically, the light from the array is demagnified and imaged to a radial line on the disk surface. In the along-array direction, the imaged line spacing is on the order of  $2\text{ }\mu\text{m}$  to match the recorded data bits. In the cross-array direction, each LED element is spread to illuminate 1000 to 2000 tracks. This is shown in Figure 3.2.2.3-1. Note: because each element of the array is spread in the cross-array direction, a staggered array format is acceptable. Minimal crosstalk in the along-array image is more critical. Table 3.2.2.3-1 summarizes the requirements for an LED array

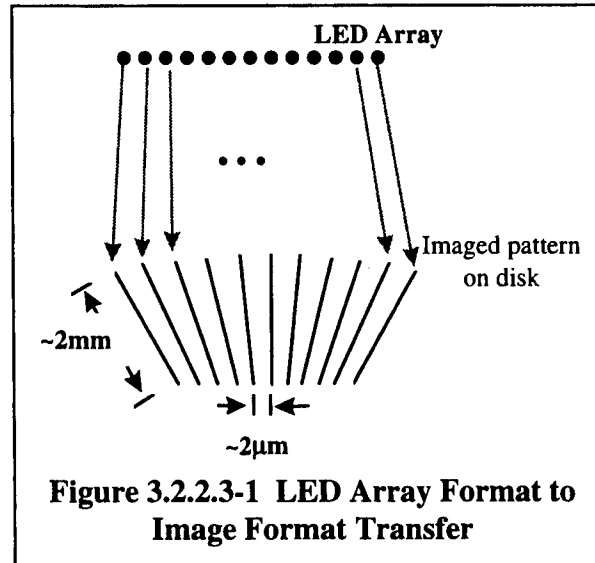


**Table 3.2.2.3-1 LED Array Requirements**

PARAMETER	REQUIREMENT
Number of Elements	The array shall have 256 individually modulatable elements.
Pitch	Center to center spacing in the along-array direction shall be $16\text{ }\mu\text{m}$ nominally. This can be accomplished by staggering rows as required.
Duty Cycle	The elements size to center spacing ratio shall be 50% (TBR).
Wavelength	The wavelength shall be centered between 800 and 850 nm.
Optical Power	Each element shall put out greater than 0.5 milliwatts of optical power.
Electrical Bandwidth	The modulation pattern shall be updatable in $50\text{ }\mu\text{sec}$ (TBR) (20 KHz bandwidth); updates will take place every 30 msec.
Modulation Requirements	Each element of the array shall be individually modulatable. The baseline requirement is for binary modulation; a possible extension will require 4 levels.
Interface	The array electronics shall be capable of being interfaced to an IBM compatible PC computer for modulation using either an RS232 or 488 interface or using a plug-in bus card.

Initial feedback from the vendors indicated that we would be pressing the state-of-the-art in several areas with our geometry, especially regarding spacing, aspect ratio, and spatial duty cycle. The output from surface emitting LEDs will almost certainly be near-Lambertian. Switching times of about 1 microsecond should be attainable. Wall-plug efficiency (optical power out compared to electrical power in) will probably be on the order of 0.1 to 1 % with 0.6% as a good working number. The optical power is measured over the entire  $2\pi$  steradian hemisphere. Maximum drive current per unit area of emitter is on the order of 100 Amps/cm<sup>2</sup>; however, it may not be possible to continuously operate the array at such a high current density. Reasonable power dissipation values may limit currents to approximately 10 Amps/cm<sup>2</sup>. Forward voltage of the emitting junction is typically assumed to be about 2 volts. The array may be difficult to fabricate at infrared wavelengths because of transparency and translucency of the materials used and the associated optical cross-talk between emitters, although the optical crosstalk problem should be significantly reduced in the 650-750 nm wavelength regime. The yield per wafer of the array may be very limited, even if the manufacturing process uses 2 inch wafers. The spatial duty cycle of the light emitting area compared to the pitch of the emitters is limited by diffusion guard bands to prevent shorting of elements and by minimum design rules for metallization which may (depending upon process) obscure a portion of the emitting area. A 50% spatial duty cycle at 10  $\mu$ m element pitch is a first cut estimate for most processes.

To evaluate how well the input optics can collect the available light from an LED, a standard device was implemented in the breadboard. The input optics consists of an F1 lens, hot mirror, beam splitter, and objective lens. The input efficiency of the demonstration system is on the order of 6.25%; this is driven by the F1 lens and the beam splitter.

The collection efficiency of the F1 lens is limited by the following geometrical factors.

Assuming the LED distribution is essentially uniform over the half sphere, its output is spread across the surface area of a hemisphere,  $A_H$ .

$$A_H = 2\pi R^2$$

A lens of diameter D on the surface of that hemisphere collects the light going through an area,  $A_L$ , of  $\pi D^2/4$ . For an F1 lens,  $D=R$ . Therefore the collection aperture of the lens is:

$$A_L = \pi R^2/4.$$

The portion of the LED emission that is collected then is  $A_L/A_H$ .

$$\frac{A_L}{A_H} = \frac{\pi R^2}{4 * 2\pi R^2} = \frac{1}{8}$$

Therefore, only 1/8 of the LED output power can be collected by an F1 lens. The main additional loss is 50% at the beam splitter.

The LED can blocks about half of the hemisphere. Therefore, for a measured 6 mW LED output, the full LED output is 12 mW. The expected best case light power at the disk is then 12/16 or 750  $\mu$ W. The maximum measured light at the disk is 450  $\mu$ W.

### 3.2.2.4 Summary of the Source Trade

Table 3.2.2.4-1 summarizes the trades between the source options. For the final system a multi-mode edge emitting laser diode, known as a superluminescent diode, was selected. This unit has 50 mW output power, centered at 810nm, with a 3 dB bandwidth of 30 nm. The output facet size is 1 $\mu$ m by 100  $\mu$ m resulting in a beam divergence and optical collection efficiency equal to that of a laser. However, because of the wide bandwidth, no speckle noise is apparent.

**Table 3.2.2.4-1 Source Trade**

PARAMETER	SINGLE MODE LASER DIODE	MULTI-MODE EDGE EMITTING LASER DIODE	SINGLE LED	ARRAY OF LED'S
AVAILABLE POWER	5 - 100 mW	300 - 3000 mW	1-50 mW	128-256 mW
WAVELENGTH	670 to 830 nm	830 nm	750-850 nm	750-850 nm
ILLUMINATION EFFICIENCY	10%	10%	1%	1%
DISADVANTAGES	SPECKLE	POWERS HIGHER THAN 50 MW HAVE NOT BEEN DEMONSTRATED	AVAILABLE POWER	CUSTOM DESIGN
ADVANTAGES	SUFFICIENT POWER	SIMPLER DESIGN HIGHER POWER	NO SPECKLE	NO SPECKLE NO SLM NEEDED

### 3.2.3 SLM

A Spatial Light Modulator (SLM) imposes a spatial modulation on light and is controlled either electrically or by an independent optical beam. In the optical correlator, when the operator enters a search request into the system, the proper key word for the data base is determined and the optical matched filter is calculated and loaded into a spatial light modulator to interface with the optical system. The SLM must provide high resolution to match the data on the disk. For an image plane correlator, a binary SLM is sufficient; the only information of interest is whether a bit is on or off. For the incoherent correlator architecture, amplitude modulation is needed. The amplitude modulation may be generated either directly by the SLM or indirectly by polarizer analyzer systems. The ability of the system to rank order the degree of

correlation depends on the signal-to-noise ratio of the system. The SLM is one of the noise contributors and, therefore must have good contrast ratio and low noise.

The time to write a new mask to the SLM directly affects system latency. While one correlation is running, the controller has a full 30 msec rotation to generate a new key word and load it into the input buffer. The keyword is then transferred into the SLM during the period of time that the disk is rotating through a sector boundary (about 100  $\mu$ sec). If this transfer rate is not maintained the system must wait for subsequent sector boundaries before it can begin the next correlation operation.

The geometry of the SLM is driven by the correlation and how the data is written on the disk. If the data bits in the SLM do not properly line up with the image from the disk, the correlation will degrade. On a standard 5 1/4" disk, data is recorded from 30 mm to 60 mm in a constant angular velocity format. Therefore, the center-to-center spacing of the channel bits in the outside track is twice that of the inside track. Assuming 20,000 tracks, and 1 bit diameter (standard inside track bit) channel bit spacing on the inside track, the outside track spacing is at 2 bit diameters. The stretch track to track is 1/20,000 of a bit. Over all 2000 tracks, the distortion from innermost to outermost track is 1/100 of a bit. Assuming the center bit on the center track is perfectly aligned, the  $\pm 128$ th bit on the  $\pm 1000$ th track will be  $128 \times 1/100 = 1.28$  bits out of the ideal position. This will destroy the correlation and needs to be corrected. The correction can come from the SLM geometry, the geometry of the data on the disk or by optically distorting the image of the disk on the SLM. For the breadboard, we chose to modify the data format on the disk so that standard format SLMs could be used.

Table 3.2.3-1 summarizes the SLM requirements. The following comments summarize the reasoning behind some of the specifications.

**Table 3.2.3-1 Spatial Light Modulator Requirements**

Parameter	Requirement
Load Time	0.12 msec goal, 1 msec maximum
Frame Rate	30 Hz
Geometry	Linear Array, 4000:1 aspect ratio desired
Element Pitch	10 $\mu$ m elements goal, 25 $\mu$ m maximum
Element Height	4 cm goal, 400 $\mu$ m minimum
Spatial Duty Cycle	$\geq 75\%$
Readout Wavelength	800 nm $\pm 25$ nm
Source Polarization	$> 500:1$ Linear
Throughput Efficiency	$\geq 80\%$
Mode	Amplitude; either transmissive or reflective
Uniformity	$\pm 0.5$ dB along the element length and between elements
Number of Elements	256 minimum, 408 maximum
Contrast Ratio	$\geq 100:1$ ; Binary
Addressability	Electronic
Flatness	$< 1/10$ wave (goal)

## Comments on the specifications

- **Load Time and Frame Rate:** The baseline plan is to load a keyword within the normal error correction period of one sector (0.24 msec) and then hold the pattern for a full revolution (30 msec). If this cannot be met or if the error correction period is used to expand the modulation code, we will use a full sector time period of 1 msec to load the new keyword and slip the rotation start by one sector on each rotation.
- **Geometry:** The geometry of the SLM must match the manner in which the data is recorded on the disk. The data will be recorded on the disk in a modified CAV format. The sector boundaries will be in a CAV format (or zoned CAV). Each correlator head will look at 1250 tracks. This defines a sector block that is part of a pie wedge. Within each sector block, the data will be recorded in a rectilinear pattern (CLV format) as shown below so that the bit spacing is always constant. The correlators are looking for the same pattern on each track, therefore all 1250 tracks must optically pass through the linear SLM. This will be easiest if the SLM elements are very tall. Ideally, they should be in the ratio of the bit spacing ( $0.5\text{ }\mu\text{m}$ ) to 1250 times the track spacing ( $1250 \times 1.6 = 2000\text{ }\mu\text{m}$ ) or 4000:1. If a lower ratio is used, the tracks can be optically compressed to match which complicates the optical system slightly.
- **Element Pitch:** The  $10\text{ }\mu\text{m}$  element spacing is to minimize the magnification ratio between the disk and the SLM to keep the optical path length as short as possible. If a two dimensional SLM is used, we would simply slave the columns together to generate the effect of tall thin elements.
- **Spatial Duty Cycle:** A 75% spatial duty cycle is desired for good optical efficiency.
- **Readout Wavelength:** The readout source will be a superluminescent diode (SLED) operating at a center frequency of about 800 nm. There are some potential advantages to bringing this down a bit in the final system, so we have defined a fairly broad range. The SLED inherently has about a 30 nm FWHM spectral width.
- **Source Polarization:** This is controlled by the characteristics of the SLED.
- **Throughput Efficiency:** As high as possible to improve the light budget.
- **Mode:** The image off the disk is an amplitude pattern, therefore the SLM will be used in an amplitude mode. If a phase device is found, a means of converting phase to amplitude will be needed (polarizers, etc.).

- **Number of Elements:** The number of elements in the linear array is defined to match the longest keyword. For a 15 bit modulation code, 256 elements are needed; for a 24 custom modulation code, 408 elements are required. It is unlikely that a code longer than 24 bits will be used.
- **Contrast Ratio:** We will use the SLM as a binary device.
- **Addressability:** To keep the system simple, we require the keywords to be electronically loaded.
- **Flatness:** This is required to be able to collect all the elements into a single PDA element. Therefore the critical dimension is across the 256 elements. The height direction of each element is less critical.

Many types of SLMs have been developed for information processing applications; some are written optically, others electronically. Only electronically written devices are considered for this application. These devices fall into two broad categories, the transmissive and reflective types. The transmissive types have been assumed as the primary baseline for the optical correlator because of the simple optical layouts achievable with them. However, very few vendors of transmissive SLMs can address the special requirements of OAM, especially the huge pixel aspect ratio and the 10 to 20  $\mu\text{m}$  pixel spacing. Therefore, reflective SLMs were also included in the trades. Key candidates include deformable membrane modulators, liquid crystal modulators, electro-optic, and magneto-optic modulators. In the breadboard, a liquid crystal SLM from Meadowlark Optics was used.

### 3.2.3.1 Liquid Crystal Spatial Light Modulators

There are various types of liquid crystal SLMs depending on the type of liquid crystal used. The liquid crystal light valve is a well developed type of SLM. A liquid crystal is a medium in which there are long molecules that are free to rotate into any orientation. Normally they are randomly oriented, but when an electric field is applied the molecules line up along the field. The polarization of light passing through the liquid crystal depends on the orientation of the molecules. Therefore, a direct polarization modulation that matches the type of modulation on a magneto-optic disk is generated. If desired, the polarization effect can be converted into amplitude modulation by passing it through a polarization analyzer.

In a liquid crystal light valve, the data can be written either by specially shaped electrodes or by a beam of light. In the CCD addressed version, the data is written to an array of CCD shift registers and then shifted into the array in parallel. For our application this allows a full disk rotation for the shift registers to be loaded. Only the final parallel transfer needs to be done at very high speeds.

The general characteristics of a liquid crystal light valve include medium speed, high transmission, low contrast, and low resolution. In addition, liquid crystals may impart phase distortion and cross modulation to the output beam.



In a ferro-electric liquid crystal, the ferro-electric fluid acts as a half wave retarder. When voltage is applied in one direction and the fast axis of the retarder is aligned with the input polarization, no effect occurs; when the polarity is flipped, the fast axis is rotated  $45^\circ$  and the polarization of the incident light is rotated by  $90^\circ$ . An output polarizer converts this to amplitude variations.

The general characteristics of ferro-electric SLMs include high speed, high transmission, medium contrast, and low resolution. Ferro-electric liquid crystals also impart phase distortion and cross modulation to the output beam.

### **3.2.3.2 Magneto-Optic SLM**

In magneto-optic SLMs each element is a single magnetic domain segment of a magneto-optic material, e.g. Yttrium Iron Garnet (YIG). Each segment can be in one of two opposite magnetic orientations depending on the electric field across the segment. The two orientations produce different  $45^\circ$  polarization rotations by the Faraday effect. Therefore, light passing through elements with opposite magnetization will come out with a  $90^\circ$  polarization difference. Operation between crossed polarizers converts this into a binary intensity modulation.

The general characteristics of magneto-optic SLM's include: very uniform polarization, zero image latency, zero cross-modulation, requires no refresh or holding power, very high contrast, high speed, binary output, medium resolution. An advantage is that magneto-optic crystals impose no phase distortion or cross modulation to the output beam.

### **3.2.3.3 Electro-optic SLMs**

Electro-Optic crystals are used to control the light in some SLMs. When a voltage is impressed across the crystal, the birefringent nature of the EO material rotates the polarization of incident light. This polarization rotation can be used directly or converted to an amplitude variation by use of an output polarizer.

The general characteristics of electro-optic SLMs include high to very high speed, medium contrast and the capability to generate continuous gray scale. Depending on configuration, EO crystals may impart cross modulation of the output beam.

### **3.2.3.4 Deformable Mirrors**

In deformable mirror SLMs a flexible reflective membrane is suspended above an electrode pattern. The voltage on the electrode deforms the membrane mirror deflecting the light at a different angle. Texas Instruments is developing a deformable mirror SLM technology for use in the high definition television industry. The technology is now commercially available. A two dimensional array of 17 micron-centered pixels has been implemented in a  $760 \times 576$  pixel format, complete with CMOS drivers. The pixel "on" state is a mechanical movement of the mirror surface of about 10 degrees (20 degrees optical). Frame rates are an impressive 10,000 frames per second. A  $1920 \times 1080$  element array has also been fabricated but CMOS drivers have not yet been implemented on this device. The biggest stumbling block to larger devices is simply the lithographic field of view limits.

The general characteristics of deformable mirror SLMs include high to very high speed, high contrast, small pixel size and high spatial duty cycle.

### 3.2.3.5 SLM Trade Summary

Table 3.2.3.5-1 summarizes the characteristics of some commercially available SLMs; Table 3.2.3.5-2 summarizes additional SLMs which were not commercially available at the time of this survey. For the breadboard, liquid crystal SLMs from Boulder Non-linear and Meadowlark Optics were procured. The liquid crystal device from Meadowlark Optics was implemented in the breadboard.

**Table 3.2.3.5-2 Additional SLMs, Not Necessarily Commercially Available**

Parameter	TI DMD	Xerox	Boulder Non-linear	Panasonic etc
Type	Deformable Mirror	TIR	Ferro-electric Liquid Crystal	Liquid Xtal TV
Wavelength	Visible - ?	Visible - ?	Visible - ?	Visible - ?
Contrast			30:1	20:1
Flatness (waves)			$1/4\lambda$	several
Transmission	Very High	Very High	High	Medium
Frame Rate (Hz)	10 KHz		>30 Hz	60
Addressability	Electronic	Electronic	Electronic	Electronic
Beam Path	Reflective	Reflective	Reflective (amplitude)	Reflective
Resolution (pix/mm)	60 pixels/mm		48 pixels/mm 21 $\mu\text{m}$ pitch	medium
Polarized Light(in/out)	Not Rqd/Not Rqd		Rqd/Rqd	
Binary or Analog	Binary		Binary	Both
Drive Control	PC		PC	
Size of Active Area	17 $\mu\text{m}$ x 17 $\mu\text{m}$		19 $\mu\text{m}$ x 19 $\mu\text{m}$	
Stability of modulation	Good		Good	
Array Sizes	760 x 576		256 x 256	
Comments	Now commercially available			

**Table 3.2.3.5-1 Commercially Available SLMs**

Parameter	GEC/ Marconi	Hughes LCLV	Hamamatsu	Display Tech	Meadowlark Optics	Semetex	Optron	Radio Shack
Wavelength	Visible - IR	Visible - IR	Visible - IR	400-1500 nm	450-1800nm	500-850 nm	Visible - ?	Visible-near IR
Contrast	NA	300:1	250:1	500:1	500:1	68000:1	500:1	10:1
Flatness (waves)	2.5	1/4	NA	1/2	1/4	1/4	NA	NA
Transmission	NAP	NAP	NAP	85%	90%	18%	75%	50%
Frame Rate (Hz)	40-50	30	30	5000	5000	1000	10s of KHz	30
Addressability	Optic	Optic	Optic	Electronic	Electronic	Electronic	Electronic	Electronic
Beam Path	Reflective	Reflective	Reflective	Transmissive/ Reflective	Transmissive	Transmissive/ Reflective	Reflective Amplitude	Transmissive/ Reflective
Resolution (pix/mm)	38	30	10	6	30	13.2	30	2.7
Polarized Light (in/out)	Not Rqd/ Rqd	Not Rqd/ Rqd	Not Rqd/ Rqd	Rqd/ Rqd	Not Rqd/ Rqd	Rqd/ Rqd	Not Rqd/ Not Rqd	Rqd/ Rqd
Binary or Analog	Both	Both	Both	Binary	Binary	Binary	Binary	6 gray levels
Drive Control	NAP	NAP	NAP	IBM PC	IBM PC	IBM PC	PC	Custom
Size of Active Area	2 x 2 cm	0.46 cm diam	2.0 cm	2.1x2.1 cm		0.97 x 0.97 cm		4.4x5.4cm
Stability of modulation	Volatile	Volatile	Volatile	Volatile	Volatile	Bistable	Bistable	Volatile
Array Sizes	760 lp	138 lp	200 lp	6x6 to 128x128	1x128 to Hex 64	5x5 to 256x256		120 x 146

**Table 3.2.3.5-3 Recent Advances, Not Part of the Original Trade**

Parameter	Silicon Light Machines	Central Research Labs Ltd.	MicroDisplay	Kopin Corp
Type	Switchable diffraction gratings	Ferro-electric & Nematic Liquid Crystal	Liquid Crystal with diffraction gratings	Nematic Liquid Crystal Cyber Display
Wavelength	Visible - ?	Visible - ?	Visible - ?	Visible - ?
Contrast	Very High	High	High	High
Transmission	High	High	~30%	High
Frame Rate (Hz)	50 MHz	>30 Hz	>30 Hz	30 Hz
Addressability	Electronic	Electronic	Electronic	Electronic
Beam Path	Reflective	Transmissive	Reflective	Transmissive
Polarized Light(in/out)	Not Rqd/Not Rqd		Coherent Light Rqd/Rqd	Not Rqd/Not Rqd
Binary or Analog	binary, uses variable duty cycle to provide gray shade	Binary for Ferro-electric LC; Analog for nematic LC	Color capability	Analog

### 3.2.3.6 Spatial Light Modulator Testing

Spatial light modulators were procured from Optron, Boulder Non-Linear and Meadowlark Optics. Table 3.2.3.6-1 summarizes the characteristics of the devices tested.

**Table 3.2.3.6-1 Characteristics of Procured & Tested SLMs**

Parameter	Optron Systems Inc.	Boulder NonLinear Systems	Meadowlark Optics
Technology	Deformed Membrane	Liquid Crystal	Liquid Crystal
Mode	Reflective	Reflective	Transmissive
Number of Pixels	128x1	128x128	128x1
Element Size	13 mm	30 mm	102 mm
Duty Cycle	77%	54%	98%
Aspect Ratio	4000:1	128:1	585:1

The Optron SLM exhibited some problems due to manufacturing defects. The very large aspect ratio that was implemented to meet our system configuration resulted in a tendency for the cell walls to collapse. In addition, the measured reflectivity was 0.33% at 632.8 nm.

The Boulder NonLinear device was an array with the columns slaved to provide a 128:1 aspect ratio. The device was an evaluation unit and had some ground problems in the driver circuit. The liquid crystals are poled and the device must be operated AC to maintain the

proper poling which results in a 50% duty cycle of useful operating time. In addition, the device required coherent light for best contrast. Our system can not use coherent light due to excessive noise that is generated in the image.

The Meadowlark SLM is a nonlinear liquid device that operates in transmissive mode with a 98% spatial duty cycle and 30dB contrast ratio. The elements are larger than desired (100  $\mu\text{m}$  rather than <30  $\mu\text{m}$ ) and the off-the-shelf device procured has only 128 pixels. This limits the keyword length for test to 5.3 characters in the 24 bit custom code. Table 3.2.3.6-2 compares the performance of the Meadowlark SLM to the system requirements. The Meadowlark SLM was integrated into the breadboard and used for system testing.

**Table 3.2.3.6-2 Meadowlark SLM Performance**

PARAMETER	GOAL	Meadowlark SLM Performance
Load Time	0.12 msec (time out/sector is 0.24 msec)	6 msec
Frame Rate	30 Hz	30 Hz
Geometry	Linear; $\Lambda$ 100:1 aspect ratio	Linear, 60:1
Size	$\leq 20 \mu\text{m}$ element pitch	102 $\mu\text{m}$
Spatial Duty Cycle	$\geq 75\%$	98%
Mode	Amplitude readout	Amplitude Readout
Readout	Reflective or transmissive	Transmissive
Throughput	$\geq 80\%$	$\geq 90\%$
Number of elements	256 min; 408 max	128 (OTS unit)
Contrast Ratio	$\geq 50:1$ binary	1000:1
Addressability	Electronic	Electronic

### 3.2.4 Disk Media Trades

The disk trades include: the recording mode (magneto-optic, phase change, ablative, etc.), disk size, recorded bit size, and data encoding (addressed in Section 3.2.1). The ideal optical disk is erasable and consists of a transparent, pregrooved substrate coated with a read/write layer followed by a reflective layer. The read/write layer is highly absorptive at the wavelength of the write laser. Record and readout take place through the substrate so that surface contaminants are out of focus, preventing them from being mistaken for data. Unfortunately, the ideal disk does not exist.

Key disk parameters are the signal-to-noise ratio and the absolute signal strength or contrast of the data in the correlation image. These limit the accuracy of the correlation. For magneto-optic materials, the reflectance is 33%. However, 99% of that reflectance is DC bias while about 1% provides contrast between 'zero' and 'one' bits. By proper use of polarizers the DC bias can be minimized thereby increasing the data contrast. This limits the overall light available to the detector. For phase change materials the reflectance is about 14% but the contrast is larger, about 8%. Write once, read many (WORM) media provide both good reflectance, about 50%, and strong contrast, about 30%.

Correlation gain is equal to the space bandwidth product of the signal, i.e. the key word length. The maximum length of the key word is determined by the disk geometry. The data is recorded on a spiral track with approximately 0.5  $\mu\text{m}$  pit spacing and 1.6  $\mu\text{m}$  track pitch. Therefore, any segment of data recorded around the tracks is recorded in an arc. The throughput of a large segment of the arc cannot be focused to a single detector element using simple spherical optics. The portion of the signal that spills over into adjacent detector elements causes crosstalk. To minimize this channel-to-channel crosstalk on the inside track, we limited the bow to half the track pitch; this limits the key word length to approximately 256 bits.

The minimum key word is limited by system noise. Shorter key words have lower signal-to-noise ratio and less dynamic range since the light intensity in the maximum correlation signal is less. This ultimately imposes a limit, based on both the signal strength and the noise levels, on how short a key word can be correlated. The minimum key word length is set by the noise characterization of large area readout from an optical disk. Current system evaluations indicate the limit is between three and six characters.

#### 3.2.4.1 Optical Correlator Disk Size Limits

In a system requiring a custom correlator disk, the disk need not be in standard format. Increasing the size of the disk to allow larger spots will ease the constraints on the optics and on the servo system. To determine the maximum feasible disk size we assumed the rotation speed and therefore the data rate remained constant at the current values. The maximum record exposure (from the ISO spec.) is 10 mW at the disk surface to record a 0.8  $\mu\text{m}$  bit with about a 1.2  $\mu\text{m}$  laser spot. This results in a power density of about 8.8 mW/ $\mu\text{m}^2$ .

Using a 100 mW laser and a measured 64% optical efficiency between the laser and the disk, we have about 64 mW at the disk surface. Imposing a 3 dB design margin, the maximum exposure power is 32 mW. This is sufficient to expose with a 2.2  $\mu\text{m}$  spot at the power density of 8.8 mW/ $\mu\text{m}^2$ . A 2.2  $\mu\text{m}$  record spot will record about a 1.8  $\mu\text{m}$  bit.

Therefore, using a 3  $\mu\text{m}$  track pitch and 20,000 tracks, the exposure region is 60 mm wide running from a 60 mm radius to a 120 mm radius. This gives a 240 mm or 9.5 inch disk diameter. This trade is summarized in Table 3.2.4.1-1

**Table 3.2.4.1-1 Correlator Disk Size Trade**

Parameter	Current	Custom
Disk Speed	30 RPS	30 RPS
Recording power density	8.8 mW/ $\mu\text{m}^2$	8.8 mW/ $\mu\text{m}^2$
Recording spot diameter	1.2 $\mu\text{m}$	2.2 $\mu\text{m}$
Recorded data bit diameter	0.8 $\mu\text{m}$	1.8 $\mu\text{m}$
Track pitch	1.6 $\mu\text{m}$	3.0 $\mu\text{m}$
Disk diameter	5.25 inches	9.5 inches

For the breadboard we used a standard optical disk. For a future system implementation, a larger disk has advantages. The advantages of going to a larger correlator disk include:

- Larger depth of focus (3.3  $\mu\text{m}$  rather than 0.64  $\mu\text{m}$ ).
- Larger hub area for increased mechanical stability.
- Lower numerical aperture on the objective lens (~2 times less).
- The larger track pitch makes it easier to fabricate accurately maintaining track concentricity.

The disadvantages include:

- Requires a custom disk size as well as format.
- Angular wobble will result in larger axial displacements (balanced by a depth of focus increase)
- Requires modifying the standard write head to accept a larger than normal ILD.

#### **3.2.4.2 Disk Type**

We reviewed the disk formats and types and identified three basic disk types to trade: magneto-optic, WORM, and rewritable Phase Change. This section discusses the differences between these types and includes simulations and laboratory measurements of their performance in the correlator configuration.

#### **WORM DISKS**

There are several different types of recording mechanisms that are utilized for WORM disks. These include Ablative, Dye/Polymer, and Coalescent & textured media. The mechanisms are described below:

Ablative - Ablative recording is essentially a thermal process. Thin metal films are locally heated by the focused laser beam and the film either beads up or forms voids. Generally in high speed recording the dominant effect is vaporization of the film surface to open holes. Since the mechanism is thermal, the film must have a low melting point. After the hole is opened, surface tension forces dominate the process to create a stable void.

Dye/Polymer - In dye/polymer materials, marks that look like holes are formed in light absorbing organic films. Since the thermal conductivity of the organics is lower than metals, higher surface temperatures are created during recording and ablation is the dominant recording mechanism. Back pressure from the ablation process pushes the material out of the hole; surface tension effects are only minimally involved. This material was developed by Kodak.

Coalescent and Textured Media - The optical properties of these materials depend on the texture. An unrecorded film has a recording layer that is deposited in the form of small separate islands of material which have high absorption. When the material is heated it coalesces into larger clumps which have high reflectance. Burroughs originally developed a material that used an aluminum recording layer. The (TeOx) media developed by Mitsushita is similar. The WORM (Moth Eye) media from Plasmon Data Systems also utilizes this basic mechanism.

Most WORM media produces marks that have a high reflectance contrast resulting in amplitude differences during readout. Generally, WORM disks are read out through the substrate as shown in Figure 3.2.4.2-1. The reflectance is different for the metal layer than for the pit resulting in high amplitude contrast. The polarity of the contrast difference depends on the recording mechanism.

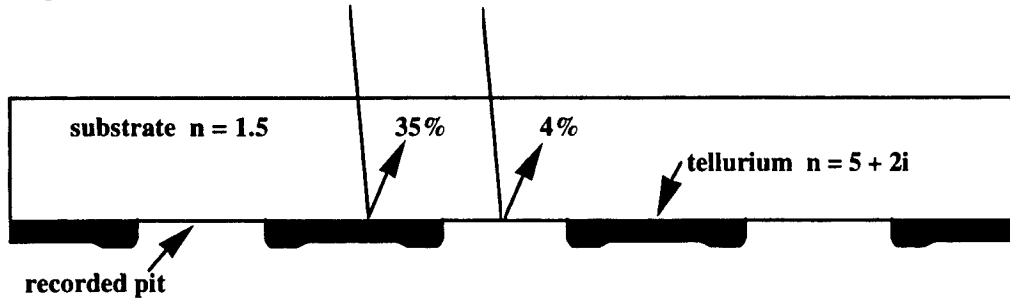


**Figure 3.2.4.2-1 WORM Readout Configuration**

The reflectance coefficients from a thick opaque film are

$$r_p = \frac{n_f^2 \cos \phi - n_0(n_f^2 - n_0^2 \sin^2 \phi)^{1/2}}{n_f^2 \cos \phi + n_0(n_f^2 - n_0^2 \sin^2 \phi)^{1/2}}$$

and

$$r_s = \frac{n_0 \cos \phi - (n_f^2 - n_0^2 \sin^2 \phi)^{1/2}}{n_0 \cos \phi + (n_f^2 - n_0^2 \sin^2 \phi)^{1/2}} ;$$

where  $\phi$  is the incident angle, and p and s refer to the polarization direction.  $n_0$  and  $n_f$  are complex indices of refraction of the film and incident media (the substrate for optical disks). For  $\phi = 0$ , this simplifies to:

$$r = \frac{n_0 - n_f}{n_0 + n_f} .$$

For normal incidence, the reflectance is independent of polarization and the reflected intensity is  $R = |r|^2$ .

For example, crystalline tellurium has a refractive index  $n_f \approx 5 + 2i$  at about 800 nm. As a result standard tellurium disks have about 35% reflectance off the tellurium layer and about 4% reflectance from the pits.

The Matsushita WORM disks ( $\text{TeOx}$ ) have the reverse contrast. The glassy  $\text{TeO}_2$  matrix encapsulates very small tellurium particles. This has an initial reflectance of 18% when illuminated through the substrate. During recording the Te crystals melt, merge, and crystallize. The resulting reflectance in the recorded areas is about 26%.



NOTE: The polarity of the contrast ratio can be varied depending on layer configuration. For some tri-layer configurations the polarity of the contrast variation on the tellurium disks is reversed from that described above.

We acquired a WORM disk written by University of Southern California. They wrote a set of test patterns for evaluation. Three different write powers (8, 9, and 10 mW) were used to record on 0.5  $\mu\text{m}$  channel spacings. We used a CCD camera frame grabber to digitize our SLED illuminated scene, then processed the image to fit the A/D values to pixel patterns and determine bright and dark field statistics. A table of those results is presented below:

**Table 3.2.4.2-1 WORM Disk Contrast Measurements**

File	Contrast	Bright	Dark	Pxls/patt	Condition
LOW2	24.7	1.125	0.877	$15.2 \pm 0.02$	WORM grating
MED2	25.5	1.127	0.873	$15.2 \pm 0.06$	WORM grating
HIH2	20.8	1.106	0.897	$15.2 \pm 0.1$	WORM grating
PHASE1	9.6	1.049	0.952	$17.2 \pm 1.1$	WORM grating
PHASE2	9.5	1.048	0.953	$17.2 \pm 0.9$	WORM grating
PHASE3	10.9	1.055	0.946	$17.2 \pm 2.2$	WORM grating
LOW1	22.0	1.118	0.898	n/a	WORM mixed
MED1	25.5	1.154	0.899	n/a	WORM mixed
HIH1	26.3	1/157	0.894	n/a	WORM mixed

The contrast is optimum for the MED2, 9 mW, write pattern. Note however, that for the mixed pattern, where off regions extend beyond the grating 3 bit length, the average contrast increases with higher write power. This may exacerbate the MTF deviation across varying mark spacings.

The column labeled Pxls/patt represents the spacing between fit grating cycles. The Panasonic phase change disk shows a deviation of 1 part in 17, or about 5%. The WORM reduces this by about an order of magnitude. It is not clear whether this level is a measurement limit but it shows a potential scale improvement of an order of magnitude by going to a controlled bit spacing writer, such as the one used by USC. The WORM spacing, 15.2 pixels, was measured on a microscope as 0.50  $\mu\text{m}$  per channel bit. Scaling our phase change to this shows a 0.56  $\mu\text{m}$  spacing.

## **PHASE CHANGE DISKS**

Phase change disks use materials that exist stably in two different structured phases, i.e., amorphous and crystalline. The heat from the focused laser beams initiates a phase change from a metastable to a stable state. Chalcogenide glasses are one example of phase change materials. This is the newest mechanism and its stability is not fully proven; unwanted phase changes can occur if the disk is stored at high temperatures.

We procured some commercial off-the-shelf phase change disks and a Panasonic disk recorder. Several controlled patterns were written on the disks which were then mounted in the breadboard. We took some frame grabs with a COHU camera off a Panasonic phase change disk illuminated by an 830nm LED. These consist of roughly 750 camera pixels along a track and

480 lines across the tracks. A FORTRAN program, GRABREAD, was written to process the frame data to determine measured channel bit levels and spacings. Bit intensity variations and locations appear to be at least as controlled as the camera bit resolution used to capture the frames.

Statistics from the frame of "FF" data and "Harris" data are presented to illustrate the outputs. To quantify statistics measured within a noise infested environment a summary is presented for the data of each file at its median (1/2 the population ranked by quantity) value.

**Table 3.2.4.2-2 Phase Change Disk Contrast Measurements**

Property	"FF" file	"Harris" file
DARK Average	0.972	0.977
Bright Average	1.029	1.036
Contrast	0.057	0.059
Dark Std Dev	0.0053	0.0092
Bright Std Dev	0.0051	0.0174
Pixels per Mark	20.5	N/A
Location Error Std Dev	0.01 ch bits	N/A
Track Location Std Dev	0.052 tracks	not measured

The measurements of the Panasonic phase change disks show a contrast ratio of about 6% with a bit intensity variation of 0.5% standard deviation (about our A/D bit resolution). The bit location error, along-track, is about 1% of a channel bit spacing and the track spacing error came out 5% of a track (1/2 camera line). In general, the disk deviations are not greater than our frame grab resolution.

## **MAGNETO OPTIC DISKS**

Magneto-Optic disks are the most common erasable disk currently available commercially and are generally read out in reflection. However, they can be custom optimized for transmissive readout rather than reflective readout. This involves a trade between the generated polarization rotation and the overall light transmission.

Transmissive readout of a magneto-optic disk involves the Faraday effect rather than the Kerr effect. The Faraday effect rotates the polarization of light with distance as the light is transmitted through the magneto-optic layer. The rotation per unit thickness is directly proportional to the product of the magnetic field strength and the Verdat constant for a specific medium. With thick films, the Faraday effect can generate more polarization rotation than the Kerr effect, thus, the tradeoff is overall transmittance. If a custom disk is optimized for the Faraday effect the overall signal (rotation x transmittance) can be stronger than that generated by the Kerr effect (rotation x reflectance). Further information on properties of custom disk formulations will have to come from disk manufacturers.

Magneto-optic disks have sufficient light reflected but inherently low contrast between 'one' bits and 'zero' bits. The normal readout enhances the contrast by utilizing differential detectors for readout. A magneto-optic based architecture has been identified that

has the potential to increase the contrast of the correlator readout using an optically implemented differential readout. Armand Tanguay at the University of Southern California has used a shearing interferometer to do direct optical correlation of images stored on a MO disk. The configuration involves inserting a birefringent material between the disk and the SLM to separate the two polarizations into separate paths one bit space apart. Each data bit is stored as two channel bits, where a data "0" is stored as a channel "1, 1" or "0, 0" (no change) and a data "1" is stored as a "0, 1" or "1, 0" (change). At the SLM plane, adjacent bits are interfered to produce the optical differential readout. This architecture requires that the bit spacing be constant which is not normally the case for a constant angular velocity system such as our baseline system. One possible solution is to record the two channel bits on two adjacent tracks which are always at constant spacing. Cross track coherence is then required in writing the disk to ensure there is no circumferential displacement between the pair of differential bits. For the breadboard we tested Panasonic phase change disks and WORM disks. No attempt was made to implement magneto-optic media.

#### **3.2.4.3 Substrate Effects**

Substrate effects, such as birefringence or surface quality and uniformity, affect how the correlator works. Large area phase effects off the Panasonic phase change and the Sundstrand WORM disks were measured on the ZYGO interferometer. A 33 mm diameter area was imaged out; this covers the entire data radius.

The Panasonic disk on a polyethylene substrate has a peak to valley phase variation of about  $6.15 \lambda$  ( $\lambda = 633\text{nm}$ ) and an RMS phase of  $1.35 \lambda$ . The shape of the phase effect is a gentle cup-like bowing. The Sundstrand MO disk is on a glass substrate. The peak-to-valley phase variation is  $3.19 \lambda$  with an RMS of  $0.85 \lambda$ . In this case the pattern is more random, like a ripple on the surface. In our application the ripple will be harder for the tracking servos to follow while the cup-like effect on the polyethylene substrate will limit the disk radius that can be maintained in focus at one time. If the cupping is too severe, more correlators looking at fewer tracks each are required.

For the breadboard, a custom WORM disk was fabricated by Harris Semiconductor. It was manufactured using semiconductor mask, e-beam technology, recording on  $1/5 \mu\text{m}$  centers. Disk flatness was better than  $1/10$  wave. Pixels are  $2.5 \mu\text{m}$  diameter holes in the chrome coating on  $1.25 \mu\text{m}$  centers and the tracks are concentric with  $5 \mu\text{m}$  centers.

#### **3.2.5 Photodetector Array**

The optical correlation of the data on the disk with the SLM mask is collected onto a photodetector array. Each element of the array corresponds to a single track on the disk. The photodetector consists of a linear array of photodiodes and associated Charge Coupled Devices (CCD). In our application, the desired correlator output is the peak correlation value rather than the integrated value in each sector. The preferred implementation is to do the peak detection directly on the CCD. This peak value is then clocked out at the end of the sector. Table 3.2.5-1 summarizes the requirements of the photodetector array.

**Table 3.2.5-1 Photodetector Array Requirements**

Parameter	Specification
Wavelength	830 nm
Max Illumination Intensity	1.8 $\mu$ Watts
Min Illumination Intensity	0.32 $\mu$ Watts
NEP (SNR=1)	1.8 nWatts
Number of elements	>1500 x 1 linear Array.
Element Pitch	< 25 $\mu$ m
Element Geometry	
Width (along array axis)	> 80% of pitch
Height (cross array axis)	200 - 1000 $\mu$ m
Physical (spatial) Linearity	$\pm 0.5$ $\mu$ m
Readout Method	CCD or Equivalent
Readout period	1 msec
Max Dead Time Between Frames	0.24 msec.
Dynamic Range	30 dB (1000:1)
Element to Element Crosstalk	
1st adjacent	< -20 dBc
2nd adjacent and greater	< -30 dBc
Pixel to Pixel Response Uniformity	0.4% (above 0.1 $\mu$ W illumination)
Amplitude Response	Linear
A/D Sampling Plateau	<sup>3</sup> 50 nsec (settled to 1 lsb out of 12 bits)
Peak hold rise time (accurate to 1%)	<90 nsec
Drop at 1 msec after hold	<1%
Element to element crosstalk	1st adjacent <-20 dBc 2nd adjacent & greater <-30 dBc
Holdover Crosstalk	<-20 dBc
Charge Transfer Efficiency	0.9999 or better
Desired Enhancements	Differential output amplifier with external reference Alignment detectors (without peak detection capability)
On-chip Processing Requirements	AC coupled filter to remove bias level variations caused by light level drifts and to allow thresholds to be set based on keyword length only. Instantaneous Peak Detection with one peak detector per detector element. Peak levels passed to processing electronics at the end of sector.

Additional on-chip processing is needed. First is an AC coupled filter to remove bias level variations caused by light level drifts. This allows thresholds to be set based on keyword length only. Second is instantaneous peak detection with 1 peak detector per detector element. At the end of the sector, the peak value for that sector is digitized and sent to the post processor. The post-processor consists of bulk digital processing which performs logical operations between previously stored intermediate match results and real-time degree of match from the optical correlator. It computes and rank orders partial match results for all sectors on the disk on each revolution of the disk. The addresses of the best correlation matches are provided to the user for direct data access.

### 3.2.6 Objective Lens

A key element in the optical subsystem is the objective lens that images the disk to the spatial light modulator. We found that this element imposes a limit on the performance of the correlator through the MTF. Measurements of the MTF of the objective lens in the OAM breadboard show that for an infinite contrast disk media we would only have about 10% contrast at the correlation plane.

The breadboard has been set up such that the image of the bits on the disk are magnified about 100X by a 4 mm (0.45 N.A.) objective lens from a CD player. The light source for this measurement is a Light Emitting Diode (LED) (Hitachi HLP50RGB) with a center frequency of about 805 nm and a spectral width of about 30 nm. A data mask is placed in the image plane and then correlation between the data and the mask is reimaged 1 to 1 to a TV camera. The image of the tracks are also imaged 1 to 1 to a detector array, but the data bits are Fourier transformed by cylindrical lenses to the detector array. The Fourier transform is the sum of 1200 data bits along each track. The beam width is 1.2 mm with the detector array intercepting the central 13 microns.

The results from the bits on the phase change disk, showed about a 10% modulation between the light level of the in between grooves (100%) and the level of the data bits (90%), with zero level (0%) being the black level of the detector array.

A CD music disk was then tested and the modulation is still only 10% when measured as the sum of the bits compared to the in between region.

The lens frequency response was the suspected cause of the limit to the 10% modulation. The disk was replaced with a series of chrome on glass Ronchi rulings, at 5, 20, 70, 105, and 250 cycles per mm resolutions and the results plotted in Figure 3.1.7-1. The 667 cycle per mm point is the result from the grooved disk measurement.

The conclusion is that even if a disk had 100% contrast, when read in the correlator the apparent contrast would be limited by the lens system MTF.

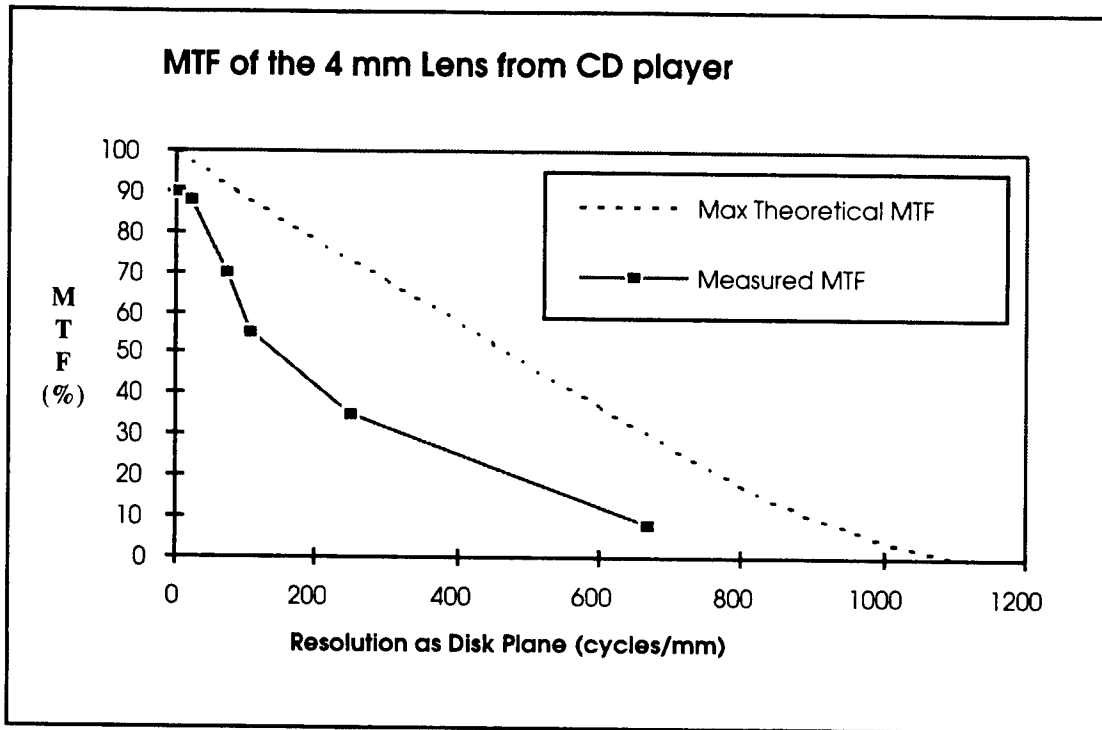


**Figure 3.2.6-1 Measure MTF of the 4mm CD player objective lens.**

### 3.2.7 Servo System

Standard optical disks must maintain focus and tracking only at the single point readout location. The large area of the correlation readout imposed additional challenges to the tracking and focus function. To meet these requirements, possible focus and tracking servo techniques were explored. This section discusses some of these techniques. After measuring the large area effects from the optical disks, a standard optical disk tracking and focus servo head was successfully implemented. The detailed electrical analysis of the focus and tracking servos is included in Appendix C.

#### TRACKING SERVO APPROACHES

1. Oversample cross-track by 2 to 4 x.
2. Center track written with a special data code.
3. Software based calibration with disk map and oversampling
4. Imaged center track or guardband tracks
5. Combination of software calibration and imaged guard band tracks
6. Auxiliary laser spot at a different wavelength. One per head.
7. Single spot/disk monitor, track correlation relative to a single point on the disk using a special track.
8. Intelligent disk hub - spec. hub runout to < 40 millionths
9. Precision write - format after mounting
10. Portahub

11. On-chip processing prior to peak detection
12. Record every other track - use a larger disk than normal
13. Write head/track through correlation optics

Two cross-track servo techniques were considered in detail: electronic tracking and mechanical tracking. In electronic tracking the data is oversampled in the cross-track direction by a factor of about 4 and the peak value is selected as the true bit value. In an alternative electronic method the tracks are oversampled by a factor of two and the true correlation value is defined to be the weighted average of several cross-track detector outputs values. After additional analysis of this approach we determined that it requires a linear rolloff in amplitude as the head moves off the center of the track. Since the correlation is not a linear process this is not a valid requirement and this alternative was eliminated. Mechanical servo techniques are similar to those used for the standard readout head servo; the center track of each correlator will contain data specifically designed to assist the servo feedback system. The objective lens, or possibly a single component of the lens, is laterally translated to keep the readout centered on the tracks. This tracking method works best if concentric tracks are used. For the breadboard, mechanical tracking was successfully implemented.

### FOCUS SERVO TECHNIQUES

Recorded spot sizes on the disk are on the order of  $1\text{ }\mu\text{m}$  and the resulting depth of focus is about  $\pm 0.5\text{ }\mu\text{m}$ . In order to maintain this tight tolerance an active focal servo system is required. The output of the servo system should be an error signal that is roughly proportional to the displacement (positive or negative) from ideal focus. A steep slope in the linear region is desirable for accuracy and, outside the linear region, the sign of the error signal should remain correct.

Standard optical focal servo techniques used in optical disk systems are some variant of the Foucault knife-edge or astigmatic lens systems. They use the same optical beam that is used to read or write the data and basically determine how far out of collimation the return beam is after passing back through the objective lens.

#### Foucault Knife-edge

For this discussion of the Foucault knife edge assume the input to the objective lens is collimated. When the objective is properly focused, the reflected light is recollimated by passing back through the objective. A field lens refocuses the reflected beam. A knife edge is positioned between the field lens and its focus to cut off half the beam. A split detector is placed in the focal plane. When the system is in focus, the output of the two detectors is equal; when it is defocused, the beam shifts laterally and the two outputs are not equal. A differential detection scheme then generates an error signal to feedback the objective positioning system.

#### Half Aperture

A similar system that requires less precision in component position is the half-aperture technique. A bi-prism acts as a dual knife edge and focused each half of the beam onto a separate split detector. Any misalignment of the system is canceled in the net error signal generated. In addition, the half aperture approach uses all the reflected light.

### **Astigmatic Lens**

A second focal sensor technique utilizes an anamorphic field lens to determine the degree of collimation of the reflected beam. The lens has different focal lengths in orthogonal directions. A quadrature detector is positioned between the primary foci in the circle of least confusion with its axes 45° with respect to the lens axes. Any shift in focus causes the beam at the detectors to become elliptical. The direction of the ellipse determines the direction of the focal shift. The output of opposite elements in the detector are either added or multiplied and difference between the resulting values is measured.

### **3.3 Breadboard Results**

The optical subsystem comprises a set of fixed optical correlation stations spaced around the disk that perform channel-encoded binary optical correlation in parallel across all tracks on the disk. As discussed previously, a space integrating correlator architecture best meets the requirements of correlation directly from an optical disk. The matched filter is a fixed spatial light modulator and the signal is automatically translated past the filter function by the rotating disk. *Because coherent noise effects require incoherent illumination, the optimum architecture is an amplitude modulated space integrating correlator with the matched filter in the image plane of the optical disk.*

During operation a defined key word is input as a matched filter reference function by computing and storing the proper density distribution in a Spatial Light Modulator (SLM). As the disk rotates past the SLM the degree of correlation between the recorded data and the key word filter is detected as a function of time at the detector plane. The correlator output is proportional to the byte-by-byte degree of match, in bits, between search mask and data on the disk. The sector and track where a correlation is found, along with a voltage level proportional to the strength of the optical correlation, are sent into the post-processor.

The optical correlator was breadboarded and tested. The purpose of the breadboard was to identify and measure critical correlation effects, identify and test critical components and demonstrate the basic feasibility and performance of the optical correlation approach. Breadboard results were compared to simulations and used to refine the assumptions in the simulations. The refined simulations were then used in additional trades. Many of the trade discussions in Section 3.2 include information derived from the breadboard. Section 3.3 describes the all optical correlator breadboard, breadboard simulations, and experimental results.

#### **3.3.1 Breadboard Description**

Figure 3.3.1-1 shows the breadboard configuration. The breadboard is essentially the combination of two optical systems operating at different wavelengths to avoid interference. The servo subsystem operates at 670 nm. It consists of a laser diode that is focused to a point source on the surface of the disk just outside the correlation area so that it will not degrade the correlation. The reflected beam is imaged onto a quadrant detector and standard optical alignment algorithms are implemented for focus and tracking. The output of the servo subsystem is fed to the mount for the objective lens to control position.



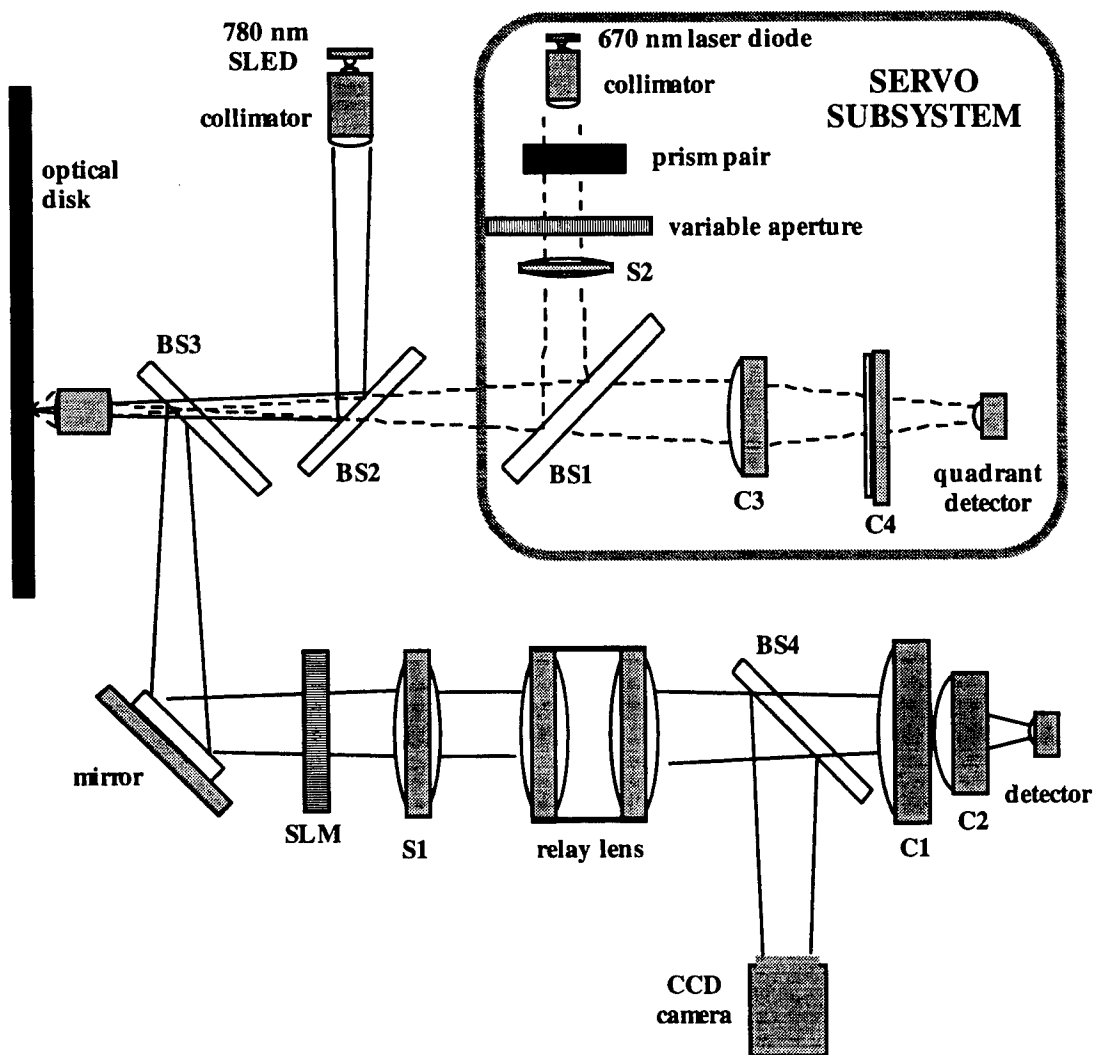


**Figure 3.3.1-1 Breadboard Layout**

The correlation system starts with a 780 nm superluminescent diode (SLED). The output of the SLED is reflected off a dichroic mirror and provides a large area illumination at the disk surface. The dichroic mirror prevents the back reflections from interfering with the servo system. In the along track direction, 408 bits around the disk are imaged onto the SLM through beamsplitter 3 (BS3). In the across track direction, the disk surface is Fourier transformed to the SLM such that the transform of 1250 tracks pass through a single element of the SLM. This allows a linear, 1 dimensional, SLM to correlate with multiple tracks simultaneously. The SLM contains the query word and the throughput of the SLM is the spatial correlation between the data on the disk and the query word. The output of the SLM is relayed to a photodetector array oriented perpendicularly to the SLM. In the along track direction, the throughput is simply collected into a single element forming a correlation sum. In the across track direction the throughput is retransformed such that each disk track is imaged onto an individual element on the array. Thus, the individual correlations from each track are separated. The correlation values

from the CCD array are captured by a high speed oscilloscope, then digitized and sent to a computer for processing. The SLM is also imaged to a CCD camera as a breadboard convenience to aid in alignment.

Table 3.3.1-1 summarizes the original design light budget and the final breadboarded measurements. The light available to the CCD in the breadboard was about 30% of the predicted levels. Some of that low level comes from operating the SLED at a lower power level to ensure device life. The remainder comes from reduced efficiency between the SLED and the disk and a higher CCD overfill ratio. The breadboard had 9.3nW of light at the CCD for an average correlation period.

**Table 3.3.1-1 Breadboard Design and Measured Light Budget**

ELEMENT	DESIGN ESTIMATES	BREADBOARD RESULTS
SLED Output	50 mW	25 mW (estimated from curves at 440 mA)
SLED Collimator	0.50	12.5 mW (measured)
Hot Mirror	0.95	
Beam Splitter	0.45	
Objective Lens	0.80	
OPTICAL EFFICIENCY TO DISK	0.17	0.12 (calculated from Collimator output and intensity at disk)
Intensity at disk	8.5 mW (=50mW*0.17)	3 mW (measured)
Recovered Disk Reflectance	0.12 (includes MTF effects)	0.12 (calculated from intensity at mask plane)
Percentage of bits ON in code =50%	0.50	0.5
Objective Lens	0.80	
Beam Splitter	0.45	
Dichroic mirror	0.95	
Light at mask plane	1.45 mW	70 $\mu$ W measured
SLM transmittance	0.60	0.60
CCD overfill ratio (F/2.8 cylinders)	0.30	
Optics	0.77 (5 elements @ 0.95 each)	0.9 (measured)
Number of Tracks	1300	1300
Track duty cycle	0.65	0.65
INTENSITY PER CCD ELEMENT	$50\text{mW} \cdot 0.17 \cdot 0.004 \cdot 0.65 / 300 = 17 \text{ nW}$	$70\mu\text{W} \cdot 0.6 \cdot 0.3 \cdot 0.9 \cdot 0.65 / 1300 = 6.3 \text{ nW}$
ENERGY PER CORRELATION PERIOD	$17 \text{ nW} \cdot 100 \text{ nsec} = 17 \times 10^{15} \text{ Joules or } 6,528 \text{ photons}$	$6.3 \text{ nW} \cdot 100 \text{ nsec} = 6.3 \times 10^{15} \text{ Joules or } 2,419 \text{ photons}$

### 3.3.2 Breadboard Development Measurements and Simulations

This section summarizes the measurements and related simulation of the optical correlation breadboard during the development phase. Results using standard disks, standard disk codes, and the custom code are included. On the breadboard, we digitize correlation outputs with a Rapid System A/D at 1.25 MHz (8 bit resolution with values ranging from 0 to 255), with the disk spinning at 1 Hz. The buffer length is 1024 KSamples (1,048,576) for a total duration of 0.83 seconds. Figure 3.3.2-1 depicts a typical sector's worth of data for the MTF calibration pattern.

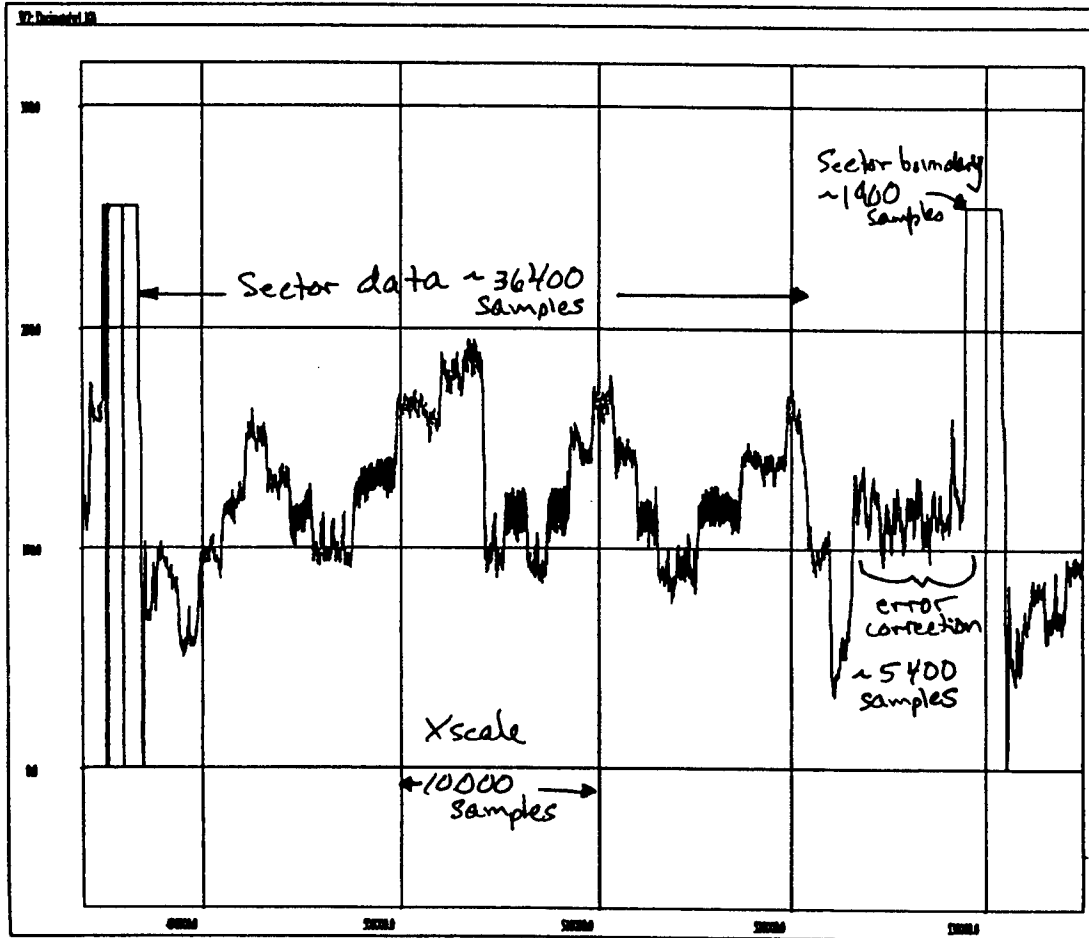


**Figure 3.3.2-1 One sector of correlation output using a standard calibration pattern.**

A sector consists of:

Boundary	1900 samples
Data Region	36400 samples
Error Correction	5400 samples
Totaling	43,700 samples.

The data region to overhead ratio is therefore  $36400/43700$  or 83%. Our RLL(2,7) disc data region is further divided into synchronization boundaries every 16 data bytes. The 1024 byte region thus includes an additional 64 resynch bytes. Every byte consists of 16 channel bits. Our sampling rate is:  $36400/64 = 570$  samples per resynch region, and  $570/(17*16) = 2.1$  samples per channel bit. Note that bit markings extend for a length of 2 channel bits, so that the informational sampling rate is 4.2 samples per data mark.

The analysis code scans an acquired data set and indicates the locations of the best correlation output regions. It does this by analyzing the distance between peak outputs and comparing those to the encoded data spacing. Thresholds and distances are operator entered to allow optimization for differing patterns and acquisition inputs. Next, varying bias levels must be compensated.

During discussions with detector vendors, various shift and difference processing algorithms were considered for the correlation output processing. Initial breadboard outputs had background level variations requiring local level referencing. Figure 3.3.2-2 shows a sample breadboard correlation acquisition. Point B is the desired output which a simple peak detect could not recognize due to the previous region's higher background. Three candidate processing algorithms were considered: two point difference, three point difference, and offset integrator. The two point difference corresponds to B-A, it removes background level variations and depends on the timing between A and B to produce a large differential. The three point difference looks ahead to point C as well as behind to point A. This strengthens the rejection of false peaks that tend to be less symmetric. However, the data stream is analog and therefore free from obvious bit timing. This can cause difficulty in acquiring the points at the optimum data extremes. If the sampling does not coincide with peaks and valleys the discrimination degrades. A close alternative is continual integration of a time corresponding to the A to B spacing of the data delta above point A. This alleviates the timing synchronization requirement but the integration must last longer than the data resolution and so must be replicated with a staggered starting interval.

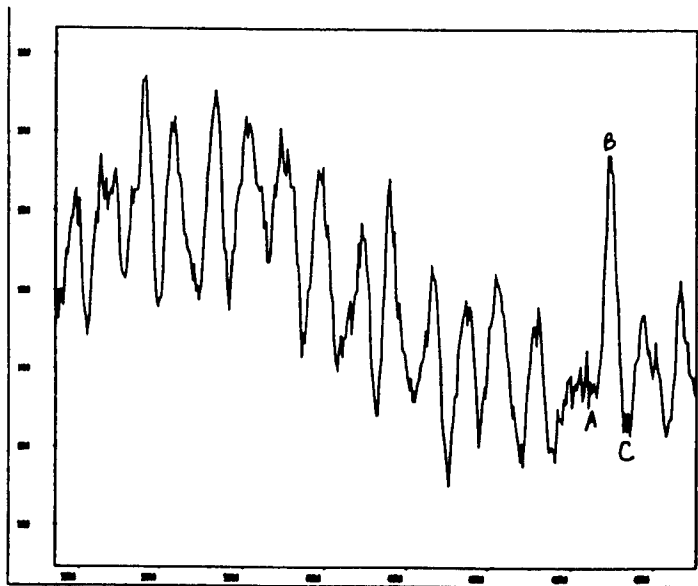


**Figure 3.3.2-2 Sample breadboard correlation output in the RLL(2,7) code**

Improvements in the breadboard focus and alignment reduced the measured data bias variation, allowing local smoothing algorithms to provide a sufficient output normalization. Figure 3.3.2-3 illustrates a form of bias subtraction processing, enabling a successful peak detect across a measured data region. The data is shown overlaid with a bias calculation. The dotted curve is the result of subtracting the bias from the direct data detect, where the processed desired output now peaks above the rest of the data field. This process does not require a time delay for the bias subtraction. The bias is determined with an exponential history of prior data as would be done by charging a parallel capacitor. Figure 3.3.2-4 shows the processing over a broader input region. Measured data is on the left; simulations are on the right. Processing is the top two panels; raw inputs are on the bottom panels. The measured data bias ranges over a larger extreme than the simulation. However, the variations are slow enough that the processed output correctly peak detects the regularly spaced desired outputs.

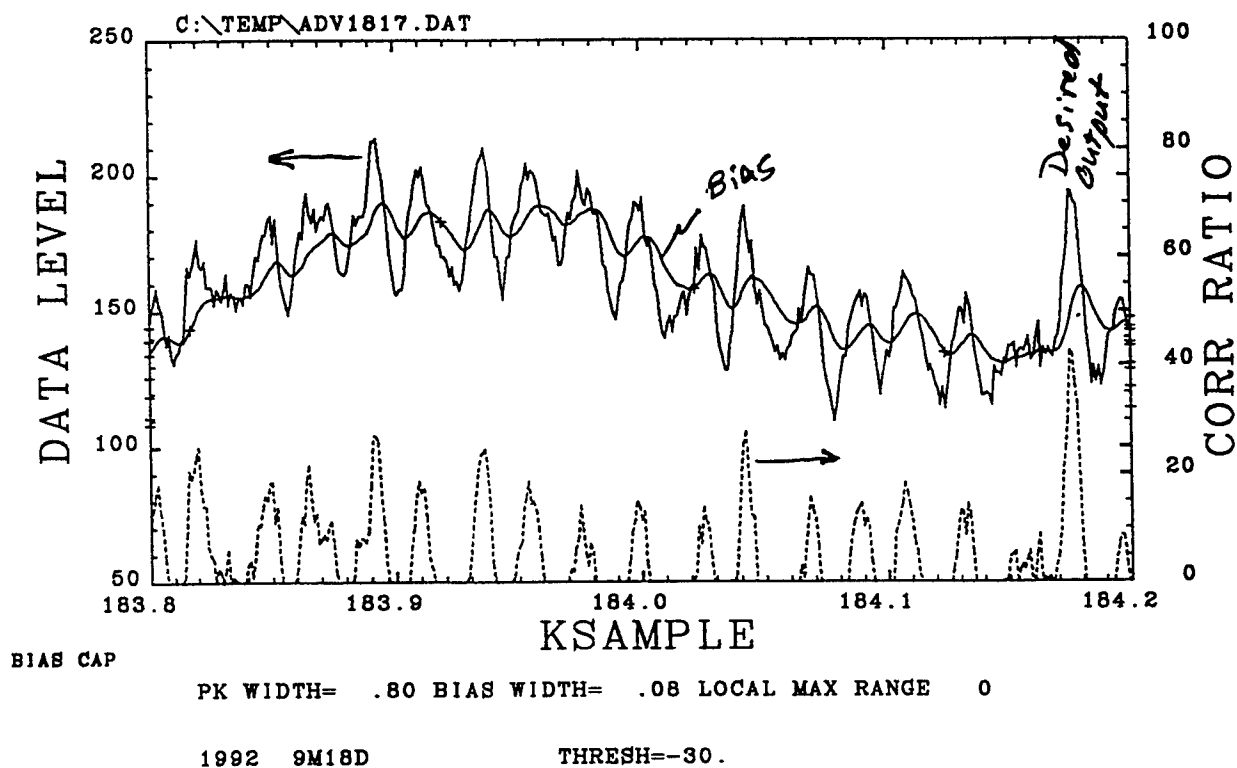


Figure 3.3.2-3 Bias subtraction processing algorithm

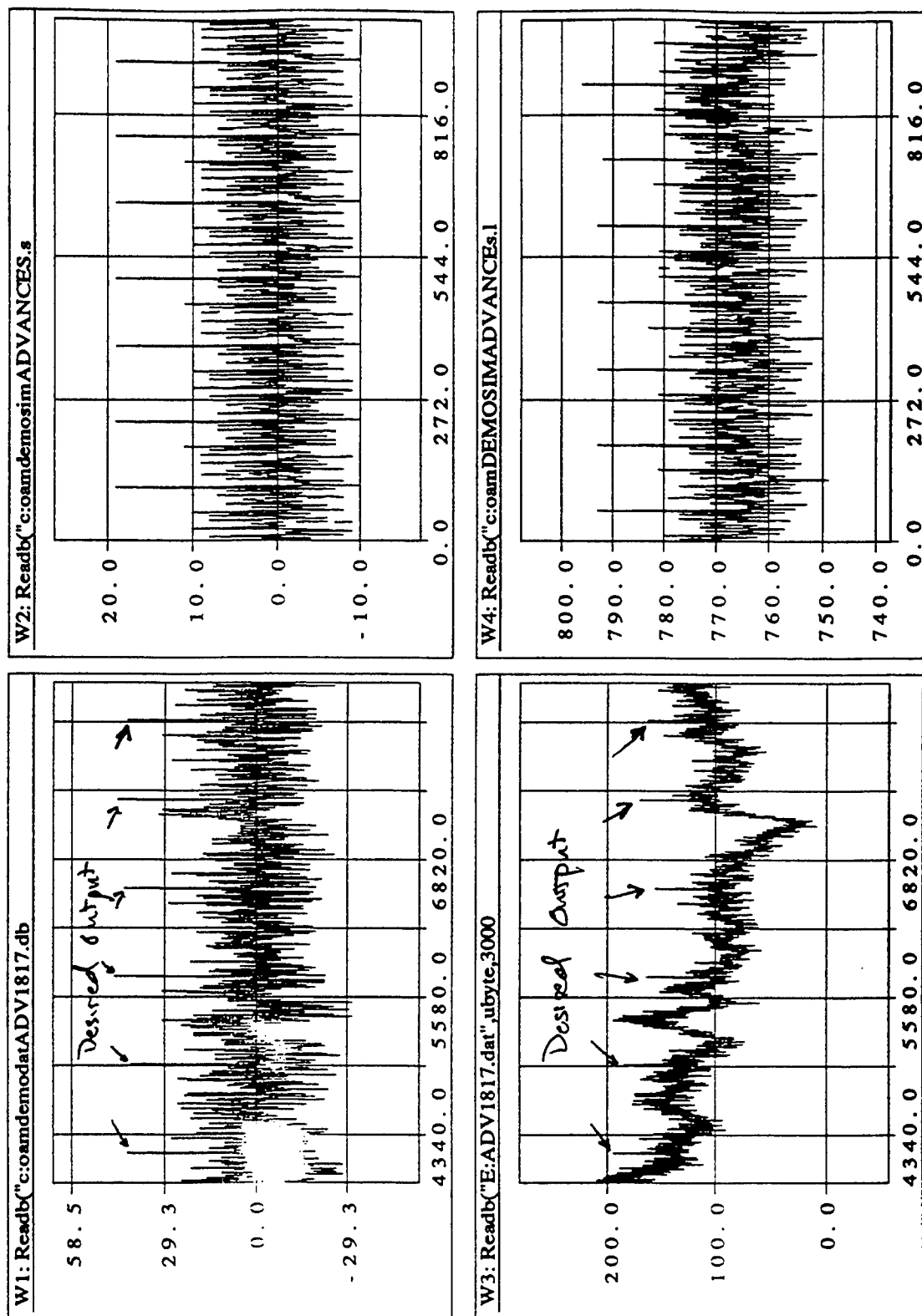


Figure 3.3.2-4 Breadboard output using the bias subtraction algorithm

A limitation of calculating the bias level from past history is identifying desired outputs in a falling bias level region (or excluding false outputs in a rising bias region). Performing a normalization with bias, ahead of the output, requires delaying the data subtraction until the bias has been calculated.

This simple noncausal bias subtraction processing algorithm is applied to the input data stream. Menu selection 3, Processed Correlation Out, allows setting the peak constant SWTP (typically 0.5-0.8) and the bias constant SWTB (0.05-0.1). These correspond to the equations for PEAK and BIAS as:

$$\begin{aligned}\text{PEAK} &= (1-\text{SWTP}) * \text{PREV\_VALUE} + \text{SWTP} * \text{NEXT\_VALUE} \\ \text{BIAS} &= (1-\text{SWTB}) * \text{PREV\_VALUE} + \text{SWTB} * \text{NEXT\_VALUE} \\ \text{CORRELATION\_OUT} &= \text{PEAK} - \text{BIAS}.\end{aligned}$$

Additional data screening is provided in two glitch filters consisting of:

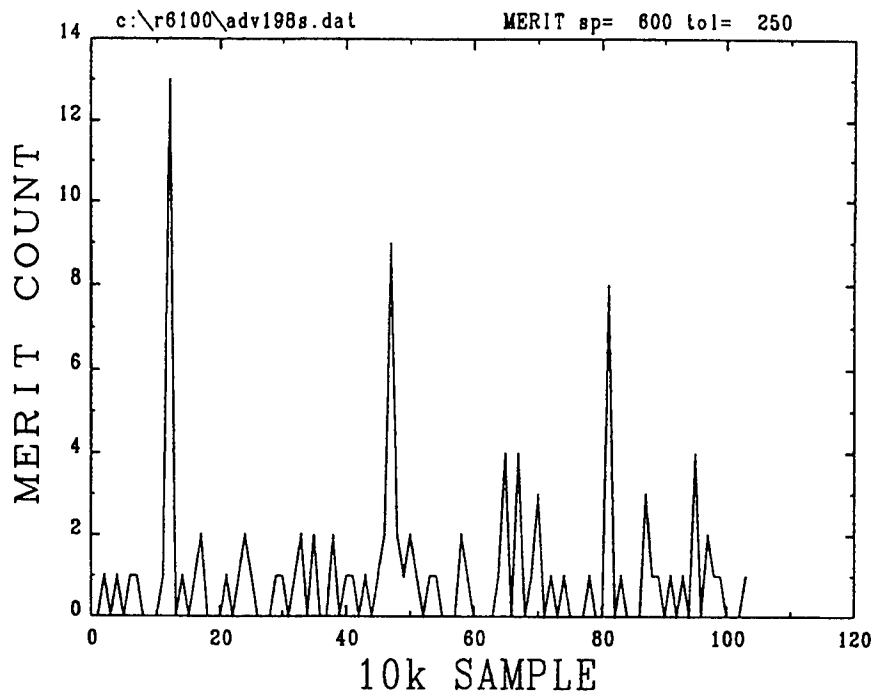
- 1) Sector boundary screen: removes the next 3/SWTB samples whenever BIAS exceeds 200. This removes the saturated sector boundary areas.
- 2) Data dropouts: removes the next 3/SWTP samples whenever consecutive samples exceed half of the data range.

Up to 2048 correlation outputs can be stored. How much of the data is read depends on the correlation output threshold. This is dependent on the condition of data acquisition (typically 20-30 counts and provides a good measure of data quality).

Next, Section 4, RUN Correlation MERIT, scans the identified correlation outputs for their spacings. The operator enters the nominal spacing expected and a tolerance factor. For instance, a pattern with one occurrence per synch region should have a spacing of 570 samples. A pattern which advances one byte per synch would be 18/17 times that, or 604 samples. The data is then tested against the spacing criteria and a count is produced for the number of matching spacings per 10,000 sample increment. Our once per synch region pattern would have 17 matched occurrences if all have been correctly identified. Figure 3.3.2-5 is a sample output indicating the best data region around 10K group 12, or samples 120,000-130,000. Note: there is presently no mechanism in the program to sift sector boundaries nor error correction from the sample areas. Thus, a strong region that includes these may incorrectly indicate a weak output.

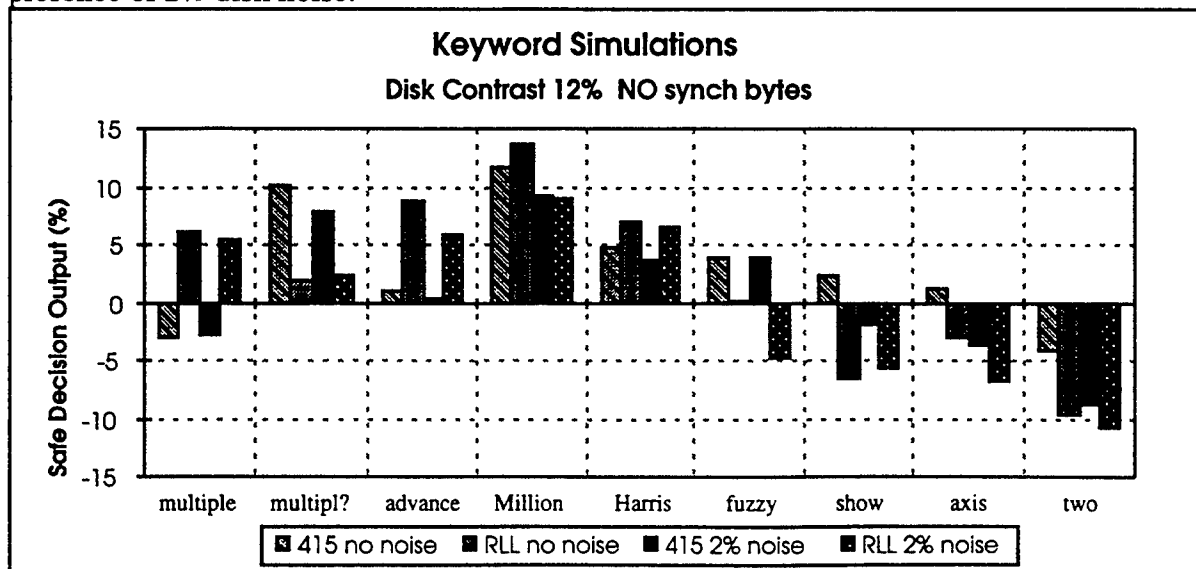
Our correlator simulations were exercised for the target file Oldprop.20 (20,480 characters) in order to estimate baseline text performance and to see if different coding schemes had much of an impact on text discrimination. No synch bytes were included within the data streams. Mask properties are 70-90% transmission and 1/2 to 1% extinction, and disk contrast was set at 12% with a 2% Gaussian noise on the level as an option. Quantization noise is included at 0.1 of a bit level. The bias subtraction is set by using a pair of leaky integrators with peak characteristic 0.75 (SWTP) and bias 0.1 (SWTB).

Figure 3.3.2-6 shows the results of testing several keywords in the above conditions. The outputs indicate the clear region separating a correct word identification from a false output. Thus the word "Million" shows about 10% of the output region as a safe threshold window and the word "two" has false readings overlapping about 5 to 10% of the output window above the



**Figure 3.3.2-5 Processed Correlation Output Example**

true threshold. The RLL code separates "multiplied" from "multiple", and variations on "advance" ("advantage", "enhance", etc.) better than the 4/15 code. This may be due to the non-unique nature of encoding bytes. Whether or not it is desirable to exclude near matches from the identified set is a system use issue. For the shorter keywords, 4/15 maintains a clear window between the true and false outputs. This advantage is eroded at the 4 character words in the presence of 2% disk noise.



**Figure 3.3.2-6 Keyword Discrimination**



These comparisons suggest that system usage influences the encoding choice and media characteristics contribute to the performance with shorter keywords.

Initial breadboard measurements were hindered by poor signal to noise ratio in the output. To ease alignment constraints during preliminary testing, we replaced the breadboard PIN detector with a CCD array. This allowed us to integrate along the data rows and display the CCD array across the disk tracks (see Figure 3.3.2-7). We "rigged" the data pattern with Hex"FF" characters to produce the repetitive code sequence 1000. For these doubled mark lengths this produces two channel bits 'dark' followed by two channel bits 'light' (1100). Correlating this data pattern against a matching mask results in alternating maximum and minimum correlations. Figure 3.3.2-8 shows a full frame display of the disc pattern when overlaid with the Hex"FF" mask. Along the time axis the first level displayed at 3.5 volts represents the dark reference (mask taped along data direction). This is followed by a bright space (no bars) at -1.6 volts. Across the mask region, levels are approximately 50% of the bright reference indicating the mask pattern is passing 50% of the incident light. The small ripple (200mv peak to peak) indicates alternating data rows with brighter track boundaries. The bump at 1.21ms is a dirt spot on the cylinder collection lens. From this curve we read an available full light swing of 5 volts for no mask and about 3 volts for the brightest illumination region between 1.2 and 1.25ms through the striped area. This area is used to evaluate the correlated output.

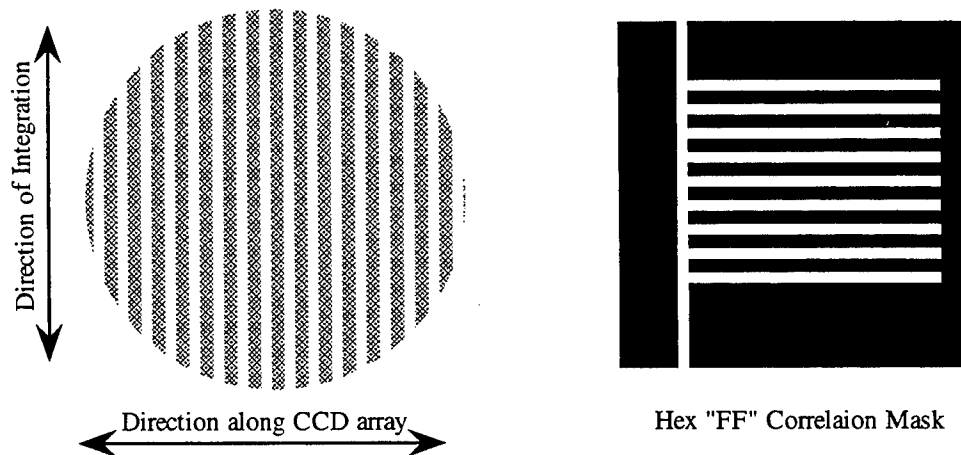


**Figure 3.3.2-7 Disk Orientation with respect to the test pattern and CCD array**

Figure 3.3.2-9 shows the first data runs for the correlation evaluation. The upper panel is six randomly timed, successive frames with the disk in a stationary condition (STILL). Each peak corresponds to a data track; each valley corresponds to the area between tracks. This run was acquired through the correlation mask and a peak may or may not be synchronized with a correlation peak. In the ROCK frame, the disk is moved slightly to cause the successive acquisitions to vary their alignment with the correlation condition. There is more variation in the outputs; this may be due either to the desired correlation deviation or just the motion itself. SU

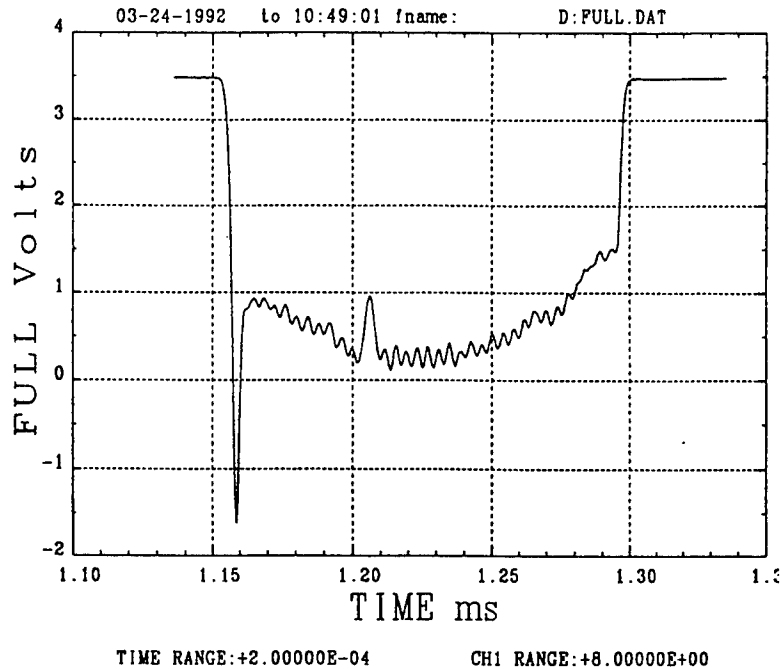


**Figure 3.3.2-8 Full CCD scan through the mask**

(Subsequent data will be presented without the mask to show that this motion is not a primary effect). The correlation outputs vary at the rate of bit procession through the mask grating. We rotate one step, at the rate of two steps per second. There are 2000 steps per revolution. We were scanning an outer track of 32 sectors, with about 1360 bytes/sector. The "FF" pattern produces 4 cycles of mark/clear per byte. Our data extent per ROCK is then:

$$\frac{\text{sectors} * \text{bytes} * \text{cycles}}{\text{steps/rev}} = \frac{32 * 1360 * 4}{2000} = 87 \text{ peaks}$$

At 2 steps/sec we have about 180 peaks per second or a period time of 5.5ms. The CCD array integrates for 1ms and is able to resolve a correlation peak by strobing the correlation output. The array output is recovered through a differential amplifier where the CCD output is DC offset and lowpass filtered at 300KHz. This output is then captured with an HP digital scope with line acquisition through an IEEE 488 interface.

The sequential line scans are processed and the appropriate statistics calculated. The 'row-statistics' processing subroutine extracts peak heights above their average neighbor valley levels. An example of this data is presented in Table 3.3.2-1. S1-S6 are the sequential line acquisitions. X is the relative scan time of an acquisition and serves as an indicator of which peak is examined. For example, consider the peak at X=3.25 for Run A. The runs in the STILL case vary from 0.19 to 0.24 volts (EXT calculates the extremes = 0.05). In the ROCKed condition the same set of peaks varied from 0.23 to 0.32 (EXT = 0.10 after roundoff). Nearly every peak showed a greater variation during ROCKing indicating a larger correlation output

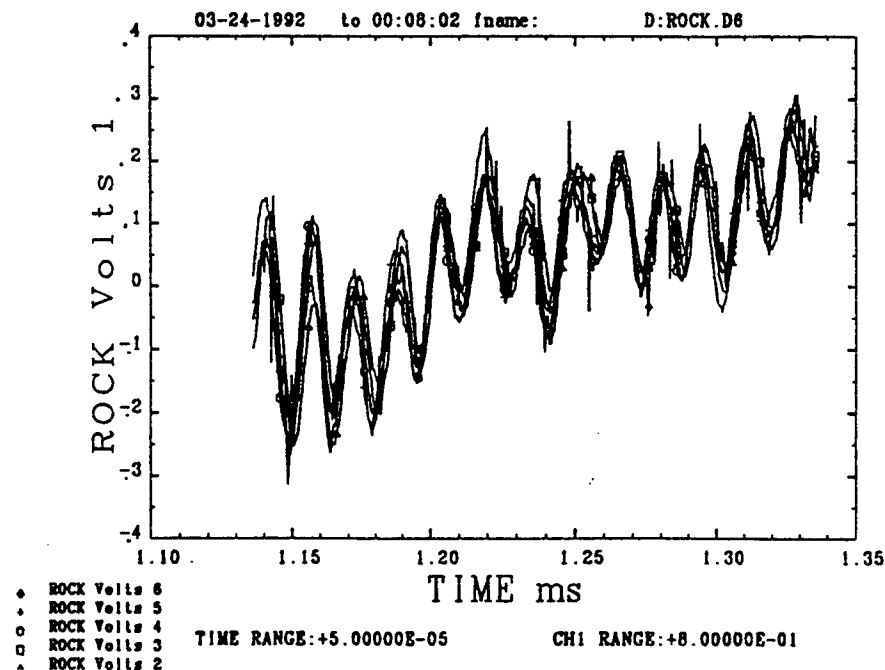
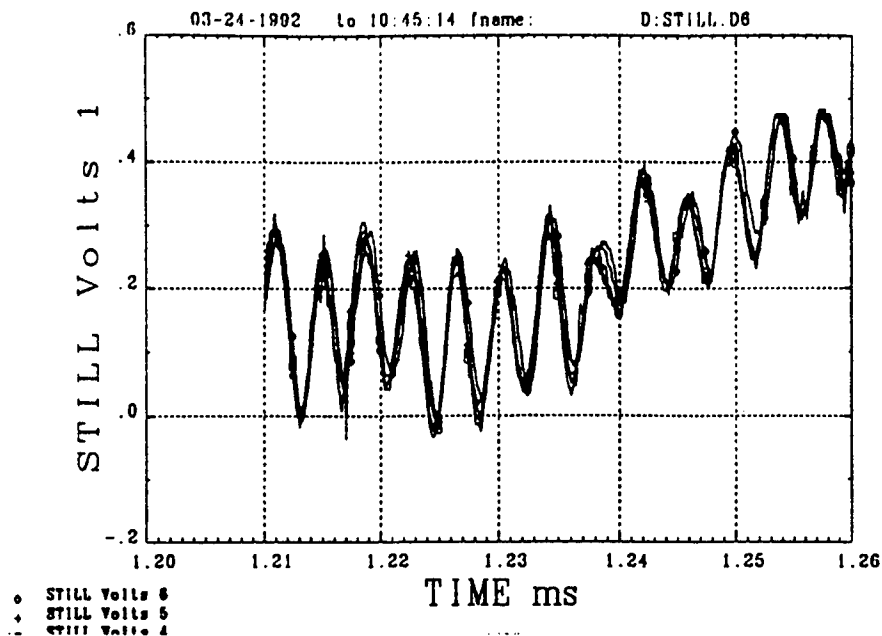


**Figure 3.3.2-9 Correlation data region Run A, through the mask**

range. The average EXT difference increased from 27mv to 56mv. The mask was removed and the data retaken to examine motion only as an effect. Correlation peaks should not change, as no mask is present to obscure disk bits. The light level was decreased to produce a comparable output for 'mask installed' case. For this case, the STILL and ROCKing sets were both at 32mV average peak to valley. The mask was reinserted and another data set taken. The resulting

averages were 31mV STILL and 79mV ROCKing. Figure 3.3.2-10 plots each set in histogram format. Run A and Run B show an extended range of output when ROCKed. The 'no mask' condition shows less difference between the ranges in the STILL and ROCKed cases.

**Table 3.3.2-1 An Example of Statistics from a set of correlation outputs**

**(Run A with MASK - Peak to Valley Statistics)**

03-24-1992 to 10:45:14 fname: D:STILL.D6

1992 3 M25D

TIME RANGE:+5.00000E-05 CH1 RANGE:+8.00000E-01

X AXIS MINs

avg	@std	X	S1	S2	S3	S4	S5	S6	EXT
0.22	0.015	3.25	0.23	0.19	0.21	0.23	0.24	0.22	0.05
0.23	0.013	6.80	0.22	0.25	0.25	0.24	0.22	0.22	0.03
0.22	0.009	11.05	0.22	0.23	0.20	0.22	0.23	0.22	0.03
0.25	0.009	14.80	0.25	0.25	0.27	0.24	0.25	0.24	0.03
0.20	0.006	18.60	0.21	0.19	0.20	0.21	0.21	0.21	0.02
0.25	0.012	22.55	0.26	0.24	0.24	0.23	0.25	0.25	0.03
0.14	0.008	26.40	0.15	0.14	0.14	0.12	0.13	0.14	0.02
0.19	0.009	30.30	0.20	0.20	0.18	0.21	0.19	0.19	0.03
0.13	0.004	34.35	0.13	0.13	0.14	0.13	0.14	0.14	0.01
0.19	0.010	37.90	0.18	0.20	0.19	0.17	0.19	0.18	0.03
0.19	0.008	41.95	0.18	0.19	0.18	0.20	0.19	0.17	0.03
		45.90			0.14				
0.20	0.009	AVE	0.203	0.200	0.199	0.200	0.203	0.199	0.027
0.04	0.003	STD	0.039	0.039	0.039	0.040	0.040	0.037	0.009
		EXT	0.13	0.13	0.13	0.12	0.12	0.12	
		EXT AVE	0.125						
		EXT STD	0.006						

03-24-1992 to 00:07:29 fname: D:ROCK.D2

1992 3 M25D

TIME RANGE:+5.00000E-05 CH1 RANGE:+8.00000E-01

avg	@std	X	R1	R2	R3	R4	R5	R6	EXT
0.22	0.033	3.20	0.28	0.23	0.27	0.33	0.26	0.32	0.10
0.19	0.018	7.20	0.21	0.21	0.17	0.21	0.19	0.17	0.04
0.19	0.031	10.90	0.14	0.21	0.21	0.17	0.24	0.17	0.09
0.20	0.015	14.92	0.20	0.21	0.19	0.21	0.23	0.19	0.04
0.20	0.018	18.75	0.22	0.20	0.17	0.21	0.19	0.18	0.05
0.15	0.019	22.85	0.16	0.19		0.14	0.14	0.13	0.05
0.17	0.020	26.40	0.15	0.15	0.16	0.20	0.17	0.19	0.05
0.16	0.020	30.35	0.17	0.14	0.16	0.19	0.15	0.19	0.05
0.15	0.009	34.40	0.16	0.15	0.14	0.16	0.16	0.15	0.03
0.18	0.021	37.90	0.18	0.20	0.14	0.20	0.19	0.19	0.06
0.20	0.015	41.75	0.20	0.19	0.22	0.22	0.19	0.21	0.04
		45.85							
0.19	0.020	AVE	0.188	0.189	0.182	0.205	0.192	0.191	0.056
0.04	0.003	STD	0.039	0.028	0.039	0.045	0.036	0.044	0.021
		EXT	0.14	0.09	0.14	0.18	0.12	0.18	
		EXT AVE	0.141						
		EXT STD	0.033						

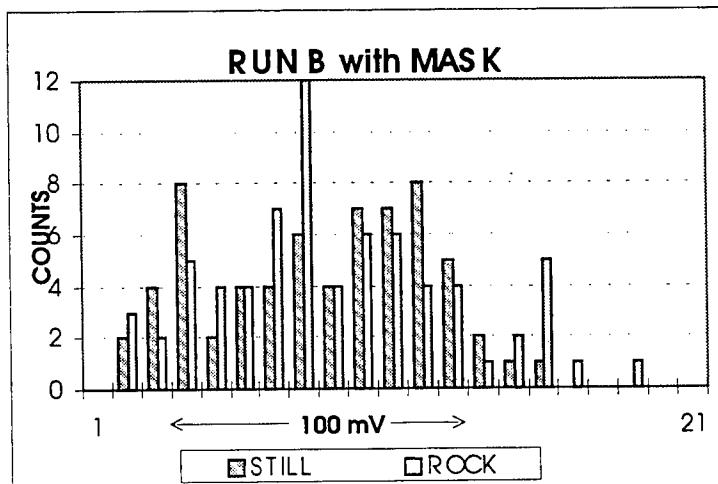
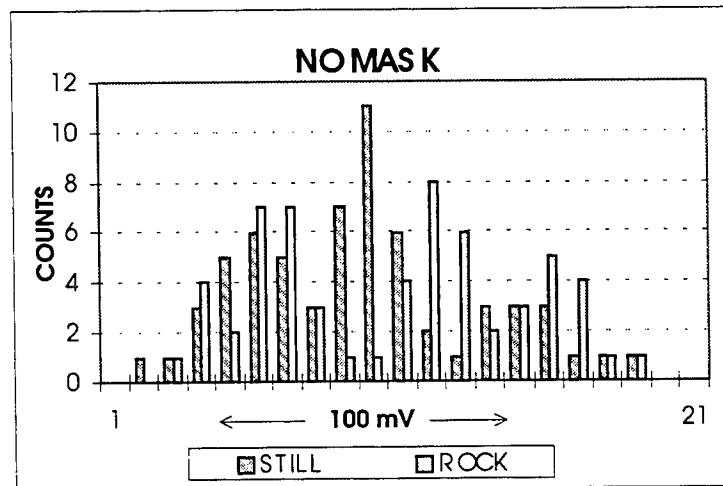
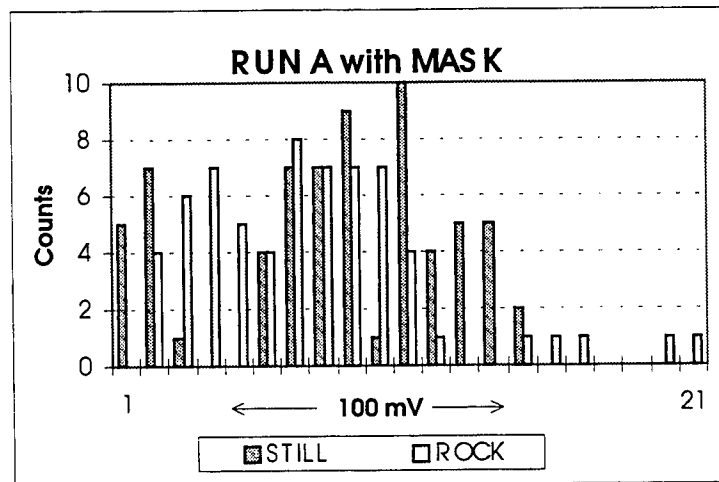


**Figure 3.3.2-10 Correlation Output Histograms**

Quantifying the correlation is more difficult to do than merely establishing its presence. Even in the STILL frame case the data may be in and out of correlation with varying track location (the tracks are not coherently aligned). The standard deviation per peak, summarized in Table 3.3.2-2 across the sequential row samples may give the best indication of what is happening.

**Table 3.2.2-2 Standard Deviation in the Correlation Peaks**

	STILL Deviation	ROCKED Deviation
Run A with the mask	9mV	20mV
With no mask	15mV	11mV
Run B with the mask	11mV	26mV

Run B suggests a correlation difference on the order of 13mV which is about 6.5% of our 200mV average peak to valley level. This agrees well with the ripple to peak ratio for the full frame scan of  $200\text{mV}/3\text{v} = 6.7\%$  (see Figure 3.3.2-7). A stronger correlation output calibration is desirable. We continued evaluating the breadboard performance to determine where improvements could be made. The breadboard was modified by installing a collimator for the super luminescent diode and replacing the beam splitters. These changes resulted in a cleaner image on the camera monitor. We took some image frame grabs off the phase change disk, the Great Books CD ROM, and the Glenn Miller CD ROM. The row statistics subroutine was used to process the frame data. Rows with excessive level standard deviation are excluded from the contrast averaging. The results are summarized in the table below.

**Table 3.3.2-3 Breadboard Contrast Measurements**

Disk type	Average Contrast	Dark level STD	Bright level STD
phase change - frame 1	11.9 %	0.030	0.030
phase change - frame FF	12.4 %	0.036	0.037
Great Books CD ROM	19.8 %	0.042	0.053
Glenn Miller CD ROM	25.8 %	0.068	0.070

Several different data regions were examined on the phase change disk. Figure 3.3.2-11 shows two rows from a Hex"FF" region with a resynch byte in the center of the pattern. The brightness levels within the resynch byte do not seem to vary from the surrounding data bits. Observations of previous Hex"FF" correlation outputs showed about 10 times the PIN voltage swing in the resynch region relative to the data region outputs; simulation does not agree with this. The discrepancy may have been due to misalignment. A realignment produced data output levels equal to the resynch levels observed on the first but resynch outputs at the second alignment were not recorded at a good resolution. Inspection of a sector scan shows that they may be no greater than the data outputs.

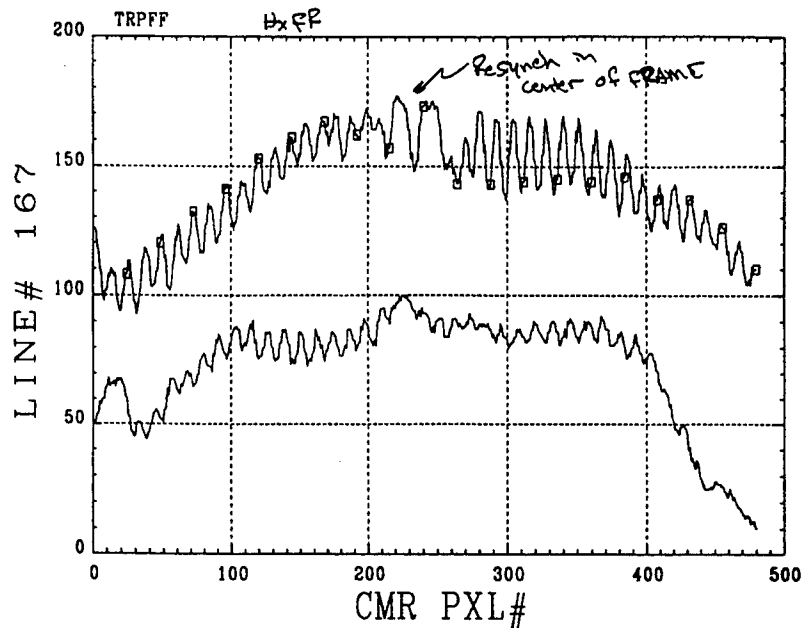


**Figure 3.3.2-11 Data scan including resynch bytes**

Figure 3.3.2-12 shows scans from data pattern spacing extremes. Sequential bytes of Hex"CC" and Hex"D2" produce the RLL(2,7) extremes of marks separated by the minimum of 2 and the maximum of 7 spaces. The simulation bit marks are overlaid on the scan. Note the wide spaced marks produce about twice the level swing as the narrow spaced marks. This is not presently incorporated in the simulation. It is caused by the setup varying MTF for the image regions and is an important design parameter for both the objective lens procurement and the development of an optimum custom code.

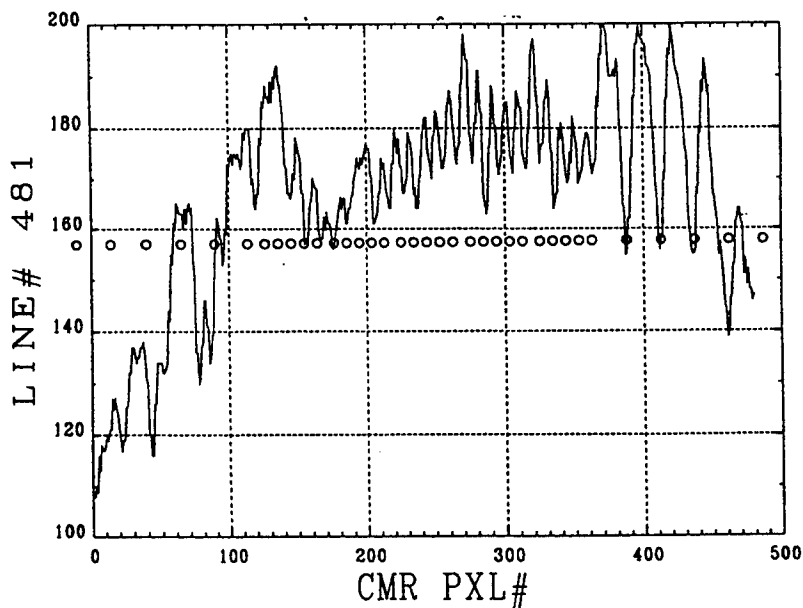


**Figure 3.3.2-12 Scans of extreme data patterns**

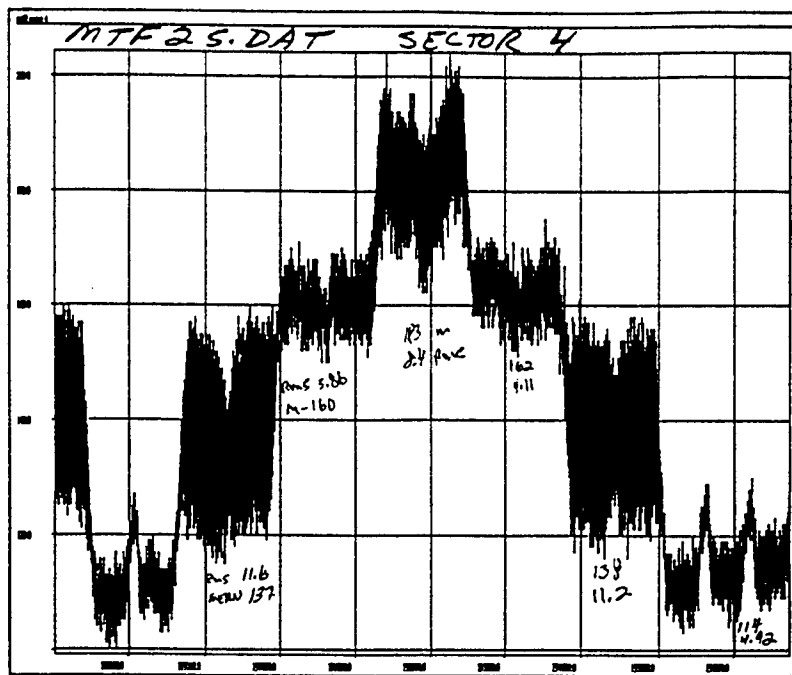
Based on the previous results we investigated the MTF of the breadboard optics. We used the RLL(2,7) code to generate patterns that are pseudo gratings, where a single mark is spaced by differing dark bit periods. The darkest pattern (the lowest responses) is coded with the letter "K". This produces a data sequenced with spaces of lengths 2-2-2-2-3. Because the size of the written marks of an optical disk are twice the bit spacing, this data pattern generates a recorded pattern of 1-1-1-1-2 spaces. The next region is split between "s" which produces 4-4-5 spaces and "@", 5-5-3 spaces. These both average a data spacing of 4.3 which narrows to 3.3 as written on the disk. The brightest output is "f" where the maximum code space length of 7 is used (again 6 as written of the disk). The periodic narrow pulses within the pattern outputs are the resynch bytes. They are brighter than the darkest pattern and darker than the brightest pattern.

Figure 3.3.2-13 shows good visual agreement between measured data and simulation for the calibration pattern. The simulation used a simple traveling 3 point average. Uniform weighting is used with each bit level replaced by the intensity average of itself with its two nearest neighbors. Figure 3.3.2-14 contains variations producing harsher intensity degradations. The upper panel is a 5 point average. The lower panel reaverages the simple 3 point, with a second pass producing a linear taper across 5 points. These both show more high frequency response loss than is observed in the data of Figure 3.3.2-13.

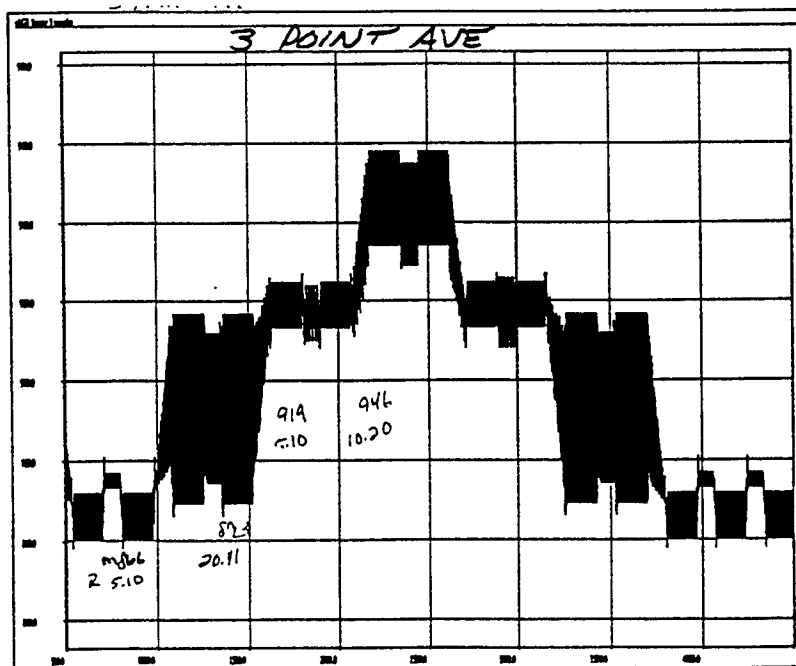
Four data sets were captured: MTFxS.DAT ( $x = 1,4$ ). These were taken with the focal servo on and tracking disabled. The best regions of the data sets repeat fairly well.

Our best observed data runs do not quite match the chosen simulation for nonrepetitive patterns. The two character pattern "ha" (Figure 3.3.2-15) still shows a strong resemblance to the simulation. The measured data are in the left panels; the simulations are in the right panels. The upper pair include bias subtraction processing, the lower pair show raw data. There are eight correlation outputs between resynch bytes. The peak to false output ratio is about two as referenced to the signal bias. A longer pattern, representative of a typical user word, appears to lose peak output relative to the bias swings. Figure 3.3.2-16 shows data using the keyword "Harris". The unprocessed simulation shows the peak output climb to about 80% of the bias swing in the extreme data regions. The measured response approaches only about 50%. At this time we attribute the loss to scaling error. A nonrepetitive pattern loses accumulation if a bit is slipped over its extent. A repetitive pattern is much less subject to loss since a bit difference can alias and recover some output by matching another pattern region.





MEASURED



SIMULATED

Figure 3.3.2-13 MTF calibration pattern

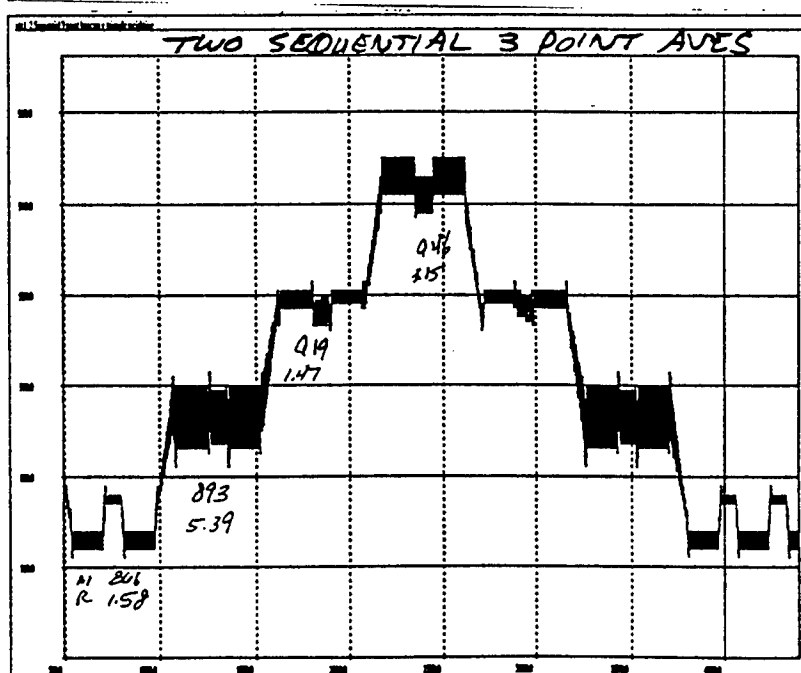
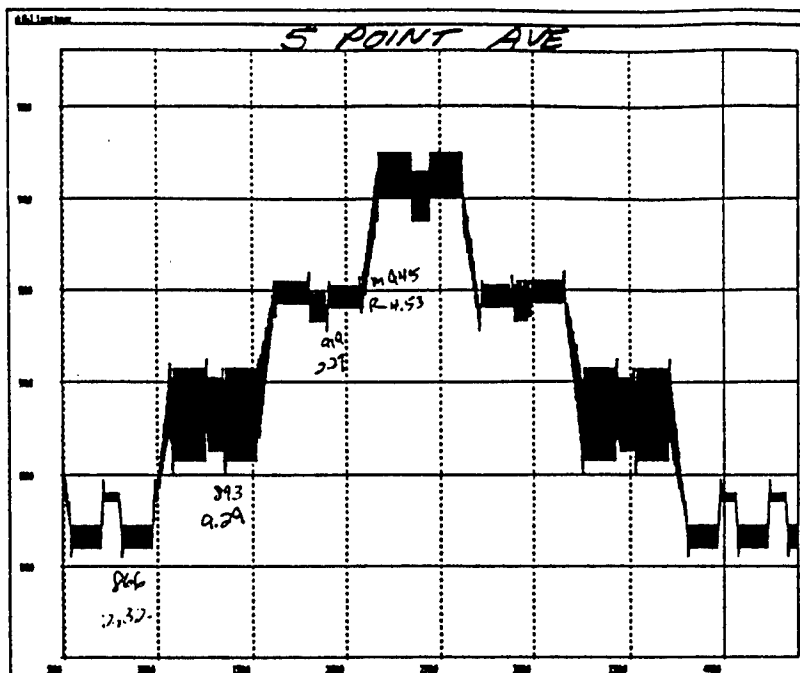
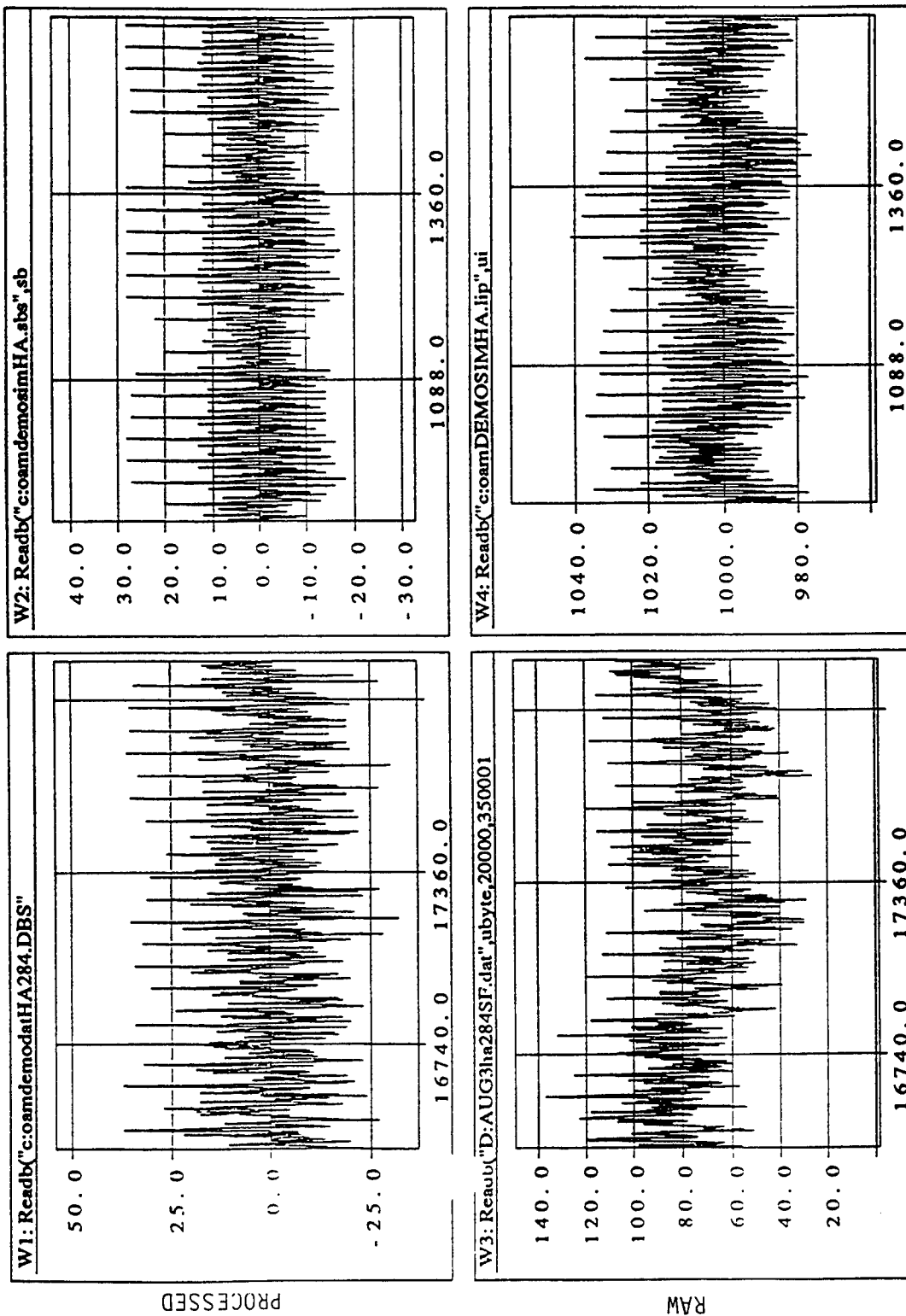


Figure 3.3.2-14 Alternative MTF simulations



MEASURED

SIMULATED

Figure 3.3.2-15 Two character repetitive pattern

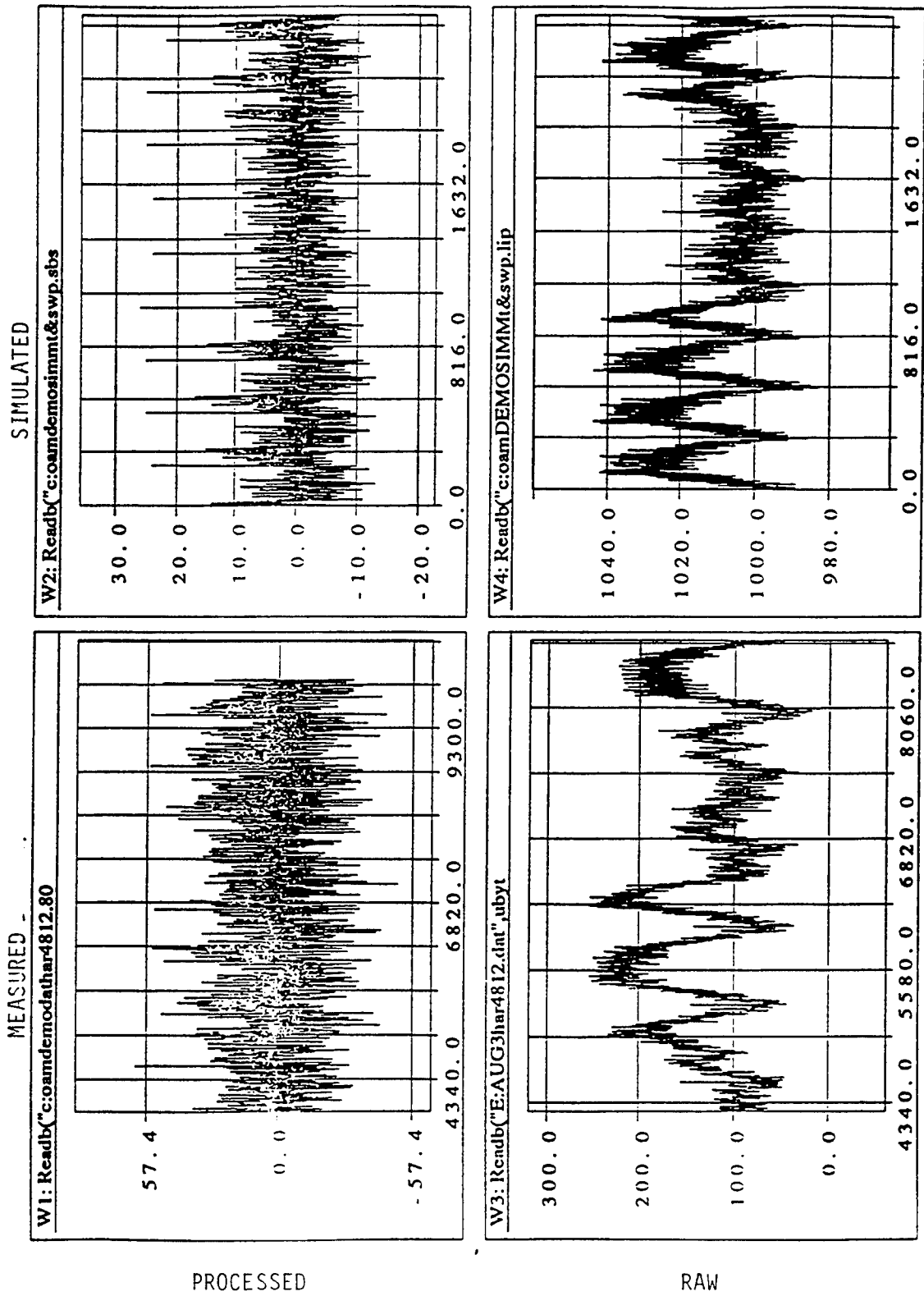


Figure 3.3.2-16 Keyword "Harris"

Since the three bit average used for MTF simulations does not provide a good match to observed data with the same scaling coefficient across varying patterns, a less efficient algorithm using an exponential weighted envelope of the  $\pm 5$  nearest neighbors at each channel bit sample was tested and did a much better job. Figure 3.3.2-17 compares patterns measured on the breadboard with simulations using the exponential average. Figure 3.3.2-18 provides an explanation for this numerical fit in terms of physical mechanisms that contribute to the image smear. The exponential fit is plotted at the points sampled with the boxes. Two Gaussian profiles that represent the effects of image broadening plus a background fogging with a wider view are line plotted. These are summed in the dark line plot which shows good agreement at the exponential envelope samples.

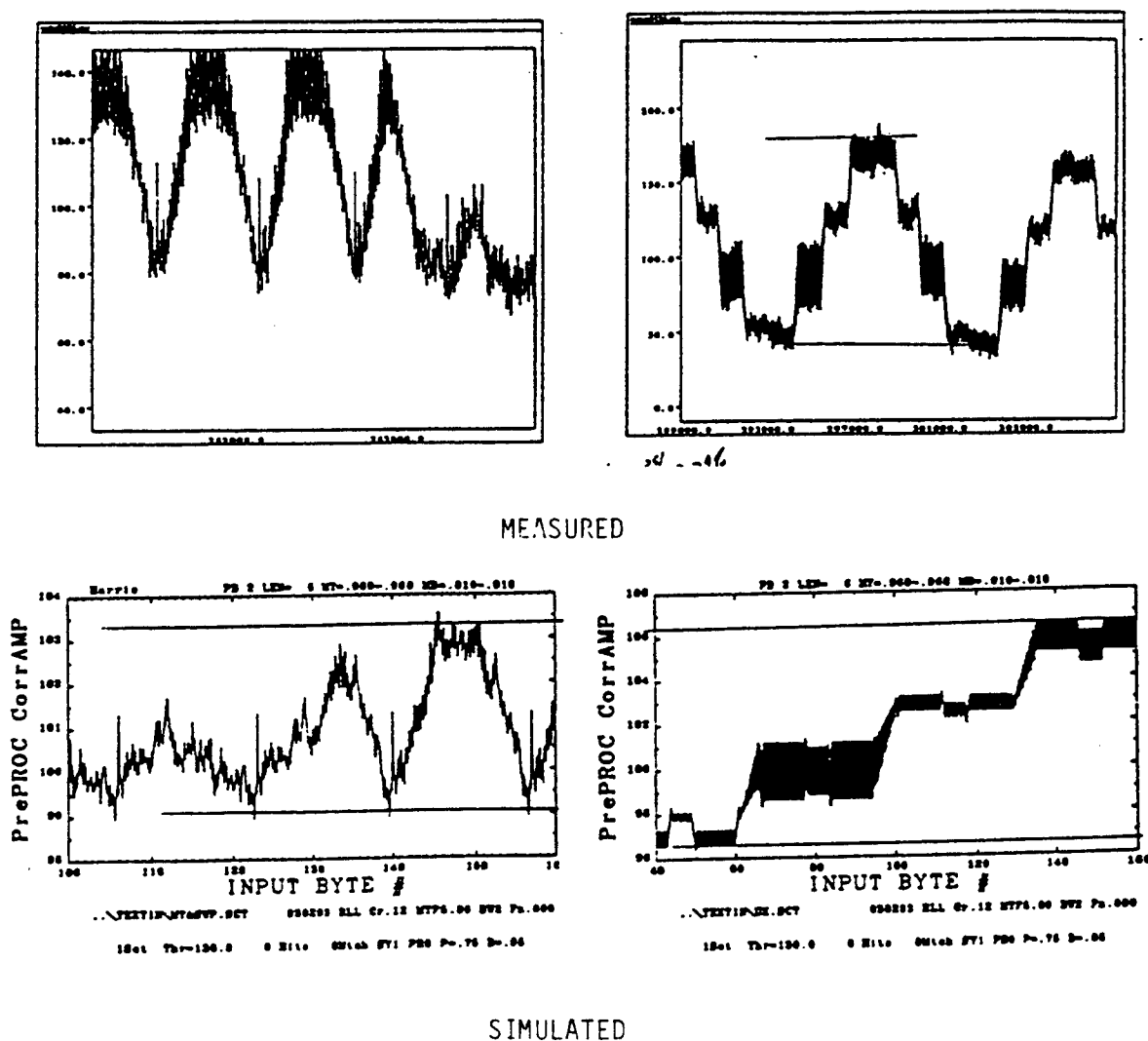
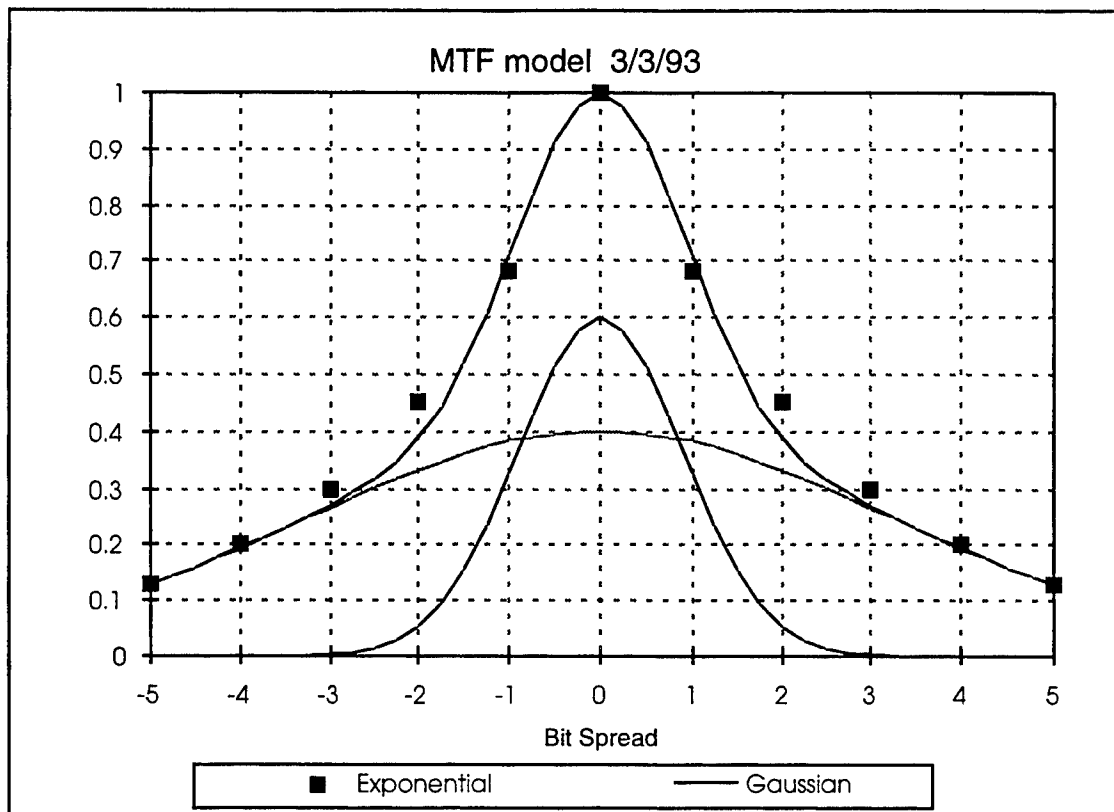


Figure 3.3.2-17 Comparison of Simulated MTF with Measured MTF



**Figure 3.3.2-18 Exponential MTF Model Contributors**

Some keywords were scanned with our sample text database, OLDPROP.20. Table 3.3.2-4 lists the correlation output statistics. The item of merit is the Safe Range. For comparison, the old three bit average MTF model is penciled in under the current model results. The RLL includes bias subtraction processing (not the more aggressive matched filter). As indicated in the custom code discussion, the 24 bit code performs better, as is readily observed for the keyword "fuzzy". This performance may be further improved if the code is "retuned" for the present MTF model. The exponential MTF model was assumed in later analyses. We next investigated the effect of scaling errors.

Disk scaling errors that accumulate across the correlation field significantly lower the correlation output. If there is a 1% scaling error between the query pattern in the SLM and the image of the disk at the SLM plane, then an image in perfect alignment at the beginning of the mask will be 1 bit out of alignment with respect to the mask after 100 bits. Figure 3.3.2-19a shows a simulation of our breadboard format with the keyword "Harris". With errors of  $\pm 1\%$ , the correlation peaks are decreased by about 10% (half their level above the false output). With errors of  $\pm 2\%$  the output falls off to the background level which is at 80% of maximum (solid line). The dashed line shows where the maximum occurs relative to the pattern alignment. When it departs from a slow pulling from the 0 offset level, the maximum output has occurred at a false correlation. The "U" pattern, shown in Figure 3.3.2-19b, is a phase shifted equivalent of

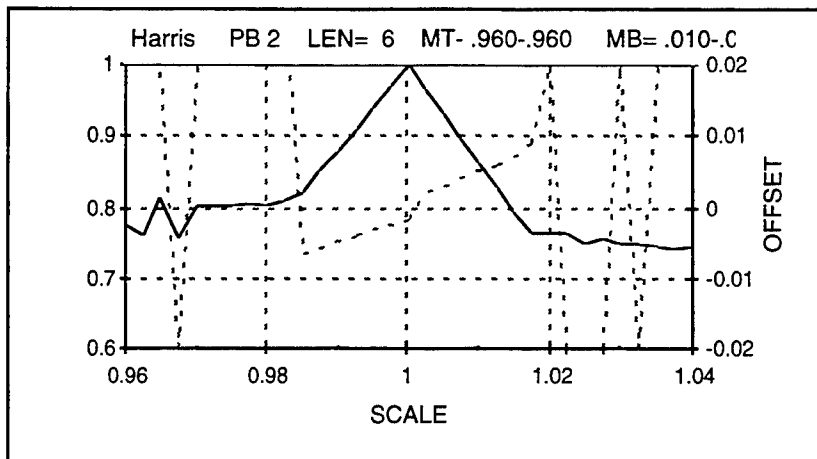
**Table 3.3.2-4 Correlation Statistics using Exponential MTF Model**

RLL Code MTF=5.0		Mar 2, 1993 20SCT SYO PR1 P=.90 B=.10		
Parameter	advance	Harris	fuzzy	axis
Present	3	9	5	3
Total for TRUE	3	9	>300	700
Safe Range	0.4%	5.8%	-10%	-15%
Safe Range for 3 bit MTF	8.7	7.1	0.25	-3%
LOW TRUE	1.29	1.36	<1.2	1.16
HIGH FALSE	1.28	1.23	1.4	
LOW FALSE	-1.02	-1.02	-1.35	-1.54
Delta Range	2.30	2.25	2.75	3.19

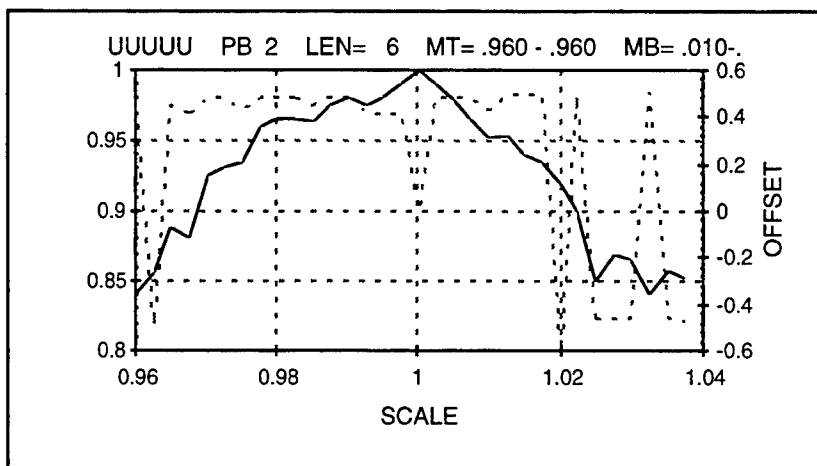
Custom Code with 16 bit mapping per ASCII character MTF=5.0		Mar 2, 1993 20SCT SYO PR1 P=.90 B=.10		
Parameter	advance	Harris	fuzzy	axis
Present	3	9	5	3
Total for TRUE	3	9	21	2000
Safe Range	4.1%	8.4%	-10%	-22%
Safe Range for 3 bit MTF			5.3%	
LOW TRUE	100.69	100.97	100.67	99.86
HIGH FALSE	100.47	100.51	101.38	101.51
LOW FALSE	95.05	95.05	94?	94.15
Delta Range	5.42	5.46	7	7.36

Custom Code with 24 bit mapping per ASCII character MTF=5.0		Mar 2, 1993 20SCT SYO PR1 P=.90 B=.10		
Parameter	advance	Harris	fuzzy	axis
Present	3	9	5	3
Total for TRUE	3	9	5	5
Safe Range	5.1%	5.0%	6.9%	-1.5%
Safe Range for 3 bit MTF			17.5%	
LOW TRUE	102.13	103.18	103.60	102.68
HIGH FALSE	101.86	102.83	103.08	102.78
LOW FALSE	96.55	95.80	95.50	95.95
Delta Range	5.31	7.03	7.58	6.83

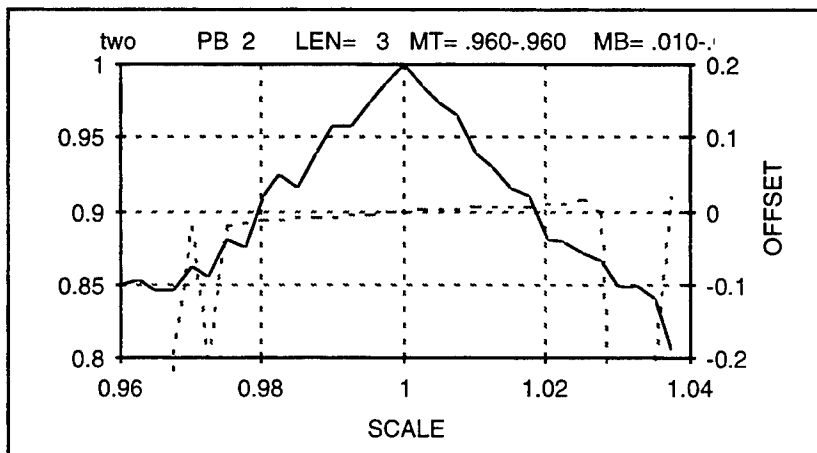
our Hex"FF". Its maximum output decreases much slower than the randomized "Harris" pattern but the offset indicates that false correlations (aliases of the pattern regularity) make correct identification difficult. Using the three letter keyword "two" shows a more discernible pattern output. This should maintain outputs at  $\pm 2\%$  errors that still track the correct alignment.



3.3.2-19a



3.3.2-19b



3.3.2-19c

Figure 3.3.2-19 Simulations of scaling errors



A series of CCD frame grabs was taken to establish the breadboard disk bit placement error: four patterns taken around a track, four patterns within a zone across tracks, and four patterns in different zones. The frame grab digitized intensity to 256 levels at a resolution of about 9 pixels per  $\mu\text{m}$  (magnified from the disk image). The field is 800 pixels across the tracks and 480 along a track. The data from the outer 150 pixels of the 800 pixel width is not processed. The data is first transposed to an effective width of 480 x 500. The upper panel of Figure 3.3.2-20 shows a typical data row. The lower panel illustrates a 1024 point FFT done in the along track direction. This quantizes to periods of  $1024/(I-1)$ . Points 60, 61, 62 correspond to periods of 17.36, 17.07, and 16.79, an increment of about 1.7%. The FFT magnitude point (typically 58-62) is stored for each of the 500 data rows. The results were averaged based on interpreting the peak magnitude detected as indicative of the position of the camera scan in relation to the disk mark row as defined by the grooves between the rows.

Various combinations of averaging groups of frames are tabulated in Table 3.3.2-4. Runs 1-4 are taken at 300 step intervals around the disk from nominally the same track (2000 steps per revolution). The data ranges in period from 16.231 to 16.592 (total excursion 2.2%). The fractional error of 0.8% gives some output as the disk turns. The camera was rescaled between runs 1-4 and runs 11-17. Runs 11-14 step across a zone at the same rotation location. The extent is 16.442 to 16.750 (1.9%). The smallest difference was the last set, runs 11 & 15-17, taken at the same rotation location and relative zone location at different zones. The extent is 16.675-16.790 (0.7%). This indicates that we can align the system based on the scaling in a reference zone and the scaling will hold in other disk locations. However, outputs may vary around the disk due to local scaling errors.

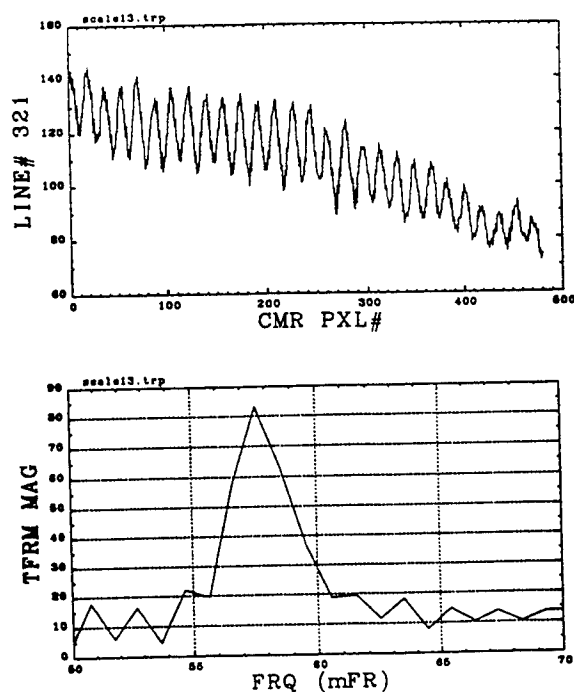


Figure 3.3.2-20 Analysis of measurements from frame grab data

**Table 3.3.2-4 Averages from Frame Grab Measurements**

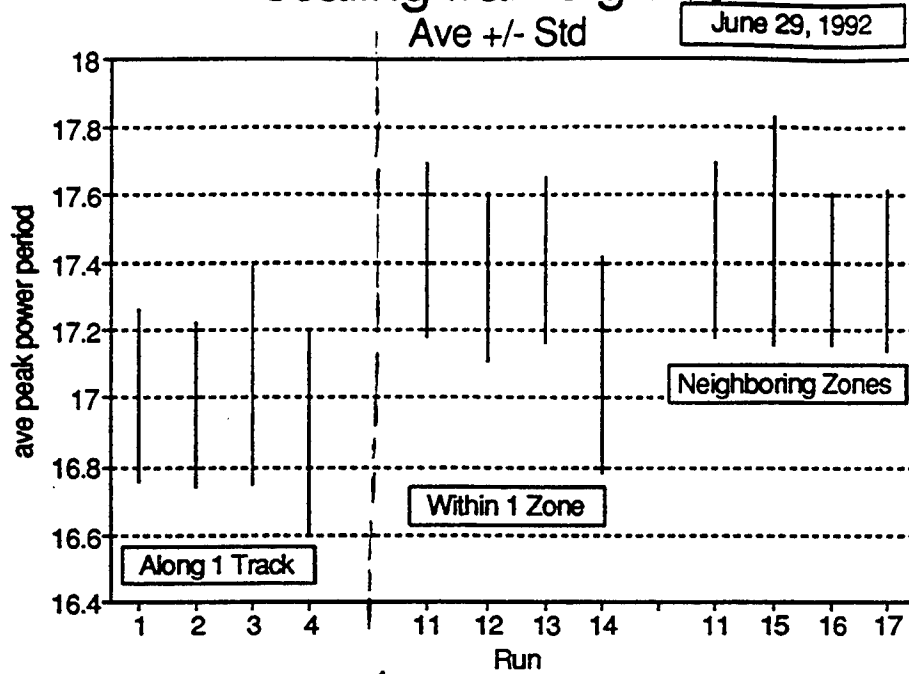
Fname	Results			Pixel spacing			
	ave	cm ave	bd ave	wt ave	cm wtd	bds wtd	
SCALE1.TRP	16.359	16.369	16.287	16.377	16.388	16.287	<b>Along a Track</b>
SCALE2.TRP	16.592	16.589	16.504	16.592	16.592	16.504	
SCALE3.TRP	16.385	16.372	16.442	16.369	16.369	16.442	
SCALE4.TRP	16.231	16.242	16.305	16.221	16.228	16.305	
	16.3918	16.393	16.385	16.39	16.394	16.385	Average
	0.12946	0.1249	0.0916	0.1324	0.1297	0.0916	Standard Deviation
	0.008	0.008	0.006	0.008	0.008	0.006	Fractional Error
SCALE11.TRP	16.750	16.756	16.753	16.764	16.770	16.753	<b>Across a Zone</b>
SCALE12.TRP	16.667	16.658	16.700	16.667	16.661	16.697	
SCALE13.TRP	16.725	16.717	16.745	16.722	16.714	16.745	
SCALE14.TRP	16.442	16.453	16.393	16.466	16.477	16.393	
	16.6461	16.646	16.648	16.655	16.656	16.647	Average
	0.12169	0.1168	0.1483	0.1143	0.11	0.148	Standard Deviation
	0.007	0.007	0.009	0.007	0.007	0.009	Fractional Error
SCALE11.TRP	16.750	16.756	16.753	16.764	16.770	16.753	<b>Different Zones</b>
SCALE15.TRP	16.790	16.807	16.841	16.784	16.795	16.838	
SCALE16.TRP	16.675	16.689	16.598	16.683	16.692	16.598	
SCALE17.TRP	16.694	16.686	16.708	16.689	16.683	16.708	
	16.7274	16.734	16.725	16.73	16.735	16.724	Average
	0.04542	0.0502	0.0876	0.0447	0.0485	0.0867	Standard Deviation
	0.003	0.003	0.005	0.003	0.003	0.005	Fractional Error

The FFT analysis was limited to less than 1.7% due to the granularity of the FFT. To improve this the data was reexamined using a DFT. This allows finer resolution on the period spacing. Figure 3.3.2-21 shows a typical frame peak scatter across the image rows. The average and standard deviation for each frame are computed and presented in the upper panel of the figure. The standard deviation of each frame is about 1%, which is at the limit of our correlation output tolerance. At 1% error, scaling may be causing some degradation in correlation output.

### 3.3.3 Optical Correlator Breadboard Results

A selection of 28 words was simulated with 8% contrast and 0.5% noise as disk intensity parameters. We selected 8 words for comparing different system configurations and for demonstrations. The data configuration is RLL(2,7) with synchronization bytes included (equivalent to the Panasonic optical disk). The selected words were limited to a maximum length of 8 characters because the breadboard SLM, a COTS unit, was only 128 bits long. Table 3.3.3-1 summarizes the results with the candidate words (multiple, advance, Million, Harris, fuzzy, show, axis, and two) highlighted. The difference between the number of keywords present and found is caused by synch bytes splintering the text on the disk. Examination of the data shows that there is no separation in correlation populations (the highest false exceeds the lowest true) for keywords of less than 4 characters.

# scaling frame grabs



← / →  
Camera  
Rescaled

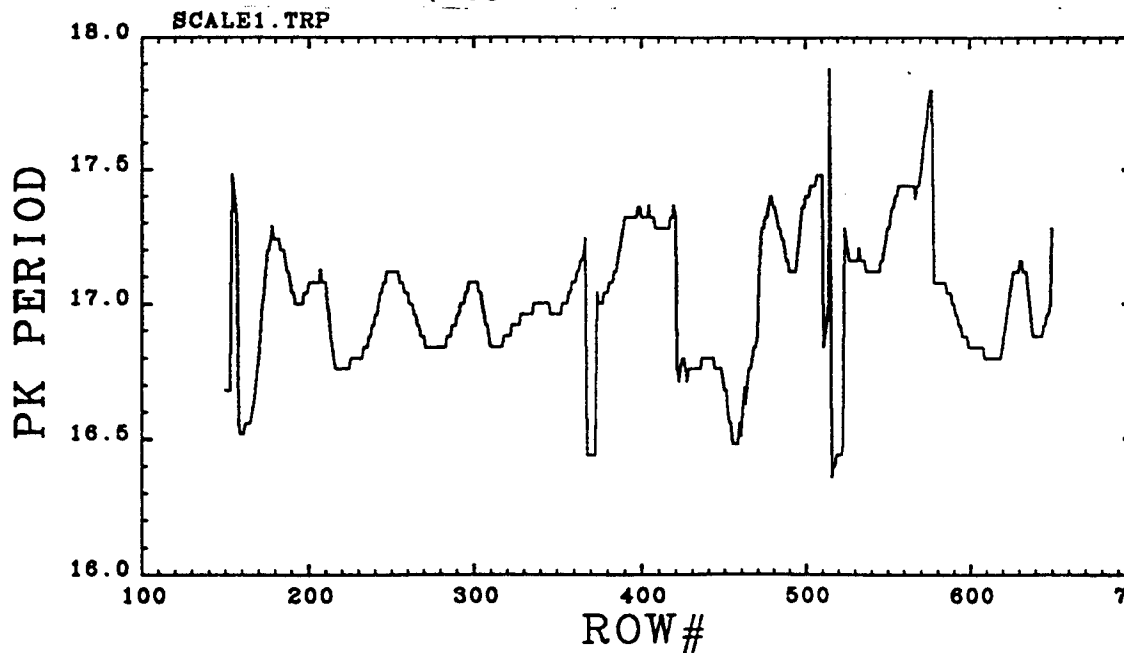
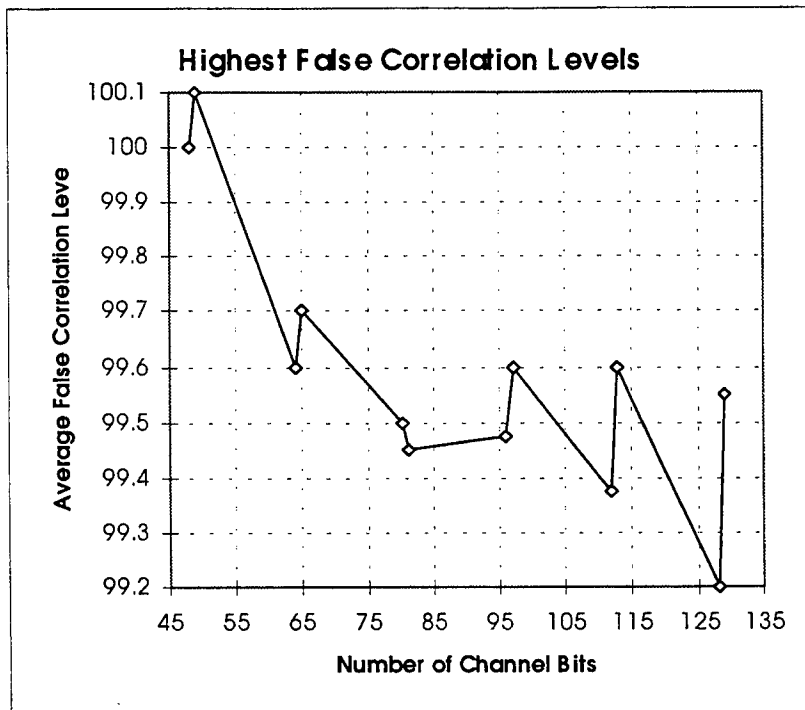


Figure 3.3.2-21 DFT analysis of Frame Grab Data

**Table 3.3.3-1 Correlation Model Results**

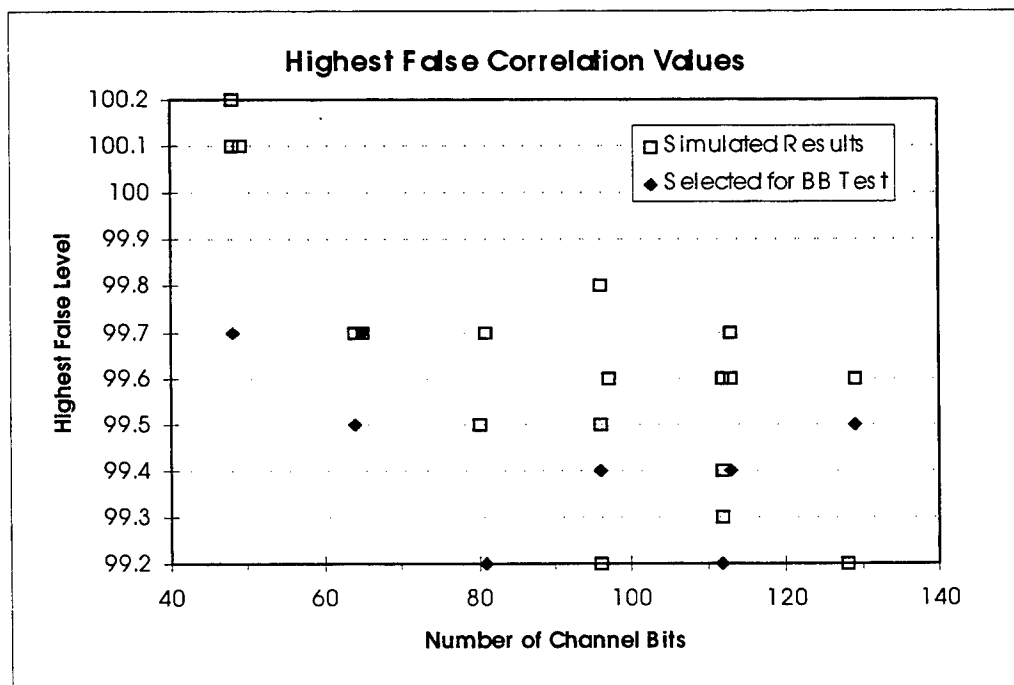
Keyword	ON bits	Marks	KW Present	KW Found	Low TRUE	High FALSE	Hits for TRUE	CH bits	PCT light
multiple	71	29	4	3	99.9	99.5		129	0.550
altitude	71	29	5	3	99.9	99.6	3	129	0.550
aircraft	70	29	4	1	100	99.2		128	0.547
propose	67	23	4	4	99.9	99.7	4	113	0.593
advance	65	24	3	2	99.9	99.4	2	113	0.575
digital	61	26	2	2	100	99.6	2	113	0.540
warfare	61	26	2	2	99.9	99.7	2	113	0.540
planned	66	23	1	0		99.3	0	112	0.589
keyword	60	26	1	1	100	99.4	1	112	0.536
Million	58	27	2	1	100	99.2		112	0.518
remarks	58	27	3	3	99.9	99.6	3	112	0.518
unique	49	24	2	2	100	99.6		97	0.505
sector	56	20	6	5	99.9	99.8	5	96	0.583
threat	52	22	7	6	99.9	99.5	6	96	0.542
SIGINT	46	25	4	3	99.9	99.2		96	0.479
Harris	46	25	9	6	99.8	99.4	6	96	0.479
fuzzy	45	18	5	4	99.9	99.2	4	81	0.556
media	41	20	4	2	99.9	99.7	2	81	0.506
radar	42	19	1	0		99.5		80	0.525
code	39	13	1	1	99.9	99.7	1	65	0.600
file	37	14	2	2	99.9	99.7	2	65	0.569
show	37	14	3	3	100	99.7	3	65	0.569
axis	34	15	3	2	100	99.5	2	64	0.531
NATO	32	16	2	2	100	99.7	2	64	0.500
TRW	21	14	2	2	100	100.1	3	49	0.429
two	28	10	3	3	99.9	99.7	3	48	0.583
EOB	24	12	3	3	99.9	100.1	11	48	0.500
mix	24	12	2	2	99.9	100.2	7	48	0.500

Figure 3.3.3-1 shows that the highest false correlation, averaged for each set of channel bit lengths, decreases to 99.6 at 64 (4 characters). Increasing the keyword length helps but improvement is less dramatic after 4 characters. This is probably due to the algorithm rather than anything linked to our signal to noise ratio. A three character word matches two of its characters to many free form text segments. The random coding nature then produces many close matches on the remaining character. As the character count increases, there are less text segments that closely resemble the keyword, allowing the false responses to separate from the spread of the true.



**Figure 3.3.3-1 Highest false correlations as a function of the number to channel bits**

Figure 3.3.3-2 shows a scatter plot of the highest false versus keyword length in channel bits with the selected words highlighted. We avoided using the worst cases, but are not exclusively using the best.



**Figure 3.3.3-2 Comparison of the highest false correlations for the selected o keywords**

When the recorded patterns are compared to the correlation levels, we find that most of the higher false readings are "fuzzy" matches with many similar characters. However, at 99.2 the resemblance becomes fairly vague. The characters matched per correlation value is an output from the simulation program. Note: the large amount of analog values produces results that are best interpreted as population statistics; forcing these into event evaluations can be misleading. *Our system best operates in a "most likely" or "least likely" mode rather than a "never" or "always" output.*

Figure 3.3.3-3 shows the system output for a short but highly repetitive pattern. The repeated characters hahaha... in the custom 24 bit code result in a grating pattern. The data shown compares measured data on the left before and after processing with simulations on the right. The bias subtraction processing reduces the background level drift making thresholding of this set reasonably easy.

Next we look at the query 'advance' in free form text. The measured and simulated outputs are shown in Figure 3.3.3-4. Advance is a relatively benign word in the custom code; the background variation is minimal. The processing cleans up the background and again makes it easy to set a useable threshold.

The final data set, shown in Figure 3.3.3-5, is from the query word 'multiple'. In the custom 24 bit code, 'multiple' is an example of a word with excessive background fluctuations. Although the processing removes much of the fluctuation, the false correlations remain strong. Any threshold set for this word that ensures finding all occurrences will also pass a large percentage of false correlations. By further refining the code to optimize the distance between common letters in the English language, it might be possible to reduce the background fluctuations in the worst cases and improve the correlation discrimination.

### **3.4 Optical Correlator Architecture Summary**

The basic functionality of the optical correlator has been demonstrated. Performance improvements are needed in developing a good statistical code that will increase accuracy by decreasing background fluctuations. The code used was not fully optimized for this purpose.

Additionally, developments are needed in the spatial light modulator and photodetector array. Because of the extensive component development required, we evaluated a different configuration. This alternative is discussed in Chapter 4.

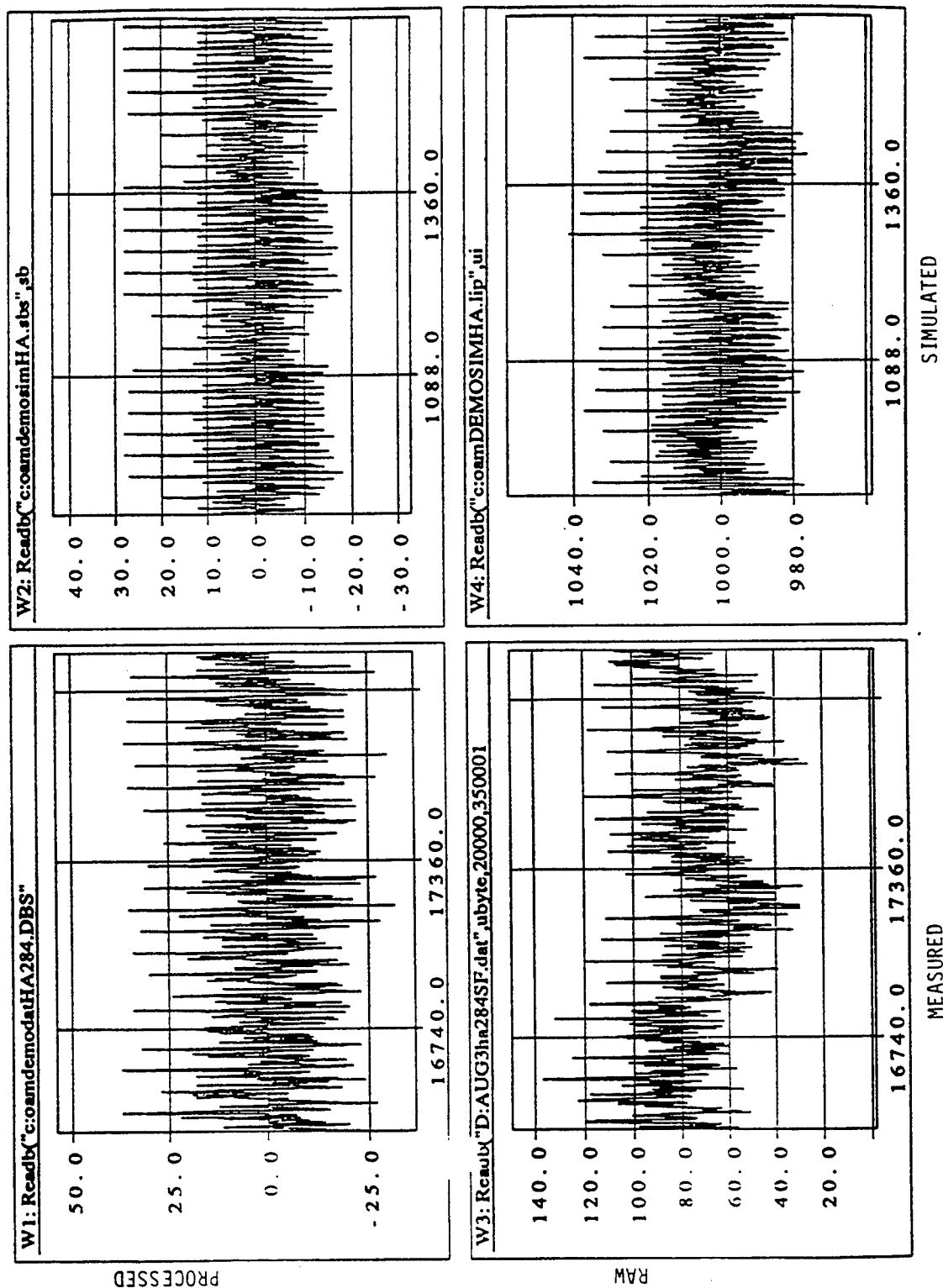


Figure 3.3.3-3 Optical Correlator Output for a Regular Grating Pattern

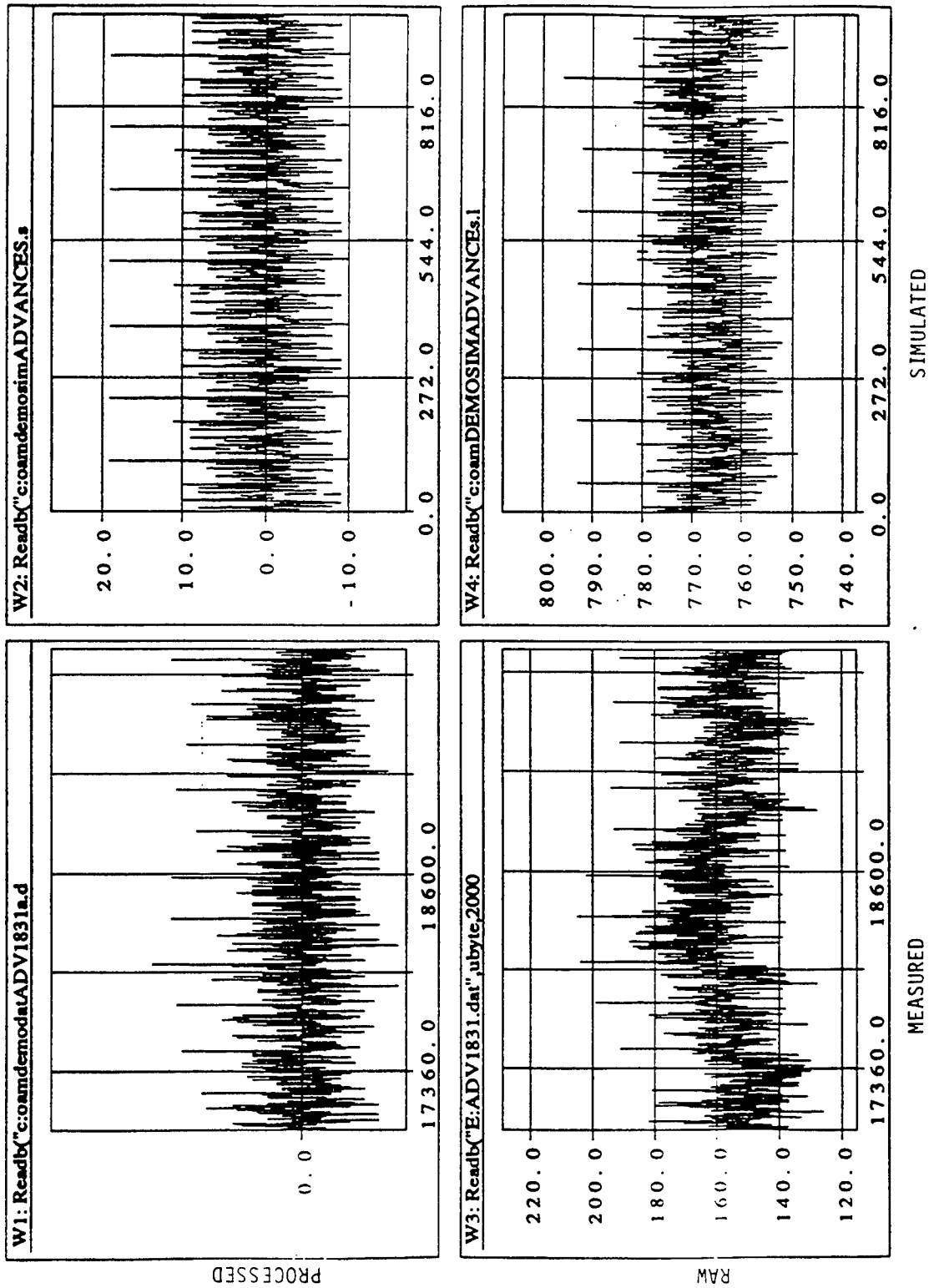


Figure 3.3.3-4 Optical Correlator Output for the Query Word 'advance'



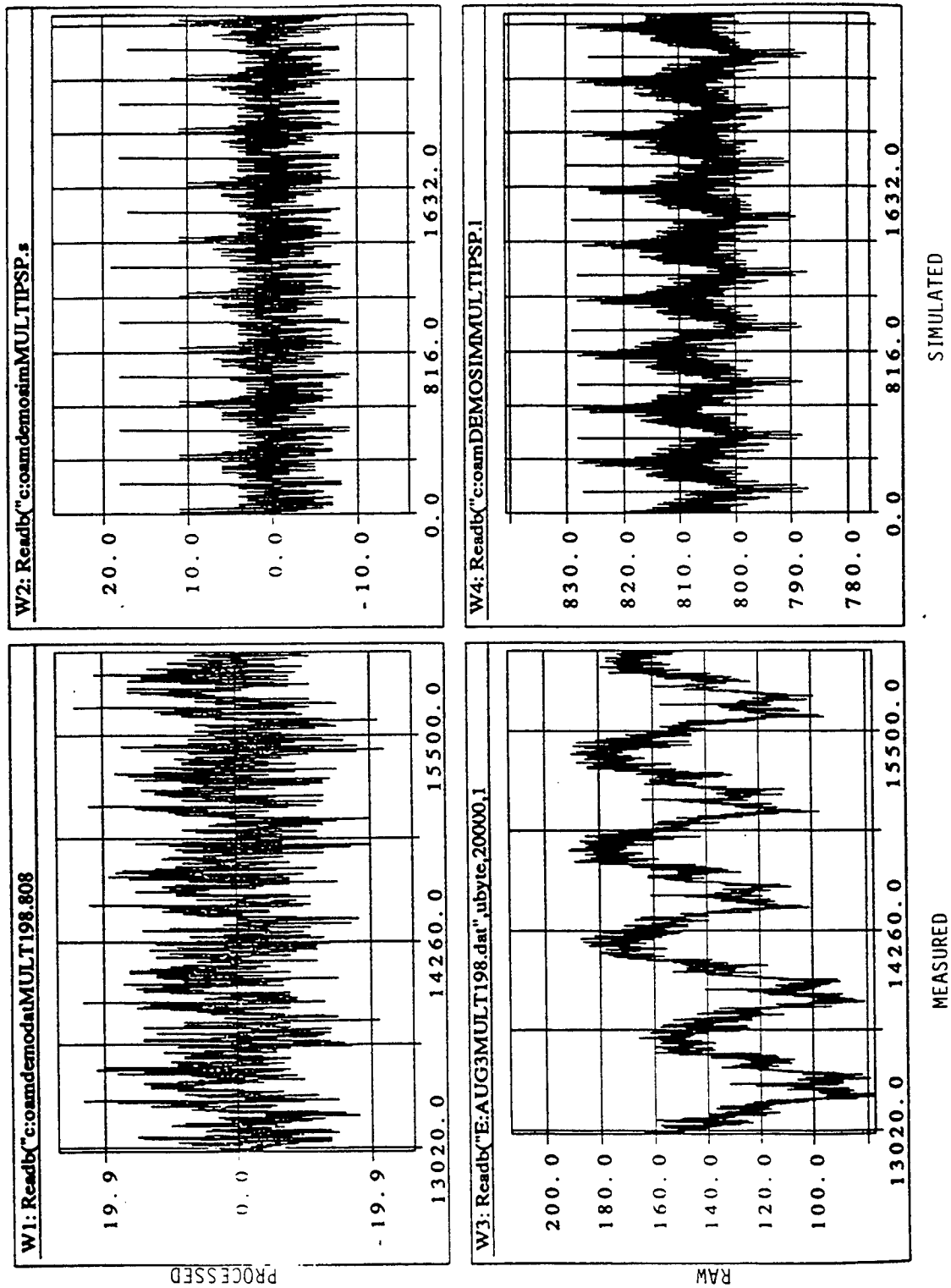


Figure 3.3.3-5 Optical Correlator Output for the Query Word 'multiple'

## 4. OPTO-ELECTRONIC CORRELATOR ARCHITECTURE

Due to the quantity of custom components required by the optical correlator architecture, we reviewed the architecture trade summarized in Section 2 and selected the opto-electronic approach as a viable alternative. This approach was analyzed in detail and a custom integrated circuit was procured from Parallel Solutions Incorporated. The breadboard was modified to accept this integrated circuit and the system performance was measured. In this section the details of the correlator chip development are summarized and the modified breadboard is described. Finally, the experimental results from the breadboard are summarized.

### 4.1 Opto-Electronic Correlator Concept

The opto-electronic correlator subsystem comprises a set of fixed correlation stations, spaced around the disk, that read the data and perform electronic correlations in parallel across all tracks on the disk. The opto-electronic correlator is a modification of the space integrating image plane architecture with the photodetector array positioned in the image plane of the optical disk (see Figure 4.1-1). The baseline design was developed in conjunction with Parallel Solutions Incorporated (PSI). It combines the optical readout developed for the optical correlator architecture with a custom opto-electronic integrated circuit (OEIC) developed by PSI. The OEIC contains both the photodetector array and the electronics to do the correlations. It replaces the spatial light modulator, photodetector array and associated detector electronics, and the focus and tracking subsystem in the optical correlator architecture.

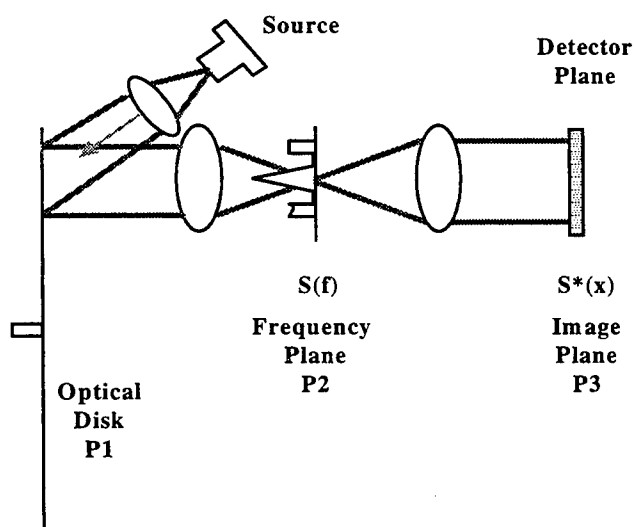


**Figure 4.1-1 Opto-Electronic Correlator Concept**

The data is stored on the disk in a radial/serial format that facilitates the electronic readout. Figure 4.1-2 shows the basic radial/serial data format and associated correlation process. Each ASCII character is stored as bits along a radius while adjacent characters are stored around the disk. The correlation is performed on a character by character basis. The output is the sum of the character correlations.

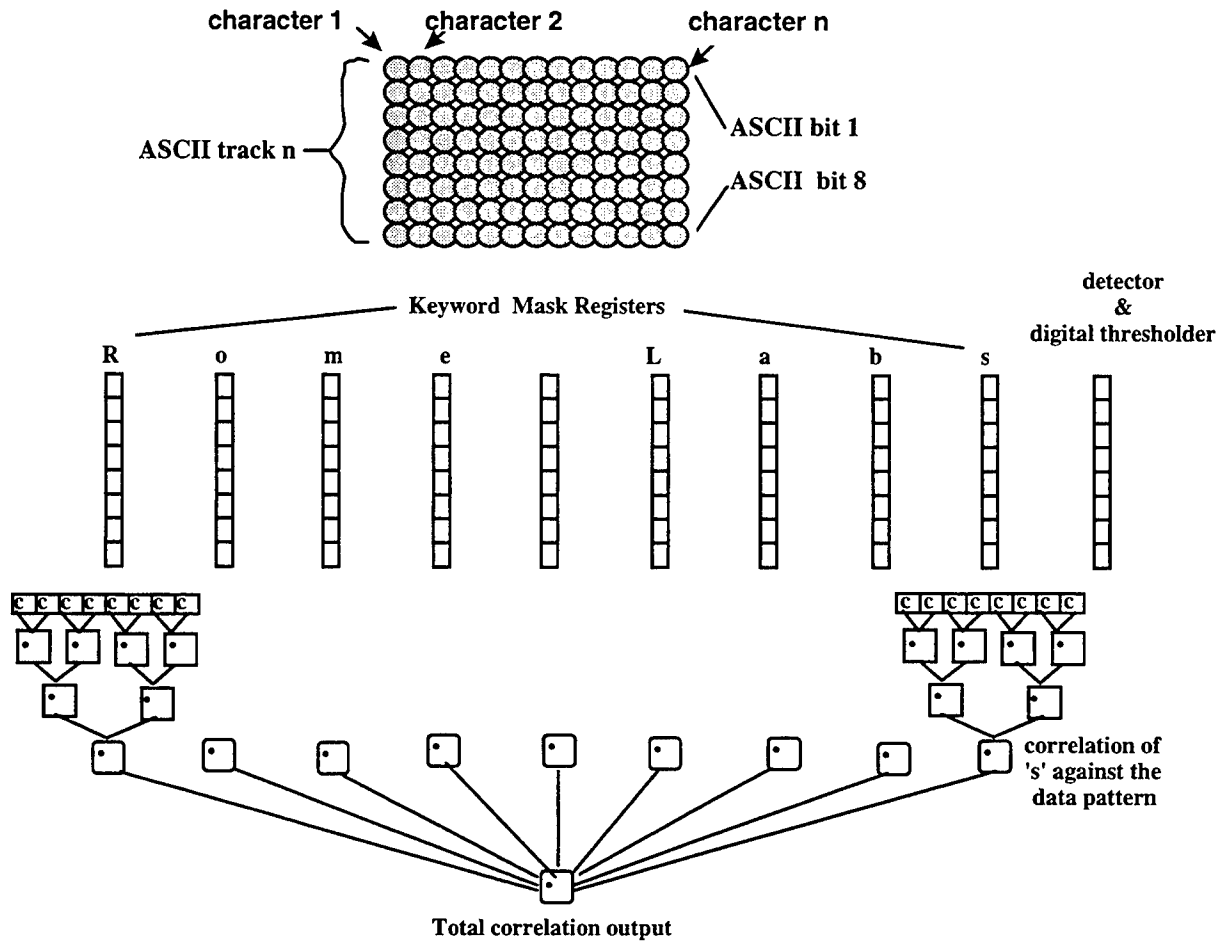


**Figure 4.1-2 Opto-electronic Correlation Tree**

To start the operation a defined key word is input to the opto-electronic integrated circuit and stored for comparison. Figure 4.1-3 shows the correlation process for the query 'Rome Labs' as a function of time. As the disk rotates past the SLM each character in turn passes under the photodetector array. In bit period 1, the bits in the character 'R' are detected and digitized into '0's and '1's. In bit period 2, 'o' is detected and digitized. The digitized 'R' is transferred to the next register and compared to the stored character 's' and the resulting correlation determined. The sum of the correlations in each register is generated and provided at the chip output ( $=0$ ). In bit time 3, 'm' is detected and digitized, 'R' is shifted down one register and compared to the stored character 'b' while 'o' is shifted into the first register and compared to the stored character 's'. The summed correlation ( $=0$ ) is provided at the output. This process continues until eventually (in bit period 10), the full term 'Rome Labs' will be in position such that each character will correlate and the resulting correlation sum will equal 9. In bit period 11, each character will shift down one register and the correlation sum will be 0. There are 16 shift registers in the OEIC to accommodate 16 character searches. The key to this process is the opto-electronic integrated circuit.

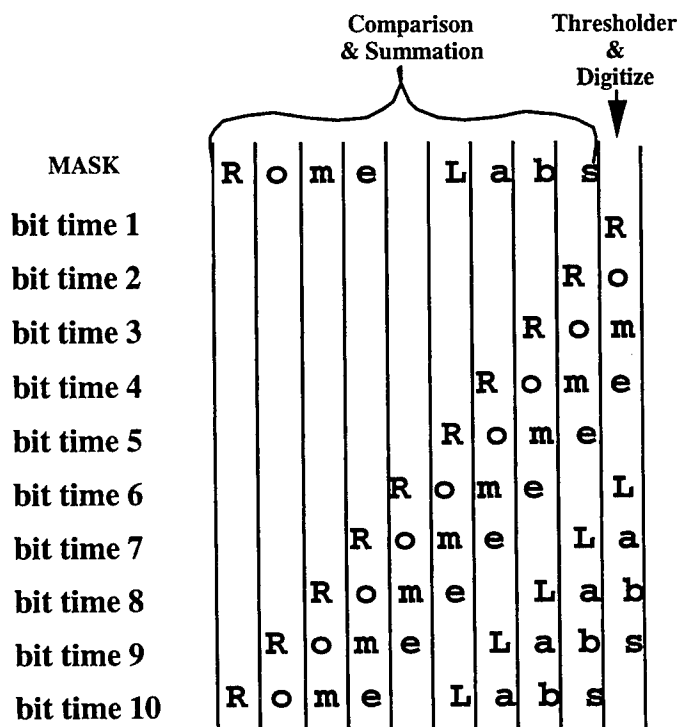
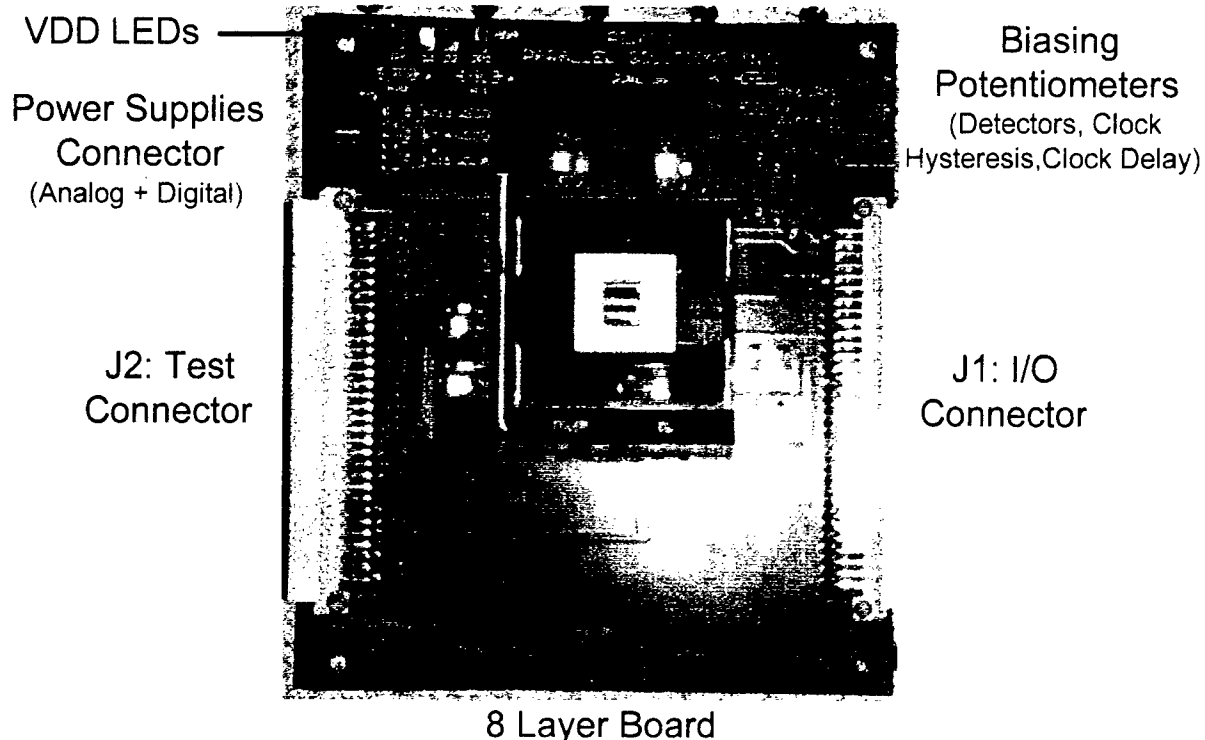


Figure 4.1-2 Electronic Correlation Process in Time

## 4.2 Opto-Electronic Integrated Circuit Development Summary

In some high-performance parallel optical access memory disks being developed, the data is retrieved by a linear photodetector array integrated into a custom VLSI chip that contains both the detectors and their associated circuits. This configuration eases the design of the custom VLSI chip because the constraint of laying out the circuitry as a 2-D matrix is removed. Thus the silicon is used more efficiently and design automation tools can be used more effectively. Use of a differential detection scheme is also easier in the 1-dimensional case.

An opto-electronic chip and associated control electronics, shown in Figure 4.2-1, was developed to correlate a programmable query entry of up to 128 bits with continuous input of optical binary data. The chip has both electrical and optical memory interface. The electrical interface provides access to high-speed small capacity silicon memory, whereas the optical interface enables direct and parallel access to optical read-out mass storage memory. The chip has been fabricated, tested, and shown to be fully functional. The chip performs four 128-bit correlation operations every 25 nsec, requiring a 40 MHz electrical interface for highest speed performance. While the electrical interface is 32 bits wide, the optical interface allows the application of 208 bits in parallel (26 ASCII characters in text recognition) at a maximum speed of 10 MHz, which allows a mass data processing throughput of 2 Gbit/sec. Several chips may be interfaced in this manner to an optical read-out memory without any speed degradation which further increases the throughput via parallelism. The prototype chip, implemented in a 1.2 micron digital CMOS process, occupies an area of about 1 cm<sup>2</sup> and integrates more than four hundred optical detectors with their associated analog circuitry and 200,000 transistors.



**Figure 4.2-1: View of the delivered chip and the interface board**

The function of the chip is to correlate a 128-bit wide query word (16 characters of 8-bit each in text recognition) with continuously input binary data, received either from the electrical or the optical memory interface. A simplified functional block diagram of the chip is shown in Figure 4.2-2. The correlator chip is composed of independent and parallel correlator blocks, a query memory block, a startup unit and a control unit.

The query to be correlated with data is written to the query memory prior to a search. The query memory is built from  $16 \times 9$ -bit latches where the 8-bit part stores a query word and the 9<sup>th</sup> location is used to store a "don't care" bit. The content of the query memory is broadcast over the correlator blocks via a 9 bit wide data bus. Each correlator block is composed of 16 row processors and a column processor, where each row processor receives 8 bits (one character) of the query. At the first time step, the first row processor, the one closest to the memory interface, receives an 8-bit word data from the off-chip storage memory. At the next time step, the content of the first row processor is transferred to the upper row processor while the first processor accepts new data from memory. In this manner, at the end of 16 time steps, the vertical pipeline composed of 16 row processors is full. At every subsequent time step the chip processes the contents of the row processors, therefore correlating the query with 8-bit wide, 16-bit long data.

Each row processor performs an 8-bit comparison operation between the 8 bits of the query, present on the query memory bus, with the 8 bit data received from the lower row processor (or the memory if the first row processor). First, all the bits are XORed in parallel and summed to find the number of bitwise mismatches between a query word and a data word, and then, the number of mismatches is compared to a preset threshold to generate a match or a

mismatch decision at the word (ASCII character) level. If the 9<sup>th</sup> query word bit (don't care bit) is a logic 1, then the corresponding row processor always generates a "match" decision independent of the comparison result. The column processor of each correlator block then sums the number of match bits generated by 16 row processors to provide the degree of match between the 16-character query and data. The process is repeated at every time step to process the 1-bit shifted data and provide full correlation of the query with the data stored in the off-chip memory.

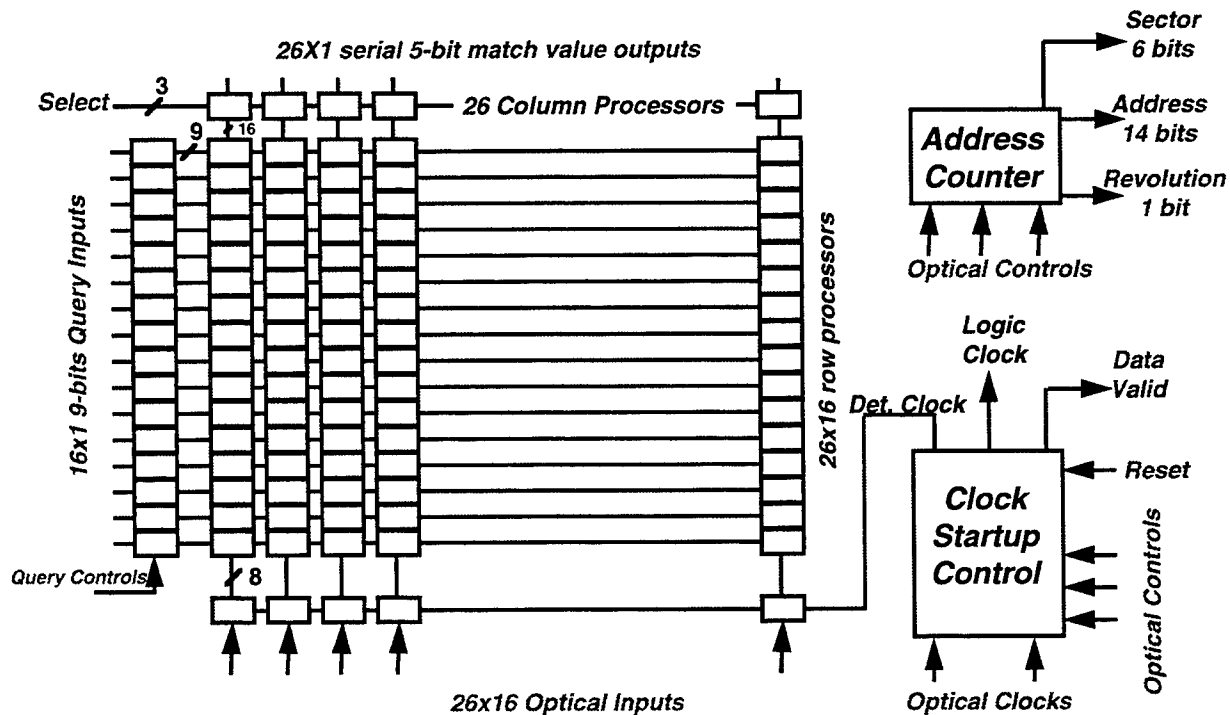


**Figure 4.2-2: Simplified Functional Diagram of the correlator chip**

If the optical memory interface, shown in Figure 4.2-3, is used, then all the clock and control signals are received from the optical memory. The startup and control units process these signals to determine the chip status and operation. From the optical clock bits, the control unit generates two frequency-doubled clock phases to properly handle the optically received data. The clock signals enable the synchronization of the chip to the memory if the memory is an optical disk, and the control signals serve to stop or restart the processing on the chip at the beginning or at the end of empty disk sectors. The control signals also enable the control unit to count the sectors and tracks to precisely locate the address of data position in conjunction with a match. A new query can be downloaded to the chip at any time during processing. When this happens, the control unit records the disk position, starts the operation and compares each new disk position with the recorded start address. This way, independent of the disk rotation speed and amount of data stored, a full rotation of the disk is precisely detected to minimize the search time. In the case of the optical disk interface, the chip also receives optical alignment and tracking signals from the disk and generates the necessary analog electrical signals that can then be used to control the disk servo mechanisms for tracking and focusing in a feedback loop.

A critical issue in optical data transmission from an optical disk to a VLSI chip is the proper coding of data. While a single bit storage/transmission scheme of each data bit is highly efficient in terms of disk capacity, it is very vulnerable to noise and optical and electrical non-uniformities. A detailed comparison analysis shows that differential detection is much more tolerant to non-uniformities in optical power as well as in photodiode responsivities and analog detector characteristics. Differential detection makes lower contrast ratio and optical power affordable while reliably transmitting the information. Differential detection is also very robust against substrate noise, ground bounce and resistive voltage drops which can easily amount to volts in a dense large-scale integration. For these reasons, we use differential coding of data in the optical correlator design. The data encoding on the disk is as follows: five radial bit locations are used to code a digital bit where 2 locations represent the positive phase, 2 locations represent



### 4.2.2 Optical Data Detector Circuits

4-6

An analog differential detector circuit has been designed specifically for this application. Because the rotation speed of the disk is slow compared to the processing speed of the chip, we chose to design a moderately fast but highly sensitive analog circuit which is capable of properly detecting an optical bit when there are only a few  $\mu\text{Watts}$  of differential optical power available per bit. In this circuit, the photocurrents are first amplified through 2 stages of current mirrors, then converted to voltage differentially and compared by a 2-stage high-gain comparator to provide an electronic bit. If the detector is a clock bit detector, then the output of the comparator is routed to the proper blocks. If the detector is a data bit detector, then the comparator output is latched in a D flip-flop by the falling edge of a clock phase. This allows the detection of data at the highest optical contrast ratio point during the rotation of the disk. Two-phase clocking allows the separation of light detection from the chip operation to minimize errors due to digital noise.

The detector circuit was tested and shown to generate the proper electronic bit when there is a minimum of  $2\mu\text{W}$  of optical power difference between positive and negative phases for an average optical power of 10 to  $100\mu\text{W}$ . The circuit operates at a nominal speed of 10 MHz, although up to 30 MHz operation is possible if more optical power is used. This performance is well within the possibilities of the optical disk.

### **4.3 Disk Data Format**

The disk data format and its relationship to the chip linear detector array is illustrated in Figure 4.3-1 through Figure 4.3-3. The linear detector array on the chip has 434 elements, where each element has a size of  $12 \times 8 \mu\text{m}^2$ . The  $5 \times 2$  (radial dimension by tangential dimension) bits on the disk are imaged on two detectors on the chip, where four bits are used for Manchester coding the data and one bit is used as a "guard" band to separate two adjacent Manchester coded sets of four bits. Thus, 1085 bits (track positions) are used for coding 26 ASCII characters including the required control signals. Thus the required magnification of the optical readout system that images the disk data onto the chip will be  $8640/(1085 \cdot t)$ , where  $t$  is the radial track spacing. For a standard track spacing of  $1.5 \mu\text{m}$ , the required magnification will be  $8640/(1085 \cdot 1.5) = 5.31$ .



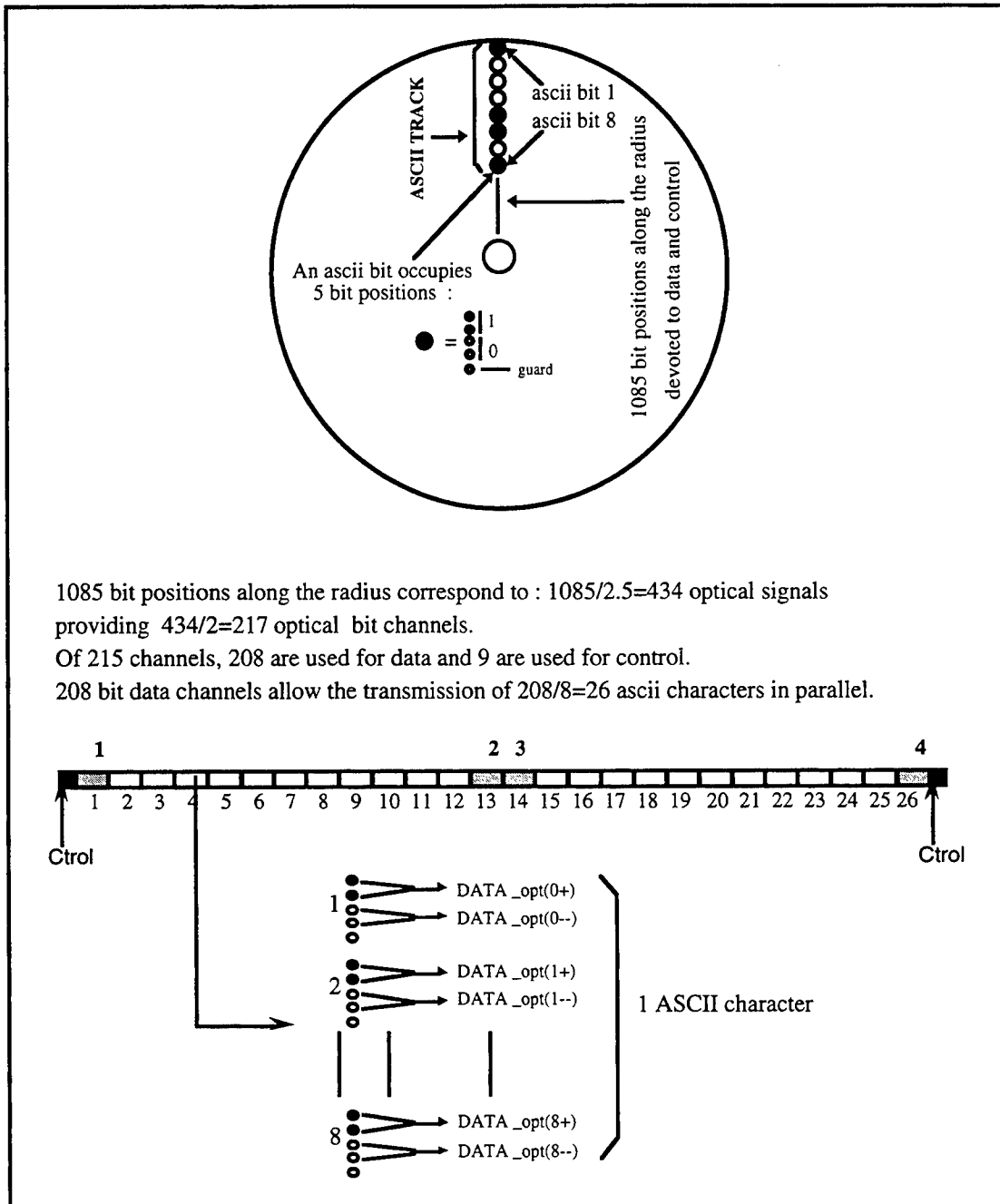


Figure 4.3-1: General disk specifications

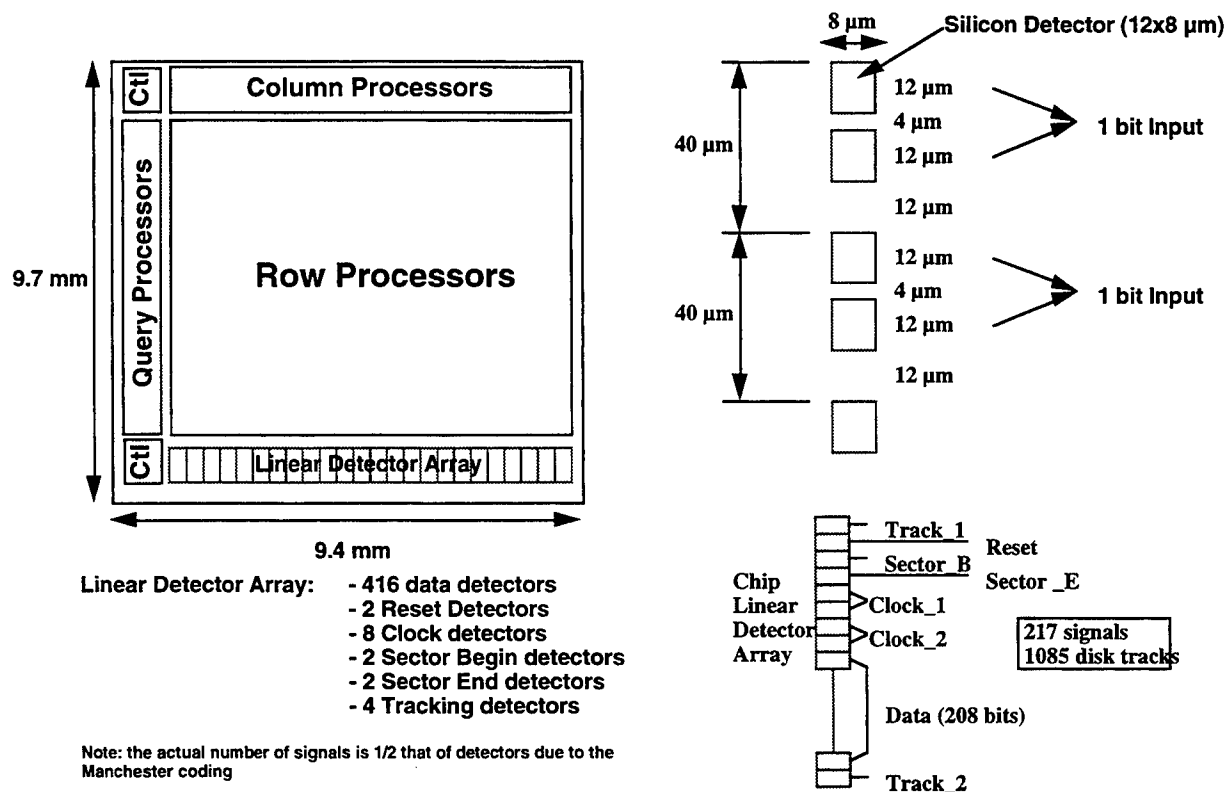


Figure 4.3-2: Physical dimensions of the detectors on the chip

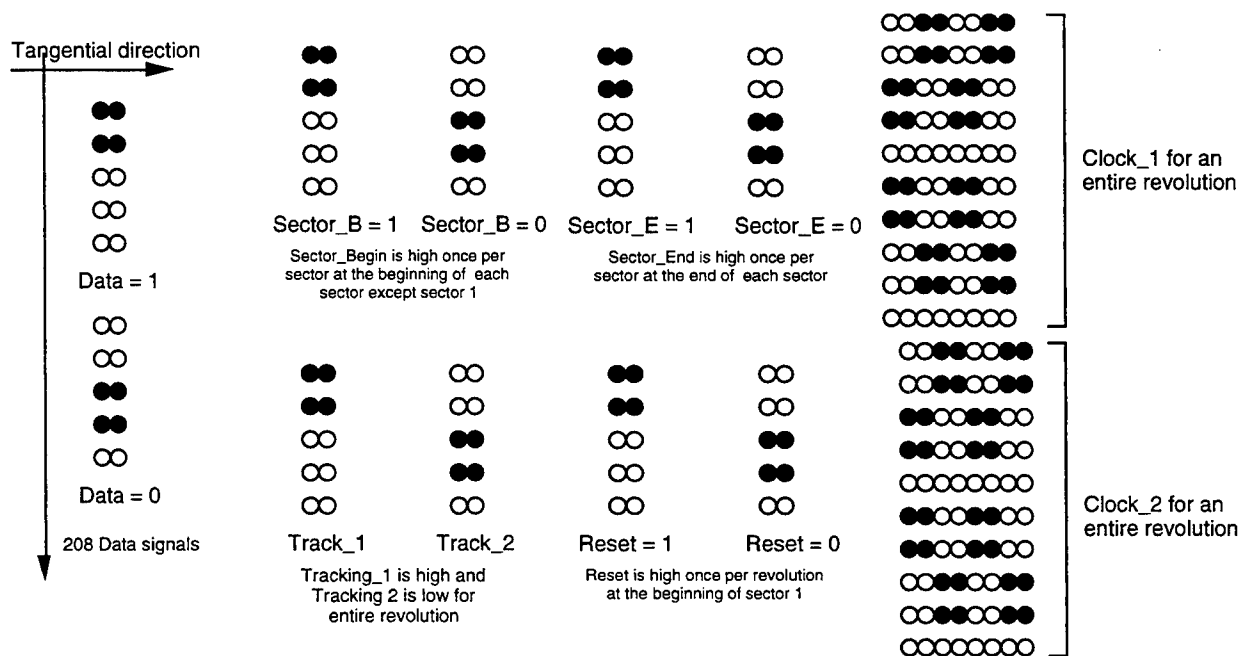
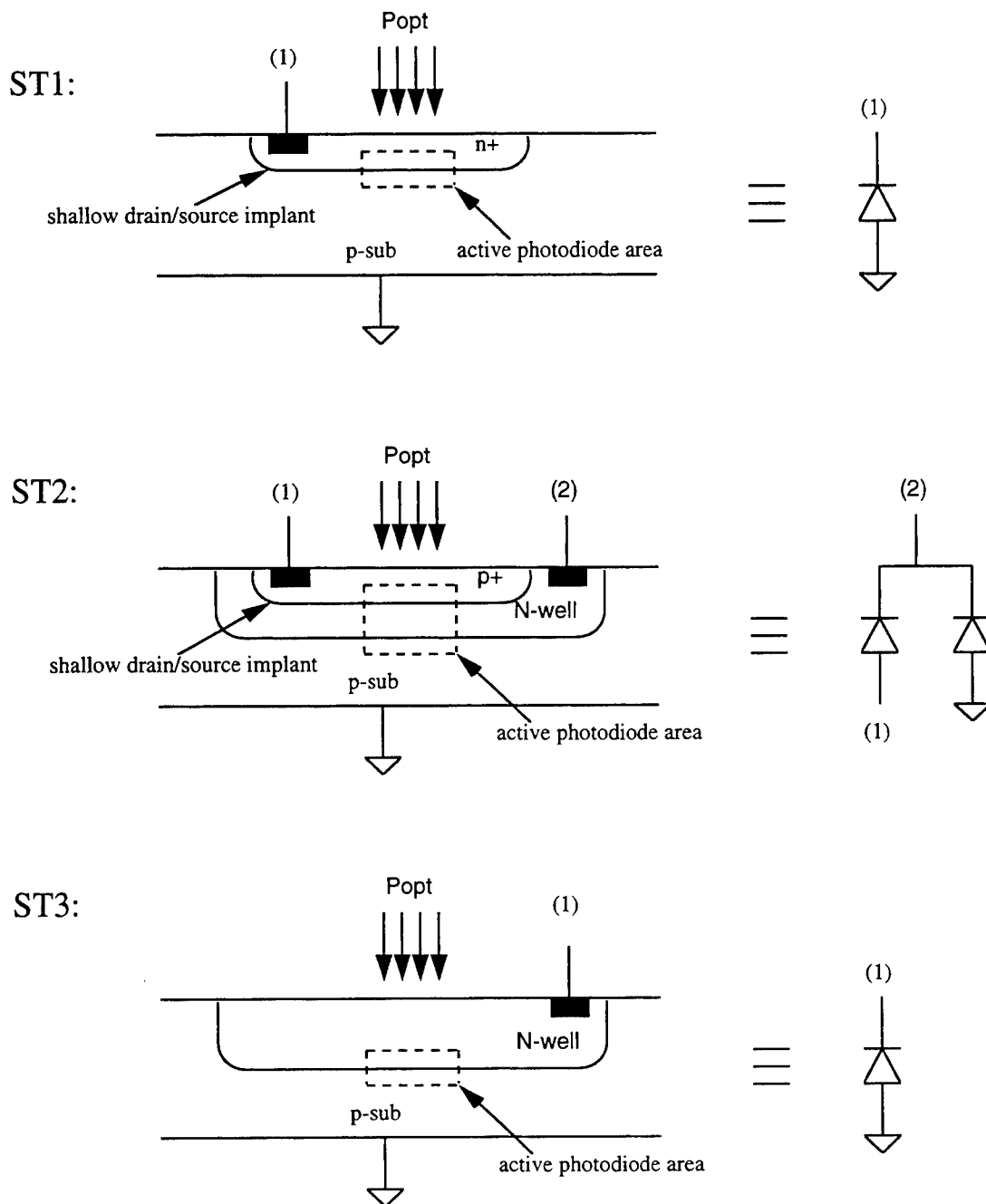


Figure 4.3-3: Descriptions of the various signal to be stored on the disk

#### 4.4 Detector Structures

Three candidate detector structures were traded for size, responsivity, and capacitance. The structures are shown in Figure 4.4-1. The qualitative comparison among them is summarized in Table 4.4-1.



**Figure 4.4-1: Possible photodiode implementations based on P-substrate N-well silicon technology**

**Table 4.4-1 Qualitative comparison of different photodiode structures**

	AREA	RESPONSIVITY	CAPACITANCE
ST1	BEST	MEDIUM	MEDIUM
ST2	WORST	BEST	WORST
ST3	MEDIUM	MEDIUM	BEST

From a qualitative point of view the detector structure of choice is ST1 since it offers the best performance overall. It also offers the best area/responsivity trade-off. Speed will not be optimized with such detectors but it is not the most critical parameter in our study, since the input data rate (from the disk to the chip) will be, at most, a few MHz.

#### **4.5 Detection Reliability and Speed Comparison of Single Bit Vs. Manchester-Coded Input Detection**

##### **4.5.1 Detection Reliability**

The detector circuits for single-bit as well as Manchester coding cases are illustrated in Figure 4.5.1-1 and Figure 4.5.1-2. In this analysis, the photodiode is modeled by a current source that sinks a photo-current as a function of the incident optical power. This assumption provides accurate enough results for a first order analysis, since the dependence of the photo-diode responsivity on voltage is weak (square-root of voltage), and voltage variations across the photodiode are small due to the limited available contrast ratio in the optical input signal.

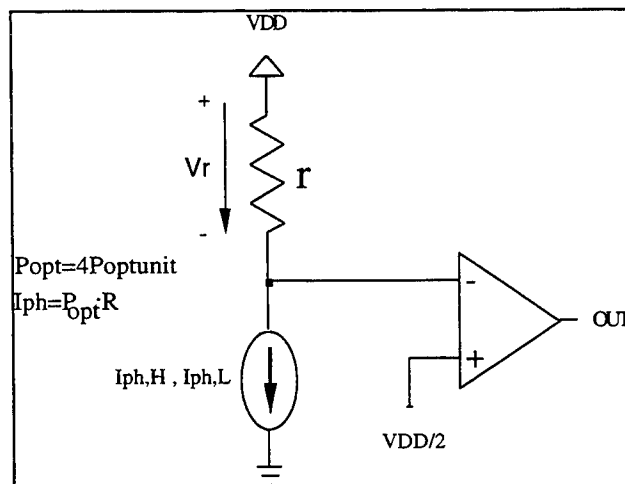


**Figure 4.5.1-1: Single bit detection circuitry**

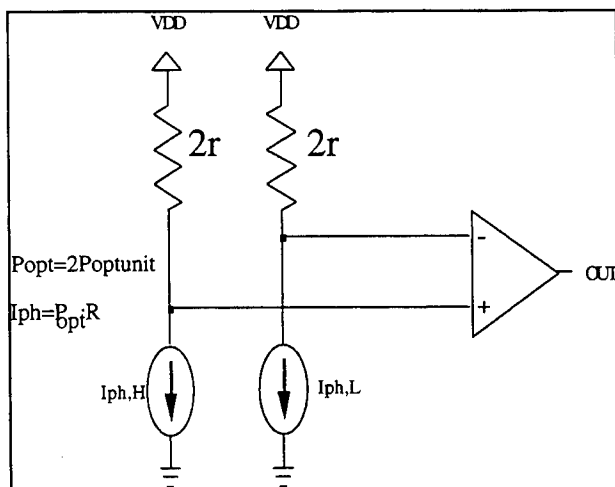


**Figure 4.5.1-2: Manchester coded input detection circuitry**

The generated photo-current as a function of incident optical power can be expressed as:

$$I_{ph} = R \cdot P_{optH, L} , \quad (1)$$

where  $R$  is the photodiode responsivity and  $P_{optH,L}$  is the high-level or low-level incident optical power:

$$P_{opt, H} = P_{opt} \frac{H}{100} , \quad (2a)$$

$$P_{opt, L} = P_{opt} \frac{L}{100} , \quad (2b)$$

where  $H$  and  $L$  are the percent high and low level modulation depths and  $P_{opt}$  is the optical power that would be received by the photodiode when the modulation is 100%. Upon the generation of the photo-current, a load resistor ( $r$ ) is used to convert the photo-current into a voltage. This resistor's value is designed such that its current is half way between high-level and low-level photo-currents when the photodiode output voltage is at mid-supply level :

$$r = \frac{V_{DD}}{2 P_{opt, M} \cdot R} , \quad (3)$$

where

$$P_{opt, M} = P_{opt} \frac{L + H}{200} , \quad (4)$$

and  $V_{DD}$  is the supply voltage level. The high and low level voltages across the load resistor can be expressed as :

$$V_{rH, L} = P_{optH, L} \cdot R \cdot r \quad (5)$$

Using (4) in (3), and then, (2) and (3) in (5) gives :

$$V_{rH} = \frac{V_{DD}}{1 + DR^{-1}} \quad (6a)$$

$$V_{rL} = \frac{V_{DD}}{1 + DR} , \quad (6b)$$

where dynamic range  $DR$  is defined as:

$$DR \equiv \frac{H}{L} . \quad (7)$$

The resistor voltage given by (6) is then thresholded by a comparator to provide a digital bit. In the single-bit scheme, the resistor voltage is compared to a threshold voltage at the half supply level ( $V_{DD}/2$ ), whereas in the Manchester decoding scheme, the positive differential resistor voltage is compared to the negative one.

#### 4.5.1.1 Single-bit detection

In this case, the power of 4 bit positions on the disk is used to illuminate a single detector;

$$P_{opt} = 4P_{optunit} \quad (8)$$

For proper detection, the minimum high-level and maximum low-level resistor voltages should satisfy:

$$V_{rH \min} = \frac{V_{DD}}{2} + V_{off} + \frac{W_c}{2} \quad (9a)$$

$$V_{rL \max} = \frac{V_{DD}}{2} - V_{off} - \frac{W_c}{2} \quad (9b)$$

where  $V_{off}$  is the comparator offset voltage and  $W_c$  is the worst-case transition region width of the comparator's transfer function.  $W_c$  is equal to  $V_{DD}/A$ , where  $A$  is the comparator gain around mid supply. From (6) and (5), minimum high-level resistor voltage can be expressed as :

$$V_{rH \min} = \frac{V_{DD}}{1 + DR^{-1}} \left( 1 - \frac{SIG\_opt\_c}{100} \right) \left( 1 - \frac{SIG\_R\_c}{100} \right) \left( 1 - \frac{SIG\_r\_c}{100} \right) \quad (10)$$

where:

$SIG\_opt\_c$  : Maximum percent variation in optical power ( $P_{opt}$ ) across the chip,

$SIG\_R\_c$  : Maximum percent variation in responsivity across the chip,

$SIG\_r\_c$  : Maximum percent variation in load resistor value across the chip.

Equating (10) to (9a), using (3) and solving for  $SIG\_opt\_c$  gives for the maximum allowable variation in optical power across the chip :

$$SIG\_opt\_c < 100 \cdot \left[ 1 - \frac{(1 + DR^{-1}) \left[ \frac{1}{2} + \frac{\frac{W_c}{2} + V_{off}}{V_{DD}} \right]}{\left( 1 - \frac{SIG\_R\_c}{100} \right) \left( 1 - \frac{SIG\_r\_c}{100} \right)} \right] \quad (11)$$

#### 4.5.2 Manchester-coded input detection

In this case, the optical power of 2 bit positions on the disk is used to illuminate each of the differential detectors;

$$P_{opt} = 2P_{optunit} \quad (12)$$

For proper detection, the following condition must be satisfied:

$$V_{rH \min} - V_{rL \max} > V_{off} + \frac{W_c}{2} \quad (13)$$

where  $V_{rHmin}$  is the minimum high-level voltage drop across the resistor given by (10) and  $V_{rLmax}$  is the maximum low-level voltage drop which can be expressed as:

$$V_{rLmax} = \frac{V_{DD}}{1+DR} \left(1 - \frac{SIG\_opt\_c}{100}\right) \left(1 - \frac{SIG\_R\_c}{100}\right) \left(1 - \frac{SIG\_r\_c}{100}\right) \times \left(1 + \frac{SIG\_opt\_s}{100}\right) \left(1 + \frac{SIG\_R\_s}{100}\right) \left(1 + \frac{SIG\_r\_s}{100}\right) \quad (14)$$

where:

$SIG\_opt\_s$  : Maximum percent variation in optical power ( $P_{opt}$ ) between adjacent spots,

$SIG\_R\_s$  : Maximum percent variation in responsivity between adjacent photodiodes,

$SIG\_r\_s$  : Maximum percent variation in load resistor value between adjacent resistors.

Note that in this case, the differential inputs to the amplifier may move together away from the half supply level (due to variations in  $P_{opt}$  across the chip), which results in the widening of  $W_c$  in (13) due to reduced gain of the comparator. In this analysis, we simplify this behavior by assuming a linear relationship between  $W_c$  and the input common-mode voltage  $V_{cm}$ :

$$W_c = \frac{V_{DD}}{A} (1 + b|V_{cm} - V_{DD}/2|), \quad (15)$$

where  $b$  is a coefficient that can be determined by simulation. In equation (15), the common-mode voltage  $V_{cm}$  is bound by the input common-mode range of the comparator. For simplicity, we will assume a practical input common-mode range of:

$$0.25V_{DD} < V_{cm} < 0.75V_{DD}. \quad (16)$$

In this range,  $V_{cm}$  is controlled by the variations across the chip:

$$V_{cm} = P_{opt} \frac{L+H}{200} \left(1 - \frac{SIG\_opt\_c}{100}\right) R \left(1 - \frac{SIG\_R\_c}{100}\right) r \left(1 - \frac{SIG\_r\_c}{100}\right). \quad (17)$$

Solving for  $SIG\_opt\_c$  yields:

$$SIG\_opt\_c < 100 \left\{ 1 - \frac{\frac{V_{off}}{V_{DD}} + \frac{1}{2A} + \frac{bV_{DD}}{4}}{gn \left[ \frac{1}{1+DR^{-1}} - \frac{fcd}{1+DR} + \frac{bV_{DD}}{4} \right]} \right\}, \quad (18)$$

where;

$$\begin{aligned} c &\equiv 1 + \frac{SIG\_R\_s}{100} & d &\equiv 1 + \frac{SIG\_r\_s}{100} \\ e &\equiv 1 - \frac{SIG\_opt\_c}{100} & f &\equiv 1 + \frac{SIG\_opt\_s}{100} \\ g &\equiv 1 - \frac{SIG\_R\_c}{100} & n &\equiv 1 - \frac{SIG\_r\_c}{100} \end{aligned}$$

Note that, if the tolerance estimated by (18) results in a  $V_{cm}$  outside the operation region given by (16), then we set the  $V_{cm}$  to one of the limits in (16), and use this value in (15).

Similarly, (18) can be solved for  $SIG_{opt\_s}$ ;

$$SIG_{opt\_s} < 100 \left\{ \frac{(1 + DR) \left[ \frac{egn}{1 + DR^{-1}} - \frac{V_{off}}{V_{DD}} - \frac{1}{2A} - \frac{bV_{DD}}{4} (1 - egn) \right]}{egn_{cd}} - 1 \right\} \quad (19)$$

### 4.5.3 Detection Speed

#### 4.5.3.1 Single-bit detection

Worst detection speed response occurs when the photo-current is lower than nominal and the load current is higher than nominal. Worst-case low photo-current occurs when optical input power and responsivity are low, whereas worst-case high load current occurs when the load resistor is low. In this case, the necessary voltage swing for proper detection is high, while the available current to induce this voltage change is small. Minimum low-level voltage drop across the load resistor is :

$$V_{rL\min} = \frac{V_{DD}}{1 + DR} \left( 1 - \frac{SIG_{opt\_c}}{100} \right) \left( 1 - \frac{SIG_{R\_c}}{100} \right) \left( 1 - \frac{SIG_{r\_c}}{100} \right) \quad (20)$$

For proper detection, voltage across the load should swing between  $V_{rL\min}$  given by (20) and  $V_{rH\min}$  given by (9a). During this swing, average load resistor current can be expressed as:

$$I_{avr} = \frac{V_{rL\min} + V_{rH\min}}{2r \left( 1 - \frac{SIG_{r\_c}}{100} \right)} \quad (21)$$

On the other hand, if we assume a fast transition in the optical input, the average photo-current during switching is equal to the minimum high-level current :

$$I_{avph} = P_{opt} \frac{H}{100} \left( 1 - \frac{SIG_{opt\_c}}{100} \right) R \left( 1 - \frac{SIG_{R\_c}}{100} \right) \quad (22)$$

Finally, the switching delay can be expressed as:

$$t_s = C_{det} \frac{V_{rH\min} - V_{rL\min}}{I_{avph} - I_{avr}} \quad (23)$$

#### 4.5.3.2 Manchester-coded input detection

In this case, worst-case speed response occurs when the detector pair receives lower than nominal optical power, and responsivities and load resistance are low. In addition, spot-to-spot variations within the detector pair should be overcome. During switching, one of the



differential photodiode outputs switches from a low to a high voltage level, whereas the other switches in the opposite direction:

$$V_{L-H} = \frac{I_{av}}{C_{det}} t + V_L(0) , \quad (24a)$$

$$V_{H-L} = -\frac{I_{av}}{C_{det}} t + V_H(0) , \quad (24b)$$

where  $I_{av}$  is the average current that induces the transition, and  $V_L(0)$  and  $V_H(0)$  are the low-level and high-level steady-state voltages (in the worst-case for speed):

$$V_H(0) = \frac{V_{DD}}{1 + DR^{-1}} \left( 1 - \frac{SIG_{opt-c}}{100} \right) \left( 1 - \frac{SIG_{R-c}}{100} \right) \left( 1 - \frac{SIG_{r-c}}{100} \right) \quad (25a)$$

$$V_L(0) = \frac{V_{DD}}{1 + DR} \left( 1 - \frac{SIG_{opt-c}}{100} \right) \left( 1 - \frac{SIG_{R-c}}{100} \right) \left( 1 - \frac{SIG_{r-c}}{100} \right) \times \left( 1 - \frac{SIG_{opt-s}}{100} \right) \left( 1 - \frac{SIG_{R-s}}{100} \right) \left( 1 - \frac{SIG_{r-s}}{100} \right) \quad (25b)$$

Where we introduced the worst-case spot-to-spot variations, which have a delaying effect on switching. The comparator switches when ;

$$V_{H-L} = V_{L-H} + V_{off} + \frac{W_c}{2} \quad (26)$$

Using (24) in (26) and solving for the switching time  $t_s$  yields:

$$t_s = \frac{C_{det}}{2 \cdot I_{av}} \left\{ [V_H(0) - V_L(0)] + V_{off} + \frac{W_c}{2} \right\} . \quad (27)$$

For the detector that switches from low to high, we can find the voltage where switching occurs by substituting  $t_s$  for  $t$  in (24a):

$$V_s = \frac{1}{2} [V_H(0) + V_L(0) + W_c + 2V_{off}] \quad (28)$$

For this detector, the average resistor current during switching is found as:

$$I_{avr} = \frac{V_L(0) + V_s}{2r(1 - \frac{SIG_{r-c}}{100})} \quad (29)$$

The average photo-current, again assuming step input, is given by (22).  $I_{av}$  is then calculated by:

$$I_{av} = I_{avph} - I_{avr} . \quad (30)$$

Thus, using (30) and (25) in (27) gives the switching delay of the differential photodiode output stage.

## **4.6 Mathcad Analysis of single-bit vs. Manchester Inputs**

### **4.6.1 Detection Reliability**

$SIG\_R\_s := 2$       percent variation in responsivity between adjacent photodiodes (spot -to-spot)

$SIG\_R\_c := 10$       percent variation in responsivity between photodiodes across the chip

$SIG\_r\_s := 2$       percent variation in photodiode load resistance between adjacent detectors

$SIG\_r\_c := 10$       percent variation in photodiode load resistance across the chip

$H := 22 \%$   
percent high-level and low-level modulation depths

$L := 13 \%$

$DR := \frac{H}{L}$  dynamic range

$$DR = 1.692$$

$VDD := 5$       supply voltage

$V_{off} := 0.02$       comparator worst-case offset voltage

$A := 50$       worst-case comparator gain around half supply level

$W_c := \frac{VDD}{A}$       worst-case comparator transfer function transition region width

$b := 0.3$       gain variation constant with input common-mode voltage

$P_{optunit} := 50 \cdot 10^{-6}$       optical intensity on the chip created by single spot on the disk

$R := 0.3$       photodiode responsivity

$C_{det} := 300 \cdot 10^{-15}$       photodiode load capacitance

#### 4.6.1.1 Single-Bit input

Given the chip non-idealities, allowable percent variation in optical intensity across the chip:

for H=22% , L=13% :

$$\text{SIG\_opt\_c} := 100 \cdot \left[ 1 - \frac{\left( 1 + \text{DR}^{-1} \right) \cdot \left( \frac{1}{2} + \frac{\frac{W_c}{2} + V_{\text{off}}}{VDD} \right)}{\left( 1 - \frac{\text{SIG\_r\_c}}{100} \right) \cdot \left( 1 - \frac{\text{SIG\_R\_c}}{100} \right)} \right]$$

$\text{SIG\_opt\_c} = -0.954$

as a function of H/L (dynamic range):

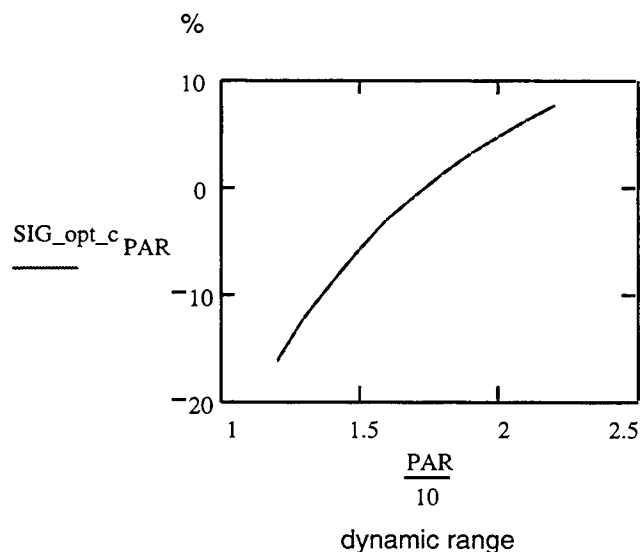
$\text{PAR} := 12..22$

$$\text{SIG\_opt\_c\_PAR} := 100 \cdot \left[ 1 - \frac{\left( 1 + \frac{10}{\text{PAR}} \right) \cdot \left( \frac{1}{2} + \frac{\frac{W_c}{2} + V_{\text{off}}}{VDD} \right)}{\left( 1 - \frac{\text{SIG\_r\_c}}{100} \right) \cdot \left( 1 - \frac{\text{SIG\_R\_c}}{100} \right)} \right]$$

$$\text{DR}_{\text{PAR}} := \frac{\text{PAR}}{10}$$

$\text{DR}_{\text{PAR}}$	$\text{SIG\_opt\_c\_PAR}$
1.2	-16.337
1.3	-12.27
1.4	-8.783
1.5	-5.761
1.6	-3.117
1.7	-0.784
1.8	1.289
1.9	3.145
2	4.815
2.1	6.326
2.2	7.699

dynamic range      allowable % intensity variation across chip



#### 4.6.1.2 Manchester Inputs

assume  $SIG\_opt\_s := 5$

some definitions:

$$C := 1 + \frac{SIG\_R\_s}{100} \quad D := 1 + \frac{SIG\_r\_s}{100}$$

$$F := 1 + \frac{SIG\_opt\_s}{100} \quad G := 1 - \frac{SIG\_R\_c}{100}$$

$$C = 1.02$$

$$D = 1.02$$

$$F = 1.05$$

$$G = 0.9$$

$$N = 0.9$$

$$N := 1 - \frac{SIG\_r\_c}{100}$$

$$DR := \frac{H}{L} \quad DR = 1.692$$

tolerable optical intensity variations across the chip for 5% spot-to-spot variations and 22% and 13% high and low level modulation depths:

$$SIG\_opt\_c := 100 \cdot \left[ 1 - \frac{\frac{V_{off}}{VDD} + \frac{1}{2 \cdot A} + \frac{b \cdot VDD}{4}}{G \cdot N \cdot \left( \frac{1}{1 + DR^{-1}} - \frac{F \cdot C \cdot D}{1 + DR} + \frac{b \cdot VDD}{4} \right)} \right]$$

$$SIG\_opt\_c = 19.666$$

$$\text{define : } E := 1 - \frac{SIG\_opt\_c}{100}$$

$$E = 0.803$$

check if  $V_{cm} > 0.25VDD$  :

$$\frac{VDD}{2} \cdot E \cdot G \cdot N = 1.627$$

similarly, for a given SIG\_opt\_c;

$$\text{SIG\_opt\_s} := 100 \cdot \left[ \frac{(1 + \text{DR}) \cdot \left[ \frac{E \cdot G \cdot N}{1 + \text{DR}} - \frac{\text{Voff}}{\text{VDD}} - \frac{1}{2 \cdot A} - \frac{b \cdot \text{VDD}}{4} \cdot (1 - E \cdot G \cdot N) \right]}{E \cdot G \cdot N \cdot C \cdot D} - 1 \right]$$

$$\text{SIG\_opt\_s} = 5$$

with DR as a parameter;

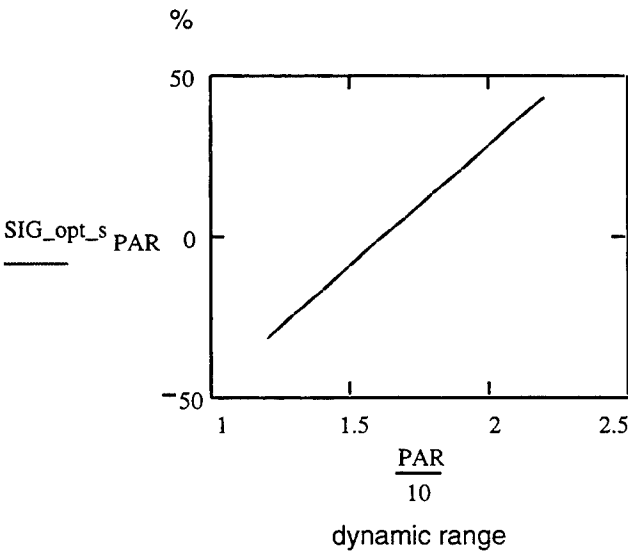
$$\text{PAR} := 12.. 22$$

$$\text{SIG\_opt\_s\_PAR} := 100 \cdot \left[ \frac{\left(1 + \frac{\text{PAR}}{10}\right) \cdot \left[ \frac{E \cdot G \cdot N}{1 + \frac{10}{\text{PAR}}} - \frac{\text{Voff}}{\text{VDD}} - \frac{1}{2 \cdot A} - \frac{b \cdot \text{VDD}}{4} \cdot (1 - E \cdot G \cdot N) \right]}{E \cdot G \cdot N \cdot C \cdot D} - 1 \right]$$

$$\text{DR\_PAR} := \frac{\text{PAR}}{10}$$

DR <sub>PAR</sub>	SIG_opt_s <sub>PAR</sub>
1.2	- 31.776
1.3	- 24.306
1.4	- 16.836
1.5	- 9.365
1.6	- 1.895
1.7	5.575
1.8	13.045
1.9	20.515
2	27.985
2.1	35.455
2.2	42.925

dynamic  
range      allowable  
% intensity  
variation  
between  
adjacent spots



## 4.6.2 Speed Analysis

### 4.6.2.1 Single-Bit Input

assume :

$$H := 16, 18.. 50 \quad L := 10 \quad \text{SIG\_opt\_c} := 0.1 \quad \text{SIG\_opt\_s} := 0.1$$

\*\*\*\*\*

$$\text{Popt} := 4 \cdot \text{Poptunit} \quad 4 \text{ spot intensity on 1 detector}$$

$$\text{DR}_H := \frac{H}{L}$$

minimum voltage drop across photodiode load resistance:

$$\text{VrLmin}_H := \frac{\text{VDD}}{1 + \text{DR}_H} \cdot \left(1 - \frac{\text{SIG\_opt\_c}}{100}\right) \cdot \left(1 - \frac{\text{SIG\_R\_c}}{100}\right) \cdot \left(1 - \frac{\text{SIG\_r\_c}}{100}\right)$$

$$\text{VrHmin} := \frac{\text{VDD}}{2} + \frac{\text{Wc}}{2} + \text{Voff} \quad \text{maximum low-level photodiode output voltage}$$

$$\text{VrHmin} = 2.57$$

photodiode load resistance design based on available optical power as a function of DR:

$$r_H := \frac{100 \cdot \text{VDD}}{\text{Popt} \cdot R \cdot (L + H)}$$

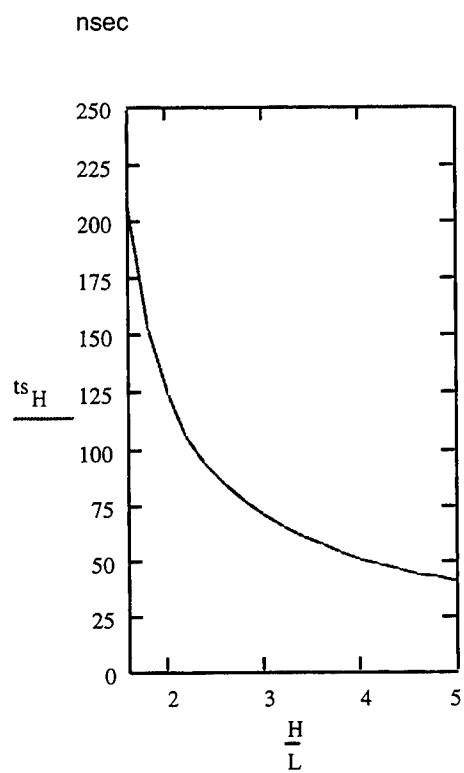
average load current during switching:

$$\text{Iav}_H := \frac{1}{2 \cdot r_H} \cdot (\text{VrLmin}_H + \text{VrHmin}) \cdot \frac{1}{1 - \frac{\text{SIG\_r\_c}}{100}}$$

average photo current during switching:

$$\text{Iavph}_H := \text{Popt} \cdot \frac{H}{100} \cdot R \cdot \left[ \left(1 - \frac{\text{SIG\_opt\_c}}{100}\right) \cdot \left(1 - \frac{\text{SIG\_R\_c}}{100}\right) \right]$$

$$\text{ts}_H := \text{Cdet} \cdot \frac{\text{VrHmin} - \text{VrLmin}_H}{\text{Iavph}_H - \text{Iav}_H} \cdot 10^9 \quad \text{nsec} \quad \text{switching delay}$$



$ts_H$	$\frac{H}{L}$	$VrHmin - VrLmin_H$
205.598	1.6	1.014
152.328	1.8	1.125
124.125	2	1.221
106.203	2.2	1.306
93.573	2.4	1.38
84.066	2.6	1.446
76.58	2.8	1.505
70.487	3	1.559
65.406	3.2	1.607
61.086	3.4	1.65
57.356	3.6	1.69
54.095	3.8	1.727
51.214	4	1.761
48.647	4.2	1.792
46.342	4.4	1.821
44.258	4.6	1.848
42.364	4.8	1.872
40.634	5	1.896

$I_{avph_H} - I_{avr_H}$	$r_H$
$1.479 \cdot 10^{-6}$	$3.205 \cdot 10^5$
$2.216 \cdot 10^{-6}$	$2.976 \cdot 10^5$
$2.952 \cdot 10^{-6}$	$2.778 \cdot 10^5$
$3.688 \cdot 10^{-6}$	$2.604 \cdot 10^5$
$4.424 \cdot 10^{-6}$	$2.451 \cdot 10^5$
$5.161 \cdot 10^{-6}$	$2.315 \cdot 10^5$
$5.897 \cdot 10^{-6}$	$2.193 \cdot 10^5$
$6.633 \cdot 10^{-6}$	$2.083 \cdot 10^5$
$7.369 \cdot 10^{-6}$	$1.984 \cdot 10^5$
$8.106 \cdot 10^{-6}$	$1.894 \cdot 10^5$
$8.842 \cdot 10^{-6}$	$1.812 \cdot 10^5$
$9.578 \cdot 10^{-6}$	$1.736 \cdot 10^5$
$1.031 \cdot 10^{-5}$	$1.667 \cdot 10^5$
$1.105 \cdot 10^{-5}$	$1.603 \cdot 10^5$
$1.179 \cdot 10^{-5}$	$1.543 \cdot 10^5$
$1.252 \cdot 10^{-5}$	$1.488 \cdot 10^5$
$1.326 \cdot 10^{-5}$	$1.437 \cdot 10^5$
$1.4 \cdot 10^{-5}$	$1.389 \cdot 10^5$

#### 4.6.2.2 Manchester Inputs

Popt := 2 · Poptunit      2 spot power on 1 detector

$$V_{cm} := \frac{VDD}{2} \cdot E \cdot G \cdot N$$

$$W_c := \frac{VDD}{A} \cdot \left[ 1 + b \cdot \left( \frac{VDD}{2} - V_{cm} \right) \right]$$

$$W_c = 0.126$$

$$V_{H0_H} := \frac{VDD}{1 + (DR_H)^{-1}} \cdot \left( 1 - \frac{SIG_{opt\_c}}{100} \right) \cdot \left( 1 - \frac{SIG_{R\_c}}{100} \right) \cdot \left( 1 - \frac{SIG_{r\_c}}{100} \right)$$

$$V_{L0_H} := \frac{VDD}{1 + (DR_H)} \cdot \left( 1 - \frac{SIG_{opt\_c}}{100} \right) \cdot \left( 1 - \frac{SIG_{R\_c}}{100} \right) \cdot \left( 1 - \frac{SIG_{r\_c}}{100} \right)$$

$$V_{L0_H} := V_{L0_H} \cdot \left( 1 - \frac{SIG_{opt\_s}}{100} \right) \cdot \left( 1 - \frac{SIG_{R\_s}}{100} \right) \cdot \left( 1 - \frac{SIG_{r\_s}}{100} \right)$$

$$V_{s_H} := \frac{1}{2} \cdot (V_{H0_H} + V_{L0_H} + W_c + 2 \cdot V_{off})$$

$$r_H := \frac{100 \cdot VDD}{Popt \cdot R \cdot (L + H)}$$

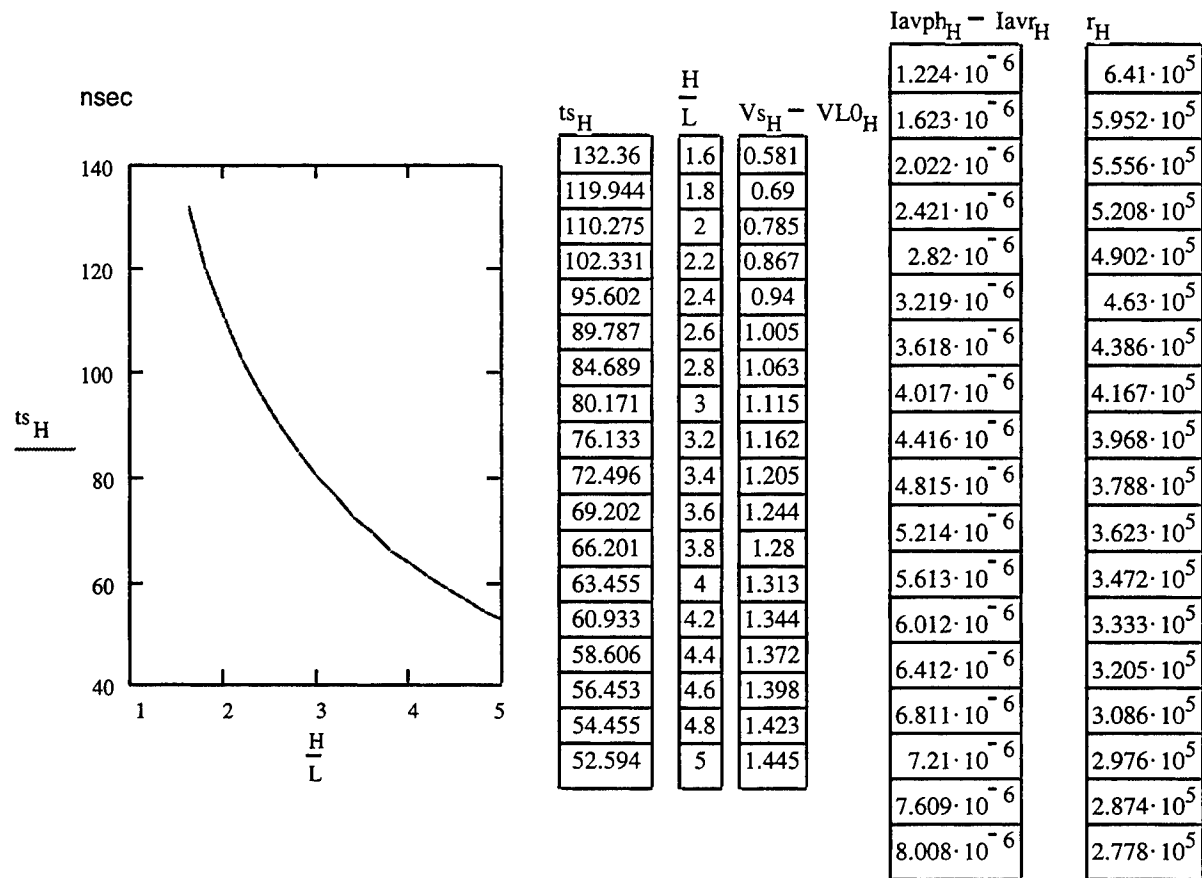
$$I_{avr_H} := \frac{1}{2 \cdot r_H} \cdot (V_{L0_H} + V_{s_H}) \cdot \frac{1}{1 - \frac{SIG_{r\_c}}{100}}$$

$$I_{avph_H} := Popt \cdot \frac{H}{100} \cdot R \cdot \left[ \left( 1 - \frac{SIG_{opt\_c}}{100} \right) \cdot \left( 1 - \frac{SIG_{R\_c}}{100} \right) \right]$$

$$t_{S_H} := t_{s_H}$$

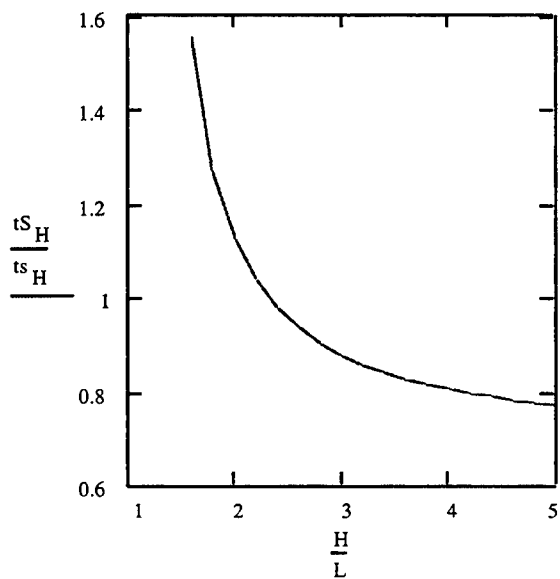
$$t_{s_H} := \frac{C_{det}}{2} \cdot \frac{V_{H0_H} - V_{L0_H} + V_{off} + \frac{W_c}{2}}{I_{avph_H} - I_{avr_H}} \cdot 10^9 \quad \text{nsec}$$





#### 4.6.2.3 Comparison

SINGLE-BIT/MANCHESTER DELAY RATIO



## 4.7 Input Detector Circuits

### 4.7.1 Data

Figure 4.7.1-1 is the schematic of the differential detectors circuitry. This section of the electronics performs a differential detection on the Manchester encoded optical bits and generates a digital '1' or '0' depending on the polarity. It operates at the bit clock rate.

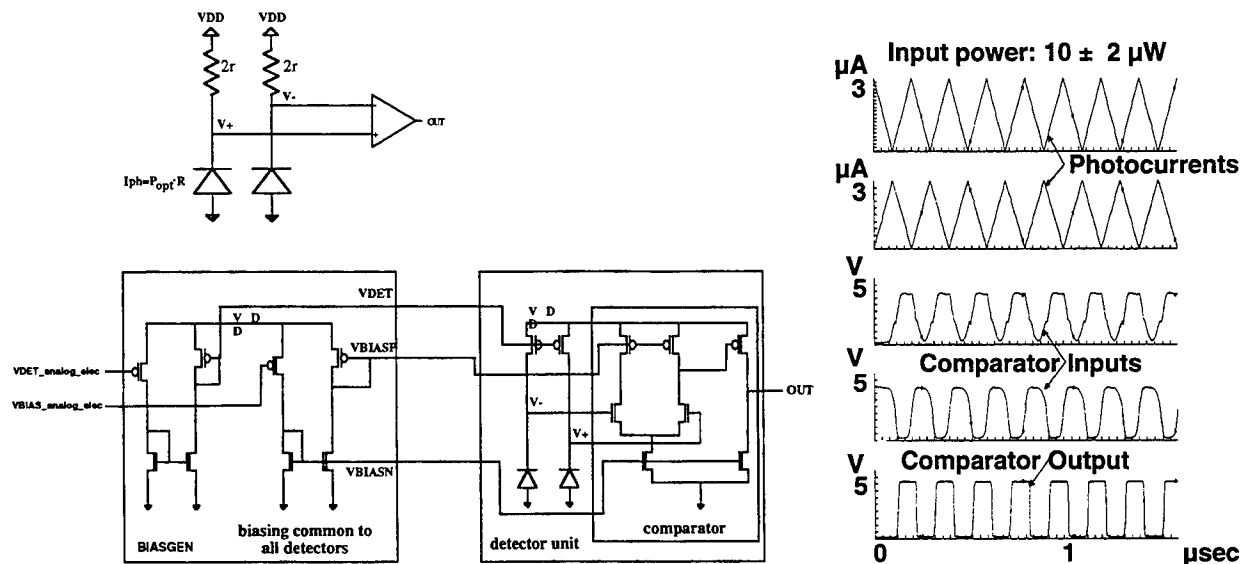
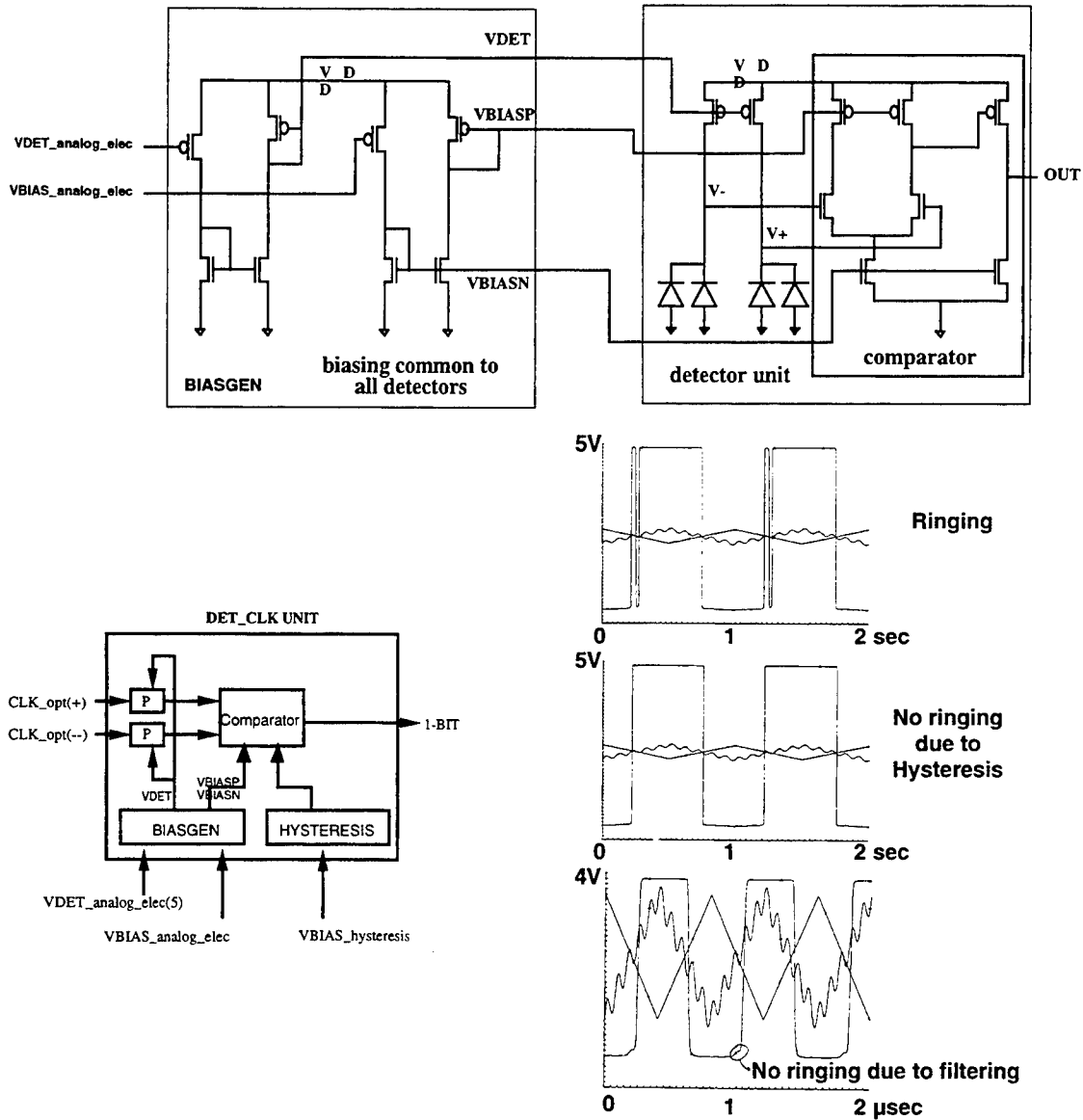


Figure 4.7.1-1: Differential Optical Input Detector Circuitry

### 4.7.2 Clock

We incorporated a hysteresis functionality into the clock detector comparators. The desired hysteresis is performed via a small positive feedback from the output by adding one inverter and three transistors to the clock circuits. From our SPICE simulations, the clock ringing problems occur if the circuits were used as originally designed and at very low frequencies (about 1 Hz on Figure 4.7.2-1). Figure 4.7.2-1 also shows the behavior of the circuit at the same frequency when the hysteresis is added, removing the double clocking effect. Finally, Figure 4.7.2-1 shows that at higher speeds (1 MHz) the ringing problem is non-existent even without adding hysteresis, due to the limited frequency response of the comparator.



**Figure 4.7.2-1: Differential Clock Detector Circuitry with Double Photodiodes and hysteresis compensation circuit**

### 4.7.3 Tracking and Alignment

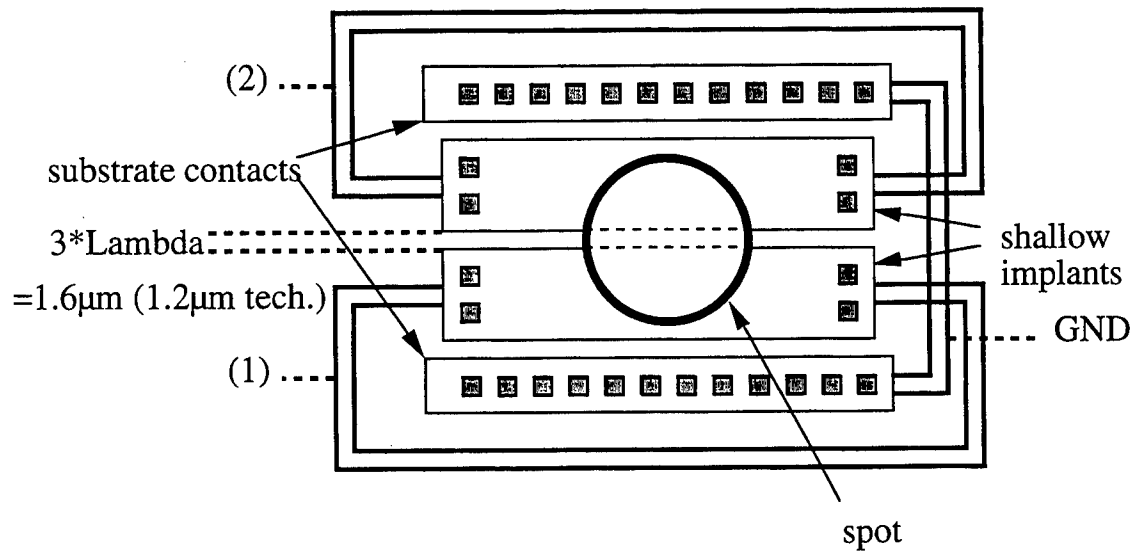


Figure 4.7.3-1: Split Detector layout based on the ST1 detector Structure

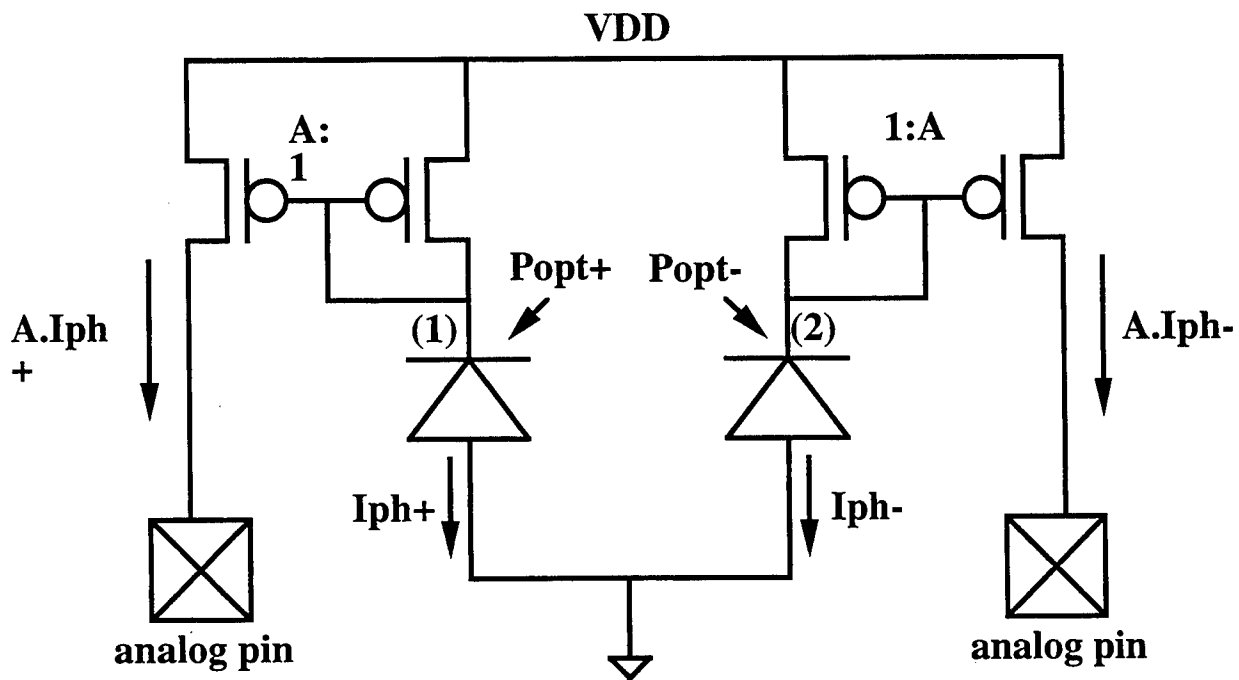
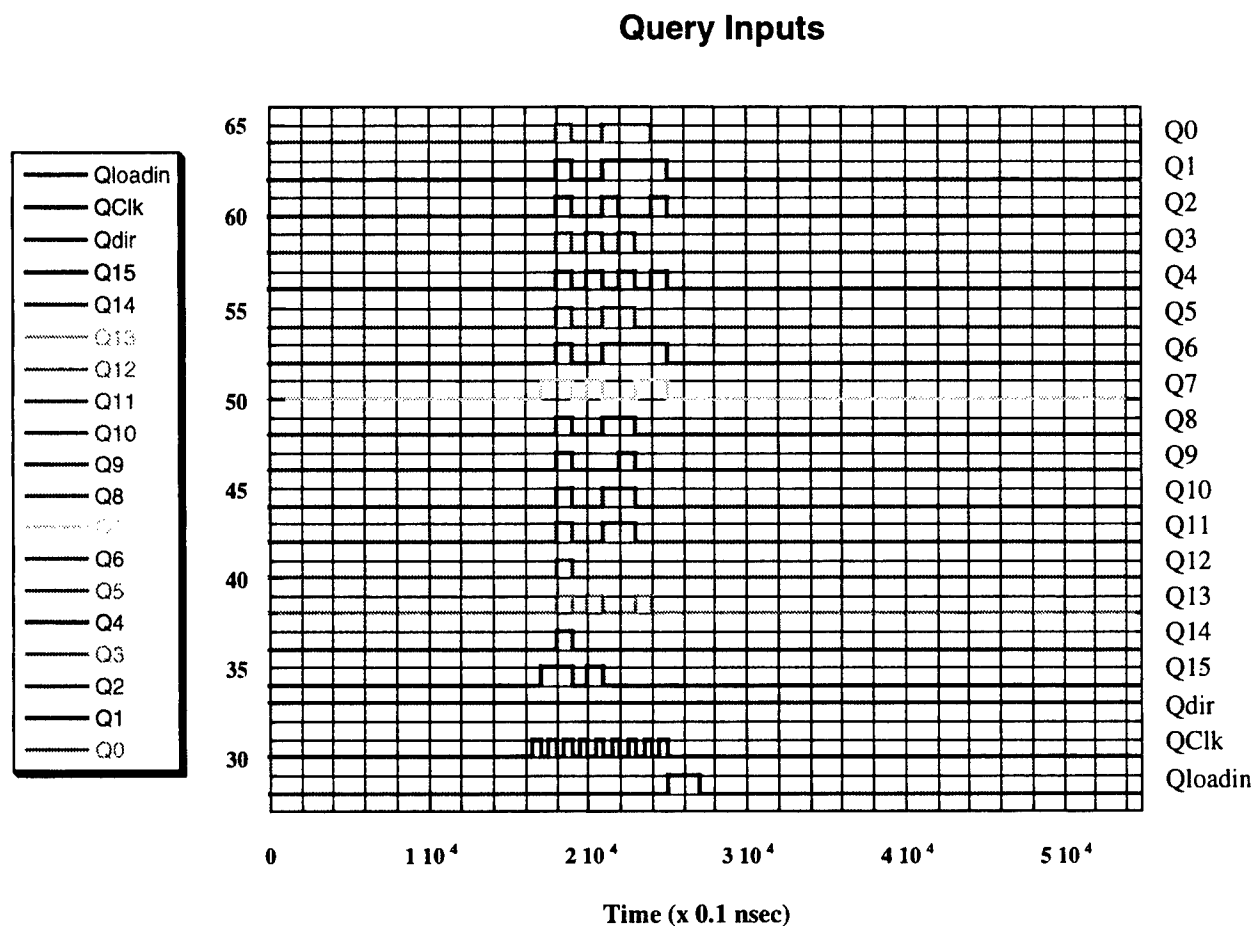


Figure 4.7.3-2: Split detector Current Amplifier Circuitry

## 4.8 Typical simulations of the chip operation

### 4.8.1 Query Loading

Figure 4.8.1-1 shows the timing for loading the query word into the on-chip registers.



**Figure 4.8.1-1: Query Loading simulations**

## 4.8.2 Perfect match Simulation

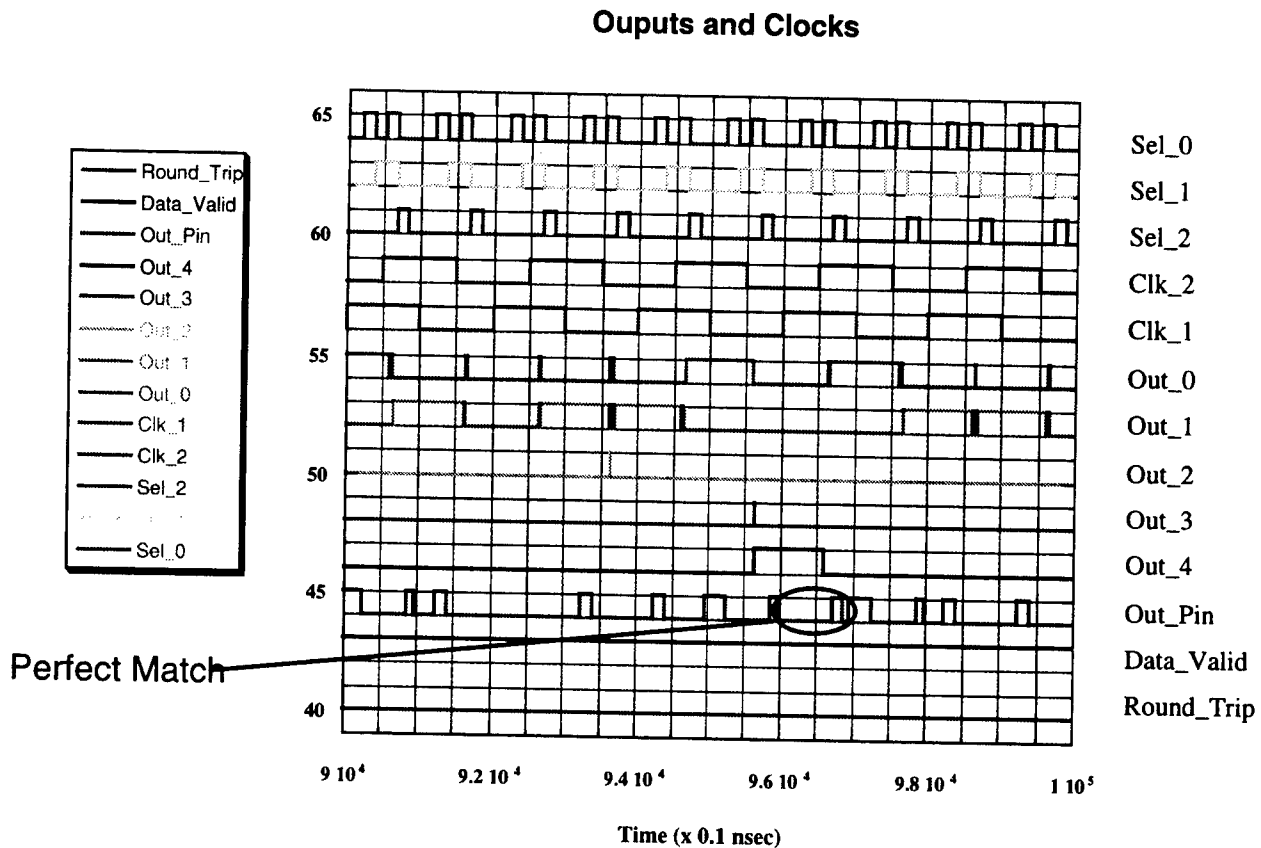


Figure 4.8.2-1 shows the simulation of a perfect correlation match.

**Figure 4.8.2-1: Perfect Match simulation**

## 4.9 Fabricated Parts

Details of the chip interface are included in Appendix B. This section shows the fabricated parts.

### 4.9.1 Correlator Chip

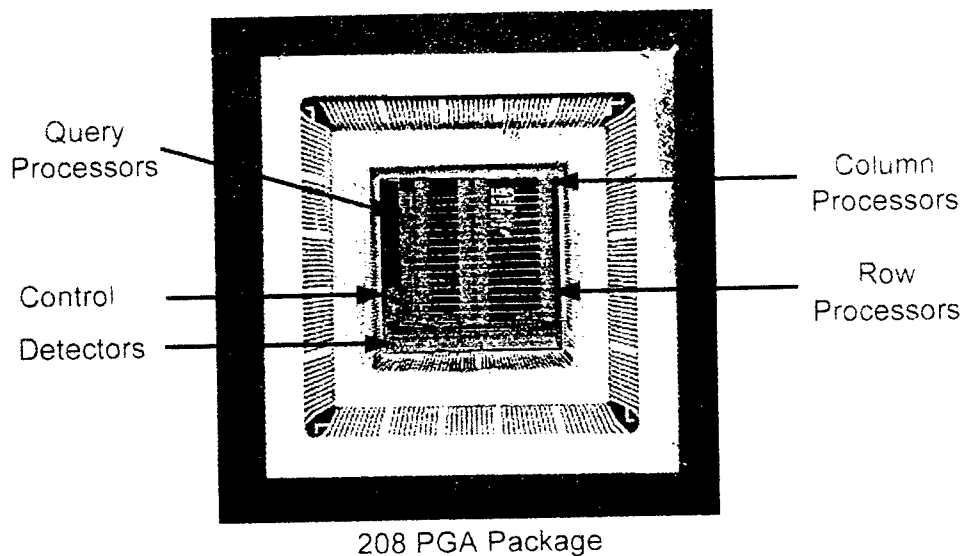


**Figure 4.9.1-1: Picture of the correlator chip**

### 4.9.2 Chip and Interface Board

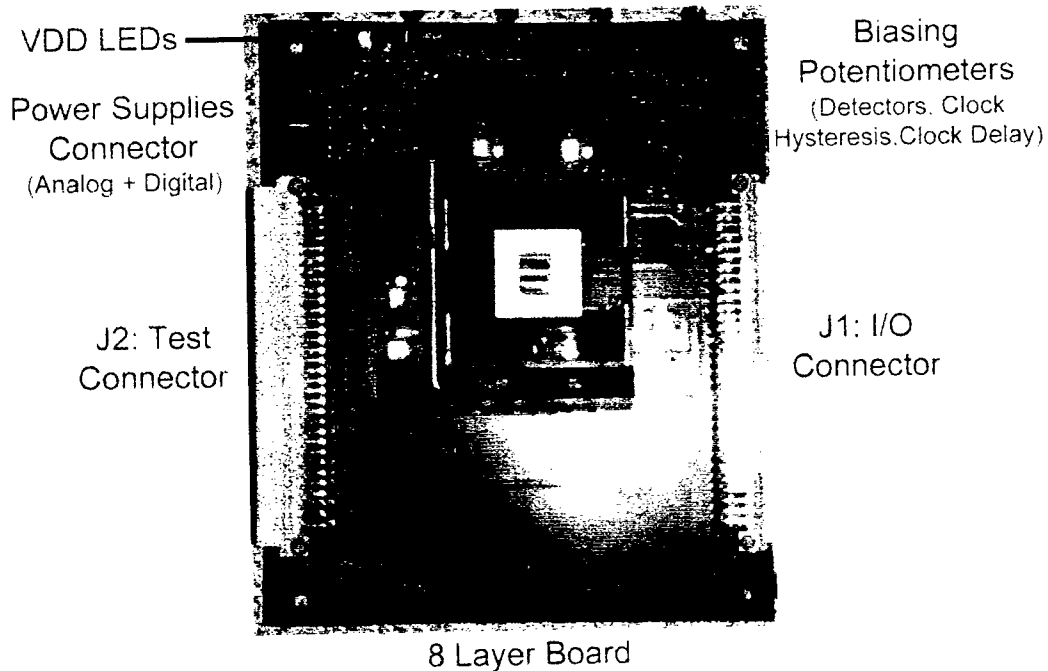


**Figure 4.9.2-1: Picture of the interface board with mounted chip**

### 4.9.3 Test Board

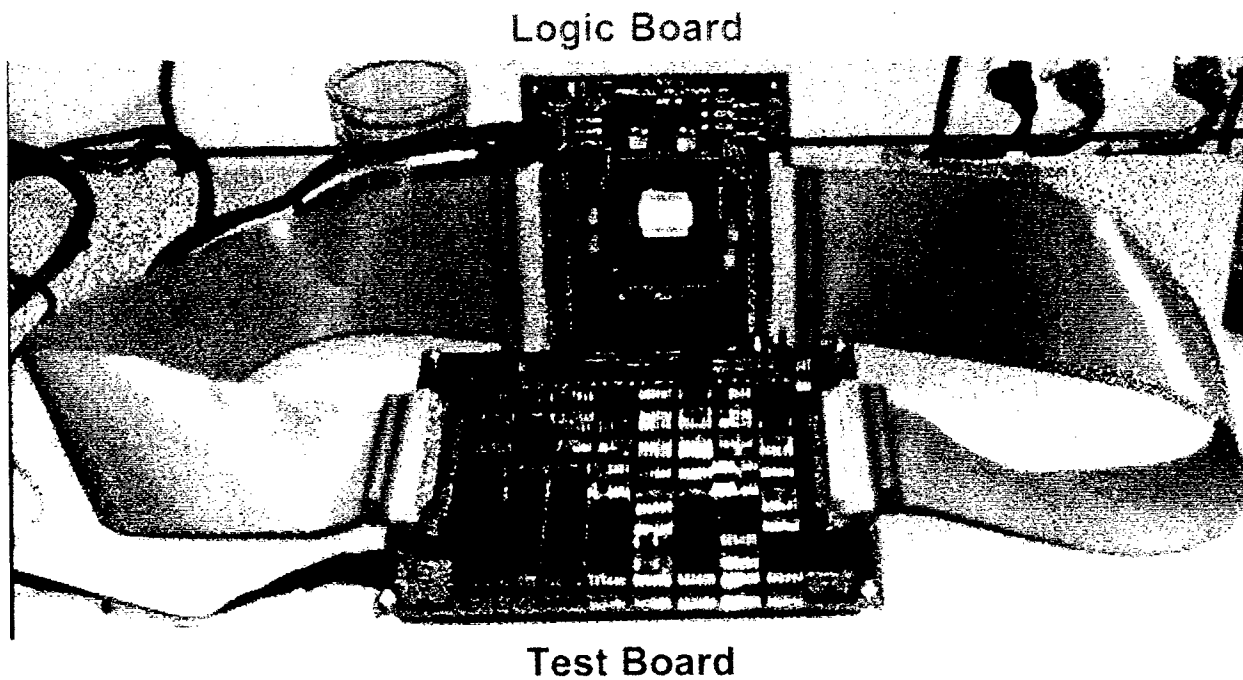


Figure 4.9.3-1: Picture of the test board connected to the interface board

### 4.9.4 Test Setups

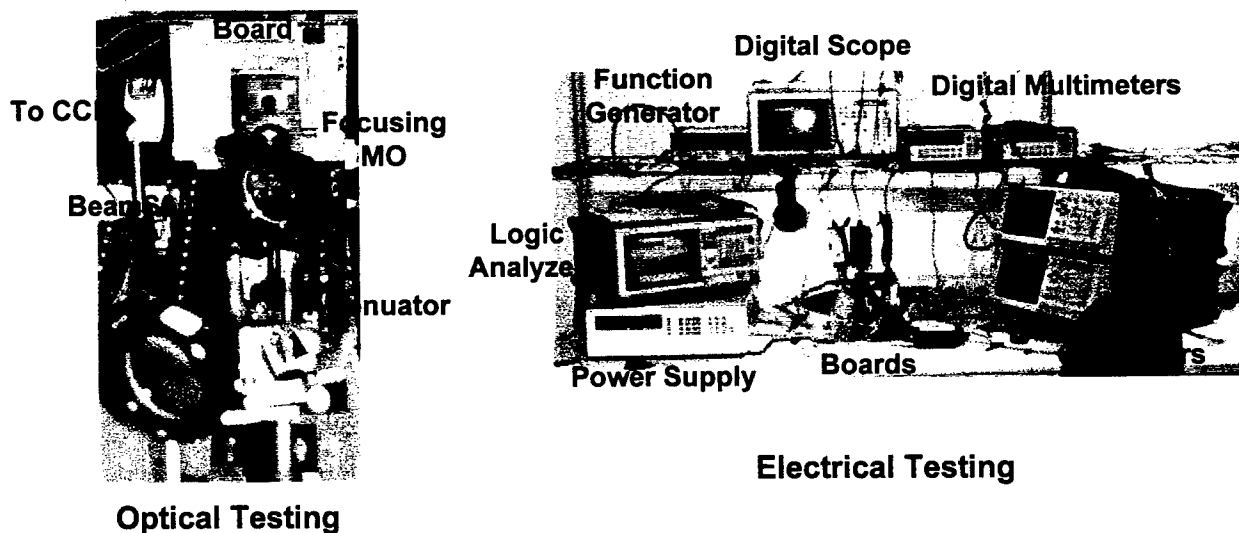
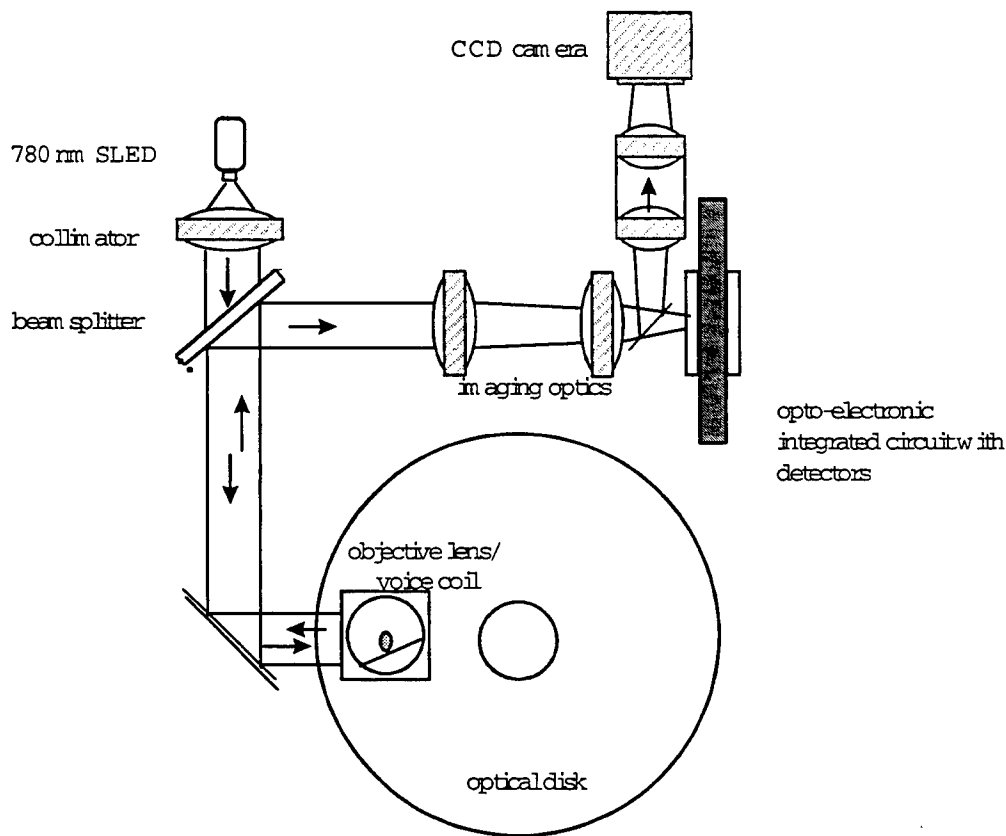


Figure 4.9.4-1: Electrical and Optical test set-ups



#### 4.10 Breadboard Experiments

After electrical check-out, the OEIC was delivered and integrated into the optical system. In the opto-electronic correlator breadboard, shown in Figure 4.10-1, the superluminescent diode illuminates a large area on the disk. The objective lens and imaging optics image the recorded pattern from the disk to the photodetector array on the OEIC. There, the data is detected, thresholded, digitized and sent to the on-chip correlation electronics. The CCD camera system is not an integral part of the correlator; it is used for set-up and lab evaluation.



**Figure 4.10-1 Opto-Electronic Correlator Breadboard**

The system light budget is summarized in Table 4.10-1. The throughput of the beamsplitter between the SLED and the disk and, on reflection, between the disk and the OEIC, could be improved by replacing it with a polarization sensitive beamsplitter. This would increase the available light to approximately  $5 \times 10^{-12}$  Joules/bit period which provides sufficient margin for a system design. In addition, higher power SLEDs are available if required.

The breadboard test disk was recorded in the same manner that the optical correlator test disk was recorded to facilitate comparisons between the systems. Quarter micron e-beam photolithography was used to produce the disk. The data was recorded in the custom radial/serial format using Manchester encoding. To match the photodetector geometry, the pixels were

**Table 4.10-1 OEIC Correlator Light Budget**

Source Power		100 mWatts
M	Sled Collimator transmittance	0.5
M	Beam Splitter transmittance	0.5
M	Objective Lens transmittance	0.9
E	No. misc. elements	2
E	Transmittance / element	0.98
C	Transmittance of misc. elements	0.96
C	Total efficiency to disk	0.22
M	Disk Reflectance (including MTF)	0.43
M	Objective Lens transmittance	0.90
M	Beam Splitter transmittance	0.5
E	No. misc. elements	2
E	Transmittance / element	0.98
C	Transmittance of misc. elements	0.96
C	Total efficiency disk to chip	0.19
C	System Optical Efficiency (= 0.22 * 0.19)	0.04
	No. tracks per head	547 tracks
	Track duty cycle	0.65
	Correlation period	274 nsec
C	Intensity per detector element	4.8 $\mu$ Watts
C	Energy per correlation period	1.31E-12 Joules
PSI	minimum detectable power	1 $\mu$ W
PSI	at	1 MHz
<b>PSI</b>	<b>Minimum Detectable Energy</b>	<b>1E-12 Joules</b>
M = Measured from the breadboard		
E = Estimated for final system implementation		
C = Calculated		
PSI = PSI design specification		

recorded as 3  $\mu$ m spots on 3  $\mu$ m centers in the along track direction and as 3  $\mu$ m spots on 4.6  $\mu$ m centers across track. The patterns were recorded in 8 sectors around the disk with 8K bytes per sector on each ASCII track. Ten bands were written; they included all necessary clocks and system control signals as well as test data. The data set recorded on the glass disk was a section of free form text drawn from the encyclopedia Britannica.

Queries tested ranged from three characters to 16 characters. Figure 4.10-3 shows the query process. The query word or phrase is loaded into the OEIC on-chip registers and the detection threshold on the detectors is set. Then, the disk is spun and the correlation values detected. The correlation levels at each bit time are transferred into computer memory. At this point, the operator can display the raw correlation data or set the detection threshold and allow the software to determine the location of the query in the text. Note: in the system concept of operations, the correlation threshold is set by the control system based on the length of the query phrase. The correlation system then collects the correlation levels and locations and passes them to the post processing subsystem at the end of each sector. The Post-Processor then combines them with previous queries as specified by the operator and returns the ranked list of correlation locations to the operator.

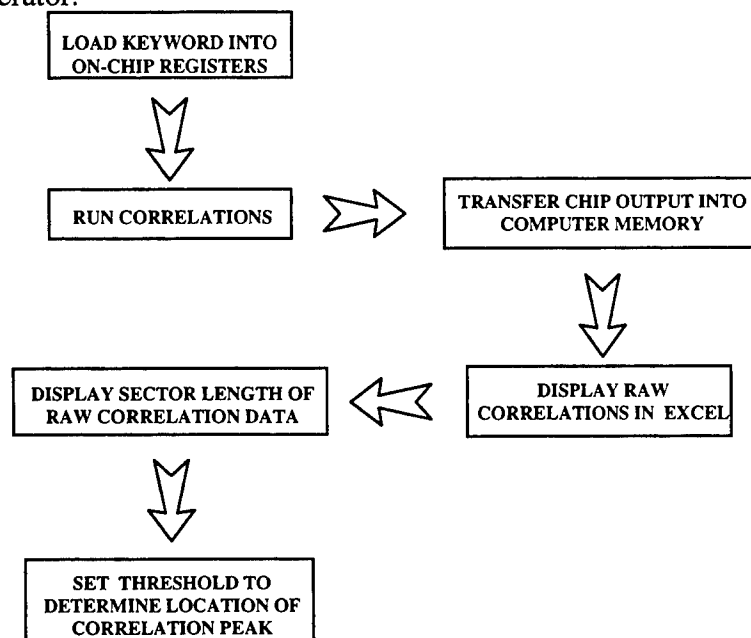
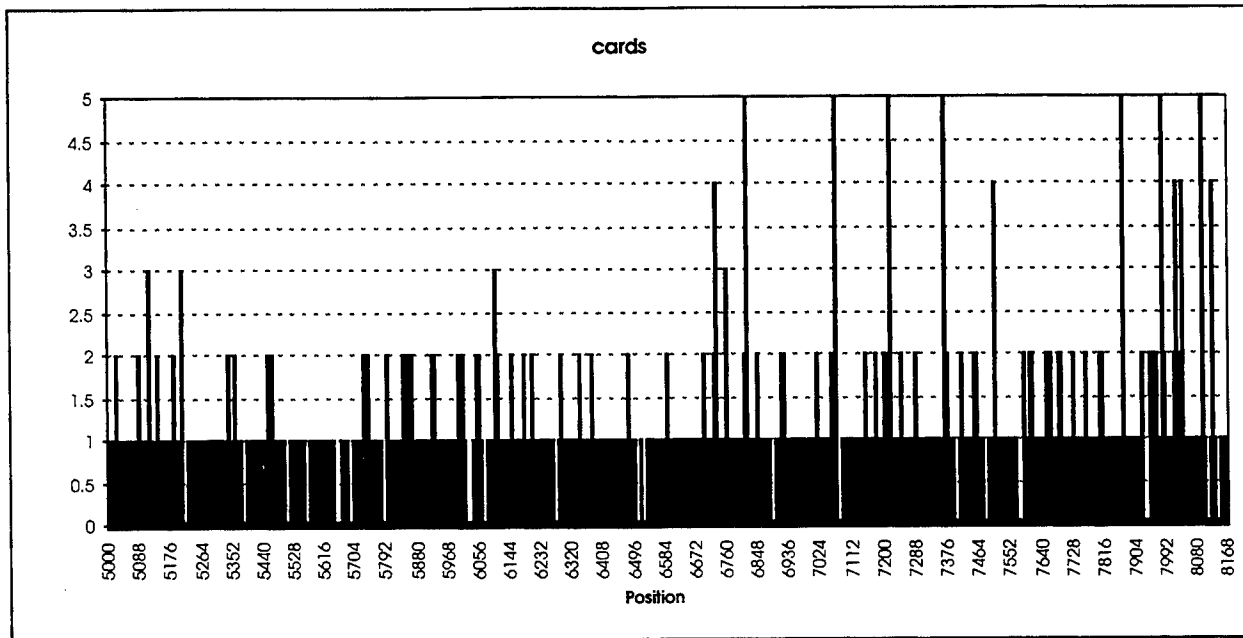


**Figure 4.10-3 Breadboard Query Process**

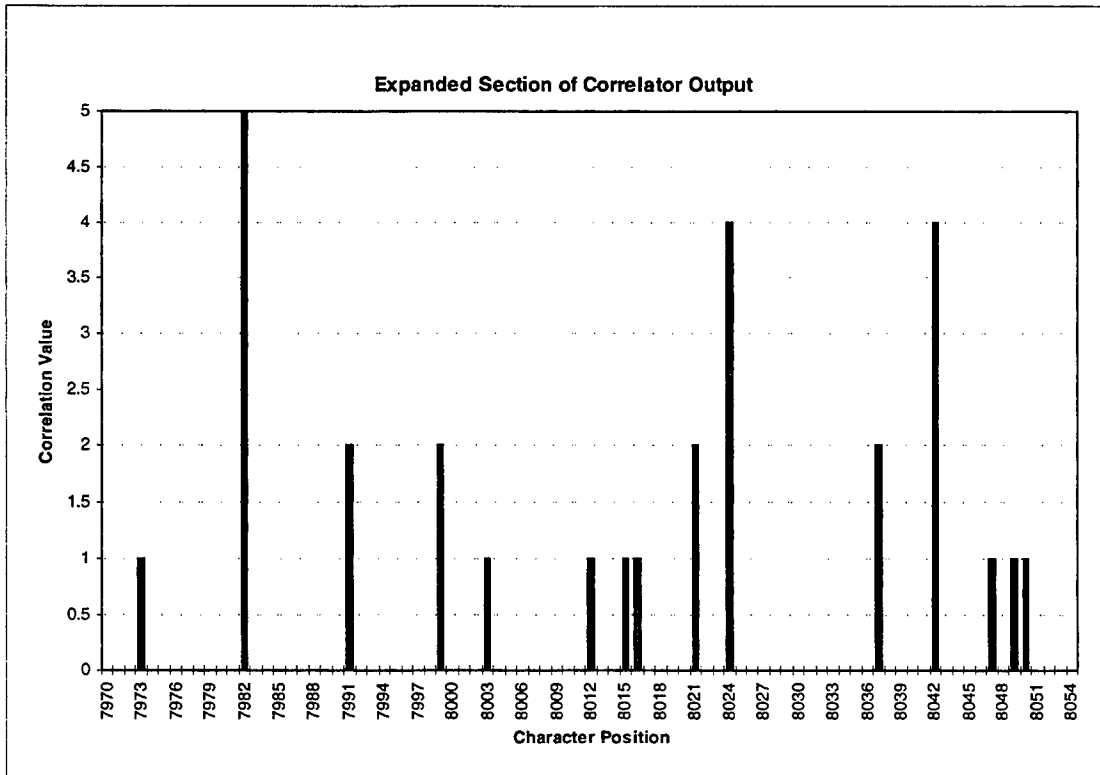
Figure 4.10-4 shows a sample correlation output for the 5 character query word 'cards' along with the end section of the text being searched that includes the last three correlations. The word 'cards' appears three times. The three four character cross correlations are generated by the word 'card' twice and by the partial word 'ards' in standards.



These advantages were noted by commercial interests and soon led to the development of improved punch-card business-machine systems by International Business Machines (IBM), Remington-Rand, Burroughs, and other corporations. These systems used electromechanical devices, in which electrical power provided mechanical motion--such as for turning the wheels of an adding machine. Such systems soon included features to feed in automatically a specified number of **cards** from a "read-in" station; perform such operations as addition, multiplication, and sorting; and feed out **cards** punched with results. By modern standards the punched-card machines were slow, typically processing from 50 to 250 **cards** per minute, with each card holding up to 80 decimal numbers. At the time, however,

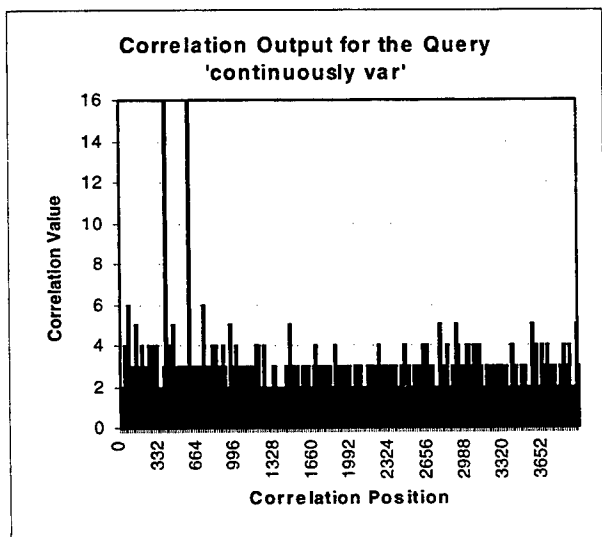
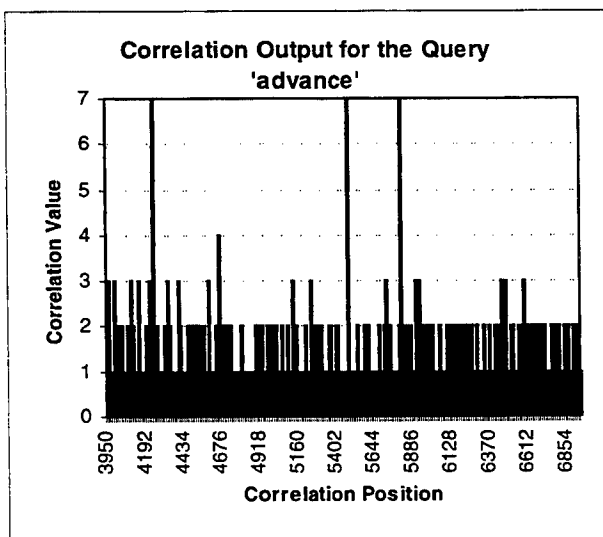
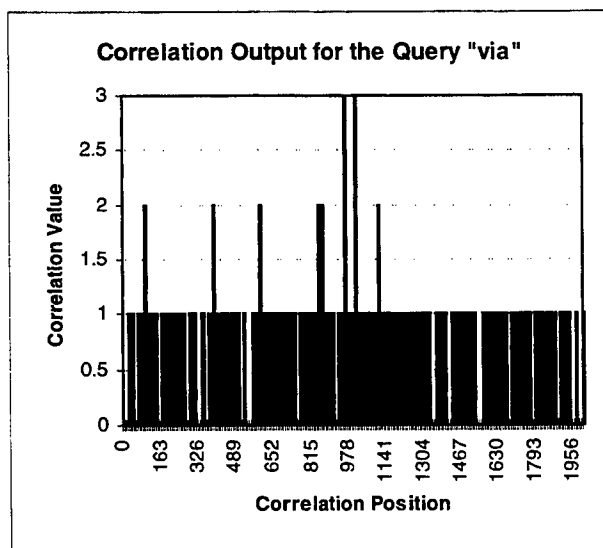
**Figure 4.10-4 Opto-Electronic correlation of the query word 'cards.'**

Figure 4.10-5 shows an expanded region of this correlation output; at most locations the correlation value is zero. Any time one of the characters in 'cards' occurs in the text, the correlation output equals one which is a relatively frequent occurrence. Correlation outputs greater than one require matched letter combinations and are relatively uncommon. Therefore, for longer query words, the correlations become more distinctive. This can be seen in Figure 4.10-6 where three different correlation plots are shown for 3 character, 7 character and 16 character queries along with a section of the associated text. For the 16 character query, the strongest false correlation is at 6 characters; for the 3 character query, the strongest false correlation is at 2 characters. Obviously, longer keywords are easier to threshold and ensure all correlations are found with no false correlations.



**Figure 4.10-5 Expanded Correlation Output**

The opto-electronic correlation system was exercised with keywords ranging from 3 to 16 characters. Table 4.10-2 summarizes the results. Ten runs were made for each query. The table includes: the query word, its length, the number of times it occurs in the test, the number of times it was expected vs. found in ten runs, the location (both expected and found), the strength of the correlation and the strength of the nearest false correlation. *When the chip is in the standard configuration, all expected correlations were found.* For short queries, it may be necessary to set a threshold that will also detect some false correlations; this is not the case for long queries. The occasional difference between expected and found location was caused by periodic missed clocks in the test software. The correlation chip was providing the correct location but the test clock sometimes went out of synch. This is not a fundamental system problem.



Digital, analog, and hybrid computers are conceptually similar in that they all depend on outside instructions; in practice, however, they differ most noticeably in the means they provide for receiving new programs to do new calculating jobs. Digital computers receive new programs quite easily **via** manual instructions or, in modern versions, **via** automatic means. For analog or hybrid computers, however, reprogramming is likely to involve partial disassembly and reconnection of mechanisms and components. Because analog computers are assemblies of physical apparatuses arranged so as to enact the specific type of mathematical relationship for which solutions are to be computed, the choice of a new relationship may require a new assembly. To the extent that analog machines can be considered programmable, their program is rebuilt into their structure for each job.

The difference engine, although of limited flexibility and applicability, was conceptually a great **advance**. Babbage continued work on it for 10 years, but in 1833 he lost interest because he had a "better idea" --the construction of what today would be described as a general-purpose, fully program-controlled, automatic mechanical digital computer. Babbage called his machine an "analytical engine"; the characteristics aimed at by this design show true prescience, although this could not be fully appreciated until more than a century later. The plans for the analytical engine specified a parallel decimal computer operating on numbers (words) of 50 decimal digits and provided with a storage capacity (memory) of 1,000 such numbers.

A computer is an apparatus built to perform routine calculations with speed, reliability, and ease. Three important types are: digital computers, which function internally and perform operations exclusively with digital (discrete) numbers (a type on which most recent progress has centered and that is the focus of much of this article); analog computers, which use **continuously variable** parts exclusively for internal representation of magnitudes and to accomplish their built-in operations; and the less-common hybrid computers (see **HYBRID COMPUTER**), which use both **continuously variable** techniques and discrete digital techniques in their operation.

**Figure 4.10-6 Correlation Outputs for different query lengths**

**Table 4.10-2 Summary of the Opto-Electronic Correlator Testing**

Keyword	# Char	Matches Expected /run	Total # Matches Expected /Found	Expected Location	Found Location	Correlation Value	Value of Highest False Correlation
via	3	2	20/20	964 1012	964 1012	3 3	2
tax	3	1	10/10	2271	2271	3	2
each	4	3	30/30	1529 3100 8126	1529 3100 8126	4 4 4	3
wide	4	3	30/30	1668 2075 2607	1667- 1668 2073- 2075 2605- 2607	4 4 4	3
sort	4	1	10/10	7960	7953- 7958	4	3
built	5	7	70/70	39 484 1498 2354 2570 2969 3822	39 484 1498 2354 2570 2969 3822	5 5 5 5 5 5 5	4
_tax_	5	1	10/10	2270	2270	5	3
_via_	5	2	20/20	963 1011	963 1011	5 5	3
_add_	5	1	10/10	2377	2338- 2352	5	4
digit	5	8	80/80	139 224 626 2116 2511 4472 4802 5769	139 224 626 2116 2511 4472 4802 5769	5 5 5 5 5 5 5 5	4
Digit	5	2	20/20	669 912	669 912	5 5	4
cards	5	7	70/70	6823 7072 7223 7375 7871 7982 8103	6823 7072 7223 7375 7871 7982 8103	5 5 5 5 5 5 5	4

**Table 4.10-2 Summary of the Opto-Electronic Correlator Testing (continued)**

Keyword	# Char	Matches Expected /run	Total # Matches Expected /Found	Expected Location	Found Location	Correlation Value	Value of Highest False Correlation
analog	6	5	50/50	350 678 1037 1184 1431	350 678 1037 1184 1431	6 6 6 6 6	4
hybrid	6	3	30/30	525 690 1047	524-525 689-690 1046-1047	6 6 6	4
depend	6	1	10/10	749	749	6	3
manual	6	2	20/20	968 3115	967-996? 3113-3115	6 6	4
Blaise	6	1	10/10	2058	2051-2058	6	3
series	6	1	10/10	3331	3318-3326	6	4
appreciate	10	1	10/10	4640	4640	9-10	5
analytical	10	3	30/30	4521 4703 5138	4521 4703 5138	10 10 10	5
prescience	10	1	10/10	4595	4595	10	7
digital comp	12	4	40/40	139 913 4472 5769	139 912 4472 5769	12 12 12-13 12	10
analog comp	11	2	20/20	350 1184	350 1184	11 11	7
differential	12	2	20/20	5952 6369	5952 6369	12 12	9
multiplicati	12	1	10/10	7940	7940	11-12	7
continuously	12	2	20/20	378 580	378 580	12 12	7
program-controll	16	1	10/10	4431	4430-4431	15	9
continuously var	16	2	20/20	378 580	378 580	15-16 15-16	6-7
calculating mach	16	2	20/20	2124 3743	2124 3743	16 16	12

Next, the system readout rate was increased. We found it necessary to increase the readout light level as the speed was increased to maintain approximately the same optical energy. If light was not increased to compensate the shorted integration times, the correlation output degraded rapidly due to two effects. First, the impact of noise increased, thereby increasing the risk that false correlations will be detected for short queries. Second, tracking degrades at reduced light levels making readout impossible. As long as sufficient light was maintained, the



system worked as well at increased speeds. Figure 4.10-7 shows the output for the 16 character query word 'apparatus built' at 1000 Hz and at 2400 Hz. The correlation is easily identified in both; the highest false correlation has the same value. Down at the noise level, some differences in cross correlations can be observed due to random noise variations.

The OEIC chip correlates each character individually and defines the character correlation to equal 1 if the bits in the ASCII code match. The chip output is the sum of the number of individual characters that properly correlate. The chip electronics include an internal threshold that defines the number of bit mismatches that are allowed for the correlation to be defined as true (=1). The mismatches can be set equal to 1, 2, 3, or 4. We tested the system at all threshold levels. The results for a 10 character keyword 'analytical' are shown in Figure 4.10-8.

For a threshold of 0 or 1, the system remains functional. There may be some advantages to setting the threshold to 1 since there is only a one bit difference in the ASCII code for a letter in upper case vs. lower case. Setting the threshold equal to 1 allows the system to simultaneously search for capital and lower case query matches. Thresholds greater than 1 result in excessive false correlations and should not be used.

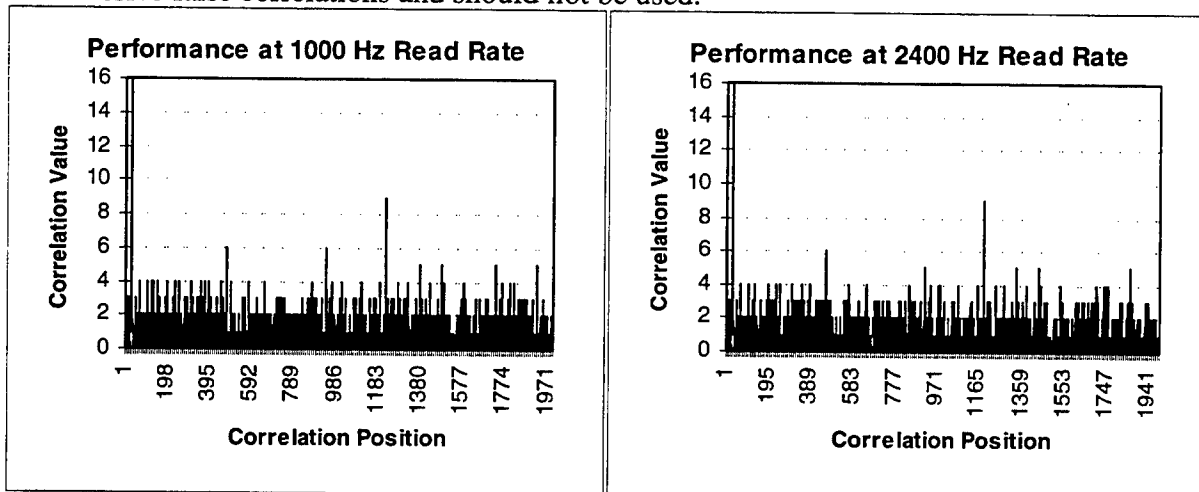


**Figure 4.10-7 Effect of Readout Speed on the Correlator Output**

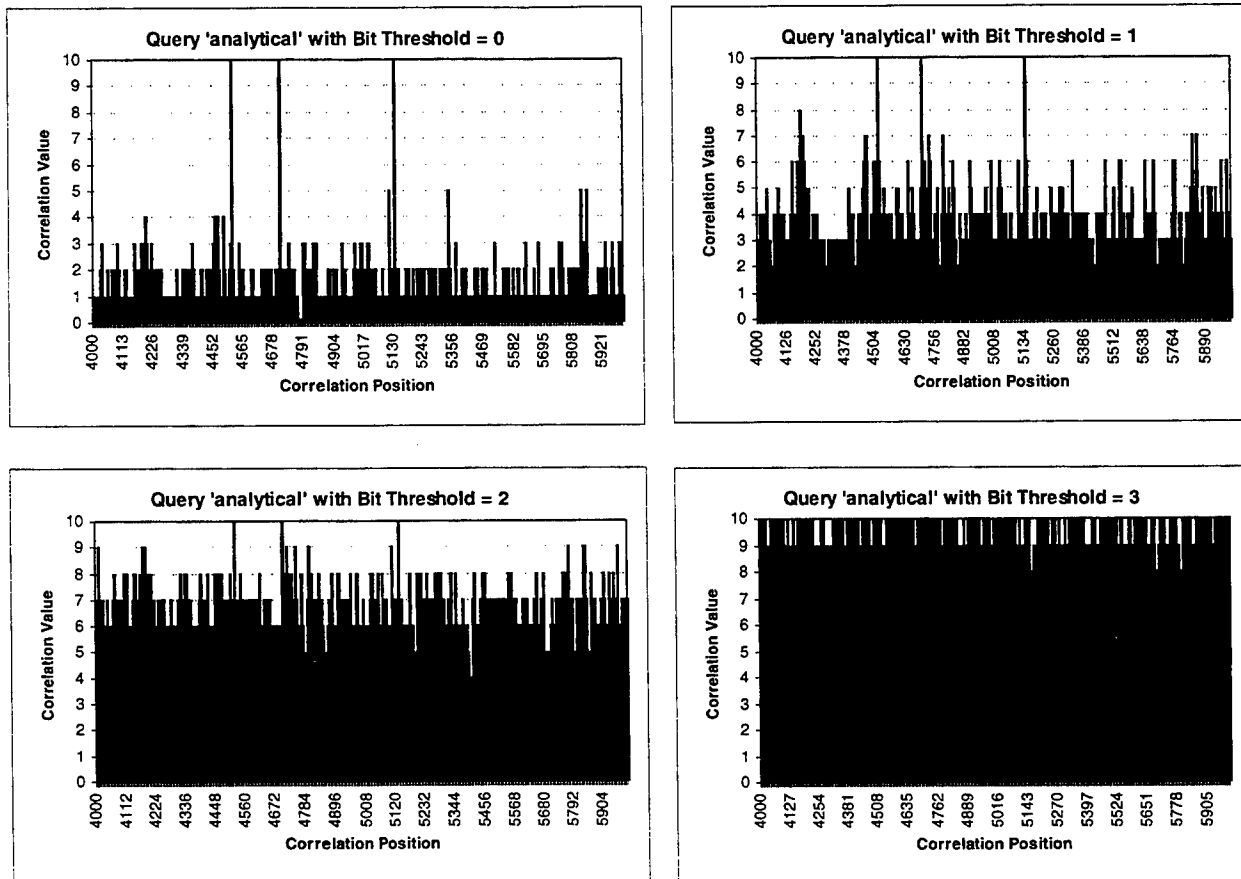


**Figure 4.10-8 Effect of the Internal Chip Threshold on Correlation Output**

Table 4.10-3 summarizes the results for varying query lengths for threshold levels of zero (perfect match) and one (single bit mismatch). For query lengths less than about 6, there are too many false correlations with the threshold set to one to make the system useful. However, at lengths greater than six, a threshold of one may have uses.

#### **4.11 Opto-Electronic Correlator Summary**

Overall, the opto-electronic correlator system worked well. The optics are simple and therefore easier to package. The correlation outputs are relatively clean and easy to threshold. Although not all channels were populated, the OEIC was fabricated at the component density required for a fully populated chip. In addition, it can be expanded by utilizing state-of-the-art semiconductor fabrication technologies. The breadboard chip was fabricated in  $1.2\ \mu\text{m}$  technology; current commercial fabrication technologies are available at  $0.8\ \mu\text{m}$  element sizes. This could be used to make the chip smaller, faster, and to increase the storage capacity of the system.

**Table 4.10-3 Summary of the Correlator Results with Thresholds of '0' and '1'**

Keyword	Keyword Length	Threshold=0			Threshold=1		
		Number Found in Sector	Height	Highest False	Number Found in Sector	Height	Highest False
via	3	2	3	2	too many	3	2
tax	3	1	3	2	16	3	2
add	3	7	3	2	too many	3	2
each	4	3	4	3	42	4	3
wide	4	3	4	3	21	4	3
feed	4	2	4	3	29	4	3
sort	4	1	4	3	4	4	3
urge	4	1	4	2	20	4	3
built	5	7	5	4	14	5	4
digit	5	8	5	4	11	5	4
Digit	5	2	5	4	10	5	4
cards	5	7	5	4	9	5	4
multi	5	3	5	4	3	5	4
tax (with spaces)	5	1	5	3	1	5	4
via (with spaces)	5	2	5	3	41	5	4
add (with spaces)	5	1	5	4	3	5	4
analog	6	5	6	4	5	6	5
hybrid	6	3	6	4	4	6	5
depend	6	1	6	3	5	6	5
manual	6	2	6	4	2	6	5
Blaise	6	1	6	3	1	6	5
series	6	1	6	4	1	6	5
system	6	3	6	4	3	6	5
advance	7	3	7	5	3	7	6
appreciate	10	1	10	5	1	10	7
analytical	10	3	10	5	3	10	8
prescience	10	1	10	7	1	10	7
analog comp	11	2	11	7	2	11	8
digital comp	12	3	12	11	4	12	10
differential	12	2	12	9	2	12	9
multiplicati	12	1	12	7	1	12	7
continuously	12	2	12	7	2	12	8
program controll	16	1	15	9	1	15	11
continuously var	16	2	16	7	2	16	10
calculating mach	16	2	16	12	2	16	13

## 5. SUMMARY AND RECOMMENDATIONS

Two versions of the optical correlation subsystem were breadboarded and tested. Both worked with varying degrees of performance. Issues of concern are system complexity, the state of development of the key components, and relative performance. This section discusses the comparison between the two systems and compares them with what is possible in electronic technologies today.

### 5.1 Correlator Design

Correlator design issues include storage capacity, how well the thresholds can be set, and mechanical packaging.

#### 5.1.1 Storage Capacity

Table 5.1.1-1 compares the performance of the optical and opto-electronic correlators for a full speed system. The disk rotation rate is assumed to be 30 Hz, the standard optical disk rate. The disk and data formats discussed in Chapters 3 and 4 are used. The optical correlator uses the 24 bit custom code developed on this program. The coded bits are recorded as standard bits with standard bit spacing. The opto-electronic correlator uses Manchester encoded ASCII characters written across-track. In the breadboard system, two tracks were used for each polarity of the Manchester code with one guard track between adjacent characters, resulting in five channel bits per ASCII bit. For this design trade, we assume that each polarity of the Manchester code requires 1 track. This reduces the coding overhead to three channel bits per ASCII bit.

**Table 5.1.1-1 Associative Memory Design Parameters - Projected System**

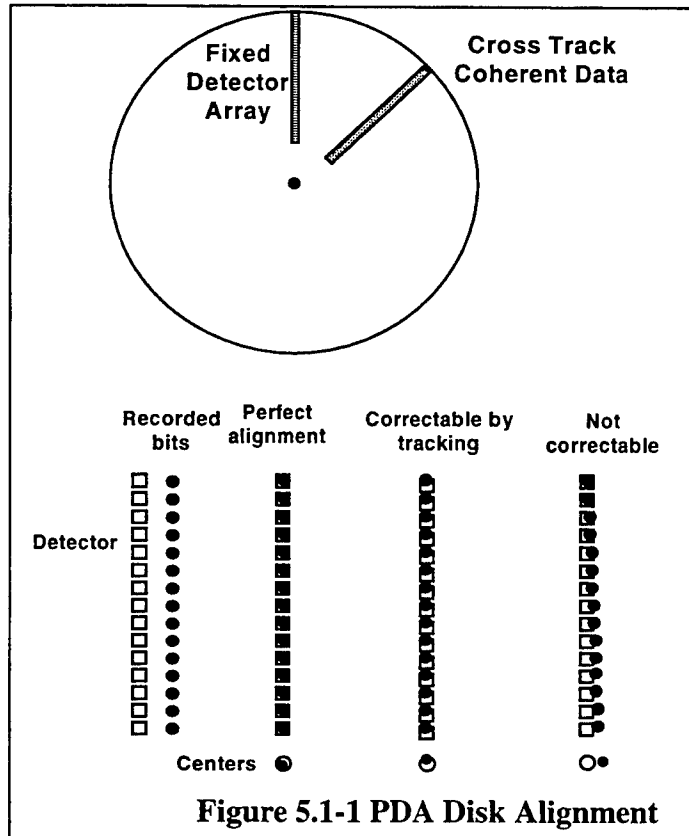
PARAMETER	Optical Correlator	Opto-Electronic Correlator
Rotation rate (rpm)	1800	1800
Rotation Period (msec)	33.33	33.33
Disk Format	Zoned CAV	Zoned CAV
Zones / disk	16	16
Recording range (cm)	3 to 6	3 to 6
Normal bit spacing ( $\mu\text{m}$ )	0.5	0.5
Long bit ratio	1	6
Channel bit center spacing ( $\mu\text{m}$ )	0.5	3
channel bits per ASCII word (bits)	24	16
Guard band bits per ASCII character (bits)	0	1
Normal track spacing ( $\mu\text{m}$ )	1.6	1.6
Tall bit ratio	1	1
Custom track spacing ( $\mu\text{m}$ )	1.6	2.4
bits per zone-sector (bits)	24,238,311	2,693,146
Sectors per disk (sector blocks)	392	392
Bytes/disk (MBytes)	396	66

In the along-track direction, we do not recommend reducing the bit size from the breadboard. The along-track bit size is  $3\text{ }\mu\text{m}$ ; this is a factor of six compared to the normal optical disk bit spacing of  $0.5\text{ }\mu\text{m}$ . This difference is included in the long bit ratio of 6 for the opto-electronic correlator vs. 1 for the optical correlator. The reason the along-track bit size can not be reduced is shown in Figure 5.1-1. The photodetector array is aligned along a radius of the correlation disk. The data is written in a cross-track coherent manner along a radius of the disk. However, the disk writer is a different mechanical system than the correlation disk drive and some eccentricity can be expected between them. An additional offset comes from the axial wobble of the correlation disk drive. If the center of the correlation disk does not line up properly with the extrapolated center of the detector array, the data line will be tilted with respect to the detector array. The data is clocked out using a clock track at the outer edge of the array. The worst case condition occurs when the offset is perpendicular to the detector array. With a tilt between the recorded radius and the detector, the inner bits may not be on a detector simultaneously with the clock. If the bits are more than 20% offset, excessive noise will degrade the readout quality. To keep the offset less than  $\pm 20\%$ , the centers must be aligned within  $\pm 10\text{ }\mu\text{m}$ . Although it is possible to adjust out most of the eccentricity differences between the two drives, the axial wobble of the correlation disk drive must still be maintained to better than the  $\pm 10\text{ }\mu\text{m}$ . Reducing the along-bit size will make this tolerance even tighter.

The recorded bit size, the disk format, and the coding scheme combine to determine the data storage capacity of the two systems. The storage capacity of the optical correlator system is 396 Mbytes. The storage capacity of the opto-electronic correlator system is 66 Mbytes.

### 5.1.2 Thresholding

The system specification is for 100% probability of detection with less than 5% probability of false correlation. This means it is more important to be sure no correlations are missed than to spend effort on weeding out false correlations. Both the optical correlator and the opto-electronic correlator have adjustable thresholds so that the user can determine the probability of detection. In the optical correlator, the threshold is set in terms of the number of acceptable bit mismatches out of the entire query word. The opto-electronic correlator threshold is set in terms of the number of characters that must properly correlate. Figures 5.1-1 and 5.1-2



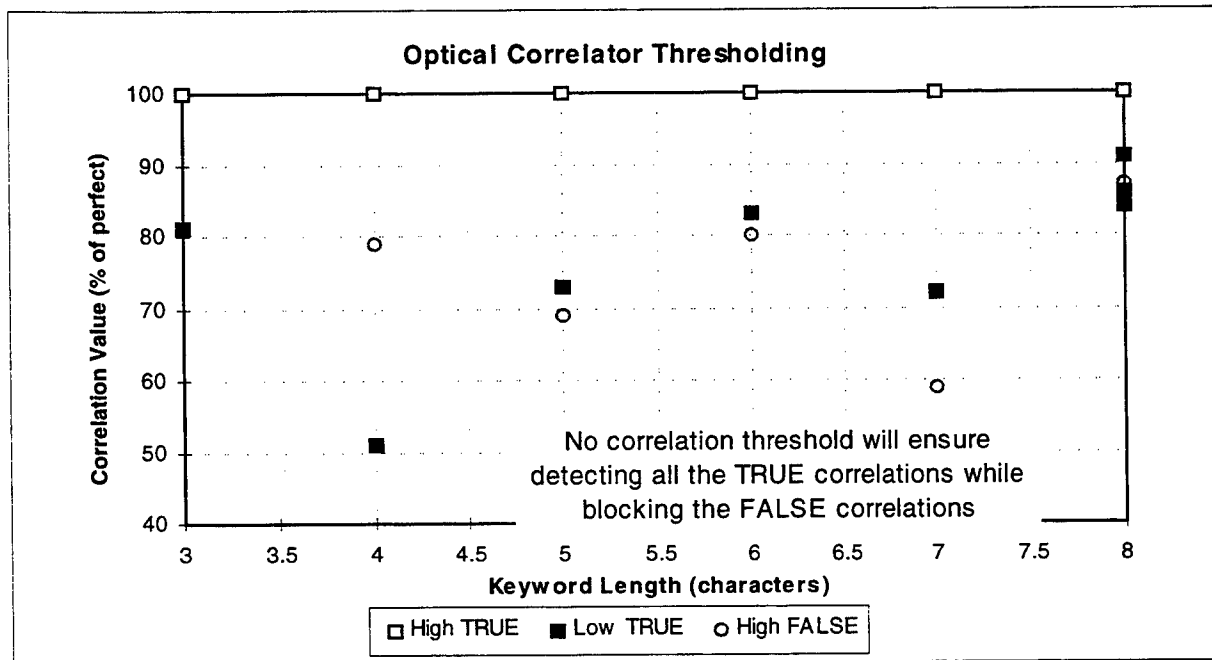


**Figure 5.1.2-1 Threshold Characteristics of the Optical Correlator**

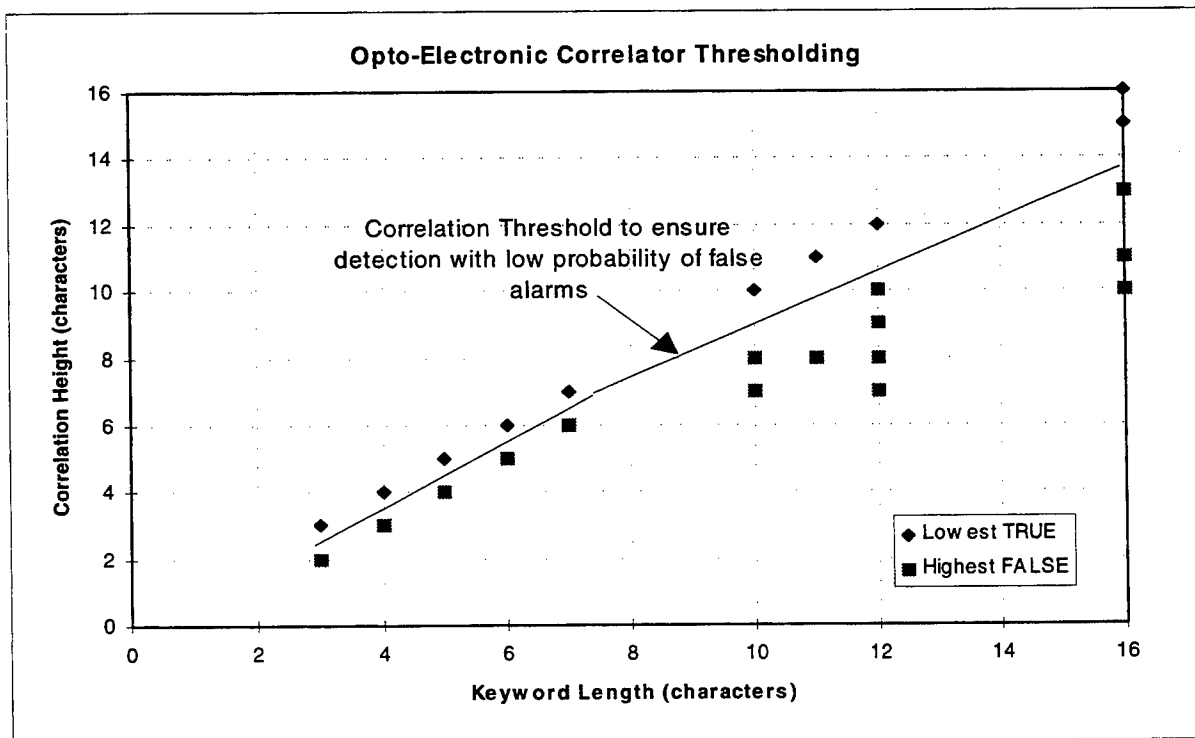


**Figure 5.1.2-2 Thresholding Characteristics of the Opto-Electronic Correlator**

show the threshold characteristics for the optical and opto-electronic correlators respectively. In the optical correlator, the highest false correlations are frequently stronger than the lowest true correlations. This occurs because the background variations are not completely removed by the bias subtraction algorithm. In Figure 5.1.2-1, setting a threshold to 70% of the maximum correlation for keywords longer than 6 characters ensures detection but results in a high false correlation level. For words of 5 characters or less, a lower threshold is required to ensure all true correlations are found; this results in an even higher probability of false correlations. For the opto-electronic correlator, the threshold is easier to set. For short keywords (5 characters or less), the threshold must be set such that only perfect matches are above the threshold. If a lower threshold is set, the number of false correlations becomes excessive. Adding spaces at the beginning and end of keywords, wherever possible, improves the thresholding by effectively increasing the keyword length. For keywords of 6 to 12 characters, it is preferable to set a threshold one character less than the query length. This ensures detection without increasing the false alarm rate. For keywords longer than 12, setting the threshold 2 or 3 characters less than the word length is acceptable. For longer queries, it is relatively simple to set a threshold that will ensure all correlations are found. In the breadboard tests, when the system was operating properly, the correlation value found was never more than the keyword length minus one.

### **5.1.3 Packaging**

Both systems require 16 correlator heads around the optical disk, one for each of the zones in the zoned CAV format. Each correlator head includes source, optics, SLM and PDA. The opto-electronic correlator concepts will be much easier to package compactly because there are fewer components. The SLM and the optics between the SLM and PDA are not required. In addition, a separate focus and tracking optical system is not required for OEIC.

## **5.2 Component Development Status**

A key consideration is how much development will be required to ensure all components of the optical system are ready for integration into a product. Table 5.2-1 identifies the components used in each correlator type and summarizes their status.

Both systems require custom disk formats with the associated custom disk writer. Such disk writers are commercially available for use in testing optical disks. Modifications are required to adapt to the specific data formats of the correlators.

Both systems use superluminescent diodes (SLED) as the source. The breadboard SLED is a 50 mW device; this will need to be increased for the final system. The vendor has analyzed the requirements for the higher power devices and considers them to be a low risk development.

The input optics and objective lens are the same for both systems. A design has been developed for the objective lens and reviewed with vendors. This lens is low risk development. The remaining optics that image the disk to the correlation plane are commercial off-the-shelf components.

The opto-electronic correlator does not require a spatial light modulator whereas the optical correlator does. The off-the-shelf liquid crystal device used in the breadboard worked well and demonstrated feasibility of the concept but a longer device will be required for the final system. The development of spatial light modulators is an active field. As discussed in Section

**Table 5.2-1 Correlator Component Status**

COMPONENT	OPTICAL CORRELATOR	OPTO-ELECTRONIC CORRELATOR
Custom Disk	<ul style="list-style-type: none"> <li>• Special data format required</li> </ul>	<ul style="list-style-type: none"> <li>• Special data format required</li> </ul>
Source	<ul style="list-style-type: none"> <li>• 500 mW SLED baseline</li> <li>• Requires a small modification to an existing device</li> </ul>	<ul style="list-style-type: none"> <li>• 100 mW SLED baseline</li> <li>• Requires a small modification to an existing device</li> </ul>
Spatial Light Modulator	<ul style="list-style-type: none"> <li>• 1 x 408 Binary</li> <li>• Liquid crystal SLM selected</li> <li>• Successful in breadboard tests</li> <li>• Modifications in size required for final system</li> </ul>	<ul style="list-style-type: none"> <li>• Not Required</li> </ul>
PDA	<ul style="list-style-type: none"> <li>• 1 x 1300 elements</li> <li>• Vendors identified</li> <li>• Required on-chip processing is feasible</li> </ul>	<ul style="list-style-type: none"> <li>• 1 x 1300 element</li> <li>• Part of OEIC</li> <li>• Vendor identified</li> <li>• Prototype procured and successfully tested</li> <li>• Higher resolution photo-lithography required for final system (commercially available)</li> </ul>
PDA Processing Electronics	<ul style="list-style-type: none"> <li>• Analog AC filter for bias subtraction</li> <li>• Peak detect and hold</li> <li>• Similar to existing vendor designs</li> </ul>	<ul style="list-style-type: none"> <li>• Differential detection &amp; threshold</li> <li>• Electronic correlation</li> <li>• Proven in breadboard</li> </ul>
Post Detection Processing	<ul style="list-style-type: none"> <li>• Digitization and thresholding</li> </ul>	<ul style="list-style-type: none"> <li>• Digital peak detect and hold</li> </ul>
Objective and imaging optics (Source to disk to image plane)	<ul style="list-style-type: none"> <li>• Custom objective lens required</li> <li>• Design is similar to existing lenses</li> <li>• Remaining optics are off-the-shelf</li> </ul>	<ul style="list-style-type: none"> <li>• Custom objective lens required</li> <li>• Design is similar to existing lenses</li> <li>• Remaining optics are off-the-shelf</li> </ul>
Transform Optics	<ul style="list-style-type: none"> <li>• COTS</li> <li>• SLM to PDA transformation</li> </ul>	<ul style="list-style-type: none"> <li>• Not Required</li> </ul>
Servo Systems	<ul style="list-style-type: none"> <li>• Uses standard optical disk servo techniques</li> <li>• Requires separate source (different wavelength) and optics</li> <li>• Tested and working in breadboard</li> </ul>	<ul style="list-style-type: none"> <li>• Integrated into OEIC chip</li> <li>• Tested and functioning in the breadboard</li> </ul>
Correlator Disk Drive	<ul style="list-style-type: none"> <li>• Standard disk drive</li> </ul>	<ul style="list-style-type: none"> <li>• Required tighter mechanical tolerances</li> </ul>
Disk Writer Electronics	<ul style="list-style-type: none"> <li>• Identified a vendor to develop the correlation disk writer</li> <li>• Data is written in rectilinear blocks (combined CAV/CLV)</li> <li>• Requires bit spacing accurate to within 0.05%</li> </ul>	<ul style="list-style-type: none"> <li>• Identified a vendor to develop the correlation disk writer</li> <li>• Data is written in parallel/serial format in 16 zones</li> <li>• Data is cross-track coherent within each zone</li> <li>• Requires bit spacing accurate to within 0.05%</li> </ul>

3.2.3, there are improved SLMs that were not available at the time the liquid crystal device was selected. We recommend reviewing the current state-of-the-art when selecting a SLM.



Both systems require a one dimensional photodetector array. A custom detector array with on-chip analog and digital processing is required for the optical correlator. The analog processing consists of a simple AC filter and a peak detection circuit. Both have been fabricated in the past. The digital processing includes an A/D converter and an externally set threshold circuit. For the opto-electronic correlator, the PDA is an integral part of the opto-electronic integrated circuit. After the initial detection and differential detection, all processing is digital; this function was demonstrated in the breadboard testing.

The optical correlator requires a transform lens between the SLM and the PDA. This lens is a standard off-the-shelf item.

The two systems use different focus and tracking approaches. The optical correlator essentially uses the same focus and tracking system as standard optical disk readers. However a different optical system is required since the correlator uses a large area illumination and the standard focus system requires a focused point at the disk plane. To ensure that it does not interfere with the correlation readout, a different wavelength source is used. This increases the number of components that need to be packaged into the correlator head. The opto-electronic correlator integrates the focus and tracking system into the OEIC which simplifies the overall optics. Both servo systems have been successfully tested on the breadboards.

### **5.3 Alternative Technologies**

At the start of this program, a review of the alternative technologies indicated that there was nothing available that could meet the operational timeline required of this system. This is not necessarily true today given the advances in hardware and software and the additional requirements identified during the design of the optical systems.

The original concept for the optical correlator was that it would be capable of using standard optical disks. A user could walk up to the system, insert a disk into the optical disk reader and run a correlation. This mode provided a major speed and simplicity advantage over any software solution. The advantage was lost when a separate correlation disk using a custom code became necessary. Use of the custom code requires doubling the storage capacity of the system since the data is written twice - once to the data disk and once to the correlation disk. The custom correlation disk is written off-line at a separate optical station and a software map is generated linking the two disks. This operation can take hours. Any time new data is added, the correlation disk must be updated. When it is inserted into the correlation station, the entire 300 Mbyte database is read in a single rotation generating the first correlations in 33 msec.

A standard indexed database has similar requirements and performance. The memory it requires is at least twice the database size. Half is for the database, half (or more) is for the index. The index is created off-line and can take hours to create. When new data is added, the index must be recreated. However, once the index is created, the binary search algorithms can be used to search it in times that are on the order of 30 msec.

The concept of using a standard optical disk was originally abandoned because the complexity of the on-chip electronics required to handle the resynch bytes in the standard optical disk recording formats was very high risk. With the development of flip-chip technologies that make it possible to easily connect the analog PDA to digital processing electronics, much of the risk is reduced. However, the excessive background fluctuations generated by the nature of both the RLL (2,7) and 4/15 codes make a custom code necessary. Therefore, the special correlation disk is still required.

A second alternative is a hardware solution. In this concept, the data is stored in RAM memory and a custom correlation chip is developed to handle the search. The entire 300 Mbyte database can now be stored in a single RAM memory chip. Custom ASICs are capable of operating at speeds up to 100 MHz. The correlation process would be pipelined through the ASIC in a manner similar to the electrical correlation in the OEIC system. Using a dedicated bus, input/output (I/O) rates on the order of 50 MHz for 32 bit wide data are attainable. This I/O rate could be pushed to 100 MHz with 64 bit wide data at an increased development risk. Assuming a 100 MHz ASIC fed with 32 bit wide data at 50 MHz, the a 300 Mbyte database can be correlated in 1.5 seconds with the limit being set by the data I/O rate. Increasing the I/O rate to 100 MHz, the correlation time drops to 750 msec. Further reduction to 375 msec is possible by postulating the use of a 64 bit wide data bus. By dividing the data storage into multiple RAM chips, a parallel readout system can be designed with one ASIC dedicated to each RAM chip. For the 32 bit wide, 50 MHz I/O, 50 ASICS with associated memory chips are required. At a 100 MHz I/O rate, this drops to 25. Finally, using a 64 bit wide bus, 13 parallel ASICS are required to correlate the 300 Mbyte database in 33 msec. Custom video chips are now available with I/O rates on the order of 128 MHz. The electrical correlator system falls within the current state-of-the-art design and product availability.

Table 5.3-1 summarizes the advantages and disadvantages of the correlator options.

#### **5.4 Summary and Recommendations**

During the span of this program, we investigated several optical correlation approaches that could perform a high speed correlation of a free form database recorded on an optical disk. The two most promising were developed and breadboarded. A combination of simulations and breadboard measurements demonstrated the basic feasibility of both approaches. Of the two optical correlation approaches, the opto-electronic correlator offers several advantages. It contains fewer components and it therefore easier to package. It is also relatively immune to noise from the optical system. A threshold level can be set based on keyword length that will ensure 100% detection with minimal false correlations. However, because of the requirement for a special correlation disk, it is not clear that either optical approach provides a major advantage over software and electronic solutions. With the technology available today, we recommend further investigation into a hardware solution.

**Table 5.3-1 Correlator Option Comparison**

	ADVANTAGES	DISADVANTAGES
OPTICAL CORRELATOR	<ul style="list-style-type: none"> <li>• Reduced data rate</li> <li>• Reduced mechanical tolerances</li> </ul>	<ul style="list-style-type: none"> <li>• Complex optics; separate focus &amp; tracking system required.</li> <li>• Several custom components</li> <li>• Custom disk format written off-line requiring hours of timeline</li> <li>• Threshold can not be cleanly set. Noise is a problem.</li> <li>• Requires packaging 2 optical systems (reader and servo) in one compact package.</li> <li>• 16 correlator heads required around the disk</li> </ul>
OPTO-ELECTRONIC CORRELATOR	<ul style="list-style-type: none"> <li>• Simpler optics</li> <li>• COTS components (except OEIC)</li> <li>• Threshold can be cleanly set. Noise is less of an issue.</li> <li>• Easier packaging</li> </ul>	<ul style="list-style-type: none"> <li>• Mechanical centering must be within <math>\pm 10 \mu\text{m}</math>.</li> <li>• Higher data rates from the chip.</li> <li>• Custom disk format written off-line requiring hours of timeline.</li> <li>• Reduced data storage</li> <li>• 16 correlator heads required around the disk</li> </ul>
SOFTWARE	<ul style="list-style-type: none"> <li>• The entire database can be scanned within 33 msec.</li> <li>• Standard binary search algorithms are used</li> <li>• Minimum development</li> </ul>	<ul style="list-style-type: none"> <li>• Database must be indexed . This requires twice the memory capacity.</li> <li>• Index must be regenerated any time new data is added. This requires hours.</li> </ul>
HARDWARE	<ul style="list-style-type: none"> <li>• The entire database can be scanned within 33 msec.</li> <li>• High capacity memory is commercially available</li> <li>• Once the database is stored in memory, no further operations are required prior to correlation (no indexing).</li> <li>• New data is added by adding it to the RAM memory</li> </ul>	<ul style="list-style-type: none"> <li>• Requires development of high speed state-of-the-art electronics</li> <li>• At least 13 parallel memory chips and correlation chips are required</li> </ul>

FRED HARITATOS 10  
RL/IRAP  
32 HANGAR RD  
ROME, NY 13441-4114

MS. LYNDAL RALSTON 5  
HARRIS CORP  
GOVERNMENT COMM SYS DIVISION  
P.O. BOX 91000  
MELBOURNE, FL 32902

ROME LABORATORY/SUL 1  
TECHNICAL LIBRARY  
26 ELECTRONIC PKY  
ROME NY 13441-4514

ATTENTION: DTIC-OCC 2  
DEFENSE TECHNICAL INFO CENTER  
8725 JOHN J. KINGMAN ROAD, STE 0944  
FT. BELVOIR, VA 22060-6218

ADVANCED RESEARCH PROJECTS AGENCY 1  
3701 NORTH FAIRFAX DRIVE  
ARLINGTON VA 22203-1714